Aerosol Technology

Properties, Behavior, and Measurement of Airborne Particles

Second Edition

William C. Hinds
Department of Environmental Health Sciences
Center for Occupational and Environmental Health
UCLA School of Public Health
Los Angeles, California

A WILEY-INTERSCIENCE PUBLICATION
JOHN WILEY & SONS, INC.
NEW YORK / CHICHESTER / WEINHEIM / BRISBANE / SINGAPORE / TORONTO

Library of Congress Cataloging-in-Publication Data

Hinds, William C.
Aerosol technology : properties, behavior, and measurement of airborne particles / William C. Hinds. —2nd ed.
p. cm.
"A Wiley-Interscience publication."
Includes bibliographical references and index.
ISBN 0-471-19410-7 (cloth : alk. paper)
1. Aerosols. 2. Aerosols—Measurement. I. Title.
QC882.42.H56 1998 98-23683
648.5'3—dc21

328828

Printed in the United States of America.
10 9 8 7 6 5 4 3 2 1

CONTENTS

PREFACE TO THE FIRST EDITION

Airborne particles are present throughout our environment. They come in many different forms, such as dust, fume, mist, smoke, smog, or fog. These aerosols affect visibility, climate, and our health and quality of life. This book covers the properties, behavior, and measurement of aerosols.

This is a basic textbook for people engaged in industrial hygiene, air pollution control, radiation protection, or environmental science who must, in the practice of their profession, measure, evaluate, or control airborne particles. It is written at a level suitable for professionals, graduate students, or advanced undergraduates. It assumes that the student has a good background in chemistry and physics and understands the concepts of calculus. Although not written for aerosol scientists, it will be useful to them in their experimental work and will serve as an introduction to the field for students starting such careers. Decisions on what topics to include were based on their relevance to the practical application of aerosol science, which includes an understanding of the physical and chemical principles that underlie the behavior of aerosols and the instruments used to measure them.

Although this book emphasizes physical rather than mathematical analysis, an important aspect of aerosol technology is the quantitative description of aerosol behavior. To this end I have included 150 problems, grouped at the end of each chapter. They are an important tool for learning how to apply the information presented in the book. Because of the practical orientation of the book and the intrinsic variability of aerosol properties and measurements, correction factors and errors of less than 5 percent have generally been ignored and only two or three significant figures presented in the tables.

Aerosol scientists have long been aware of the need for a better basic understanding of the properties and behavior of aerosols among applied professionals. In writing this book, I have attempted to fill this need, as well as the long-standing need for a suitable text for students in these disciplines. The book evolved from class notes prepared during nine years of teaching a required one-semester course on aerosol technology for graduate students in the Department of Environmental Health Sciences at Harvard University School of Public Health.

Chapters are arranged in the order in which they are covered in class, starting with simple mechanics and progressing to more complicated subjects. Particle statistics is delayed until the student has a preliminary understanding of aerosol properties and can appreciate the need for the involved statistical characterization. Applications are discussed in each chapter after the principles have been presented. The more complicated applications, such as filtration and respiratory deposition, are

introduced as soon as the underlying principles have been covered. The operating principles of different types of aerosol measuring instruments are given in general terms so that one may correctly interpret data from them and explain the frequent differences in results between instruments. Discussion of specific instruments is limited because they change rapidly and are covered well in *Air Sampling Instruments,* 5th edition, ACGIH, Cincinnati, OH (1978). The latter (or any future edition) makes an excellent companion to this text. Several general references are given at the end of each chapter. Tables and graphs are provided in the appendix for general reference and for help in dealing with the problems at the end of each chapter.

While many people have contributed to this book, I would like to acknowledge particularly Klaus Willeke of the University of Cincinnati, who reviewed the manuscript and made many helpful suggestions; Kenneth Martin, who provided the SEM photos; and Laurie Cassel, who helped prepare and type the manuscript.

WILLIAM C. HINDS

Boston, Massachusetts
February 1982

PREFACE TO THE SECOND EDITION

More than 16 years have passed since the first edition of *Aerosol Technology* was published in 1982. During this time the field of aerosol science and technology has expanded greatly, both in technology and in the number of scientists involved. When the first edition was published there were two national aerosol research associations, now there are 11 with regular national and international meetings. Growth areas include the use of aerosols in high-technology material processing and the administration of therapeutic drugs, and there is an increased awareness of bioaerosols, aerosol contamination in microelectronic manufacturing, and the effect of aerosols on global climate. While the first edition proved to be popular and useful, and became a standard textbook in the field, changes in technology and growth of the field have created the need to update and expand the book.

The objective of the book has remained the same: to provide a clear, understandable, and useful introduction to the science and technology of aerosols for environmental professionals, graduate students, and advanced undergraduates. In keeping with changes in the field, this edition uses dual units, with SI units as the primary units and cgs units as secondary units. Besides updating and revising old material, I have added a new chapter on bioaerosols and new sections on resuspension, transport losses, respiratory deposition models, and fractal characterization of particles. The chapter on atmospheric aerosols has been expanded to include sections on background aerosols, urban aerosols, and global effects. There are 26 new examples and 30 new problems. The latest edition of *Air Sampling Instruments* remains an excellent companion book, as does *Aerosol Measurement*, by Willeke and Baron. Both provide greater depth and detail on measurement methods and instruments.

Of the many people who have helped with this edition, I would like to particularly acknowledge Janet Macher, Robert Phelan, and John Valiulis for reviewing specific chapters; Rachel Kim and Vi Huynh for typing manuscript changes; doctoral student Nani Kadrichu for entering the equations; and finally, my wife Lynda for her continued support during this long process.

WILLIAM C. HINDS

Los Angeles, California

LIST OF PRINCIPAL SYMBOLS

a	acceleration, particle radius
a_c	centrifugal acceleration, Eq. 3.15
A	area, cross-sectional area
A_p	cross-sectional area of a particle
A_s	surface area
b	coefficient for Hatch–Choate equation, Eq. 4.47
B	particle mobility, Eq. 3.16
B_0	luminance of an object, Eq. 16.26
B'	luminance of background, Eq. 16.26
c	molecular velocity; velocity of light
$\bar{c}$	mean molecular velocity, Eq. 2.22; mean thermal velocity of a particle, Eq. 7.10
c_{rms}	root mean square molecular velocity, Eq. 2.18; root mean square thermal velocity of a particle, Eq. 7.9
c_x, c_y, c_z	velocity in the x, y, z directions
C	particle concentration in sampling probe
C_c	Cunningham correction factor, Eq. 3.19; slip correction factor, Eq. 3.20
C_D	drag coefficient, Eq. 3.4
C_m	mass concentration, mass of particles per unit volume of aerosol
CMD	count median diameter
C_N	number concentration, number of particles per unit volume of aerosol
C_R	apparent contrast, reduced contrast, Eqs. 16.27 and 16.33
C_0	true concentration, inherent contrast, Eq. 16.26
CE_R	collection efficiency for respirable precollector, Eq. 11.14
CE_T	collection efficiency for thoracic precollector, Eq. 11.18
d	particle diameter; derivative
$\bar{d}$	arithmetic mean diameter, Eq. 4.11
d^*	Kelvin diameter, Eq. 13.5
d_a	aerodynamic diameter, Eq. 3.26
d_A	specified average diameter, Eq. 4.47
d_c	diameter of cylinder
d_d	droplet diameter
d_e	equivalent volume diameter, Eqs. 3.23 and 19.3
d_f	fiber diameter
d_F	Feret's diameter, Fig. 20.1
d_g	geometric mean diameter, Eq. 4.14

a_i midpoint diameter of the ith group
d_m diameter of a gas molecule
$d_{\bar{m}}$ diameter of average mass, Eq. 4.19
d_{mm} mass mean diameter, Eq. 4.26
d_M Martin's diameter, Fig. 20.1
d_p particle diameter
$d_{\bar{p}}$ diameter of average property proportional to d^p, Eq. 4.22
d_{PA} projected-area diameter, Fig. 20.1
$(d_{qm})_{\bar{p}}$ p moment average of the qth moment distribution, Eq. 4.36
d_s Stokes diameter, Eq. 3.26
$d_{\bar{s}}$ diameter average surface, Eq. 4.22
d_{sm} surface mean diameter, Eqs. 4.27 and 4.31
d_t tube diameter
$d_{\bar{v}}$ diameter of average volume, Eq. 4.22
d_w wire diameter
d_{50} particle diameter for 50% collection efficiency, Eqs. 5.28 and 19.1
D particle diffusion coefficient, Eqs. 7.1 and 7.7
D_{ba} diffusion coefficient of gas b in air, Eq. 2.35
D_F fractal dimension, Eq. 20.5
D_j impactor jet diameter
D_s sampling probe diameter
D_v diffusion coefficient of vapor in air
D_0 duct diameter
DF deposition fraction, total, Eq. 11.5
DF_{AL} deposition fraction, alveolar, Eq. 11.4
DF_{HA} deposition fraction, head airways, Eq. 11.1
DF_{TB} deposition fraction, tracheobronchial, Eq. 11.3
e charge of an electron; coefficient of restitution, Eq. 6.6; base for natural logarithms
E efficiency; electrical field strength, Eqs. 15.6 and 15.10
E overall filter efficiency, Eqs. 9.1 and 9.2
E_D single-fiber efficiency for diffusion, Eq. 9.27
E_{DR} single-fiber efficiency for diffusion-interception interaction, Eq. 9.28
E_G single-fiber efficiency for settling, Eq. 9.30
E_I impactor efficiency, Eq. 5.27; single-fiber efficiency for impaction, Eq. 9.24
E_L surface field limit, Eq. 15.28
E_q single-fiber efficiency for electrostatic attraction, Eq. 9.32
E_R single-fiber efficiency for interception, Eq. 9.21
E_Σ total single-fiber efficiency, Eqs. 9.14 and 9.33
f fraction; frequency; frequency of light, fraction of sites with colonies, Eq. 19.3
f_{ab} fraction between sizes a and b
$f(d_p)$ frequency function of particle size distribution, Eq. 4.4
f_n fraction of particles having n charges, Eqs. 15.30 and 15.31

F	force
$F(a)$	cumulative frequency at a, Eq. 4.8
$F(x)$	cumulative fraction at x, Eq. 11.12
F_{adh}	force of adhesion, Eqs. 6.1-6.4
F_D	drag force, Eqs. 3.4 and 3.8
F_E	electrical force, Eq. 15.8
F_f	frictional force on a fluid element, Eq. 2.36
F_G	force of gravity, Eq. 3.11
F_I	inertial force on a fluid element, Eq. 2.39
F_n	form component of Stokes drag, Eq. 3.6
F_{th}	thermal force, Eqs. 8.1 and 8.4
F_v	volume fraction of spheres in liquid, Eq. 21.6
F_τ	frictional component of Stokes drag, Eq. 3.7
g	acceleration of gravity
G	gravitational settling parameter, Eq. 9.29; ratio of cloud velocity to particle velocity, Eqs. 17.6 and 17.7
GSD	geometric standard deviation, σ_g, Eq. 4.40
h	height; velocity head, Eq. 2.43
H	height of chamber; thermophoretic coefficient, Eq. 8.5; latent heat of evaporation of a liquid
	Mie intensity parameter for perpendicular component of scattered light, Eqs. 16.23 and 16.24
i_2	Mie intensity parameter for parallel component of scattered light, Eqs. 16.23 and 16.25
I	number of intervals for grouped size data, Eq. 4.14; light intensity, Eq. 16.7
I_0	incident light intensity, Eq. 16.7
$I_1(\theta)$	intensity of scattered light at angle θ, perpendicular polarization, Eq. 16.24
$I_2(\theta)$	intensity of scattered light at angle θ, parallel polarization, Eq. 16.25
IF	inhalable fraction, Eq. 11.7, 11.8
IF_N	inhalable fraction for nose breathing, Eq. 11.9
J	diffusion flux, Eqs. 2.30 and 7.1
k	Boltzmann's constant
k_v	thermal conductivity of a gas or vapor
K	a constant; corrected coagulation coefficient, Eq. 12.13
K_0	uncorrected coagulation coefficient, Eq. 12.9
$\overline{K}$	effective coagulation coefficient for polydisperse aerosols, Eq. 12.17
K_E	electrostatic constant of proportionality (SI units), Eq. 15.1 and Table 15.1
KE	kinetic energy
Kn	Knudsen number = $2\lambda/d_p$
Ku	Kuwabara hydrodynamic factor, Eq. 9.22
K_R	Kelvin ratio, Eq. 13.5
K_{st}	Pressure rise index, Eq. 18.1

$K_{1,2}$ coagulation coefficient of particle size 1 with size 2, Eq. 12.16
L length; length of fluid element, length of chamber, duct, or tube; path length of light beam, Eq. 16.7
L_R limit of resolution, Eq. 20.9
L_V visual range, Eq. 16.35
m mass of molecule; mass of particle; index of refraction, Eq. 16.2
m_r relative index of refraction, Eq. 16.5
M molecular weight; total mass
MMD mass median diameter
n number of molecules per unit volume; number concentration; number of elementary charges
n_A number concentration at A
n_c rate of capture, Eq. 12.20; number of organisms collected, Eq. 19.3
n_i number of particles in the ith group
n_L charge limit, Eqs. 15.28 and 15.29
n_m number of moles
$n(t)$ number of charges at time t, Eqs. 15.24, 15.25, and 15.33
rate of molecular collisions, Eq. 2.24
n_0 initial number concentration; initial number of charges
N number of molecules; total number of particles in sample; particle number concentration
N_a Avogadro's number
NA numerical aperture, Eq. 20.8
N_i ion concentration
$N(t)$ particle number concentration at time t, Eq. 12.12
N_0 particle number concentration at time zero
p pressure; partial pressure
p_A partial pressure of component A, Eq. 13.1
p_d partial pressure of vapor at droplet surface, Eq. 13.5
p_s saturation vapor pressure, Eq. 13.2
p_T total pressure
p_v velocity pressure, Eqs. 2.43 and 2.44
p_∞ partial pressure of vapor away from droplet
P pressure, perimeter
P penetration, overall filter penetration, Eqs. 9.3 and 9.4
Pe Peclet number, Eq. 9.26
PF PM-10 fraction, Eq. 11.19
$P(n)$ probability of n solid spheres in a droplet, Eq. 21.5
q amount of charge; amount of charge on a particle, Eq. 15.2; weighting parameter for moment distributions
q_F filter quality, Eq. 9.12
qMD median of the qth moment distribution, Eq. 4.48
Q flow rate
Q_a absorption efficiency, Eq. 16.10
Q_e extinction efficiency, Eq. 16.8

Q_s	sample flow rate; scattering efficiency, Eq. 16.10
Q_0	duct flow rate
r	radial position
R	gas constant, Eq. 2.1; radius; interception parameter, Eq. 9.20; separation distance of electric charges, Eq. 15.2
Re	Reynolds number, particle or flow, Eq. 2.41
Re_f	fiber Reynolds number, Eq. 9.13
Re_0	initial Reynolds number, Eq. 5.21
RF	respirable fraction, Eq. 11.10
S	stopping distance, Eq. 5.19
S_R	saturation ratio, Eq. 13.3
SMD	surface median diameter
Stk	Stokes number, Eqs. 5.23 and 5.24
Stk_{50}	Stokes number for 50% collection efficiency, Eq. 5.28
t	time; thickness of filter
T	temperature
T_d	temperature at droplet surface
TF	thoracic fraction, Eq. 11.15
T_∞	temperature away from droplet
U	velocity; gas velocity; gas velocity inside filter, Eq. 9.6; gas velocity in sampling probe
$\overline{U}$	average velocity in duct
U_0	face velocity of filter; free-stream velocity
	gas volume
v_d	droplet volume
v_p	particle volume
v_m	volume of a molecule, Eq. 13.9
v_1, v_2	volume of gas or vapor at state 1 or 2
V	velocity of particle; relative velocity between particle and gas
V_c	critical velocity for bounce, Eq. 6.5; cloud velocity, Eq. 17.4
V_{dep}	deposition velocity, Eq. 7.27
V_f	final velocity
VMD	volume median diameter
V_r	gas velocity in the r direction, Eq. 3.41
$V(t)$	particle velocity at time t, Eq. 5.15
V_{th}	thermophoretic velocity, Eqs. 8.2 and 8.6
V_T	tangential velocity, Eq. 3.15
V_{TC}	terminal centrifugal velocity, Eq. 3.14
V_{TE}	terminal electrical velocity, Eq. 15.15
V_{TF}	terminal velocity for constant external force F, Eq. 5.5
V_{TS}	terminal settling velocity, Eqs. 3.13 and 3.21
$\overline{V}_x$	average velocity in the x-direction, Eq. 3.37
V_0	initial velocity; velocity at time zero
V_∞	gas velocity far away from particle or fiber
V_θ	gas velocity in the θ direction, Eq. 3.42
W	width of slot; voltage

	separation distance; distance from wall
$\bar{x}$	average number of spheres per droplet, Eq. 21.6
$\bar{x}_{MMD}$	average number of spheres in an MMD-sized droplet, Eq. 21.7
x_{rms}	rms displacement of particle, Eq. 7.18;
$x(t)$	position of particle at time t, Eq. 5.18
y	vertical distance
z	number of molecular collisions per unit area, Eq. 2.15
Z	electrical mobility, Eq. 15.21
Z_i	ion mobility
α	volume fraction of fibers in a filter, solidity, Eq. 9.7; size parameter for light scattering, Eq. 16.6
α_v	volume shape factor, Eq. 20.2
β	correction factor for coagulation coefficient, Eq. 12.13
	surface tension; fraction captured per unit thickness of filter, Eqs. 9.11 and 9.19
Γ	velocity gradient
δ	diffusion boundary-layer thickness, Eq. 7.30
∂	partial derivative
Δd	diameter interval
Δp	pressure drop, pressure differential, Eqs. 2.47, 2.52, and 9.36
∇T	temperature gradient
	relative permittivity (dielectric constant); threshold of brightness contrast, Eq. 16.34
ϵ_0	permittivity of vacuum, Eq. 15.2
η	viscosity, Eq. 2.26
Θ	angle between flow direction and sampling probe
θ	scattering angle
λ	gas mean free path, Eq. 2.25; wavelength of light; step size, Eq. 20.5
λ_p	particle mean free path, Eq. 7.11
	deposition parameter for diffusion loss in tubes, Eqs. 7.28 and 7.33
ρ	density of gas; density of particle
ρ_b	density of bulk material
ρ_c	density of cloud, Eq. 17.2
ρ_g	density of gas
ρ_L	density of liquid
ρ_p	density of particle
ρ_0	standard density, 1000 kg/m^3 [1.0 g/cm^3]
σ	standard deviation, Eq. 4.38
σ_a	absorption coefficient, Eq. 16.11
σ_e	extinction coefficient, Eq. 16.7
σ_g	geometric standard deviation, GSD, Eq. 4.40
σ_s	scattering coefficient, Eq. 16.11
	relaxation time, Eq. 5.3
φ	bend angle, Eq. 10.17; Fuchs-effect correction factor, Eq. 13.16
χ	dynamic shape factor, Eq. 3.23
ω	angular frequency, rotational velocity

1 Introduction

The microscopic particles that float in the air are of many kinds: resuspended soil particles, smoke from power generation, photochemically formed particles, salt particles formed from ocean spray, and atmospheric clouds of water droplets or ice particles. They vary greatly in their ability to affect not only visibility and climate, but also our health and quality of life. These airborne particles are all examples of *aerosols.* An aerosol is defined in its simplest form as a collection of solid or liquid particles suspended in a gas. Aerosols are two-phase systems, consisting of the particles *and* the gas in which they are suspended. They include a wide range of phenomena such as dust, fume, smoke, mist, fog, haze, clouds, and smog. The word *aerosol* was coined about 1920 as an analog to the term *hydrosol,* a stable liquid suspension of solid particles. Aerosols are also referred to as suspended particulate matter, aerocolloidal systems, and disperse systems. Although the word *aerosol* is popularly used to refer to pressurized spray-can products, it is the universally accepted scientific term for particulate suspensions in a gaseous medium and is used in that sense in this book.

Aerosols are but one of the several types of particulate suspensions listed in Table 1.1. All are two-component systems having special properties that depend on size of the particles and their concentration in the suspending medium. All have varying degrees of stability that also depend on particle size and concentration.

An understanding of the properties of aerosols is of great practical importance. It enables us to comprehend the process of cloud formation in the atmosphere, a key link in the hydrological cycle. Aerosol properties influence the production, transport, and ultimate fate of atmospheric particulate pollutants. Measurement and control of particulate pollutants in the occupational and general environments require the application of this knowledge. Aerosol technology has commercial application in the manufacture of spray-dried products, fiber optics, and carbon black; the production of pigments; and the application of pesticides. Because the toxicity of inhaled particles depends on their physical as well as their chemical properties, an understanding of the properties of aerosols is required to evaluate airborne particulate hazards. The same knowledge is used in the administration of therapeutic aerosols for the treatment of respiratory and other diseases.

Aerosol technology is the study of the properties, behavior, and physical principles of aerosols and the application of this knowledge to their measurement and control. The particulate phase of an aerosol represents only a very small fraction of its total mass and volume, less than 0.0001%. Bulk properties of aerosols, such as viscosity and density, differ imperceptibly from those of pure air. Consequently, to study the properties of aerosols, one must adopt a *microscopic point of view.* This

TABLE 1.1 Types of Particulate Suspensions

Suspending Medium	Type of Suspended Particles		
	Gas	Liquid	Solid
Gas	—	Fog, mist, spray	Fume, dust
Liquid	Foam	Emulsion	Colloid, suspension, slurry
Solid	Sponge	Gel	Alloy

reduces the problem of understanding the complex properties of aerosols to that of understanding the properties of individual particles. The microscopic approach considers one particle at a time and deals with questions about the forces on that particle, its motion, and its interaction with the suspending gas, with electromagnetic radiation, and with other particles.

At the beginning of the 20th century, the study of aerosols was at the forefront of physical science because aerosols represented the smallest observable division of matter. Aerosol science contributed to the early understanding of Brownian motion and diffusion, Millikan's measurement of the charge on the electron, and Wilson's cloud chamber experiments for the study of ionizing radiation. This classical period of aerosol science research continued through the first half of the century, concluding with the publication of *The Mechanics of Aerosols* by Fuchs in 1955. Following World War II, and particularly during the 1970s and 1980s, aerosol technology grew in importance because of an increased environmental awareness and a concern for the health effects arising from air pollution in community and occupational environments. The field expanded rapidly in the 1980s to include the use of aerosols in high-technology production processes and a concern for aerosol contamination in the semiconductor industry (clean technology). The decade of the1990s has seen increased research on the properties of ultrafine particles (<0.1 μm) and on the effect of aerosols on global climate. Aerosol technology has become an important tool in understanding the effect we have on our environment and the impact of that environment on us.

Any subject that touches upon such diverse phenomena as sunsets, silicosis, rain, cascade impactors, global climate change, cross pollination, electrostatic precipitation, and rainbows is not a simple one. Aerosol technology draws on physics, chemistry, physical chemistry, and engineering. It uses some tools, concepts, and terminology of powder technology. It is used in the fields of occupational hygiene, air pollution control, inhalation toxicology, atmospheric physics and chemistry, and radiological health.

A dual system of units is used in this book, with the primary system being the the International System of Units (SI units, or meter-kilogram-second units). Because of a tradition of using cgs (centimeter-gram-second) units in this field, especially in the United States, cgs units are included in square brackets, and some equations and most examples are presented both ways.

Figures 1.1–1.5 show sources of aerosols paired with microscope photographs of the particles produced. They illustrate the range of aerosol-producing activities and the complex nature of the resulting particles.

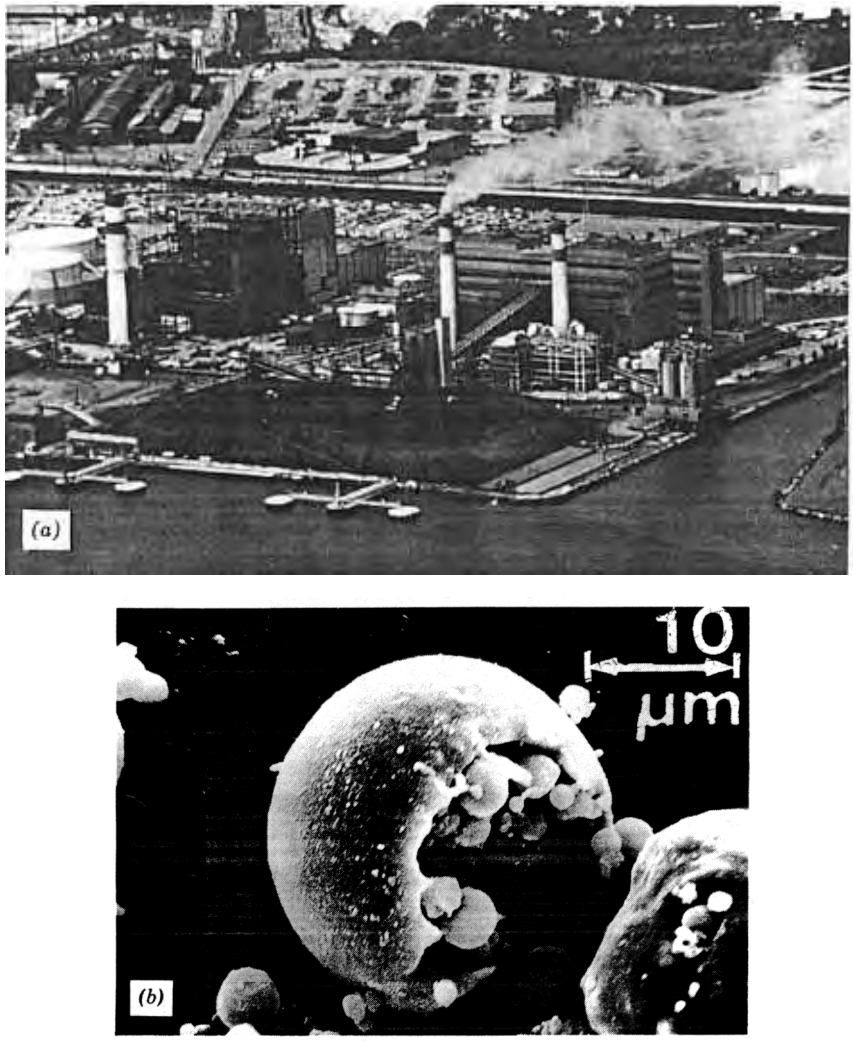

FIGURE 1.1 (*a*) Coal-burning power plant. (*b*) Scanning electron microscope (SEM) photograph of coal fly ash particles.

1.1 DEFINITIONS

Aerosols can be subdivided according to the physical form of the particles and their method of generation. There is no strict scientific classification of aerosols. The following definitions correspond roughly to common usage and are precise enough for most scientific description.

Aerosol A suspension of solid or liquid particles in a gas. Aerosols are usually stable for at least a few seconds and in some cases may last a year or more. The

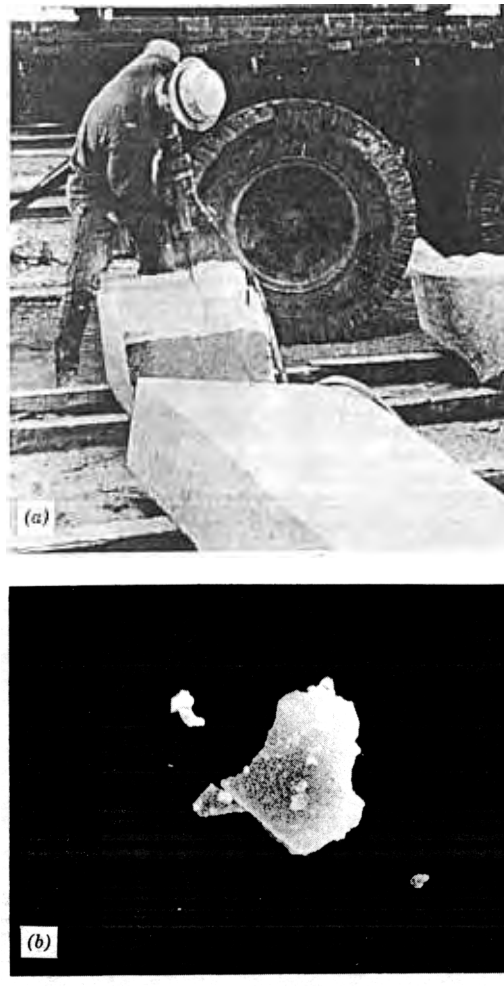

FIGURE 1.2 (*a*) Granite cutting. (*b*) SEM photograph of quartz particles. Magnification 2650×.

term *aerosol* includes both the particles and the suspending gas, which is usually air. Particle size ranges from about 0.002 to more than 100 μm.

Bioaerosol An aerosol of biological origin. Bioaerosols include viruses, viable organisms, such as bacteria and fungi, and products of organisms, such as fungal spores and pollen.

Cloud A visible aerosol with defined boundaries.

Dust A solid-particle aerosol formed by mechanical disintegration of a parent material, such as by crushing or grinding. Particles range in size from submicrometer to more than 100 μm and are usually irregular.

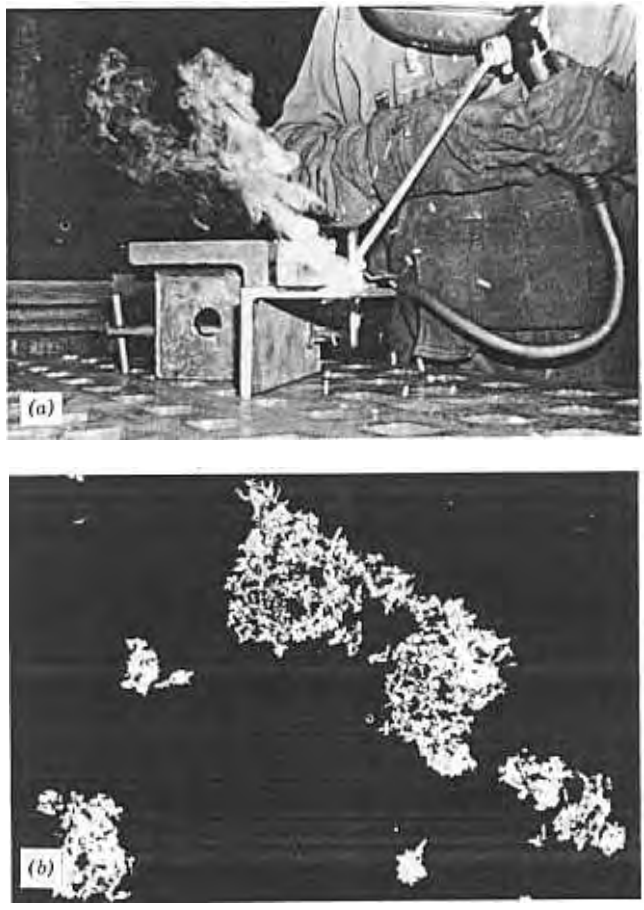

FIGURE 1.3 (*a*) Arc welding. (*b*) SEM photograph of iron-oxide particles. Magnification 2300×.

Fume *A* solid-particle aerosol produced by the condensation of vapors or gaseous combustion products. These submicrometer particles are often clusters or chains of primary particles. The latter are usually less than 0.05 μm. Note that this definition differs from the popular use of the term to refer to any noxious contaminant in the atmosphere.

Haze An atmospheric aerosol that affects visibility.

Mist and Fog Liquid-particle aerosols formed by condensation or atomization. Particles are spherical with sizes ranging from submicrometer to about 200 μm.

Smog 1. A general term for visible atmospheric pollution in certain areas. The term was originally derived from the words *smoke* and *fog*. 2. *Photochemical smog* is a more precise term referring to an aerosol formed in the atmosphere by the action of sunlight on hydrocarbons and oxides of nitrogen. Particles are generally less than 1 or 2 μm.

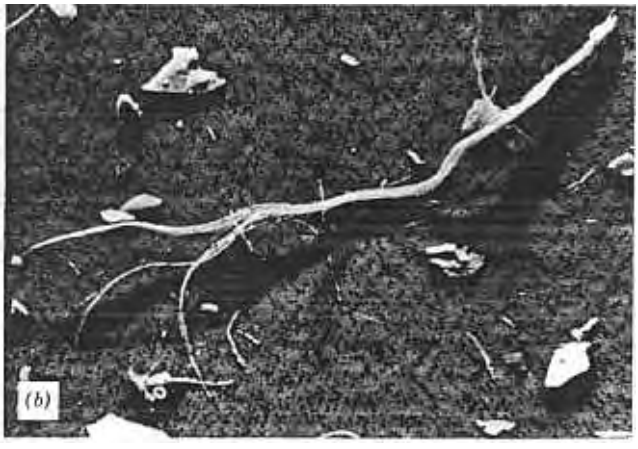

FIGURE 1.4 (*a*) Removal of asbestos pipe covering. (*b*) SEM photograph of asbestos fibers. Magnification 1250×.

Smoke A visible aerosol resulting from incomplete combustion. Particles may be solid or liquid, are usually less than 1 μm in diameter, and may be agglomerated like fume particles.

Spray A droplet aerosol formed by the mechanical breakup of a liquid. Particles are larger than a few micrometers.

In this book the preceding distinctions are usually not necessary, and the general term *aerosol* is used. Liquid particles are referred to as *droplets*. The term *par-*

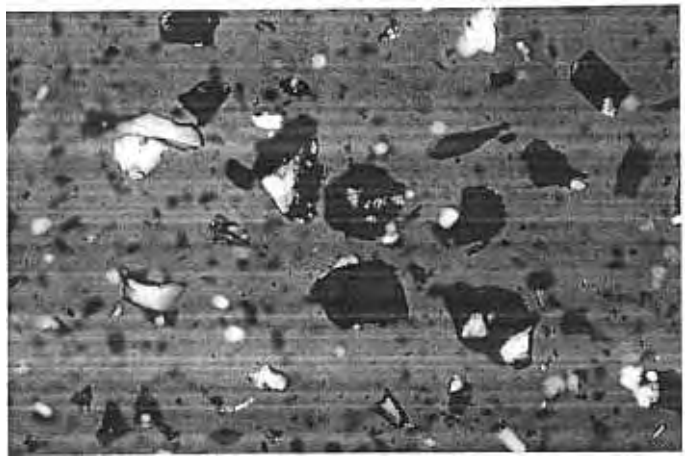

FIGURE 1.5 (a) Volcanic eruption of Mount St. Helens, May 1980. (b) Optical microscope photograph of volcanic ash. Magnification 125×. USGS photograph by Austin Post. Reprinted from *Mount St. Helens: Five Years Later*. Courtesy of Eastern Washington University Press and W. C. McCrone and J. G. Delly, *The Particle Atlas*. Reprinted by permission from McCrone Research Institute.

ticulate matter refers to either solid particles or liquid droplets. A *primary aerosol* has particles that are introduced directly into the atmosphere, whereas a *secondary aerosol* has particles that are formed in the atmosphere by chemical reactions of gaseous components (gas-to-particle conversion). A *homogenous aerosol* is an aerosol in which all particles are chemically identical. *Monodisperse aerosols* have particles that are all the same size and can be produced in the laboratory for use as test aerosols. Most aerosols are *polydisperse*, with a wide range of particle sizes, and statistical measures should be used to characterize their particle size.

In this text, *standard conditions* are defined as a temperature of 293 K [20°C] and an atmospheric pressure of 101 kPa (1Pa = $1N/m^2$) [760 mm Hg].

1.2 PARTICLE SIZE, SHAPE, AND DENSITY

Particle size is the most important parameter for characterizing the behavior of aerosols. All properties of aerosols depend on particle size, some very strongly. Furthermore, most aerosols cover a wide range of sizes; a hundredfold range between the smallest and largest particles of an aerosol is common. Not only do aerosol properties depend on particle size, but the nature of the laws governing these properties may change with particle size. This emphasizes the need to adopt a microscopic approach and characterize properties on an individual particle basis. Average properties can then be estimated by integrating over the size distribution. An appreciation of how aerosol properties vary with particle size is fundamental to an understanding of their properties.

The "yardstick" for particle size is the micrometer (μm) or its older equivalent, the micron (μ), which is 10^{-6} m, 10^{-4} cm, or 10^{-3} mm. The micron is no longer acceptable as an SI unit. Particle size can refer to particle radius, but in this book it refers to particle diameter. For consistency it is expressed in micrometers for all particle sizes, even though nm is more appropriate for particles less than 0.1 μm. Particle diameter is given the symbol d or, where confusion with other symbols might arise, the symbol d_p. It is customary to refer to particle size in micrometers, but calculations require converting micrometers to meters (SI units) by multiplying by 10^{-6} or to centimeters (cgs units) by multiplying by 10^{-4}.

Figure 1.6 shows size ranges for aerosols and other phenomena. A major dividing line is 1 μm, which marks the upper limit of the submicrometer range (less than 1.0 μm) and the lower limit of the micrometer size range (1–10 nm). Figure 1.6 covers a size range of 10^7, from gas molecules to millimeter-sized particles. The particle sizes of the aerosols shown in the figure range from 0.01 to 100 μm, the size range addressed in this book. In general, dusts, ground material, and pollen are in the micrometer range or larger, and fumes and smokes are submicrometer. The smallest aerosol particles approach the size of large gas molecules and have many of their properties. Ultrafine particles cover the range from large gas molecules to about 100 nm (0.001 to 0.1 μm). Particles less than 50 μm are called nanometer particles or nanoparticles. Particles greater than 10 μm have limited stability in the atmosphere, but still can be an important source of occupational exposure because

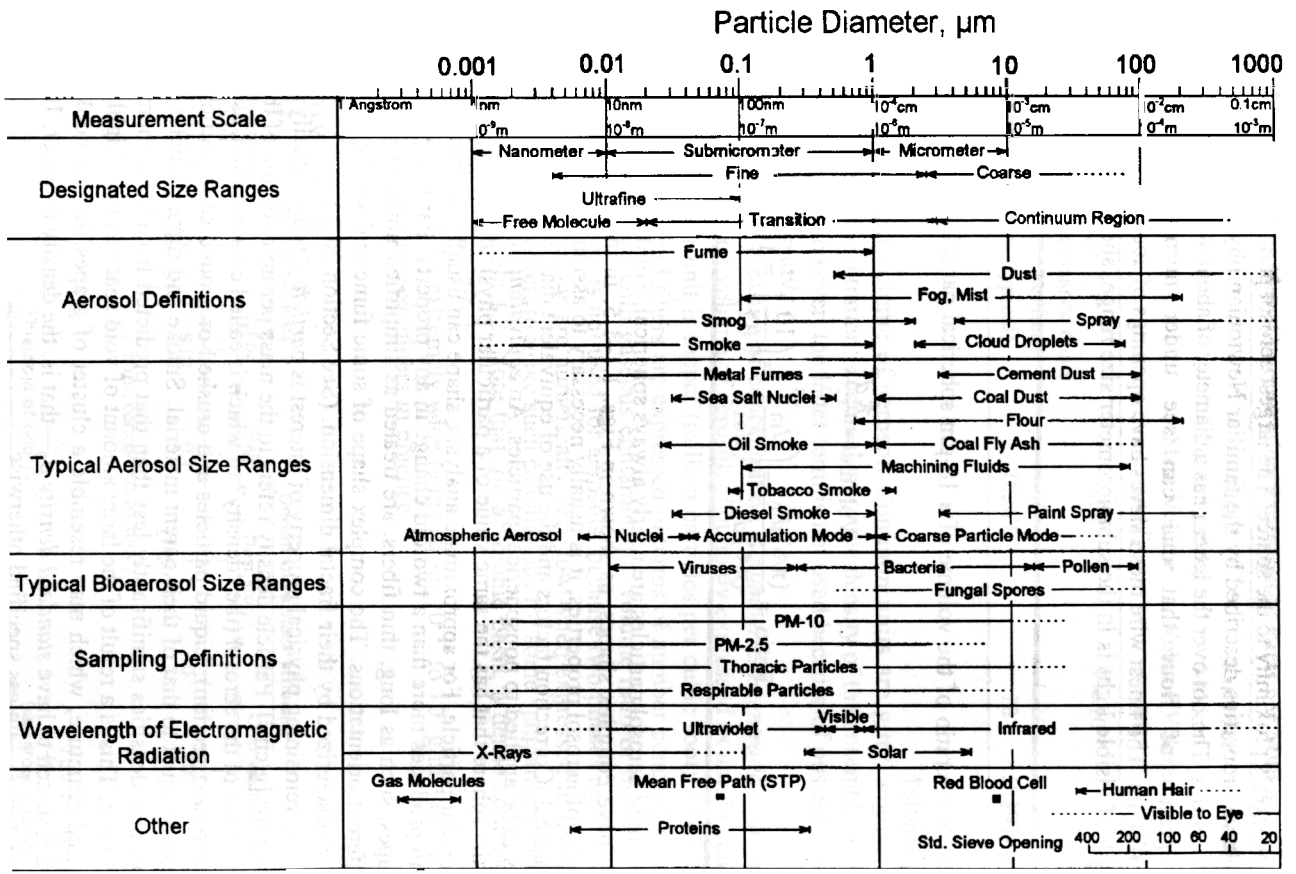

FIGURE 1.6 Particle size ranges and definitions for aerosols.

of a worker's proximity to the source. The largest aerosol particles are visible grains that have properties described by the familiar Newtonian physics of baseballs and automobiles. The dot over the letter *i* has a diameter of about 400 μm, and the smallest grains of flour that one can see under normal conditions are 50–100 μm. The finest wire mesh sieves have openings of about 20 μm. The wavelength of visible light is in the submicrometer size range, about 0.5 μm.

EXAMPLE

What is the ratio of the volume of a 10-μm spherical particle to that of a 0. ·μm particle?

$$\text{Volume} = \frac{\quad}{6}$$

$$\text{Ratio} = \frac{(\pi/6)\, d_{10}^3}{(\pi/6)\, d_{0.1}^3} = \left(\frac{d_{10}}{d_{0.1}}\right)^3 = \left(\frac{10}{0.1}\right)^3 = 10^6$$

Liquid aerosol particles are nearly always spherical. Solid aerosol particles usually have complex shapes, as shown in Figs. 1.1–1.5. In the development of the theory of aerosol properties, it is usually necessary to assume that the particles are spherical. Correction factors and the use of equivalent diameters enable these theories to be applied to nonspherical particles. An *equivalent diameter* is the diameter of the sphere that has the same value of a particular physical property as that of an irregular particle. For approximate analysis, shape can usually be ignored, as it seldom produces more than a twofold change in any property. Particles with extreme shapes, such as long, thin fibers, are treated as simplified nonspherical shapes in different orientations. The complex shape of some fume and smoke particles can be characterized by their fractal dimension. (See Section 20.2.)

The remaining physical property of interest is *particle density,* usually expressed in kg/m^3 [g/cm^3]. Particle density refers to the mass per unit volume of the particle itself, not of the aerosol (the "density" of which is called concentration, as described in the next section). Liquid particles and crushed or ground solid particles have a density equal to that of their parent material. Smoke and fume particles may have apparent densities significantly less than that predicted from their chemical composition. This is a result of the large amount of void space in their highly agglomerated structure, which may resemble a cluster of grapes. In this book particles are assumed to have *standard density* ρ_0—that is, the density of water, 1000 kg/m^3 [1.0 g/cm^3]—unless specified otherwise.

1.3 AEROSOL CONCENTRATION

The most commonly measured aerosol property, and the most important one for health and environmental effects, is the *mass concentration,* the mass of particu-

TABLE 1.2 Examples of Mass Concentration Expressed in Parts per Million[a]

	Mass Concentration, Mass/Volume (mg/m^3)	Parts per Million, Volume/Volume (ppm)	Parts per Million, Mass/Mass (ppm)
U.S. PM-10, annual average	0.05		0.04
Threshold limit value for nuisance dusts (Particulates not otherwise classified)	10	0.01	8
Uncontrolled stack effluent (typical)	10,000	10	8,000

[a]Standard-density spheres.

late matter in a unit volume of aerosol. Common units are g/m^3, mg/m^3, and $\mu g/m^3$. The mass concentration is equivalent to the density of the ensemble of aerosol particles in air; however, the latter term is not used because of possible confusion with particle density.

Another common measure of concentration is *number concentration,* the number of particles per unit volume of aerosol, commonly expressed as number/cm^3 or number/m^3. An older unit is mppcf (million particles per cubic foot). Concentrations of bioaerosols and fibers are expressed in terms of number concentration.

Unlike the situation with gaseous contaminants, volume ratio or mass ratio in parts per million (ppm) is not used for aerosols, because two phases are involved and aerosol concentrations are numerically very low when expressed in this way. It is informative, however, to make such calculations for some standard concentrations, as shown in Table 1.2. Note that, on a volume basis, a dense combustion plume is 99.999% pure air.

Figure 1.7 shows the extremely wide range (from 10^{-13} to 10^3 g/m^3) of aerosol concentrations that one encounters in practice.

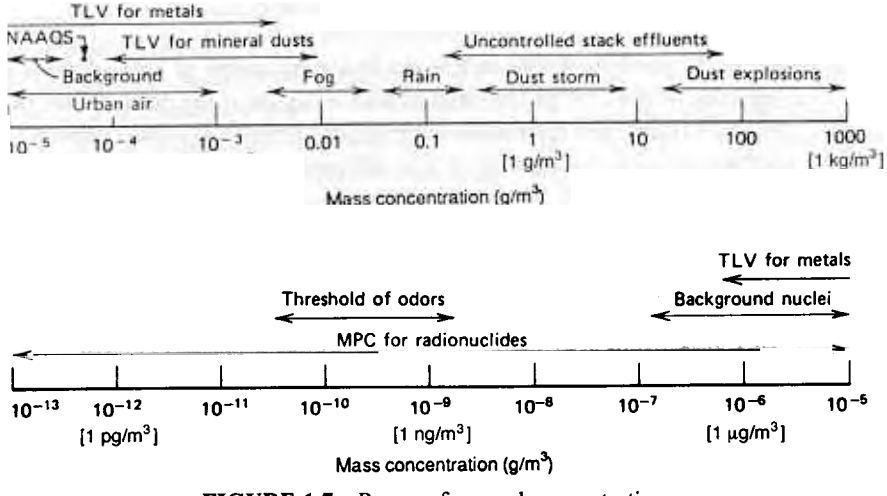

FIGURE 1.7 Range of aerosol concentration.

If you have not already done so, now is a good time to read the preface, which contains important information about this book and how to use it.

PROBLEMS

1.1 How many 1.0-μm-diameter particles are required per cubic centimeter of aerosol for the mass concentration to be 10 mg/m^3? Assume that the particle density is 1000 kg/m^3 [1 g/cm^3].
ANSWER: 19,100/cm^3.

1.2 In smoking one nonfilter cigarette, a person inhales 350 mL of aerosol containing 20 mg of tobacco smoke particles. If these particles are standard-density spheres 0.4 μm in diameter, how many particles does the smoker inhale from one cigarette? What is the mass concentration of the smoke? Make a ratio comparison of this smoke concentration to the U.S. PM-10 standard (annual average) of 50 μg/m^3.
ANSWER: 6.0×10^{11}, 0.057 kg/m^3 [57 g/m^3], 1.1×10^6.

1.3 How many molecules are in a 0.l-μm diameter water droplet?
ANSWER: 1.8×10^7.

1.4 By what factor does the total surface area of a 5-cm-diameter sphere of coal increase on being dispersed into 0.l-μm-diameter spheres?
ANSWER: 5×10^5.

1.5 A person inhales approximately 20 mg of tobacco smoke particles from one cigarette. If smoke particles are standard-density spheres 0.4 μm in diameter, what is the surface area of this amount of smoke?
ANSWER: 0.30 m^2 [3000 cm^2].

1.6 How many particles would be present in a cubic meter of aerosol at the concentration of the U.S. PM-10 standard of 50 μg/m^3 if the particles are (a) 0.1 μm, (b) 1.0 μm, and (c) 10 μm in diameter? Assume standard density.
ANSWER: (a) 9.5×10^{10}, (b) 9.5×10^7, (c) 9.5×10^4.

1.7 If aerosol particles were considered to be extremely large gas molecules, what would be the gram molecular weight of a "gas" of 1.0-μm particles having a density of 1000 kg/m^3?
ANSWER: 3.2×10^{11} g/mole.

1.8 Derive an expression for the surface area per kilogram of material as a function of particle size. Assume that the material is divided into spheres, each

having a diameter d and a density $\rho = 1000$ kg/m^3 [1.0 g/cm^3]. What is the surface area of 1 g of 0.1-μm-diameter particles?
ANSWER: 60 m^2.

1.9 Determine the ratio of the surface area of a sphere to that of a fiber with the same volume. Assume that the fiber is a cylinder with a diameter equal to 20% of the diameter of the sphere. Assume that the sphere and the fiber have standard density.
ANSWER: 0.3.

REFERENCES

Listed below are some general references on aerosol science and technology. A comprehensive list of books and journals is given in *Aerosol Science and Technology*, **14**, 1–4 (1990).

Cadle, R. D., *The Measurement of Airborne Particles,* Wiley, New York, 1975. (Emphasizes microscopic measurement.)

Clift, R., Grace, J. R., and Weber, M. E., *Bubbles, Drops, and Particles*, Academic Press, New York, 1978. (Reference textbook on fluid dynamics, heat transfer, and mass transfer of single bubbles, drops, and particles.)

Davies, C. N. (Ed.), *Aerosol Science,* Academic Press, New York, 1966. (Thorough coverage on selected topics.)

Friedlander, S. K., *Smoke, Dust and Haze,* Wiley, New York, 1977. (Good coverage; oriented toward air pollution.)

Fuchs, N. A., *The Mechanics of Aerosols,* Pergamon, Oxford, UK., 1964. (This outstanding classic has been republished in paperback by Dover Publications, New York, 1989).

Hidy, G. M., and Brock, J. R., *The Dynamics of Aerocolloidal Systems,* Pergamon Press, New York, 1971. (A mathematical approach to the theory of aerosol science.)

Hinds, W. C., *Aerosol Technology: Properties, Behavior and Measurements of Airborne Particles*, Wiley, New York, 1982. (The predecessor to this edition.)

Mercer, T. T., *Aerosol Technology in Hazard Evaluation,* Academic Press, New York, 1973. (Good coverage; oriented toward occupational hygiene.)

Reist, P. C., *Introduction to Aerosol Science*, McGraw-Hill, New York, 1993. (An introductory textbook on aerosol science.)

Shaw, D. T. (Ed.), *Fundamentals of Aerosol Science,* Wiley, New York, 1978. (Detailed coverage of selected topics.)

Vincent, J. H., *Aerosol Science for Industrial Hygienists*, Pergamon, Oxford, UK., 1995. (A textbook on the application of aerosol science and technology to the field of occupational hygiene.)

Vincent, J. H., *Aerosol Sampling: Science and Practice*, Wiley, New York, 1989. (Comprehensive coverage of aerosol sampling, especially with blunt samplers.)

Willeke, K., and Baron, P., *Aerosol Measurement: Principles, Techniques, and Applications*, Van Nostrand Reinhold, New York, 1993. (Comprehensive coverage of aerosol measurement.)

Williams, M. M. R., and Loyalka, S. K., *Aerosol Science: Theory and Practice*, Pergamon, Oxford, 1991. (Strong theoretical coverage.)

Two international journals are devoted to aerosol science and technology:

Journal of Aerosol Science, Pergamon, Elsevier, Exeter, U.K.

Aerosol Science and Technology, Elsevier, New York.

4 Particle Size Statistics

The size of the particles of a monodisperse aerosol is completely defined by a single parameter, the particle diameter. Most aerosols, however, are polydisperse and may have particle sizes that range over two or more orders of magnitude. Because of this wide size range and the fact that the physical properties of aerosols are strongly dependent on particle size, it is necessary to characterize these size distributions by statistical means. For the purposes of this chapter, we neglect the effect of particle shape and consider only spherical particles.

We begin by characterizing size distributions in a general way without specifying the type or shape of the distribution used. Later we apply these concepts to the most common aerosol size distribution, the lognormal distribution.

4.1 PROPERTIES OF SIZE DISTRIBUTIONS

In this section, we characterize size distributions and their properties by using examples based on a specific set of particle size data. The result of a careful size analysis might be a list of 1000 particle sizes. In some situations, keeping the data in this form may be desirable—for example, if the list is stored in a computer. In most situations, however, we would like to have a picture of how the particles are distributed among the various sizes and to be able to calculate several different kinds of statistics that describe the properties of the aerosol. For that purpose, a list of 1000 numbers is an awkward format, so it is necessary to resort to descriptive statistics to summarize the information.

The first step in such a summarization is to divide the entire size range into a series of successive particle size intervals and determine the number of particles (the count) in each interval. The intervals must be contiguous and cover the entire size range, so that no particles are left out. If there are 10 size intervals, our list of 1000 numbers is reduced to 20 numbers, the lower (or upper) size limits and the count for each interval, as shown in Table 4.1. The upper size limit of each interval coincides with the lower limit of the next-higher interval. If a particle size falls exactly on the interval limit, it is grouped in the higher interval. These grouped data are much easier to deal with and give the first glimpse of the shape of the size distribution.

One graphical representation of grouped data is the histogram, shown in Fig. 4.1, where the width of each rectangle represents the size interval and the height represents the number of particles in the interval. Unfortunately, the figure gives a dis-

TABLE 4.1 Example of Grouped Data

Size Range[a] (μm)	Count	Fraction/μm	Percent	Cumulative Percent
0–4	104	0.026	10.4	10.4
4–6	160	0.080	16.0	26.4
6–8	161	0.0805	16.1	42.5
8–9	75	0.075	7.5	50.0
9–10	67	0.067	6.7	56.7
10–14	186	0.0465	18.6	75.3
14–16	61	0.0305	6.1	81.4
16–20	79	0.0197	7.9	89.3
20–35	90	0.0060	9.0	98.3
35–50	17	0.0011	1.7	100.0
>50	0	0.0	0.0	100.0
Total	1000		100.0	

[a]Intervals are equal to or greater than the lower limit and less than the upper limit.

torted picture of the size distribution because the height of any interval is dependent on the width of that interval. Thus, doubling an interval's width results in roughly twice as many particles falling into that interval and the interval growing to twice its height. To prevent this distortion, the histogram is normalized for interval width by dividing the number of particles in each interval by the width of that interval. As shown in Fig. 4.2, the height of each rectangle now equals the

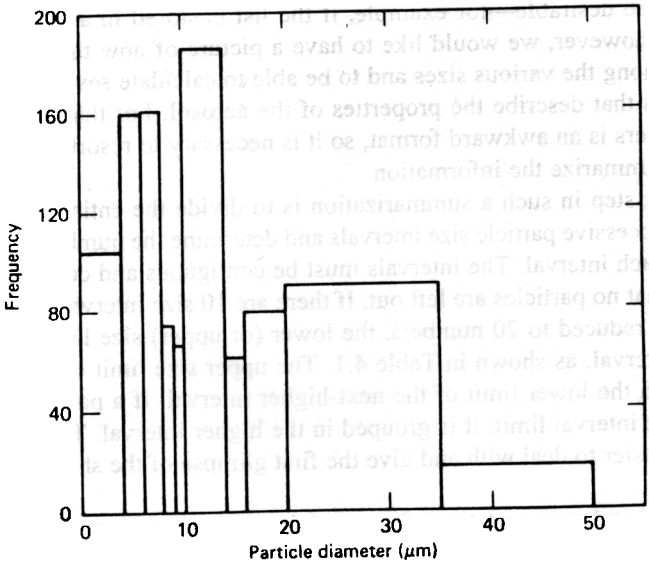

FIGURE 4. Histogram of frequency versus particle size.

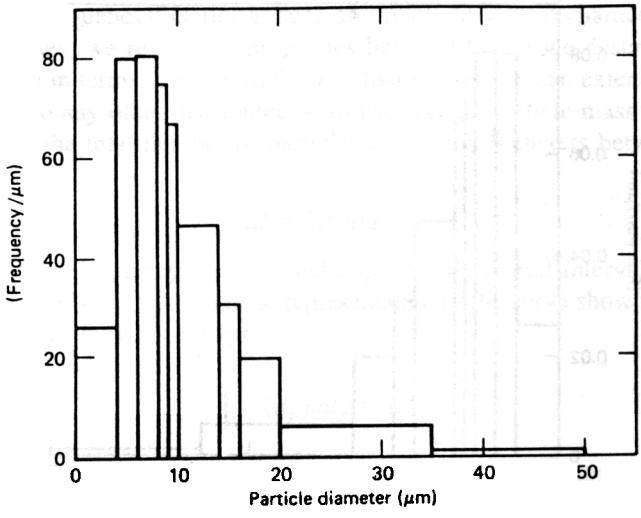

FIGURE 4.2 Frequency/μm versus particle size.

number of particles per unit of size interval (number/μm), and the heights of intervals with different widths are comparable. Furthermore, the area of each rectangle is proportional to the number, or frequency, of particles in that size range. This relationship can be seen from the units of the graph: The height h_i' in number/μm times the width Δd_i in μm gives an area equal to the number of particles in the interval. The total area of all the rectangles is the total number of particles in the sample N.

$$N = \sum (h_i' \Delta d_i)$$

The histogram is usually standardized for sample size by dividing the heights of the rectangles h_i (in frequency/μm) by the total number of particles observed in the sample, giving heights as fraction/μm. The area of each rectangle in the units of the graph, $h_i \Delta d_i$, *is* equal to the fraction f_i of particles in that size range, and the total area is equal to 1.0. This change allows direct comparison of histograms obtained from samples of different size.

$$f_i = \frac{n_i}{N} = (h_i \Delta d_i)$$

$$\Sigma f_i = \sum_i (h_i \Delta d_i) = 1.0$$

As shown in Fig. 4.3, the shape of the distribution is the same as that shown in Fig. 4.2, but the ordinate is now the fraction of the total number of particles per unit of size interval.

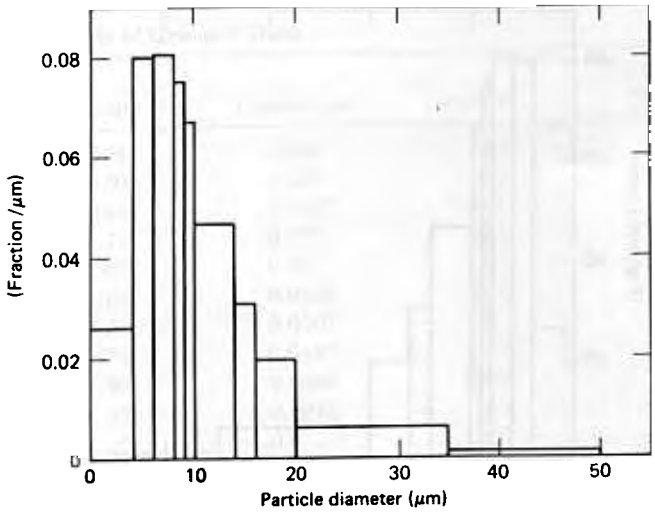

FIGURE 4.3 Fraction/μm versus particle size, count distribution.

Finally, by using many rectangles and drawing a smooth curve through their tops, we obtain the particle size distribution curve that is the graphical representation of the frequency function, or probability density function. Figure 4.4 is an accurate picture of how the particles are distributed among the various sizes; it has the same characteristics as Fig. 4.3, but may be amenable to mathematical interpretation.

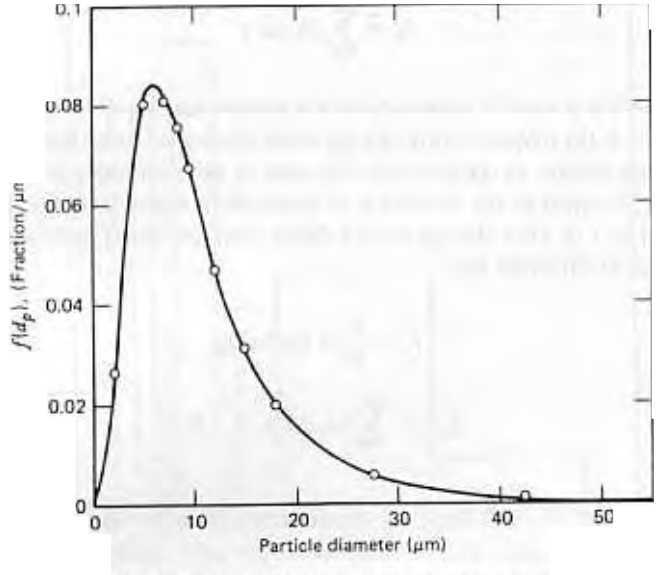

FIGURE 4.4 Frequency distribution curve

Because the frequency function is such an important way of characterizing distributed quantities, we review its properties here. Although we describe the frequency function in terms of the particle size distribution, we can extend the analysis by analogy to any other distributed quantity, such as particle mass or velocity. The fraction of the total number of particles *df* having diameters between d_p and $d_p + dd_p$ is

$$df = f(d_p)dd_p \tag{4.4}$$

where $f(d_p)$ *is* the frequency function and dd_p *is* a differential interval of particle size. This function is the mathematical representation of the curve shown in Fig. 4.4. The area under the curve is always

$$\int_0^\infty f(d_p)dd_p = 1.0$$

which is equivalent to Eq. 4.3. In thinking about frequency functions, always keep in mind which interval is under consideration. The interval may be from zero to infinity, as in Eq. 4.5, or it may be between given sizes a and b, or it may even be the tiny interval dd_p.

The area under the frequency function curve between two sizes a and b equals the fraction of particles whose diameters fall within this interval. Mathematically, this is expressed as

$$f_{ab} = \int_a^b f(d_p)dd_p$$

which is equivalent to Eq. 4.2. Note that the fraction of particles having diameters *exactly* equal to diameter b is zero, because the interval width is zero:

$$f_{bb} = \int_b^b f(d_p)dd_p = 0$$

Size distribution information can also be presented as a cumulative distribution function, $F(d_p)$, which is defined by

$$F(a) = \int_0^a f(d_p)dd_p$$

$F(a)$ gives the fraction of the particles having diameters less than a. Note that the cumulative distribution function has the size interval built into its definition. Figure 4.5 shows the cumulative distribution function for the data given in Table 4.1. The fraction less than a particular size is obtained from the location on the vertical axis associated with the point on the curve directly above that particular size.

An alternative cumulative distribution function can be constructed by considering the number of particles whose size is greater than, instead of less than, a particular size. A plot of this function contains the same information as is in Fig. 4.5, but has the S-shaped curve reversed. In this book we consider only the more common variety, the "less than indicated size" cumulative distribution.

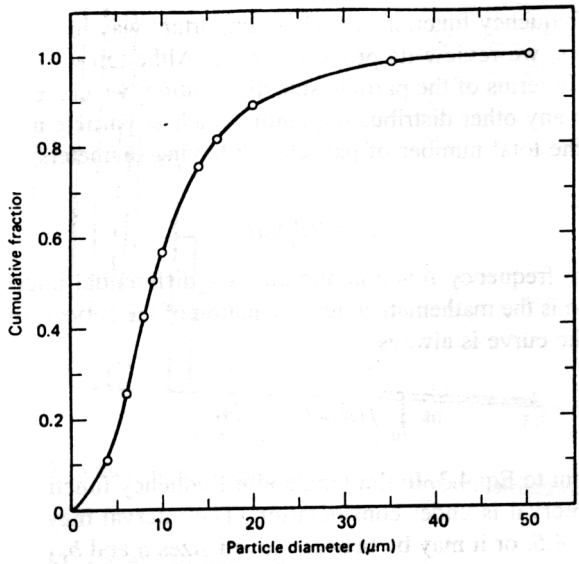

FIGURE 4.5 Cumulative distribution curve.

The cumulative distribution enables one to determine readily quantitative information about the particle size distribution. The fraction less than a given size can be read directly from the graph. The fraction of particles having diameters between sizes a and b (Eq. 4.6) can be determined directly by subtracting the cumulative fraction for size a from that for size b.

$$f_{ab} = F(b) - F(a) \tag{4.9}$$

The slope of the cumulative distribution function at any point is equal to the value of the frequency function at that size.

$$f(d_p) = \frac{\quad}{dd_p} \tag{4.10}$$

As a means of further summarizing the grouped data, a mathematical distribution function is assumed and parameters are calculated that define this function for a particular data set. Most distribution functions require two parameters: one that identifies the location, or center, of the distribution and one that characterizes the width, or spread, of the distribution. These parameters will be discussed more fully in connection with specific distribution functions in subsequent sections.

The most commonly used quantities for defining the location of a distribution are the mean, mode, median, and geometric mean. These and others to be discussed are included in the general term "average." The mean, or arithmetic average, $\bar{d}_p$ is simply the sum of all the particle sizes divided by the number of particles. The mean for listed data, for grouped data, and for a frequency function is given by

$$\bar{d}_p = \frac{\Sigma d}{N} = \frac{\Sigma n_i d_i}{\Sigma n_i} = \int_0^\infty d_p f(d_p) dd_p \tag{4.11}$$

where n_i is the number of particles in group i, having a midpoint of size d_i, and where $N = \Sigma n_i$, i.e., the total number of particles, and the summations are over all intervals. The midpoint size d_i can be the geometric midpoint—the square root of the product of the upper and lower limits of the interval—or the arithmetic midpoint—the mean of the limits. The former is often preferred, but causes a distortion when the first interval has a lower limit of zero. The arithmetic midpoint is used here for simplicity.

The *median* is defined as the diameter for which one-half the total number of particles are smaller and one-half are larger. The median is also the diameter that divides the frequency distribution curve into equal areas, and the diameter corresponding to a cumulative fraction of 0.5. The *mode is* the most frequent size, or the diameter associated with the highest point on the frequency function curve. The mode can be determined by setting the derivative of the frequency function equal to zero and solving for d. For symmetrical distributions such as the normal distribution, the mean, median, and mode will have the same value, which is the diameter of the axis of symmetry. For an asymmetrical or skewed distribution, these quantities will have different values. The median is commonly used with skewed distributions, because extreme values in the tail have less effect on the median than on the mean. Most aerosol size distributions are skewed, with a long tail to the right, as shown in Fig. 4.4. For such a distribution,

$$\text{mode} < \text{median} < \text{mean}$$

The *geometric mean*, d_g, is defined as the Nth root of the product of N values,

$$d_g = (d_1 d_2 d_3 \quad d_N)^{1/N} \tag{4.13}$$

For grouped data with I intervals,

$$d_g = (d_1^{n_1} d_2^{n_2} d_3^{n_3} \quad d_I^{n_I})^{1/N}$$

where $n_1, n_2, n_3, \ldots, n_I$ are the number of particles in intervals 1 through I and $d_1, d_2, d_3, \ldots, d_I$ are the midpoints, or some other characteristic diameter for intervals 1 through I.

The geometric mean can also be expressed in terms of $\ln(d)$ by converting Eq. 4.14 to natural logarithms:

$$\ln d_g = \frac{\Sigma n_i \ln d_i}{N} \tag{4.15}$$

$$d_g = \exp\left(\frac{\Sigma n_i \ln d}{N}\right) \tag{4.16}$$

For a monodisperse aerosol, $\bar{d}_p = d_g$; otherwise, $d_g < \bar{d}_p$. The geometric mean will be discussed further in Section 4.4; it is used widely for characterizing aerosols having lognormal size distributions.

EXAMPLE

Using Fig. 4.4 or 4.5 or Table 4.1, determine the mean, median, mode, and fraction between 5 and 15 μm for the given particle size distribution.

Mean. Use Eq. 4.11 and columns 1 and 2 of Table 4.1. Use midpoint values from column 1 to obtain

$$\bar{d}_p = \frac{\Sigma n_i d_i}{\Sigma n_i} = \left(\frac{1}{1000}\right)[(2 \times 104) + (5 \times 160) + (7 \times 161) + \quad + (42.5 \times 17)]$$

$$\bar{d}_p = \frac{1}{1000}(111' \quad = 11.2\mu m$$

Median. Use Fig. 4.5. The particle size corresponding to the cumulative fraction of 0.5 is approximately 9 μm. For this data set, one can also use Table 4.1. In the table, the upper limit of the interval with a cumulative percent of 0.5 is 9 μm.

Mode. Use Fig. 4.4. The size associated with the highest point on the curve is approximately 6 μm.

Fraction between 5 and 15 μm. Use Fig. 4.5 and Eq. 4.9. From the graph, the fraction less than 15 μm is 0.79 and that less than 5 μm is 0.18. From the equation,

$$f_{5\text{–}15\mu m} = 0.79 - 0.18 = 0.61$$

4.2 MOMENT AVERAGES

The concepts described in Section 4.1 apply equally well to particle size distributions and to other quantities commonly characterized by number statistics—for example, dollars, populations, or the dimensions of machined parts. What makes particle size statistics more complicated is that we frequently measure or need to know some quantity that is proportional to particle size raised to a power (moment), such as surface area, which is proportional to d^2, or mass, which is proportional to d^3. There is no counterpart of this in number statistics, for what is the meaning of $\$^2$ or (people)^3? The need to use moment averages for particle statistics arises because aerosol size is frequently measured indirectly. For example, if you have a basket of apples of different sizes, you could determine the average size by measuring each apple with calipers, summing the results, and dividing by the total number of apples. This procedure is direct measurement. If, however, each apple were

weighed on a balance and the weights summed and divided by their number, the average mass would be obtained.

$$\overline{m} = \frac{\Sigma m_i}{N} \tag{4.17}$$

Note that $\overline{m}$ could, of course, be obtained more easily by weighing the whole basket and counting the apples. In either case, this is the first step of indirect size measurement. Assuming a spherical apple, the average mass is related to the size (diameter) of the apple with average mass $d_{\overline{m}}$ by

$$\overline{m} = \frac{\pi}{6}\rho_p d_{\overline{m}}^3 \tag{4.18}$$

Combining Eqs. 4.17 and 4.18 gives the diameter of average mass for a basket of apples, or, a sample of particles,

$$d_{\overline{m}} = \left(\frac{6}{\rho_p \pi N}\right)^{1/3} = \left(\frac{6}{\rho_p \pi N}\frac{\pi \rho_p \Sigma d^3}{6}\right)^{1/3} = \left(\frac{\Sigma d^3}{N}\right)^{1/3} \tag{4.19}$$

The diameter of average mass (the third-moment average) has a different value from the mean diameter (the first-moment average). Nonetheless, it is a very useful quantity, because it provides the link between the number and the aggregate mass of aerosol particles in a sample and between the number concentration C_N and the mass concentration C_m. The total mass of the particles in a sample, M, is

$$M = N\overline{m} = N\frac{\rho\pi}{6} d_{\overline{m}}^3$$

and

$$C_m = C_N\overline{m} = C_N\frac{\rho\pi}{6} d_{\overline{m}}^3$$

The preceding discussion deals with only one of a whole family of moment averages. The diameter of a particle with average surface area or average settling velocity is defined similarly. The general form for the diameter of an average property proportional to d^p is

$$d_{\overline{p}} = \left(\frac{\Sigma d^p}{N}\right)^{1/p}$$

or, for grouped data,

$$d_{\overline{p}} = \left(\frac{\Sigma n_i d_i^p}{N}\right)^{1/p}$$

These moment averages represent means calculated for different moments (powers of d), converted back to units of diameter. They are moments about zero and should not be confused with moments about the mean, which define variance and skewness. For the same distribution, the higher the moment, the larger the moment average.

$$\bar{d} < d_{\bar{s}} < d_{\bar{m}} \tag{4.23}$$

The second-moment average $d_{\bar{s}}$ is identical to the rms average (square root of the mean of the squares) discussed in Chapter 2. For the lognormal size distribution—the most common aerosol size distribution—there are explicit equations for converting between any of the average diameters discussed in this chapter. These moment averages are based on the count distribution, the fraction of the total particle count in each size category. In the next section we explore other distributions, such as the distribution of mass.

4.3 MOMENT DISTRIBUTIONS

The count, or number, distribution discussed in the preceding sections is only one of a whole family of distributions. Another member is the distribution of mass (the third-moment distribution), or, more correctly, the mass distribution as a function of particle size. While the number distribution gives the fraction of the total number of particles in any size range, the distribution of mass gives the fraction of the total mass of the particles contributed by particles in any size range. A graph of the mass distribution shows how the mass is distributed among the various particle sizes. The distribution of mass and the distribution of count for the same sample of particles have different means, medians, geometric means, graphical representations, and probability density functions. The median of the distribution of mass is called the *mass median diameter* (MMD), to distinguish it from the count median diameter (CMD) discussed in Section 4.2. The latter is the particle size for which half the total *number* of particles are larger and half are smaller. The MMD is defined as the diameter for which half the *mass* is contributed by particles larger than the MMD and half by particles smaller than the MMD. It is the diameter that divides the graphical representation of the distribution of *mass* into two segments of equal area.

A cumulative distribution function similar to Fig. 4.5 can be constructed for the distribution of mass. The vertical axis is changed to represent the fraction of total mass attributable to particles less than the indicated size. Figures 4.6 and 4.7 show the distribution of mass and the cumulative distribution of mass for the particle size data given in Table 4.1 and shown in Figs. 4.1–4.5.

As a simple illustration of different moment distributions, consider an aerosol composed of equal numbers of two particle sizes, one in which 50 particles are 1 μm in diameter and 50 are 10 μm in diameter. While half the number are in each size category, most of the mass is represented by the 10-μm particles. Each 10-μm

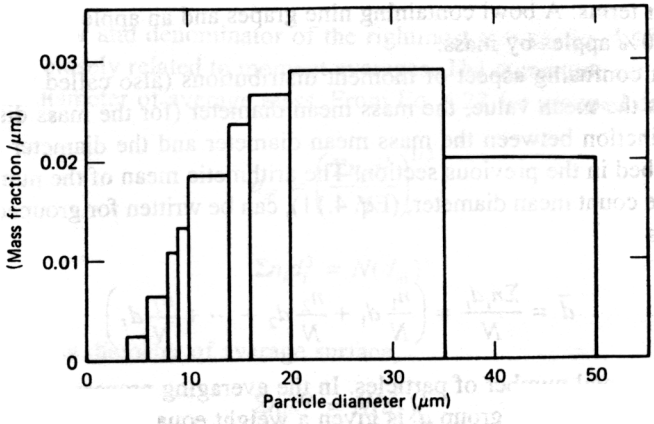

FIGURE 4.6 Mass distribution.

particle has 1000 times the mass of a 1-μm particle. The 10-μm particles contribute 50,000 units of mass to the total mass of the particles, whereas the 1-μm particles contribute only 50 units of mass; thus, the mass is distributed such that 99.9% is in the 10-μm particles and 0.1% in the 1-μm particles. A similar analysis for surface area attributes 99% of the surface area to the 10-μm particles and 1% to the 1-μm particles. The distinction between count and mass distributions can be put in

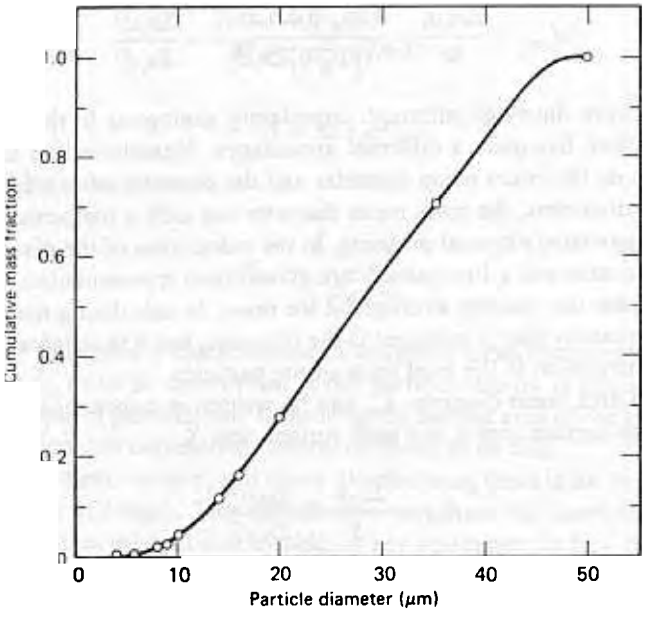

FIGURE 4.7 Cumulative mass distribution.

even simpler terms: A bowl containing nine grapes and an apple is 90% grapes by count, but 90% apples by mass.

The most confusing aspect of moment distributions (also called weighted distributions) is the mean value, the mass mean diameter (for the mass distribution), and the distinction between the mass mean diameter and the diameter of average mass, described in the previous section. The arithmetic mean of the number distribution, or the count mean diameter, (Eq. 4.11), can be written for grouped data with I intervals as

$$\frac{\Sigma n_i d_i}{N} \quad \left(\frac{n_1}{N} d_1 + \frac{n_2}{N} d_2 + \quad + \frac{n_I}{N} d_I\right) \tag{4.24}$$

where N is the total number of particles. In the averaging process, the characteristic diameter for each size group d_i is given a weight equal to n_i/N, or the fraction of the total number of particles in that group.

For the distribution of mass, which describes the fraction of the total mass in the various size ranges, the mass mean diameter can be written in a completely analogous fashion. Let m_i be the mass of all the particles in group i (midpoint diameter d_i) and let M be the total mass for all groups.

$$\text{mass mean diameter} = d_{\text{mm}} = \left(\frac{m_1}{M} d_1 + \frac{m_2}{M} d_2 + \quad + \frac{m_I}{M} d_I\right) \tag{4.25}$$

Equation 4.25 can be rewritten for spherical particles of uniform density.

$$d_{\text{mm}} = \frac{\Sigma m_1 d_i}{M} = \frac{(\pi \rho_p/6)\Sigma n_i d_i^3 d_i}{(\pi \rho_p/6)\Sigma n_i d_i^3} = \frac{\Sigma n_i d_i^4}{\Sigma n_i d_i^3} \tag{4.26}$$

The mass mean diameter, although completely analogous to the mean of the count distribution, has quite a different appearance. Nonetheless, it has units of length (d^1), as do the count mean diameter and the diameter of average mass. As with all mean diameters, the mass mean diameter has only a mathematical definition with no associated physical meaning. In the calculation of the diameter of average mass, a coarse and a fine particle are given equal representation in the averaging process, but the quantity averaged is the mass. In calculating the mass mean diameter, the quantity that is averaged is the diameter, but it is *weighted* according to its mass contribution to the total mass of the particles.

The surface area mean diameter d_{sm} can be written in a form analogous to Eq. 4.26 with group surface area s_i and total surface area S.

$$d_{\text{sm}} = \frac{\Sigma s_1 d_i}{S} = \frac{\Sigma n_i d_i^3}{\Sigma n_i d_i^2} \tag{4.27}$$

This average diameter is also called the *Sauter diameter* or the *mean volume–surface diameter.*

The numerator and denominator of the rightmost side of Eq. 4.27 are moment sums and are closely related to moment averages. The numerator can be written in terms of the diameter of average mass. From Eq. 4.22 for grouped data,

$$d_{\bar{m}} = \left(\frac{\Sigma n_i d_i^3}{N}\right)^{1/3}$$

$$\Sigma n_i d_i^3 = N(d_{\bar{m}})^3$$

Similarly, for the diameter of average surface,

$$\Sigma n_i d_i^2 = N(d_{\bar{s}})^2$$

Substituting into Eq. 4.27 gives

$$d_{\text{sm}} = \frac{N(d_{\bar{m}})^3}{N(d_{\bar{s}})^2} = \frac{(d_{\bar{m}})^3}{(d_{\bar{s}})^2} \tag{4.31}$$

Thus, each weighted mean diameter can be written as the ratio of two moment averages.

Weighted mean diameters can also be expressed in terms of aggregate quantities. If M and S are the total mass and surface area, respectively, of an aerosol sample, then

$$M = \left(\frac{\rho_p \pi}{6}\right)\Sigma n_i d_i^3$$

$$S = \pi \Sigma n_i d_i^2 \tag{4.33}$$

and Eq. 4.27 becomes

$$d_{\text{sm}} = \left(\frac{6}{\rho_p}\right. \tag{4.34}$$

Equation 4.34 illustrates a characteristic of weighted mean diameters: An average particle size (d_{sm}) can be determined if the particle density is known by simply weighing a sample of particles and measuring the surface area of the sample. There are gas adsorption and radioactive coating methods to do this.

In addition to mass, surface, and count distributions, there is the less commonly used distribution of length. This distribution expresses the fraction of the total length, if all particles are laid side by side, in any size range. In fact, there can be a moment distribution for any property that is proportional to a constant power of diameter. The general form for the distribution function giving the fraction of a quantity proportional to d_p^x in an interval between d_p and $d_p + dd_p$ is

$$df_x = f_x(d_p)d_p = \frac{d_p^x f(d_p)}{\int_0^\infty d_p^x f(d_p)dd_p} dd_p$$

There is a set of moment averages for each moment distribution. The general form for the p moment average of the q moment distribution is

$$(d_{qm})_{\bar{p}} = \left(\frac{\Sigma n_i d_i^q d_i^p}{\Sigma n_i d_i^q}\right)^{1/p}$$

When $q = 0$, the weighting is by number; when $p = 1$ and $q = 0$, we have Eq. 4.11, the arithmetic mean; when $p = 1$ and $q = 3$, we have the mass mean diameter, Eq. 4.26, and when $p = 3$ and $q = 0$ we have the diameter of average mass, Eqs. 4.19 and 4.22. The names used here are common, but hardly universal. Some authors use mean mass diameter for the diameter of average mass, but this is easily confused with the mass mean diameter. The latter can best be remembered as the mass (distribution) mean diameter or mass (weighted) mean diameter. One often encounters the terms *CMAD* and *MMAD*, which refer to the count and mass medians of the distributions of count or mass with respect to aerodynamic diameter. Graphs for these distributions are constructed by plotting frequency or fraction versus aerodynamic diameter. The term *AMD* refers to the activity median diameter and is the median of the distribution of radioactivity or toxicological or biological activity with respect to size.

EXAMPLES

As an example of moment averaging, suppose that you have a list of heights for 20 geometrically similar people and you wish to select the person with the average surface area for a heat stress experiment. Surface area is difficult to measure, but height is easy to measure. Assume that surface area is proportional to height squared, h^2, and is related to height by some constant (which we do not need to know). Then the person with the average surface area will have a height given by

$$\left(\frac{\Sigma h^2}{N}\right)^{1/2}$$

which is the square root of the arithmetic average of height squared, or the second-moment average.

Similarly, if we wanted the person with average mass, we could determine that person's height by taking the cube root of the arithmetic average of the heights cubed:

$$\left(\frac{\Sigma h^3}{N}\right)^{1/3}$$

If we desired the total weight to determine whether all 20 people could ride together on an elevator, we need only weigh that person whose height is given by the previous equation (or interpolate between the two nearest people) and multiply his or her weight by 20. The person with the median height will also have the median weight, because the order will not change by cubing heights.

2 An example of a moment distribution is that obtained from an analysis of the grain size of sand by sieving. The sand is passed through a stack of sieves arranged in order of decreasing mesh size. The mass of sand retained on each sieve is determined. From the characteristics of the screens, we can assign a diameter to each mass of sand retained. With these data, we can determine the distribution of mass and calculate the mass mean diameter of the sand particles as follows:

Calculation of Mass Mean Diameter

Sieve Opening (mm)	Midsize of Collected Sand, d_i (mm)	Mass Collected, m_i (g)	Percent of Total Mass (%)	$m_i d_i$ (g·mm)
1.0	1.5	8		12.0
0.50	0.75	34		25.5
0.25	0.375	40		15.0
0.125	0.188	12		2.26
Final Pan	0.062	3		0.19
	Total	97		54.9

$$d_{mm} = \frac{\Sigma m_i d_i}{M} = \frac{54.9}{97} = 0.57 \text{ mm}$$

3 A simple numerical example

n	d	nd	nd^2	nd^3	nd^4
3	1.0	3	3	3	
5	2.0	10	20	40	
2	6.0	12	72	432	
	9.0	25	95	475	

Arithmetic average, or count mean diameter = $\Sigma nd/N = 2.50$

Median = 2.0

Mode = 2.0

Diameter of average surface = $(\Sigma nd^2/N)^{1/2} = (9.5)^{1/2} = 3.08$

Diameter of average volume = $(\Sigma nd^3/N)^{1/3} = (47.5)^{1/3} = 3.62$

Length mean diameter = $\Sigma nd^2/\Sigma nd = 95/25 = 3.80$

Surface mean diameter = $\Sigma nd^3/\Sigma nd^2 = 475/95 = 5.00$

Volume mean diameter = $\Sigma nd^4/\Sigma nd^3 = 2675/475 = 5.63$

Note that the surface mean diameter can also be calculated by Eq. 4.31

$$d_{sm} = (d_{\bar{m}})^3/(d_{\bar{s}})^2 = 3.62^3/3.08^2 = 5.00$$

4.4 THE LOGNORMAL DISTRIBUTION

The preceding sections have focused on the properties of distributions in general without considering any particular type of distribution. In this section, we describe the characteristics and applications of the lognormal distribution for aerosol particle size analysis. As discussed below, the normal distribution, although widely used elsewhere, is not suitable for most aerosol particle size distributions.

The characteristics of other distributions that have been applied to aerosol particle size, such as the Rosin–Rammler, Nukiyama–Tanasawa, power law, exponential, and Khrgian–Mazin distributions are given in the appendix to this chapter. These distributions apply to special situations and find limited application in aerosol science. They (and the lognormal distribution) have been selected empirically to fit the wide range and skewed shape of most aerosol size distributions.

The normal distribution function is rarely used to describe aerosol particle size distributions because most aerosols exhibit a skewed (long tail at large sizes) distribution function. The normal distribution is, of course, symmetrical. It can be applied to monodisperse test aerosols, to certain pollens and spores, and to specially prepared polystyrene latex spheres. The number frequency function is given by

$$df = \frac{1}{\sigma\sqrt{2\pi}} \exp\left(-\frac{(d_p - \bar{d}_p)^2}{2\sigma^2}\right) dd_p \tag{4.37}$$

where $\bar{d}_p$ is the arithmetic mean diameter and σ is the standard deviation, defined for grouped data as

$$\sigma = \left[\frac{\Sigma n_i (d_i - \bar{d}_p)^2}{N -}\right]^{1/2} \tag{4.38}$$

A second problem in applying the normal distribution to any quantity that varies over a wide range, such as aerosol particle size, is that such a wide normal distribution requires a certain fraction of the particles to have negative size, a physical impossibility. This problem combined with the frequently observed skewed shape of the distribution, led to the use of the logarithmic transformation of size data to obtain the lognormal distribution. With the logarithm of particle size (actually, the logarithm of (d_p/d_0), where d_0 is 1 μm) plotted, instead of size, along the horizontal axis, the frequency distribution shows the symmetrical form of the normal distribution. This has been done in Fig. 4.8, using a logarithmic scale and the

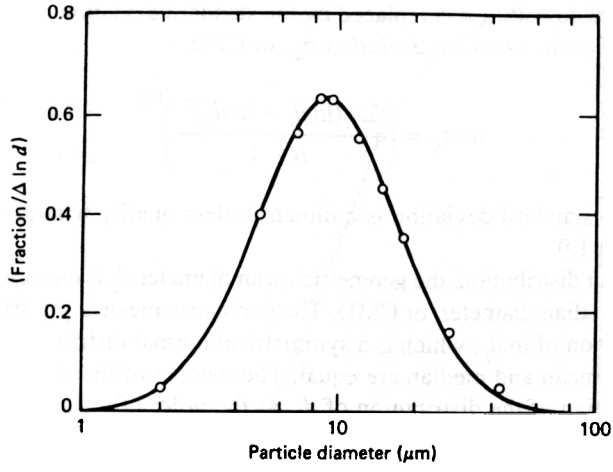

FIGURE 4.8 Frequency distribution curve (logarithmic size scale).

size data given in Table 4.1. Note that the logarithmic scale has no negative values, thus overcoming the problem of negative particle size.

The lognormal distribution has been applied to such diverse distributions as incomes, populations (of both people and bacteria), prices of stocks listed on the New York Stock Exchange, concentrations of environmental contaminants, and particle sizes of aerosols. There is no fundamental theoretical reason why particle size data should approximate the lognormal distribution, but it has been found to apply to most single-source aerosols. (See Appendix 2 at the end of the Chapter.) Mixtures of lognormal distributions will not be lognormal.

The lognormal distribution is most useful in situations where the distributed quantity can have only positive values and covers a wide range of values—that is, where the *ratio* of the largest to the smallest value is greater than about 10. When this range is narrow, the lognormal distribution approximates the normal distribution. The lognormal distribution is used extensively for aerosol size distributions because it fits the observed size distributions reasonably well and its mathematical form is convenient for dealing with the moment distributions and moment averages described in the preceding sections.

Because the logarithm of d_p *is* normally distributed, the lognormal distribution frequency function can be formed by replacing $\bar{d}_p$ and σ in Eq. 4.37 with their logarithmic counterparts. Thus, $\bar{d}_p$ is replaced by the arithmetic mean of ln d, defined by Eq. 4.15 as the geometric mean diameter d_g,

$$\ln d_g = \frac{\Sigma n_i \ln d_i}{N} \tag{4.39}$$

Either the natural logarithm or the logarithm to the base 10 can be used, but the natural logarithm is more common and is used here.

The standard deviation σ is replaced by the standard deviation of the logarithms, called the *geometric standard deviation* σ_g, or GSD.

$$\ln \sigma_g = \left(\frac{\Sigma n_i (\ln d_i - \ln d_g)^2}{N - 1} \right) \tag{4.40}$$

The geometric standard deviation is a dimensionless quality with a value equal to or greater than 1.0.

For the count distribution, the geometric mean diameter d_g is customarily replaced by the count median diameter, or CMD. The geometric mean is the arithmetic mean of the distribution of $\ln d_p$, which is a symmetrical normal distribution, see Fig. 4.8, and hence, its mean and median are equal. The median of the distribution of $\ln d_p$ is also the median of the distribution of d_p, as the order of values does not change in converting to logarithms. Thus, for a lognormal count distribution, d_g = CMD. The frequency function can be expressed as

$$df = \frac{1}{\sqrt{2\pi} \ln \sigma_g} \exp\left(- \frac{(\ln d_p - \ln \text{CMD})^2}{2(\ln \sigma_g)^2} \right) d \ln d_p \tag{4.41}$$

which gives the fraction of the particles having diameters whose logarithms lie between $\ln d_p$ and $\ln d_p + d \ln d_p$. It is more convenient, however, to express the frequency function in terms of the particle size d_p rather than $\ln d_p$. Rewriting Eq. 4.41 in terms of d_p, using the fact that $d \ln d_p = dd_p/d_p$, gives

$$df = \frac{}{\sqrt{2\pi}\, d_p \ln \sigma_g} \exp\left(- \frac{(\ln d_p - \ln \text{CMD})^2}{2(\ln \sigma_g)^2} \right) dd_p \tag{4.42}$$

The cumulative distribution for the lognormal distribution is obtained as described in Section 4.1. The cumulative plot shown in Fig. 4.9 is the same as Fig 4.5, but diameter is plotted on a logarithmic scale. Note that the median size is the same for both figures.

For the normal distribution, 95% of the particles fall within a size range defined by $\bar{d} \pm 2\sigma$. For the lognormal count distribution, the distribution is normal with respect to $\ln d$, so that 95% of the particles fall within a size range defined by

$$\exp(\ln \text{CMD} \pm 2 \ln \sigma_g) \tag{4.43}$$

This range is asymmetrical and goes from CMD/σ_g^2 to $\text{CMD} \times \sigma_g^2$. For $\sigma_g = 2.0$, 95% of the particles have sizes between one-fourth and four times the count median diameter.

All moment distributions of any lognormal distribution will be lognormal and have the same geometric standard deviation. This means that they will have the same shape when they are plotted on a logarithmic scale. The lognormal distribution is the only common distribution that has this property. Figure 4.10 shows the distri-

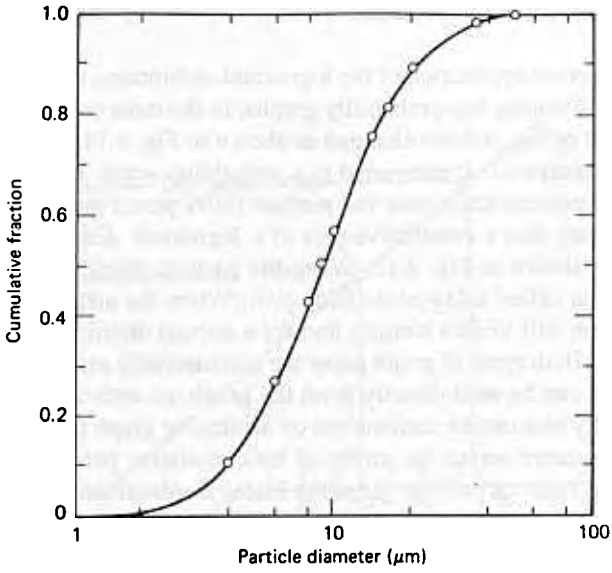

FIGURE 4.9 Cumulative distribution curve (logarithmic size scale).

bution of count and mass plotted on the same logarithmic diameter scale. For the mass distribution, we replace the geometric mean diameter with the mass median diameter MMD, analogous to what we did for the count distribution. The mass distribution has the same shape as the count distribution but is displaced along the size axis by a constant amount equal to MMD/CMD. The ratio MMD/CMD can be calculated knowing only the GSD. This calculation is covered in Section 4.6.

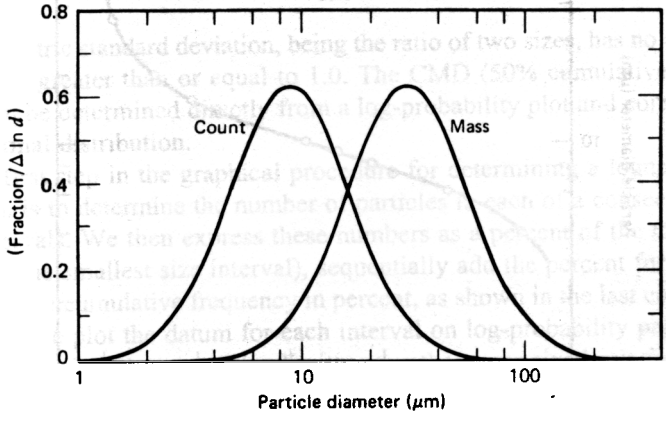

FIGURE 4.10 Count and mass distributions (logarithmic size scale).

4.5 LOG-PROBABILITY GRAPHS

Much of the practical application of the lognormal distribution to particle size analysis is facilitated by using log-probability graphs. In the most common form of these graphs, the axes of Fig. 4.9 are changed as shown in Fig. 4.11, and the cumulative fraction (or percent) scale is converted to a probability scale. The probability scale compresses the percent scale near the median (50% point) and expands the scale near the ends such that a cumulative plot of a lognormal distribution will yield a straight line, as shown in Fig. 4.12. When the particle diameter scale is logarithmic, the graph is called a *log-probability plot.* When the size scale is linear, the cumulative graph will yield a straight line for a normal distribution and is called a *probability plot.* Both types of graph paper are commercially available. In either case the median size can be read directly from the graph, as with any cumulative plot. A log-probability plot can be constructed on arithmetic graph paper by plotting the logarithm of diameter versus the probit of the cumulative percentages. The latter, obtained from a table of probits, gives the linear displacement from the midpoint (50%) in units of standard deviations. The slope of the straight line is related to the geometric standard deviation. A line with a steep slope is associated with a wide distribution, and a line with a shallow slope represents a narrow distribution. A horizontal line in Fig. 4.12 characterizes a monodisperse aerosol—that is, one in which all particles have the same size.

For any *normal* distribution, one standard deviation represents the *difference* between the size associated with a cumulative count of 84.1% and the median size (a cumulative count of 50%) or between the 50% cumulative size and the 15.9% cumulative size.

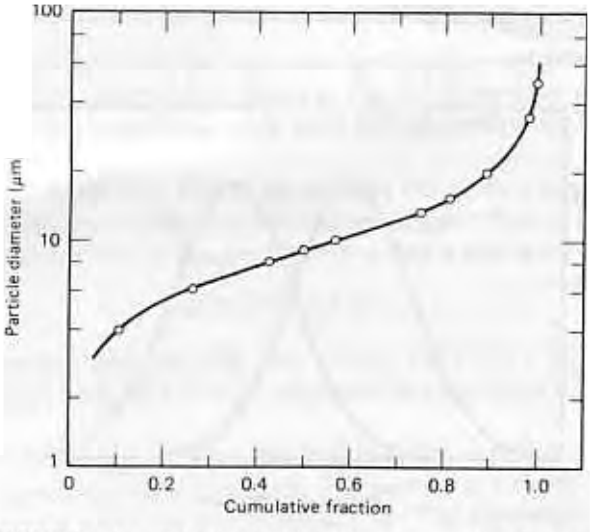

FIGURE 4.11 Particle diameter versus cumulative fraction

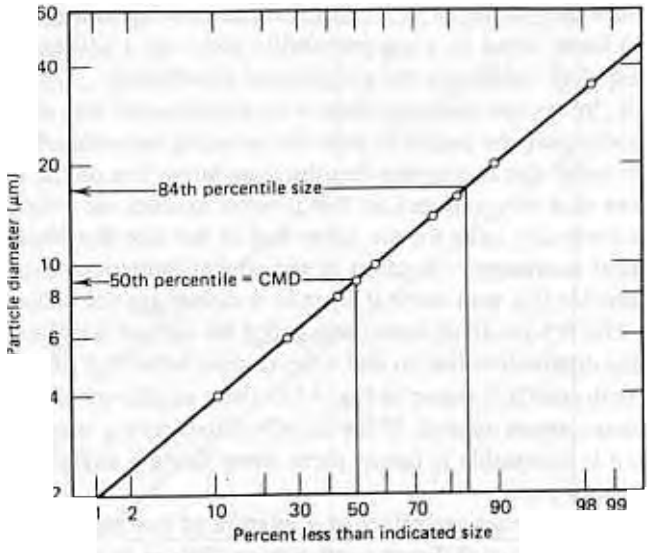

FIGURE 4.12 Log-probability graph

$$\sigma = d_{84\%} - d_{50\%} \tag{4.44}$$

For a lognormal distribution, which is normal with respect to ln d, these differences become ratios

$$\begin{aligned} \ln \sigma_g &= \ln d_{84\%} - \ln d_{50\%} \\ &= \ln(d_{84\%}/d_{50\%}) \end{aligned}$$

$$\text{GSD} = \sigma_g = \frac{d_{84\%}}{d_{50\%}} = \frac{d_{50\%}}{d_{16\%}} = \left(\frac{d_{84\%}}{d_{16\%}}\right)^1$$

The geometric standard deviation, being the ratio of two sizes, has no units and must always be greater than or equal to 1.0. The CMD (50% cumulative size) and the GSD can be determined directly from a log-probability plot and completely define a lognormal distribution.

The first step in the graphical procedure for determining a lognormal size distribution is to determine the number of particles in each of a consecutive series of size intervals. We then express these numbers as a percent of the total and (starting with the smallest size interval), sequentially add the percent for each interval, to obtain the cumulative frequency in percent, as shown in the last column of Table 4.1. Next we plot the datum for each interval on log-probability paper as the percentage less than the upper size limit versus the upper size limit for that interval. If a straight line fits the data, the distribution can be represented by a lognormal distribution and the CMD and GSD can be determined from the 50th percentile size and Eq. 4.46. While there will usually be some scatter about the straight line, the

trend of the data must be linear. If the distribution is not lognormal–that is, if it does not display a linear trend on a log-probability plot—the CMD can still be determined, but Eq. 4.46 holds only for a lognormal distribution.

Frequently, in aerosol sampling there is an aerodynamic size above which particles are aerodynamically unable to enter the sampling apparatus. This is called the *aerodynamic cutoff size* and means that the cumulative line on the log-probability plot will curve near its upper end, so that it never exceeds the cutoff size.

A similar limit may exist for the lower end of the size distribution if sizing is done by optical microscopy. Because of the optical limitations explained in Section 20.2, particles less than about 0.3 μm in diameter are not included in the size distribution. This 0.3-μm limit, sometimes called the *optical cutoff*, curves the lower end of the size distribution line so that it never goes below 0.3 μm. An example of data having both cutoffs is shown in Fig. 4.13. These cutoffs are artifacts of the sampling and measurement system. If the cutoffs affect only a small fraction of the distribution, it is acceptable to ignore them when fitting a straight line to the data on a log-probability plot.

Figure 4.13 also shows the effect of a mixture of two lognormal distributions having the same GSD but different median sizes. This is an example of a *bimodal distribution*, because its frequency function has two peaks. It is often possible to

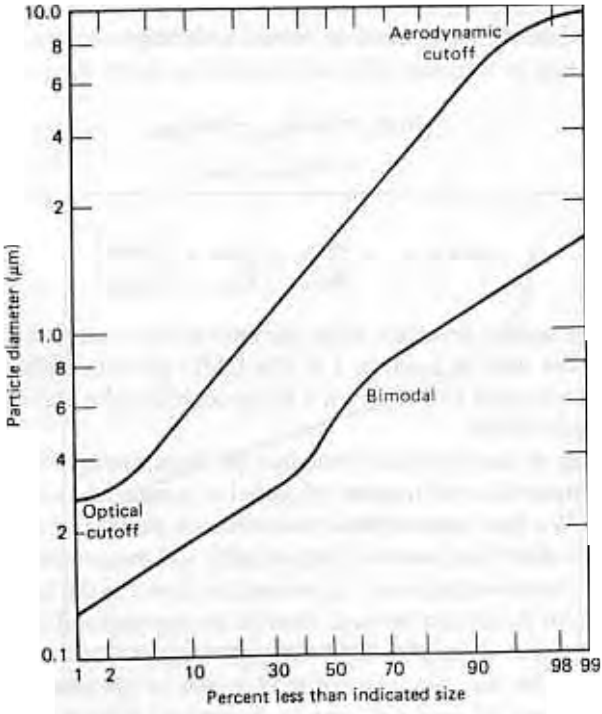

FIGURE 4.13 Nonlinear log-probability graphs

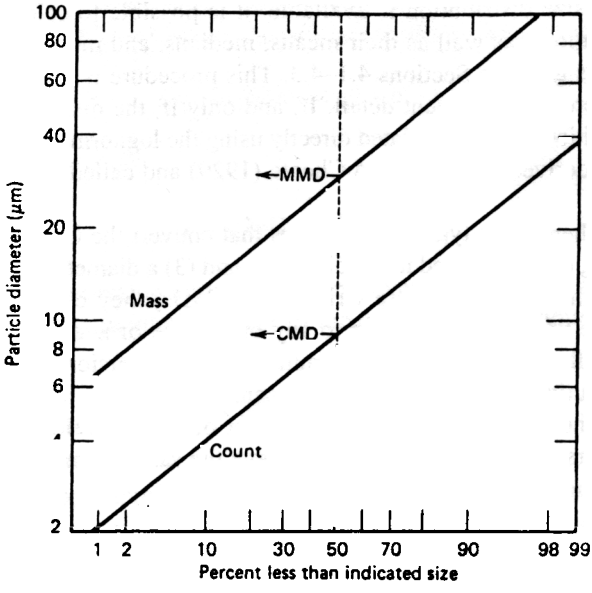

FIGURE 4.14 Cumulative count and cumulative mass distributions on log-probability graph.

represent a bimodal distribution by two overlapping lognormal distributions. (See Knutson and Lioy (1995).)

One great advantage of the lognormal distribution is that, for a given distribution, the geometric standard deviation remains constant for all moment distributions. If the GSD is the same, the ratio $d_{84\%}/d_{50\%}$ will be the same, for each distribution, and the cumulative distribution lines for other moment distributions will be parallel to the cumulative count distribution line on a log-probability graph. The separation between the lines (and between median diameters) is a function only of GSD. (See Section 4.6.) Figure 4.14 shows both count and mass distributions for the data given in Table 4.1, plotted as cumulative distributions on log-probability graph paper. The horizontal axis refers to cumulative percent of mass for the mass distribution line and cumulative percent of count for the count distribution line.

4.6 THE HATCH–CHOATE CONVERSION EQUATIONS

The real power and utility (and perhaps the popularity) of the lognormal distribution comes from the fact that any type of average diameter discussed in this chapter can easily be calculated for any known lognormal distribution—that is, a distribution for which one average diameter and the GSD are known. This is useful because it is frequently necessary to measure one characteristic of the size distribution, such as the number distribution, when what is really needed is another characteristic, such as the mass distribution or the diameter of average mass.

If a detailed size distribution is available, it is possible to calculate the other moment distributions, as well as their means, medians, and moment averages, using the equations given in Sections 4.1–4.3. This procedure is tedious and may be inaccurate if there is insufficient detail. If, and only if, the distribution is lognormal, these quantities can be calculated directly using the lognormal conversion equations originally derived by Hatch and Choate (1929) and called the *Hatch–Choate equations*.

We consider here three types of equations that convert the CMD to (1) another median diameter, (2) a weighted mean diameter, and (3) a diameter of average property. Although these equations are written for CMDs, they can be combined to convert any type of average diameter to any other type of average diameter. The examples that follow are for the most common case, conversions between number and mass distribution. Analogous equations can be written for any moment distribution, such as the distribution of surface area or of settling velocity.

All the conversion equations that follow have the same form, namely,

$$d_A = \text{CMD} \exp(b \ln^2 \sigma_g) \tag{4.47}$$

where b is a constant that depends only on the type of conversion—that is, on what type of average diameter d_A is. For a given type of conversion, the ratio of the two diameters depends only on the value of σ_g. A derivation of these lognormal conversion equations is given in Appendix 3 to this chapter.

To convert the CMD to the median diameter of the qth moment distribution (qMD), we use the general conversion equation

$$q\text{MD} = \text{CMD} \exp(q \ln^2 \sigma_g) \tag{4.48}$$

where qMD is the median of the qth moment distribution. For this conversion, b in Eq. 4.47 is set equal to q. For example, the MMD is obtained from Eq. 4.47 by setting $b = q = 3$:

$$\text{MMD} = \text{CMD} \exp(3 \ln^2 \sigma_g) \tag{4.49}$$

To convert the CMD to the *mean* diameter of the qth moment distribution, d_{qm}, we use the conversion equation

$$d_{qm} = \text{CMD} \exp\left[\left(q + \frac{}{2}\right) \ln^2 \sigma_g\right] \tag{4.50}$$

For example, the mass mean diameter is given by

$$d_{mm} = \text{CMD} \exp(3.5 \ln^2 \sigma_g) \tag{4.51}$$

To convert the CMD to the diameter of average, d^p, where $p =$ for length, 2 for surface, and 3 for mass or volume, we use the equation

$$d_{\bar{p}} = \text{CMD} \exp\left(\frac{p}{2} \ln^2 \sigma_g\right. \tag{4.52}$$

Thus, the diameter of the particle with average mass (that size particle whose mass multiplied by the total number of particles gives the total mass) is

$$d_{\bar{m}} = \text{CMD} \exp(1.5 \ln^2 \sigma_g) \tag{4.53}$$

The mode, $\hat{d}$, is given by

$$\hat{d} = \text{CMD} \exp(-1 \ln^2 \sigma_g) \tag{4.54}$$

The general conversion equation for any average diameter described by Eq. 4.36—that is, the pth moment average of the qth moment distribution—is given by

$$(d_{qm})_{\bar{p}} = \text{CMD} \exp\left[\left(q + \frac{p}{2}\right) \ln^2 \sigma_g\right] \tag{4.55}$$

For use with the logarithm to the base 10, the $(q + p/2)$ term is multiplied by 2.303, and $\log_{10}$ and 10^x are used. When $q = 0$, Eq. 4.55 becomes the conversion equation for the diameter of average d^p (Eq. 4.52). When $p = 0$, Eq. 4.55 becomes the conversion equation for the median of the qth moment distribution (qMD). When $p = 1$, we get the conversion equation for the mean of the qth moment distribution, d_{qm}. Table 4.2 gives the value of b to be used in Eq. 4.47 for the most common conversions. Figure 4.15 shows the relative positions of several average diameters on an arithmetic plot of the count distribution data given in Table 4.1. The larger the coefficient in the conversion equation, the further that converted average diameter is from the CMD. Also, the larger the GSD, the greater the ratio between the MMD and the CMD, as shown in Fig. 4.16.

Table 4.3 summarizes information about the various types of averages we have discussed and gives the coefficient b for the lognormal conversion equation, Eq. 4.47. There is an obvious pattern to the values of b, and the table can be extended by analogy in any direction. However, as will be discussed in the next section, care must be taken to ensure that the data are accurate and properly represent a lognormal distribution in the region of the converted average diameter.

TABLE 4.2 Coefficients for Equation 4.47 for the Most Common Conversions

To Convert from CMD to[a]	Use, for the value of b in Eq. 4.47,
Mode, $\hat{d}$	
Count mean diameter, $\bar{d}$	0.5
Diameter of average mass, $d_{\bar{m}}$	1.5
Mass median diameter, MMD	3
Mass mean diameter, d_{mm}	3.5

[a]Diameters listed replace d_A in Eq. 4.47.

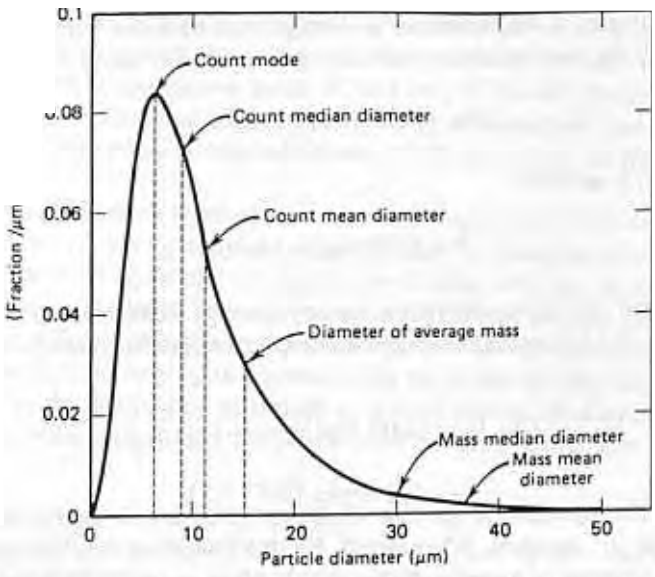

FIGURE 4.15 Arithmetic plot of the size data from Table 4.1 (count distribution with CMD = 9.0 μm and GSD = 1.89), showing the locations of various average diameters.

EXAMPLE

Calculate the MMD and the diameter of average mass, $d_{\overline{m}}$, for a lognormal size distribution with CMD = 3.5 μm and GSD (σ_g) = 2.2.

For the MMD, use Eq. 4.47 with $b = 3$:

$$\text{MMD} = \text{CMD} \exp(b \ln^2 \sigma_g) = 3.5 \exp(3 (\ln 2.2)^2)$$

$$\text{MMD} = 3.5 \exp(3 \times 0.622) = 3.5\, e^{1.865} = 3.5 \times 6.46 = 23\ \mu\text{m}$$

For $d_{\overline{m}}$, $b = .5$, and

$$d_{\overline{m}} = \text{CMD} \exp(1.5 \ln^2(2.2)) = 3.5\, e^{0.932} = 8.9\ \mu\text{m}$$

4.7 STATISTICAL ACCURACY

Great care must be exercised in calculating the mass mean or mass median diameter based on count data. As shown in Fig. 4.15, the distribution of mass is centered (MMD) well out on the tail of the number distribution. Thus, it is important to ensure that this region of the number distribution is accurately represented. When there are errors or scatter in the data, calculated values for different moment distri-

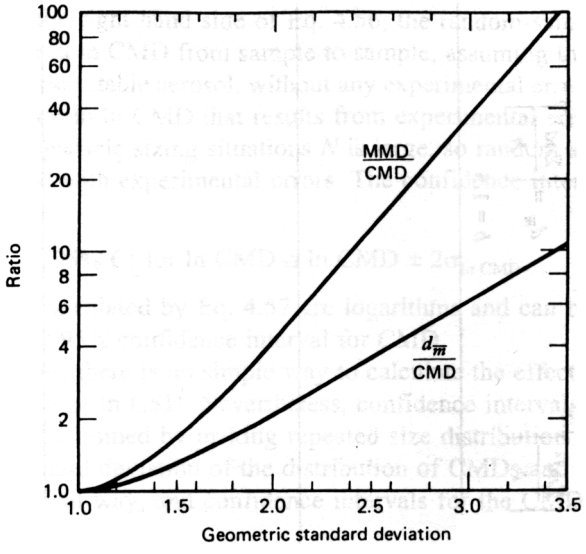

FIGURE 4.16 Ratios of mass median diameter and diameter of average mass to count median diameter versus geometric standard deviation.

butions should be considered estimates and used cautiously. For example, a 10% error in the 84% size changes the GSD from 2.0 to 2.2 and the calculated MMD by 53%. The converse is also true: When deriving count sizes from mass data, care must be taken to ensure that the lower end of the mass distribution is statistically accurate.

Most of the particles in a sample will be in a relatively few size intervals, and intervals in the tail of a distribution will contain few particles. To ensure statistical reliability of the measurements at the tail, a common criterion is to observe at least 10 particles in every size interval of importance to the distribution (either mass or count) curve. An efficient procedure for doing this for microscopic sizing is described in Section 20.1.

Confidence intervals for the CMD and GSD can be constructed to provide a measure of the range in which the true CMD and GSD values are likely to lie. Thus, the 95% confidence interval for the CMD expresses the likelihood (19 chances out of 20) that the true CMD lies within the range defined by the confidence interval of a random sample.

For a lognormal distribution the distribution of ln d is normal, and a confidence interval for ln CMD (and CMD) can be constructed using the standard deviation of ln CMD, $\sigma_{\ln \text{CMD}}$,

$$\sigma_{\ln \text{CMD}} = \left[\frac{\ln^2 \sigma_g}{N} + \sigma_{\text{EE}}^2\right]^{1/2} \tag{4.56}$$

TABLE 4.3 Names, Defining Equations, and Coefficients[a] for the Lognormal Conversion Equations for Common Types of Average Diameters

	Types of Average[b]			
	ln [$p = 0$]: Median, Geometric	$p = 1$: Diameter	$p = 2$: Area, V_{TS}	$p = 3$: Volume, Mass
Count (d^0)	Count median diameter, geometric mean: $\text{CMD} = \exp\left[\frac{\Sigma n \ln d}{N}\right]$ $b = 0$	Count mean diameter: $\bar{d} = \frac{\Sigma nd}{N}$ $b = 0.5$	Diameter of average surface: $d_{\bar{s}} = \left[\frac{\Sigma nd^2}{N}\right]^{1/2}$ $b = 1$	Diameter of average volume, diameter of average mass: $d_{\bar{m}} = \left[\frac{\Sigma nd^3}{N}\right]^{1/3}$ $b = 1.5$
Length (d^1)	Length median diameter $\text{LMD} = \exp\left[\frac{\Sigma nd \ln d}{\Sigma nd}\right]$ $b = 1$	Length mean diameter: $d_{lm} = \frac{\Sigma nd^2}{\Sigma nd}$ $b = 1.5$		
Area (d^2)	Surface median diameter: $\text{SMD} = \exp\left[\frac{\Sigma nd^2 \ln d}{\Sigma nd^2}\right]$ $b = 2$	Surface mean diameter, Sauter diameter, Mean volume–surface diameter: $d_{sm} = \frac{\Sigma nd^3}{\Sigma nd^2}$ $b = 2.5$		
Volume (d^3) or mass (d^3)	Volume median diameter mass median diameter: $\text{MMD} = \exp\left[\frac{\Sigma nd^3 \ln d}{\Sigma nd^3}\right]$ $b = 3$	Volume mean diameter mass mean diameter: $d_{mm} = \frac{\Sigma nd^4}{\Sigma nd^3}$ $b = 3.5$		

[a] b values for Eq. 4.47 and $b = q + p/2$ for Eq. 4.55

[b] p = moment of diameter.

The first term on the right-hand side of Eq. 4.56, the random-sampling error, reflects the variation in ln CMD from sample to sample, assuming that each sample is taken from the same stable aerosol, without any experimental error. The term σ_{EE} reflects the variation in ln CMD that results from experimental error due to measurement. In most particle sizing situations N is large, so random sampling errors are small compared with experimental errors. The confidence interval (CI) for ln CMD is given by

$$95\%\ \text{CI for ln CMD} \cong \ln \text{CMD} \pm 2\sigma_{\ln \text{CMD}} \tag{4.57}$$

Confidence limits calculated by Eq. 4.57 are logarithms and can be converted to diameters to get the 95% confidence interval for CMD.

In most situations, there is no simple way to calculate the effect of experimental error on ln CMD or ln GSD. Nevertheless, confidence intervals for CMD and GSD can still be determined by making repeated size distribution measurements. The mean and standard deviation of the distribution of CMDs and GSDs are then calculated in the usual way, and confidence intervals for the CMD and GSD are calculated by

$$95\%\ \text{CI for CMD} = \overline{\text{CMD}} \pm t\sigma_{\text{CMD}}$$

$$95\%\ \text{CI for GSD} = \overline{\text{GSD}} \pm t\sigma_{\text{GSD}} \tag{4.59}$$

where t is the t-test value, obtained from statistical tables ($P = 0.05$ and degrees of freedom $= N' - 1$, where N' is the number of replications). On the log-probability plot, the confidence interval of CMD defines the range of vertical positions of the size distribution line, and the confidence interval of GSD defines the range of slopes. Statistical tests such as the t-test and F-test can be used to compare the parameters of one aerosol size distribution with those of another. These tests are discussed by Cooper (1993), Land (1988), Herdan (1960), and Aitchison and Brown (1957).

The cumulative log-probability plot assumes that the data cover the size range from zero to infinity. If there are significant numbers of particles lost by truncation at either end of the size range, the cumulative plot should not be used, but a frequency histogram can still be constructed without bias.

Because of the expansion of the scale at the ends of log-probability graph paper, an error in cumulative frequency is about four times wider on the graph at 5% and 95% than it is at 50%. The rule of thumb for fitting a straight line on a log-probability plot by eye is to give the most weight to the central region (20–80%) and little weight to those points at less than 5% and greater than 95%. The use of least squares regression to find the best fitting straight line on an arithmetic plot of ln(d) versus probit of the cumulative frequency is not recommended, because it overemphasizes the tails of the distribution. There are iterative computer procedures for finding the best fitting line that give proper weight to all points in the distribution. [See Raabe (1978) and Kottler (1951).]

Because of the convenience of the lognormal distribution, there is a tendency to try to fit a straight line to points that clearly do not follow a straight line. This is a risky procedure, especially if other average diameters are to be calculated using the

[b] values for
[b] p = moment

lognormal conversion equations. When the data do not follow the lognormal distribution, it is often better not to assume any distribution function and to use percentile diameters from the cumulative plot to describe the distribution. Statistical tests such as the Kolmogorov-Smirnov (number of intervals > 10) or the chi-square goodness of fit (for count data) can be used to determine whether the distribution departs significantly from a lognormal distribution. [See Cooper (1993) and Waters et al. (1991).]

Calculation of a particle size distribution from measured data, especially when the measurement method does not sharply delineate size ranges, is called *data inversion* or *deconvolution*. The subject is complicated and beyond the scope of this text. [See Knutson and Lioy (1995) and Cooper (1993) for a summary of different approaches.]

4.8 APPENDIX 1: DISTRIBUTIONS APPLIED TO PARTICLE SIZE

The most commonly used distribution for characterizing aerosol particle size is the lognormal distribution described in Sections 4.4–4.7. Several less common distributions, however, have been found useful for specific types of aerosols. In the equations that follow, a and b are empirical constants having different values for each distribution.

The Rosin–Rammler distribution [Rosin and Rammler (1933)], originally devised for sizing crushed coal, is applicable to coarsely dispersed dusts and sprays. It is particularly useful for size distributions that are more skewed than the lognormal distribution and for sieve analysis. The weight fraction between d_p and $d_p + dd_p$ is given by

$$df_m = abd_p^{b-1} \exp(-ad_p^b)dd_p \tag{4.60}$$

where a depends on the fineness of the particles and b depends only on the their material. This distribution can be used when cutoff points for the smallest and largest diameters are well defined. Expressed in differential form, as in Eq. 4.60, the Rosin–Rammler distribution has the same form as the Weibull distribution.

2 The Nukiyama–Tanasawa distribution [Nukiyama and Tanasawa (1939)] is used for sprays having extremely broad size ranges. The number of particles with diameters between d_p and $d_p + dd_p$ is given by

$$df = ad_p^2 \exp(-b/d_p^3)dd_p \tag{4.61}$$

where the empirical constants a and b are functions of a nozzle constant c.

3 The power function distribution has been applied to the size distribution of atmospheric aerosols. (See Chapter 14.) The number of particles with sizes between d_p and $d_p + dd_p$ is given by

$$df = ad_p^{-b}dd_p \tag{4.62}$$

4 The exponential distribution has been applied to powdered materials. The number of particles with sizes between d_p and $d_p + dd_p$ is given by

$$df = a \exp(-bd_p)dd_p \tag{4.63}$$

The total number of particles is a/b.

5 The size distributions of cloud droplets are described by the Khrgian–Mazin distribution (Pruppacher and Klett, 1997). The number of droplets per unit volume with sizes between d_p and $d_p + dd_p$ is given by

$$df = ad_p^2 \exp(-bd_p)dd_p \tag{4.64}$$

Total number concentration is $2a/b^3$, and the mean diameter is $3/b$.

4.9 APPENDIX 2: THEORETICAL BASIS FOR AEROSOL PARTICLE SIZE DISTRIBUTIONS

Section 4.4 states that there is no fundamental theoretical basis for aerosols having a lognormal size distribution. While this is true in general, several authors have noted that when the particle formation process follows the "law of proportionate effect," a lognormal size distribution results. This law requires changes in size to occur in steps, with the particle size for each step being a random multiplicative factor of the size of the previous step. Breakage (crushing) of solid particles is an example of such a process. Brown and Wohletz (1995) give physically based derivations of the Weibull and Rosin–Rammler distributions based on fractal cracking, a breakage process that produces a branched tree of cracks that looks the same on any scale. (See Chapter 20.) Brown and Wohletz note that certain of the resulting distributions are very similar to the lognormal distribution.

4.10 APPENDIX 3: DERIVATION OF THE HATCH–CHOATE EQUATIONS

The diameter of average d^p, where $p = 2$ for surface area and 3 for mass, is given by Eq. 4.22 as

$$d_{\bar{p}} = (\overline{d^p})^{1/p} = \left(\int_0^\infty d^p f(d)dd\right)^{1/p} \tag{4.65}$$

To evaluate $d_{\bar{p}}$ for a lognormal distribution, we must first express the quantity $d^p f(d)$ in terms of the CMD, σ_g, and p. Expressing $f(d)$ in terms of Eq. 4.42 and making the substitution $d^p = \exp(p \ln d)$ gives

$$d^p f(d) = \frac{e^{p \ln d}}{\sqrt{2\pi}\, d \ln \sigma_g} \exp\left(\frac{-(\ln d - \ln \mathrm{CMD})^2}{2 \ln^2 \sigma_e}\right)$$

Combining and expanding the exponent yields

$$d^p f(d) = \frac{}{\sqrt{2\pi}\, d \ln \sigma_g}$$

$$\times \exp\left(\frac{+2(\ln^2\sigma_g)p \ln d - \ln^2 d + 2(\ln d)\ln \text{CMD} - \ln^2 \text{CMD}}{2 \ln^2 \sigma_g} \right) \quad (4.67)$$

We can complete the square in the exponential term of Eq. 4.67 by multiplying the entire equation by

$$1 = \left[\exp\left(p \ln \text{CMD} + \frac{p^2}{2} \ln^2 \sigma_g \right) \right] \left[\exp\left(-p \ln \text{CMD} - \frac{p^2}{2} \ln^2 \sigma_g \right) \right] \quad (4.68)$$

The second factor of Eq. 4.68 is combined with the exponential term in Eq. 4.67 to give a new exponential term,

$$\frac{}{2 \ln^2 \sigma_g} [\ln^2 d - 2(\ln d)(\ln \text{CMD} + p \ln^2 \sigma_g)$$

$$+ \ln^2 \text{CMD} + 2p(\ln \text{CMD}) \ln^2 \sigma_g + (p \ln^2 \sigma_g)^2] \quad (4.69)$$

which is equal to

$$\frac{-[\ln d - (\ln \text{CMD} + p \ln^2 \sigma_g)]^2}{2 \ln^2 \sigma_g} \quad (4.70)$$

Thus,

$$d^p f(d) = \exp\left(p \ln \text{CMD} + \frac{p^2}{2} \ln^2 \sigma_g \right)$$

$$\times \left[\frac{1}{\sqrt{2\pi}\, d \ln \sigma_g} \exp\left(- \frac{[\ln x - (\ln \text{CMD} + p \ln^2 \sigma_g)]^2}{2 \ln^2 \sigma_g} \right) \right] \quad (4.71)$$

We can now substitute Eq. 4.71 into Eq. 4.65 and integrate the resulting expression. The first exponential in Eq. 4.71 is a constant term. The bracketed term is identical in form to the frequency function of a lognormal distribution. Equation 4.65 becomes

$$d_{\bar{p}} = \left(\overline{d^p} \right)^{1/p} = \exp\left[p \ln \text{CMD} + \frac{p^2}{2} \ln^2 \sigma_g \right]^{1/p} \quad (4.72)$$

$$\ln d_{\bar{p}} = \frac{1}{p} \ln \overline{d^p} = \frac{1}{p}\left[p \ln \text{CMD} + \frac{p^2}{2} \ln^2 \sigma_g \right] \tag{4.73}$$

$$\ln d_{\bar{p}} = \ln \text{CMD} + \left(\frac{p}{2}\right) \ln^2 \sigma_g \tag{4.74}$$

and $d_{\bar{p}}$, the diameter of average d^p, is

$$d_{\bar{p}} = \text{CMD} \exp\left[\frac{p}{2} \ln^2 \sigma_g\right]$$

which is identical to Eq. 4.52.

To obtain the conversion equation for the median (qMD) of the qth moment distribution, we start with the distribution function, Eq. 4.35. Substituting Eq. 4.71, with p replaced by q, for the numerator and using the procedure just outlined in Eqs. 4.66–4.72 to evaluate the integral of Eq. 4.71 for the denominator, we get

$$df_q = \frac{1}{\sqrt{2\pi}\, d \ln \sigma_g} \exp\left(- \frac{[\ln d - (\ln \text{CMD} + q \ln^2 \sigma_g)]^2}{2 \ln^2 \sigma_g} \right) \tag{4.76}$$

This equation has the form of a lognormal distribution, Eq. 4.42, with a median diameter given by

$$\begin{aligned} \ln q\text{MD} &= \ln \text{CMD} + q \ln^2 \sigma_g \\ q\text{MD} &= \text{CMD} \exp(q \ln^2 \sigma_g) \end{aligned} \tag{4.77}$$

which is identical to Eq. 4.48.

We can use Eq. 4.71 to get d_{qm}, the mean of the qth moment distribution. This mean is the ratio of two moments of diameter and has the general form

$$d_{qm} = \frac{\int_0^\infty x^{q+1} f(x)\, dx}{\int_0^\infty x^q f(x)\, dx}$$

Both the numerator and denominator of Eq. 4.78 are equivalent to the integrals of Eq. 4.71. Evaluating Eq. 4.78 using the procedure followed in Eqs. 4.66–4.72 gives

$$d_{qm} = \frac{\exp\left[(q+1) \ln \text{CMD} + \dfrac{(q+1)^2}{2} \ln^2 \sigma_g\right]}{\exp\left[q \ln \text{CMD} + \dfrac{q^2}{2} \ln^2 \sigma_g\right]} \tag{4.79}$$

$$\ln d_{qm} = \ln \text{CMD} + \frac{[(q+1)^2 - q^2] \ln^2 \sigma_g}{2} \tag{4.80}$$

$$d_{qm} = \text{CMD} \exp[(q + \tfrac{1}{2}) \ln^2 \sigma_g] \tag{4.81}$$

which is identical to Eq. 4.50.

PROBLEMS

4.1 For the following particle size distribution data, calculate the arithmetic mean, geometric mean, count median, and diameter of the particle with average surface area.

Particle size (μm)	Number
	3
3	5
5	2
8	1

ANSWER: 3.27 μm, 2.67 μm, 3.0 μm, 3.84 μm.

4.2 A frequency function has a constant value between 1.5 and 6.5 μm and is zero elsewhere. Determine the arithmetic mean, number median, diameter of average mass, and surface mean diameter. [*Hint*: Divide the distribution into five equal intervals with midpoints at 2, 3, 4, 5, and 6 μm.]

ANSWER: 4.0 μm, 4.0 μm, 4.45 μm, 4.89 μm.

4.3 An aerosol has a lognormal particle size distribution with a mass median diameter of 10.0 μm and a geometric standard deviation of 2.5. What is the count median diameter? Assume ρ_p = 3000 kg/m^3 [3.0 g/cm^3].

ANSWER: 0.81 μm.

4.4 You are given the following data, obtained by sequential sieving of a sample of granite dust:

Sieve Opening (μm)	Mass Captured on Sieve (g)
200	4.0
100	21.6
50	38.4
40	8.0
Final Pan	8.0
Total	80.0

Determine the mass median diameter and geometric standard deviation of this distribution using log-probability graph paper. Use the appropriate conversion equation to determine the count median diameter.

ANSWER: 80 μm, 1.75, 31 μm.

4.5 An aerosol with a lognormal size distribution has a count median diameter of 2.0 μm and a geometric standard deviation of 2.2. If the mass concentration is 1.0 mg/m^3, what is the number concentration? Assume spherical particles with ρ_p = 2500 kg/m^3 [2.5 g/cm^3].
ANSWER: 5.8×10^6/m^3 [5.8/cm^3].

4.6 Consider an aerosol with a lognormal size distribution (GSD = 1.8). The size distribution is in a range where slip correction can be neglected and Stokes's law holds. If the diameter of the particle of average settling velocity is determined to be 6.0 μm, what is the count median diameter?
ANSWER: 4.2 μm.

4.7 An aerosol with a lognormal size distribution has a count median diameter of 0.3 μm and a GSD of 1.5. If the number concentration is 10^6 particles/cm^3, what is the mass concentration? The particles are spheres with a density of 4500 kg/m^3 [4.5 g/cm^3].
ANSWER: 130 mg/m^3.

4.8 An aerosol is known to have a lognormal size distribution with a geometric standard deviation σ_g. The average time required for the particles to settle a known distance h is t. Derive an expression for the diameter of average settling time. Neglect slip correction. Also, give the equation for converting this diameter to the count median diameter. Assume spherical particles.
ANSWER: $d_t = (\Sigma d^{-2}/N)^{-0.5}$, $b = +1$.

4.9 An aerosol is mixed with radon gas, resulting in a surface coating of radioactive radon decay products on the particles. The aerosol is then divided into eight aerodynamic size groups, and the radioactivity of each size group is measured. How can this information be used to calculate the count median diameter if the distribution is lognormal? All particles have the same density and are geometrically similar. Assume that log-probability graph paper is available.

4.10 For particles less than 0.05 μm, light extinction efficiency is proportional to d^4. If an aerosol is lognormally distributed with a CMD of 0.01μm and a GSD of 1.8, what is the diameter of average extinction efficiency?
ANSWER: 0.020 μm.

4.11 Measurements of specific surface indicate that 16% of the total specific surface is contributed by particles less than 0.3 μm and 84% by particles less than 1.5 μm. Assuming that the particle size distribution is lognormal, calculate (without the aid of log-probability graph paper) the specific surface median diameter, the CMD, and the GSD. The specific surface is the surface area per gram of particles.
ANSWER: 0.67 μm, 1.28 μm, 2.24.

4.12 Specific surface is defined as surface area per gram of particles. Set up the conversion equation that will give the diameter of the particle with average specific surface in terms of the CMD and σ_g.
ANSWER: $b = -½$.

REFERENCES

Aitchison, J., and Brown, J. A. C., *The Lognormal Distribution Function*, Cambridge University Press, Cambridge, U.K., 1957.

Brown, W. K., and Wohletz, K. H., "Derivation of the Weibull distributions based on physical principles and its connection to the Rosin–Rammler and lognormal distribution," *J. Appl. Phys.*, **52**, 493–502 (1995).

Cooper, D. W., "Methods of Size Distribution Data Analysis and Presentation, in Willeke, K., and Baron, P. A., (Eds), *Aerosol Measurement*, Van Nostrand, Reinhold, New York, 1993.

Crow, E. L., and Shimizu, K. (Eds.), *Lognormal Distributions: Theory and Applications*, Marcel Dekker, New York, 1988.

Hatch, T., and Choate, S. P., "Statistical Description of the Size Properties of Non-Uniform Particulate Substances," *J. Franklin Inst.*, **207**, 369 (1929).

Herdan, G., *Small Particle Statistics*, 2d ed., Academic Press, New York, 1960.

Knutson, E. O., and Lioy, P. J., Measurement and Presentation of Aerosol Size Distributions, in Cohen, B. S., and Hering, S. V., (Eds.), *Air Sampling Instruments*, 8th ed., ACGIH, Cincinnati, 1995.

Kottler, F. J., *J. Franklin Inst.*, **251**, 449, 515 (1951).

Land, C. E., "Hypothesis Tests and Interval Estimates," in Crow, E. L., and K. Shimizu, K. (Eds.), *Lognormal Distributions*, Marcel Dekker, New York, 1988.

Mercer, T. T., *Aerosol Technology in Hazard Evaluation*, Academic Press, New York, 1973.

Nukiyama, S., and Tanasawa, Y., *Trans. Soc. Mech. Eng. (Japan)*, **5**, 63 (1939).

Pruppacher, H. R., and Klett, J. D., *Microphysics of Clouds and Precipitation*, 2d ed., Kluwer, Dordrecht, the Netherlands, 1997.

Raabe, O. G., "Particle Size Analysis Utilizing Grouped Data and the Log-Normal Distribution," *J. Aerosol Sci.*, **2**, 289–303 (1971).

Raabe, O. G., *Env. Sci. Tech.*, **12**, 1162 (1978).

Rosin, P., and Rammler, E., *J. Inst. Fuel*, **7**, 29 (1933).

Silverman, L., Billings, C., and First, M., *Particle Size Analysis in Industrial Hygiene*, Academic Press, New York, 1971.

Waters, M. A., Selvin, S., and Rappaport, S. M., "A Measure of Goodness-of-Fit for the Lognormal Model Applied to Occupational Exposures," *Am. Ind. Hyg. Assoc. J.*, **52**, 493–502 (1991).

14 Atmospheric Aerosols

The atmospheric aerosol—that is, the particles that are normally found in our atmosphere—is a complex and dynamic mixture of solid and liquid particles from natural and anthropogenic sources. We consider first the natural background aerosol—the aerosol that would be present in the absence of human activity. At the other extreme the urban aerosol is dominated by anthropogenic sources. In both cases, primary particles are continuously emitted into, and secondary particles are formed in, the atmosphere. Both kinds of particles may undergo growth, evaporation, or chemical reactions and are subject to various removal mechanisms. The size distributions one finds in the atmosphere reflect the complex interaction of all these processes. We omit from this discussion the largest and most important atmospheric aerosol: natural clouds of water droplets.

14.1 NATURAL BACKGROUND AEROSOL

Sources of natural background and anthropogenic (related to human activity) aerosols are shown in Table 14.1. The wide range of the estimates given for natural aerosol sources reflects the uncertainty of the assumptions upon which these estimates are based. Soil dust includes windblown soil particles from arid regions and the natural weathering of rock. A comparison of sources can be misleading, because their contribution to the atmospheric aerosol varies greatly due to differences in transport distances and removal mechanisms. The majority of the particulate mass from soil dust, volcano aerosol emissions, and anthropogenic direct emissions is likely to be large particles that fall out near the source. The other sources shown—fires and secondary particles—produce fine particles that remain suspended for many days, long enough to travel global distances. Most of the natural photochemical smog is formed by the action of sunlight on isoprene and monoterpene vapor emissions from trees.

The majority of the particulate mass in the atmosphere, both natural and anthropogenic is formed in the atmosphere from gaseous emissions. Although there are large uncertainties in the emission estimates given in Table 14.1, on a global scale natural sources exceed anthropogenic sources by a wide margin. The anthropogenic sources contribute from less than 10 to 50% of the global particulate emissions. The natural sources are well distributed around the globe, and most of their mass contribution comes from vast area sources. The anthropogenic sources, on the other hand, are smaller in amount, but are concentrated in a small portion of the globe:

TABLE 14.1 Sources and Estimates of Global Emissions of Atmospheric Aerosols[a]

Source	Amount, Tg/yr [10^6 metric tons/yr]	
	Range	Best Estimate
Natural		
Soil dust	1000–3000	1500
Sea salt	1000–10000	1300
Botanical debris	26–80	50
Volcanic dust	4–10000	30
Forest fires	3–150	20
Gas-to-particle conversion[b]	100–260	180
Photochemical[c]	40–200	60
Total for natural sources	2200-24000	3100
Anthropogenic		
Direct emissions	50–160	120
Gas-to-particle conversion[d]	260–460	330
Photochemical[e]	5–25	10
Total for anthropogenic sources	320–640	460

[a]Data primarily from Andreae (1995) and SMIC (1971).
[b]Includes sulfate from SO_2 and H_2S, ammonium salts from NH_3, and nitrate from NO_x.
[c]Primarily photochemical particle formation from isoprene and monoterpenes vapors from trees.
[d]Includes sulfate from SO_2 and nitrate from NO_x.
[e]Primarily photochemical particle formation from anthropogenic volatile organic compounds.

the industrialized regions of the world. In these areas, the human contribution exceeds that from natural sources.

Once emitted into or formed in the atmosphere, particles can grow by vapor condensation or by coagulation with other particles. Particles are removed after growing to micrometer or larger sizes by settling or impaction on surfaces such as tree leaves. Small particles may diffuse to surfaces or serve as nucleation sites for raindrops (rainout). Larger particles may be swept out by falling rain or snow (washout). Small particles have lifetimes of days in the troposphere; large particles ($d_a > 20$ μm) are removed in a matter of hours.

Although most of the atmospheric particulate mass is confined to the troposphere (region below an altitude of 11 km), the *stratospheric aerosol* can have significant effects on climate. This subject has been reviewed by Pueschel (1996). The primary source of particulate in the stratosphere (altitude from 11 to 50 km) is the formation of sulfuric acid droplets by gas-to-particle conversion of SO_2 injected into the stratosphere by major volcanic eruptions. These droplets are formed by homogeneous nucleation involving photochemical reactions of SO_2 and water vapor. They spread widely over the hemisphere (north or south) in which they originated.

The ozone layer in the lower stratosphere absorbs solar radiation and heats up relative to the surrounding air. This heating creates a temperature inversion and a region of atmospheric stability. The sulfuric acid droplets formed in the stratosphere

accumulate in this stable layer at 18–20 km. This aerosol layer is called the *Junge layer*, after its discoverer.

Major volcanos can increase the stratospheric particulate concentration by two orders of magnitude. The Mount Pinatubo eruption in 1991 injected 14–20 Tg of SO_2 into the stratosphere, causing the aerosol concentration to increase from 2–5 $\mu g/m^3$ to 20–100 $\mu g/m^3$. Before this eruption the particle size distribution had a CMD of 0.14 μm and a GSD of 1.6; after, it had a CMD of 0.66 μm and a GSD of 1.5. The only significant anthropogenic source of particles in the stratosphere is soot from high-altitude aircraft, but this represents less than 1 percent of the total stratospheric aerosol.

Because of the stability and low moisture content of the stratosphere, clouds do not form in it. The absence of cloud formation prevents particle removal by rainout. Also, since particle concentrations are only a few per cubic centimeter, growth by coagulation with subsequent removal by settling is negligible. Similarly, growth by condensation is slow because of low vapor concentration. Consequently, particle lifetimes in the stratosphere are 1–2 years, compared with 1–2 weeks in the lower troposphere. Climatic and global effects of the stratospheric aerosol are described in Section 14.3.

The natural background aerosol in the troposphere depends on direct emissions and gas-to-particle formation from natural sources, as shown in Table 14.1. On a mass basis, direct emissions from deserts, the oceans, and vegetation are the largest sources of particles. Eighty percent of direct emissions go to the lowest kilometer of the troposphere. Consequently, the *tropospheric background aerosol* varies significantly with altitude. Above an altitude of a few kilometers, particle concentrations are influenced little by direct emissions from the earth's surface, and the size distribution in this region resembles that of the background aerosol. A further distinction can be made, between continental and marine background aerosols. Whitby (1978) summarizes available data on the size distribution of average ground-level *background* aerosol in terms of three modes, nuclei, accumulation, and coarse particle. The number concentrations for the three modes are $6400/cm^3$, $2300/cm^3$, and $3/cm^3$ respectively. Each mode can be represented as a lognormal distribution. The size distributions for the modes are as follows: nuclei—CMD = 0.015 μm, GSD = 1.7; accumulation—CMD = 0.076 μm, GSD = 2.0; and coarse particle—CMD = 1.02 μm, GSD = 2.16.

Measurements by Nyeki et al. (1997) of the background aerosol at an elevation of 8.5 km found the accumulation mode to have an average CMD of 0.12 μm and a GSD of 1.57. Concentrations ranged from $1.5 \times 10^7/m^3$ [$15/cm^3$] in winter to $6.6 \times 10^7/m^3$ [$66/cm^3$] in summer. Figure 14.1, based on Jaenicke (1986), summarizes available data on background aerosol size distributions. Defining the term "clean air" is difficult because of the substantial contribution of natural background aerosol. A useful, although arbitrary, definition is "air with a total particle content, measured by a condensation nuclei counter, of less than $700/cm^3$." Natural background aerosol at remote locations and at altitudes greater than 2 km usually fit this definition of clean air.

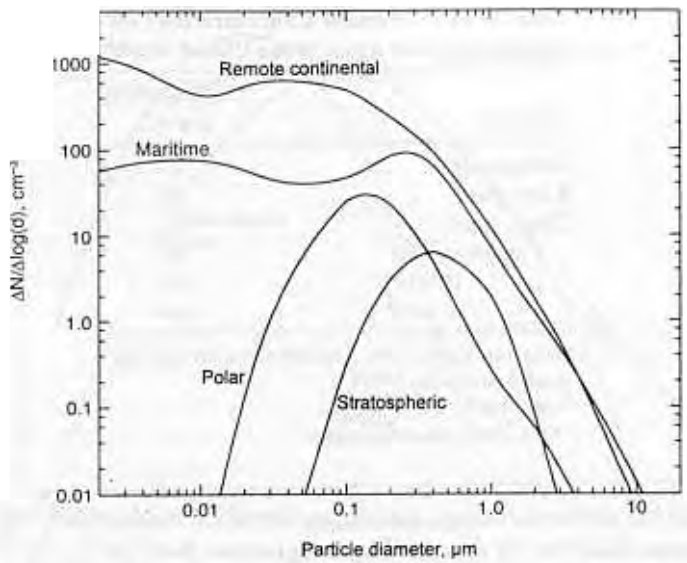

FIGURE 14.1 Particle size distribution by number for background atmospheric aerosols Data from Jaenicke (1986).

Ions are formed continuously in the atmosphere by the action of cosmic radiation and radioactive gases emanating from soil. Over land, about 10 ion pairs (a positive and a negative ion) are formed in every cubic centimeter every second. These ions attach to aerosol particles and recombine with each other at a rate that yields an equilibrium concentration of small ions (charged molecular clusters) of 100–5000/cm^3 with an average value of 8×10^8/m^3 [800/cm^3].

14.2 URBAN AEROSOL

The urban aerosol—that found in the lowest kilometer of the atmosphere over large cities—is dominated by anthropogenic sources. Aerosol mass concentrations in urban areas range from a few tens of micrograms per cubic meter to 1 mg/m^3 during air pollution episodes in heavily polluted cities in developing countries. The horizontal distribution of aerosol concentration in urban areas varies greatly, depending on the proximity to natural and anthropogenic sources. Atmospheric stability and the thickness of the mixing layer (usually 0–2 km) also affect local concentrations. Table 14.2 gives historical particulate concentrations for different types of land areas.

The particle size distribution of urban aerosol is complex, because it is a mixture of aerosols from various sources, each with a different size distribution, and is modified by size-dependent processes of growth, evaporation, and removal. The most common way to present particle size distribution data for the urban aerosol is in terms of the three modes, the nuclei, accumulation, and coarse particle modes.

TABLE 14.2 Aerosol Concentrations for Various Types of Areas of the United States[a]

	Concentration ($\mu g/m^3$)
Background[b]	20
Rural areas[b]	40
Urban areas[c]	
Population $<10^5$	86
10^5–10^6	104
$>10^6$	154

[a]Data from Corn (1976). Concentrations are total suspended particulate (TSP).
[b]1966–1967.
[c]1957–1963, geometric means.

Each mode has different sources, size range, formation mechanisms, and chemical compositions. Each can be described by a lognormal distribution, see Table 14.3. Figure 14.2a shows the average urban aerosol size distribution on a log–log graph. The combined distribution, represented by the solid line, masks the contributions of the individual modes, shown by dashed lines and does not show the nature of the surface or mass distributions.

The more or less straight-line portion of the distribution between 0.1 and 10 μm can be represented by an inverse power law distribution (the Junge distribution). For the data shown in Figure 14.2a,

$$\frac{\Delta N}{\Delta \log(d_p)} = 24.0 d^{-3.08} \tag{14.1}$$

for d in μm. Equation 14.1 is empirical; there is no fundamental or theoretical reason that the atmospheric aerosol should have this distribution function.

Figure 14.2b presents the urban aerosol size distribution as cumulative number and volume distributions on a log-probability graph. (See Section 4.5.) The distributions show significant departures from a lognormal distribution, and the contributions of the individual modes are hidden. Figures 14.2c and 14.2d respectively show particle number and volume per unit log interval on an arithmetic scale ver-

TABLE 14.3 Modal parameters for average urban aerosol.[a]

Mode				C_{vol} ($\mu m^3/cm^3$)
Nuclei	0.014	1.80	106,000	0.63
Accumulation	0.054	2.16	32,000	38.4
Coarse Particle	0.86	2.21	5.4	30.8

[a]Data from Whitby (1978).

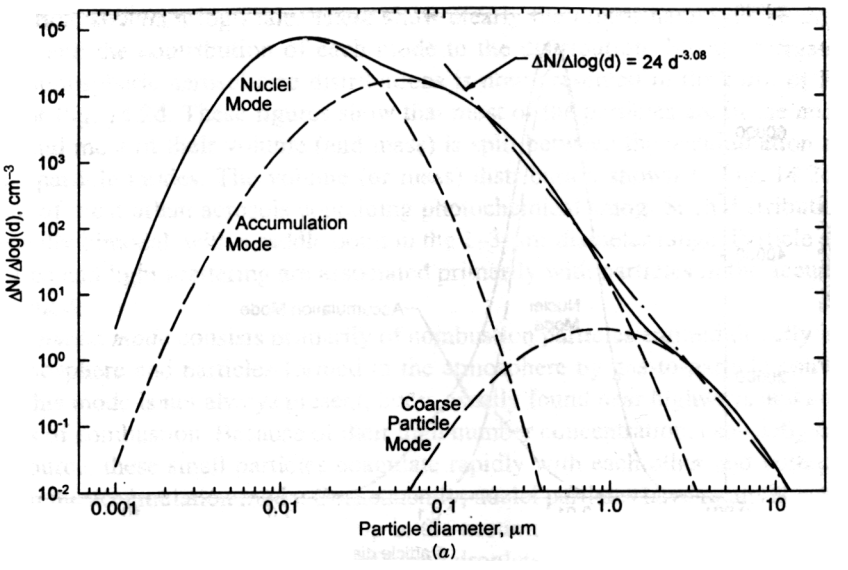

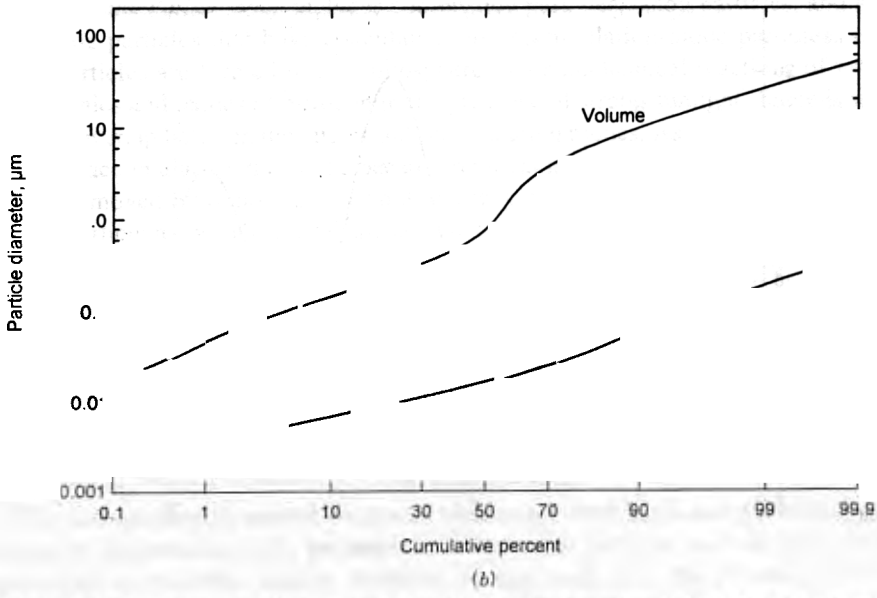

FIGURE 14.2 Average urban aerosol size distributions represented by three lognormal distributions. The modal parameters are given in Table 14.3. (a) Log–log plot of number distribution. (b) Log-probability plot of number and volume distributions. (c) Linear–log plot of number distribution. (d) Linear–log plot of volume distribution. Data from Whitby (1978).

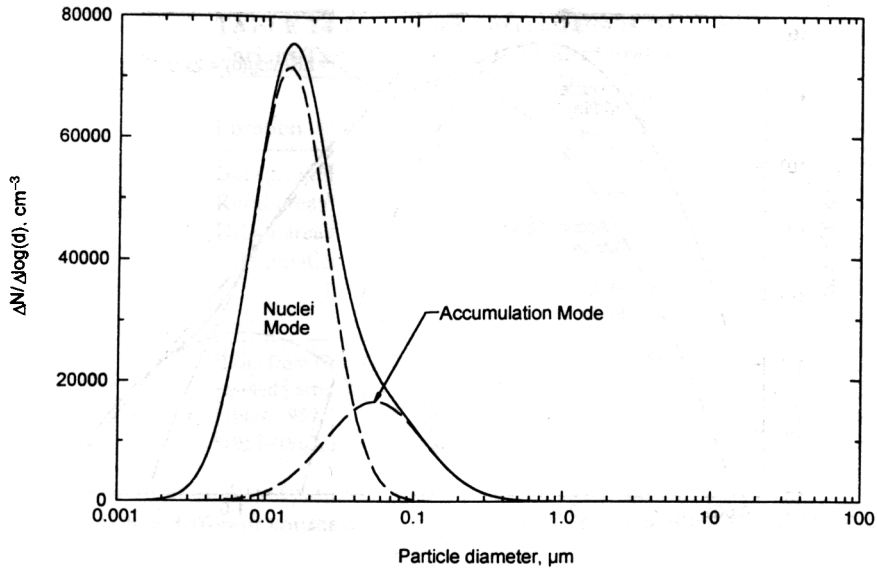

(*c*)

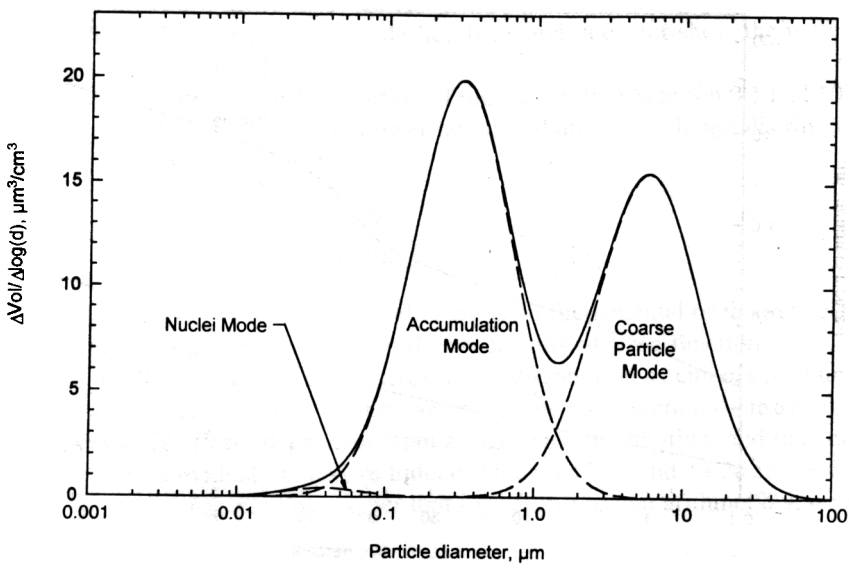

(*d*)

FIGURE 14.2 Continued.

sus particle size on a log scale. These show clearly the modal nature of the urban aerosol and the contribution of each mode to the distribution. Most information about atmospheric aerosol size distributions is now presented in the form of Fig. 14.2c or Fig. 14.2d. These figures show that most of the particles are in the nuclei mode and most of their volume (and mass) is split between the accumulation and coarse-particle modes. The volume (or mass) distribution shown in Fig. 14.2d is typical of most urban aerosols containing photochemical smog. Such distributions are usually bimodal, with a saddle point in the 1–3-μm-diameter range. Particle surface area and light scattering are associated primarily with particles in the accumulation mode.

The *nuclei mode* consists primarily of combustion particles emitted directly into the atmosphere and particles formed in the atmosphere by gas-to-particle conversion. This mode is not always present, but is usually found near highways and other sources of combustion. Because of their high number concentration, especially near their source, these small particles coagulate rapidly with each other and with particles in the accumulation mode. Consequently, nuclei particles have relatively short lifetimes in the atmosphere and end up in the accumulation mode. Nuclei particles may serve as sites for the formation of cloud droplets and may subsequently be removed from the atmosphere as rain droplets (rainout).

The *accumulation mode* includes combustion particles, smog particles, and nuclei-mode particles that have coagulated with accumulation-mode particles. The smog particles are formed in the atmosphere by photochemical reactions of volatile organics and oxides of nitrogen in the presence of strong sunlight. There is significant overlap between the nuclei and accumulation modes. As the name suggests, particles accumulate in this mode because removal mechanisms are weak. Particles can be removed by rainout or washout, but they coagulate too slowly to reach the coarse-particle mode. The nuclei and accumulation modes together constitute "fine" particles. The size range of the accumulation mode includes the wavelengths of visible light, and these particles account for most of the visibility effects of atmospheric aerosols. (See Section 16.4.)

Under conditions of high humidity, such as in a cloud or fog, the accumulation mode may itself have two submodes: a condensation mode with MMAD of 0.2–0.3 μm and a droplet mode with MMAD of 0.5–0.8 μm. The droplets are formed by the growth of hygroscopic condensation-mode particles. This process may be facilitated by chemical reactions in the droplet.

The *coarse-particle mode* consists of windblown dust, large salt particles from sea spray, and mechanically generated anthropogenic particles such as those from agriculture and surface mining. Because of their large size, the coarse particles readily settle out or impact on surfaces, so their lifetime in the atmosphere is only a few hours or days. The dividing line between coarse and fine particles is the saddle point between 1 and 3 μm. The fine-particle mode contains from one-third to two-thirds of the total mass, with the remainder in the coarse particle mode. The ratio varies according to the region of the country. Fine and coarse-particles have different chemical compositions, sources, and lifetimes in the atmosphere. There is comparatively little mass exchange between the two modes. In some locations, there

is an inverse correlation between mass concentration in the two modes. Low wind velocity reduces the concentration of windblown soil particles, but favors photochemical particle formation, and high wind velocity does the opposite.

The size distribution of the urban aerosol, shown in Figs. 14.2a–14.2d, is the steady-state result of the different sources of particles and the processes of formation (gas-to-particle conversion and photochemical reactions), growth (coagulation, condensation and evaporation) and removal (settling, deposition, rainout, and washout) that they are subject to. Figure 14.3 shows these processes schematically.

The chemical compositions of fine and coarse particles differ greatly. Because there is little mass transfer between the fine and coarse particles, they exist together in the atmosphere as two chemically distinct aerosols. As a group, the fine particles are acidic and contain most of the sulfates, ammonium compounds, hydrocarbons, elemental carbon (soot), toxic metals, and water in the atmosphere. The coarse particles are basic and contain most of the crustal materials and their oxides, such as silicon, iron, calcium, and aluminum, as well as large sea salt particles and vegetation debris. Table 14.4 gives data on the chemical composition of fine and coarse particles. Data for the table were obtained using the dichotomous virtual impactor that separates fine and coarse particles during sampling. (See Section 5.7.)

14.3 GLOBAL EFFECTS

The atmospheric aerosol, described in Section 14.1, has a significant influence on two important global atmospheric processes: global warming and ozone depletion. The stratospheric aerosol concentration can increase by up to two orders of magnitude following major volcanic eruptions. These particles have half-lives in the stratosphere of about a year. This stratospheric haze directly affects the earth's radiation balance by scattering incoming solar radiations back into space. (See Section 16.3.) This represents a change in the earth's albedo (reflectivity). Stratospheric particles have little effect on long-wave terrestrial radiation, so the net result is a cooling of the troposphere and the earth's surface. Pueschel (1996) estimates that the eruption of Mount Pinatubo in June 1991 caused a change in solar radiation reaching the earth's surface and troposphere of -2.7 W/m^2 [-2700 erg/s $\cdot$ cm^2] by September 1991. (This was partially offset by an increase in tropospheric clouds, due to the increase in tropospheric nuclei from the eruption, that reduced terrestrial radiation to space.) By comparison, the effect of the CO_2 buildup in the atmosphere since the Industrial Revolution has caused a net change of $+1.25$ W/m^2 [$+1250$ erg/s $\cdot$ cm^2]. Thus, the stratospheric aerosol can have an effect on global surface temperature that is the same order of magnitude, but in the opposite direction, as greenhouse gases and must be included in any analysis of global warming.

The tropospheric aerosol can also affect climate. Tropospheric particles scatter incoming solar radiation back into space by two mechanisms. The first is direct scattering by the tropospheric aerosol. The second mechanism is due to an increase in cloud reflectively because of a higher number concentrations of cloud droplets, resulting from an increased concentration of tropospheric condensation nuclei. Both

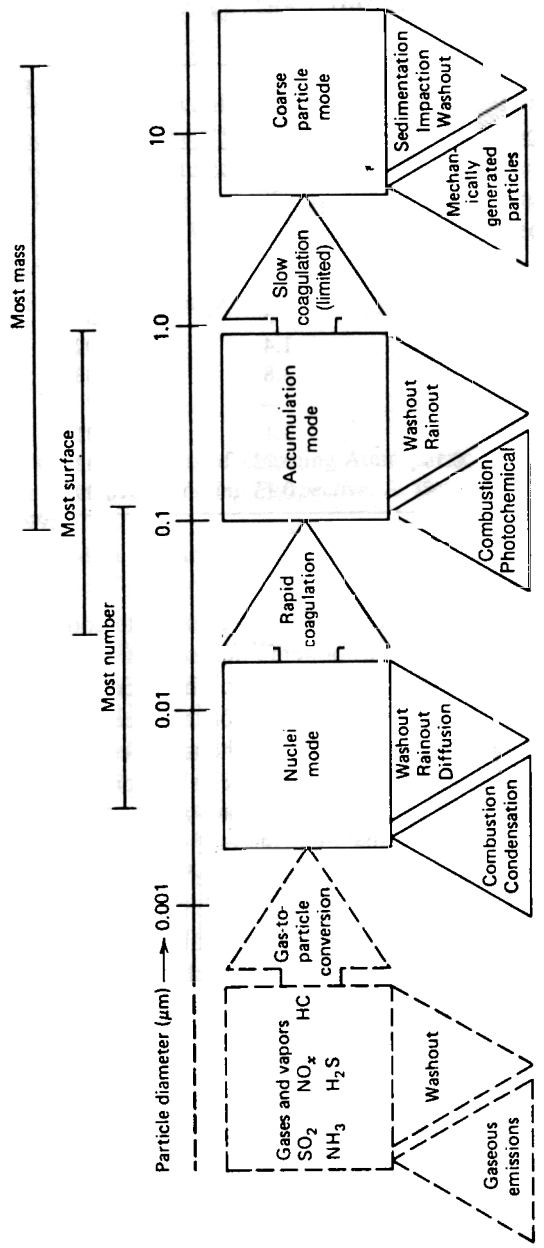

FIGURE 14.3 Schematic representation of the urban aerosol and the processes that modify it.

TABLE 14.4 Average composition of fine and coarse particles in $\mu g/m^3$ at an urban and a rural site.[a]

	Urban		Rural	
		Coarse		Coarse
Total Mass	42	27	24	5.6
SO_4^-	17	1.1	12.0	—
NO_3^-	0.25	1.8	0.30	
NH_4^+	4.3	<0.19	2.3	—
H^+	0.067	<0.01	0.114	—
C	7.6	3.3	3.3	1.3
Al	0.095	1.4	0.020	0.20
Si	0.20	3.8	0.038	0.58
S		—	3.7	0.20
Ca	0.15	3.1	0.016	0.32
Fe	0.17	0.73	0.028	0.12
Pb	0.48	0.13	0.097	0.014

[a]Data from Finlayson-Pitts and Pitts (1986).

mechanisms modify the earth's radiation balance so as to cool the earth's surface. The combined effect due to anthropogenic aerosols is called the "whitehouse" effect, as an analogue to the greenhouse effect. The uncertainty of the magnitude of the whitehouse effect is greater than that for the greenhouse effect. Schwartz (1996) estimates the cooling due to the whitehouse effect to be 20–100% of the heating due to the greenhouse effect. The particles responsible for the whitehouse effect have a lifetime in the troposphere of about a week, whereas the gases responsible for the greenhouse effect have atmospheric lifetimes of decades.

Stratospheric particles play a key role in ozone depletion. In the cold temperature of the polar stratosphere during winter, nitric acid and water vapor condense to form polar stratospheric clouds. The surfaces of these cloud particles serve as sites for the catalytic conversion of stratospheric chlorine compounds, such as anthropogenic chlorofluorocarbons (CFCs), to molecular chlorine (Cl_2) and hypochlorous acid (HOCl). In the polar spring, the sun photodissociates these compounds to atomic chlorine (Cl), which reacts with ozone (O_3) to form oxygen (O_2) and chlorine monoxide (ClO). The latter is photolyzed back to atomic chlorine, and the cycle keeps repeating with the continued destruction of ozone. Volcanic eruptions enhance this process by increasing the stratospheric aerosol, which migrates to the poles and provides additional surface for the catalytic activation of chlorine. See Seinfeld and Pandis (1998).

PROBLEMS

14.1 For the modal data given in Table 14.3, what is the particle number per unit mass for each mode? Assume standard particle density.

ANSWERS: 1.4×10^{20}/kg, 8.7×10^{17}/kg. 8×10^{14}/kg $.4 \times 10^{17}$/g 8.7×10^{14}/g, 1.8×10^{11}/g].

14.2 Estimate how long it would take for the diameter of average mass of the nuclei mode to equal the CMD of the accumulation mode if the nuclei mode particles were allowed to coagulate by themselves. Use modal data given in Table 14.3. Assume that the GSD is constant at its initial value and K is constant at 30×10^{-16} m^3/s [30×10^{-10} cm^3/s] (an interpolated average value from Table 12.4).

ANSWERS: 3.3×10^4 s (9.1 hrs).

REFERENCES

Andreae, M. O., "Climatic Effects of Changing Atmospheric Aerosol Levels," in *Future Climates of the World: A Modelling Perspective*, A. Henderson-Sellers (Ed.), Elsevier, Amsterdam, 1995.

Corn, M., "Aerosols and the Primary Air Pollutants—Nonviable Particles, Their Occurrence, Properties, and Effects," in Stern, A. C. (Ed.), *Air Pollution*, Academic Press, New York, 1976.

Finlayson-Pitts, B. J., and Pitts, J. N., "*Atmospheric Chemistry: Fundamentals and Experimental Techniques*, Wiley, New York, 1986.

First, M. W., "Aerosols in Nature," *Arch. Intern. Med.*, **131**, 24–32 (1973).

Hidy, G., Mueller, P., Grosjean, D., Appel, B., and Wesolowski, J., *The Character and Origins of Smog Aerosols*, Wiley, New York, 1980.

Jaenicke, R., "Physical Characterization of Aerosols," in Lee, S. D., Schneider, T., Grant, L. D., and Verkerk, P. J., (Eds.), *Aerosols: Research, Risk Assessment, and Control Strategies*, Lewis Publishers, Chelsea, MI, 1986.

Kiehl, J. T. and Rodhe, H., "Modeling Geographical and Seasonal Forcing due to Aerosols," in Charlson, R. J. and Heintzenberg, J., (Eds.), *Aerosol Forcing of Climate*, Wiley, New York, 1995.

National Research Council, *Airborne Particles*, University Park Press, Baltimore, 1979.

Nyeki, S., Li, F., Rosser, D., Colbeck, I., and Baltensperger, U., "The background aerosol size distribution at a high alpine site: An analysis of the seasonal cycle," *J. Aerosol Sci.*, **28**, 5211–5212 (1997).

Pueschel, R. F., "Stratospheric aerosols: Formation, properties, effect," *J. Aerosol Sci.*, *27*, 383–402 (1996).

Schwartz, S. E., "The Whitehouse Effect—shortwave Radiative Forcing of Climate by Anthropogenic Aerosols: an Overview," *J. Aerosol Sci.*, **27**, 359–382 (1996).

SMIC, *Inadvertent Climate Modification, Report of the Study of Man's Impact on Climate*, MIT Press, Cambridge, MA, 1971.

Sienfeld, J. H. and Pandis, S. N., *Atmospheric Chemistry and Physics*, Wiley, New York, 1998.

Whitby, K. J., "The Physical Characteristics of Sulfur Aerosol," *Atmos. Env.*, **12**, 135–159 (1978).

15 Electrical Properties

In aerosol mechanics, the most important electrostatic effect is the force exerted on a charged particle in an electrostatic field. Most aerosol particles carry some electric charge, and some may be highly charged. For highly charged particles, the electrostatic force can be thousands of times greater than the force of gravity. The motion induced by electrostatic forces forms the basis for important types of air-cleaning equipment and aerosol sampling and measuring instruments.

15.1 UNITS

A charged particle is acted upon by an electrostatic force near charged surfaces or other charged particles. The force acts remotely through air or vacuum and does not require the flow of current. The charge on a particle can be negative or positive, depending on whether the particle has an excess or deficiency, respectively, of electrons. In this section, we review the basic principles of electrostatics and the system of units used to express electrostatic quantities.

The fundamental equation of electrostatics is *Coulomb's law*, which gives the electrostatic repulsive force F_E between two point charges of like sign separated by a distance R:

$$F_E = K_E \frac{qq'}{R^2} \tag{15.1}$$

where q and q' represent the amount of charge at the two points, and K_E is a constant of proportionality that depends on the system of units used.

Equation 15.1 takes on a different form in the SI and cgs systems of units, because of the way the amount of charge is defined in each system.

In the SI system of units, the ampere (A), one of the seven SI base units, is defined as the current required to produce a specified force between two parallel wires 1 m apart. The units of charge and potential difference are derived from the ampere. The unit of charge, the coulomb (C), is defined as the amount of charge transported in 1 s by a current of 1 A. The unit of potential difference, the volt (V), is defined as the potential difference between two points along a wire carrying 1 A and dissipating 1 watt (W) of power between the points. In the SI system of units, the value of K_E in Eq. 15.1 is

$$K_E = \frac{}{4\pi\epsilon_0} = 9.0 \times 10^9 \quad \mathrm{N \cdot m^2/C^2} \tag{15.2}$$

where ϵ_0 is the permittivity of a vacuum, 8.85×10^{-12} C^2/N · m. Combining Eqs. 15.1 and 15.2 gives

$$F_E = 9.0 \times 10^9 \frac{qq}{R^2} \quad \text{in SI units} \tag{15.3}$$

where F_E is expressed in N, q and q' are in C, and R is in m.

In the cgs electrostatic system of units (esu), the amount of charge is expressed in terms of the statcoulomb (stC), which is defined by Eq. 15.1 as the amount of charge that causes a repulsive force of 1 dyn when two equal charges are separated by 1 cm. The prefix "stat" is used to distinguish cgs units from SI units. Thus, in the cgs system, $K_E = 1$ (dimensionless) and Eq. 15.1 can be simplified to

$$F_E = \frac{qq'}{R^2} \quad \text{in cgs units} \tag{15.4}$$

where F_E is in dyn, q and q' are in stC, and R is in cm. Having defined charge in this way, we must define unit current and unit potential difference in consistent units. Unit current, the statampere (stA), is equal to a flow of charge of 1 stC/s along a wire. Unit potential difference, the statvolt (stV), is defined as the voltage between two points that causes 1 erg of work to be done moving 1 stC of charge between the two points.

The cgs system has the advantage of simplified equations, but the disadvantage of having to use "stat" units. The SI system has the advantage of using common electrical units, but requires including the constant K_E in the equations. Table 15.1 gives conversion factors relating the two systems of units. From the definitions given and Coulomb's law, the following relationships can be derived:

$$\begin{aligned} \text{A} &= \text{C/s} & \text{stA} &= \text{stC/s} \\ \text{V} &= \text{N} \cdot \text{m/C} & \text{stV} &= \text{dyn} \cdot \text{cm/stC} \\ \text{N} &= K_E\text{C}^2/\text{m}^2 & \text{dyn} &= \text{stC}^2/\text{cm}^2 \\ \text{V} &= K_E\text{C/m} & \text{stV} &= \text{stC/cm} \end{aligned} \tag{15.5}$$

where $K_E = 9.0 \times 10^9$ N · m^2/C^2, as defined by Eq. 15.2.

TABLE 15.1 Conversion Factors and Constants for SI and cgs Electrostatic Units

Quantity	SI	cgs
Charge	1 C	3.0×10^9 stC
Current	1 A	3.0×10^9 stA
Potential difference	1 V	0.0033 stV
K_E	9.0×10^9 N · m^2/C^2	
Charge on an electron, e	1.60×10^{-19} C	4.80×10^{-10} stC
Electrons per unit charge	6.3×10^{18}/C	2.1×10^9/stC
Electrical mobility	1 m^2/V · s	3.0×10^6 cm^2/stV · s
Field strength	1N/C or V/m	3.3×10^{-5} dyn/stC or stV/cm

15.2 ELECTRIC FIELDS

An electric field exists in the space around a charged object and causes a charged particle in this space to be acted upon by a force—the electrostatic force. We express the strength of such a field in terms of the magnitude of the force F_E produced per unit charge on the particle. The field strength, or intensity, E is

$$E = \frac{F_E}{q} \tag{15.6}$$

where q is the charge on the particle. The units of field strength are N/C [dyn/stC]. Field strength is a vector that has the same direction as the force F_E. It is common to express the amount of charge q as n multiples of the smallest unit of charge, the charge on an electron e, 1.6×10^{-19} C [4.8×10^{-10} stC].

$$q = ne \tag{15.7}$$

Thus, the force on a particle with n elementary units of charge in an electric field E is

$$F_E = qE = neE \tag{15.8}$$

Equation 15.8 is the basic equation for the electrostatic force acting upon an aerosol particle. The application of the equation is straightforward if the values of n and E are known. The central problem in the application of electrostatic theory to aerosols is the determination of these two quantities. Both n and E can change with time and position, and the magnitude of one can affect the other. Sections 15.1–15.7 address this problem.

Because Coulomb's law provides a relationship between charge, force, and geometry, it can be used to determine the field strength at any point near a charged surface. An imaginary unit charge is positioned at the desired location, and the total electrostatic force on this unit charge is calculated by the vector sum of the Coulombic force due to each charge on the charged surface. The field strength is then computed from the total force by Eq. 15.6. The utility of this method is limited, because we usually do not know the location and magnitude of all the charges on a surface. In theory, the field strength at any point could be determined by placing a real test charge at the point and measuring the electrostatic force on it, but there are many practical difficulties with such measurements.

An alternative definition of field strength is based on voltage or potential, a relatively easy quantity to measure. The potential difference ΔW between two points can be defined as the work required to move a unit charge between the two points. This work is equal to the force per unit charge (the field strength) times the distance between the points, Δx:

$$\Delta W = \frac{\text{force} \times \text{distance}}{q} \tag{15.9}$$

When F_E is expressed by Eq. 15.8 and Eq. 15.9 is rearranged, an alternative definition of field strength is obtained:

$$E = \frac{\Delta W}{\Delta x} \tag{15.10}$$

Thus, the field strength in any direction at a point is equal to the potential gradient in that direction at the point. The determination of field strength is primarily a problem of determining the potential gradient near charged surfaces.

The solution for an electric field (that is, an equation that gives the field strength at any point), can be determined for simple geometries. Three such cases are considered here. The field around a *single point charge q* can be determined easily by placing an imaginary test charge q' in the field and determining the force on it by Coulomb's law and the field strength by Eq. 15.6.

$$E = \frac{F_E}{q'} = \frac{K_E q}{R^2} \tag{15.11}$$

The field strength between two oppositely charged, closely spaced *parallel plates* is uniform in the region between the plates (neglecting edge effects) and is given by

$$E = \frac{\Delta W}{x} \tag{15.12}$$

where ΔW is the algebraic difference in voltage between the two plates and x is the separation between the plates. In a uniform field, the electrostatic force on a charged particle is constant everywhere between the plates. For a positively charged particle, the direction of the force is toward the more negatively charged plate; for a negatively charged particle, the force is directed toward the more positively charged plate.

The field strength inside a *cylindrical tube* with a wire along its axis is given by

$$E = \frac{\Delta W}{R \ln(d_t/d_w)} \tag{15.13}$$

where ΔW is the algebraic difference in voltage between the wire and the tube, R is the radial position for which the field is being calculated, and d_t and d_w are the diameters of the tube and the wire, respectively. Equation 15.13 indicates that the field strength goes to infinity as R goes to zero. The finite diameter of the conducting wire precludes a field at $R = 0$. The maximum field will be at the surface of the wire and will increase as the wire diameter decreases. Equation 15.13 can also be used for the field strength in the space between two concentric cylinders. It becomes much more difficult to calculate the field strength for complex geometries or when there is significant space charge (ions or charged particles in the field region).

In the troposphere, near the earth's surface there is an electric field caused by the difference in potential between the earth's surface (negative) and the upper layers of the atmosphere (positive). In normal, clear weather, the average field strength at sea level is 120 V/m [1.2 V/cm], but it can be 10,000 V/m [100 V/cm] beneath thunderclouds and much higher at the site of a lightning discharge.

EXAMPLE

A particle is positioned 4 cm from a point charge of 10^{-14} C. What is the field strength at the particle? What is the electrostatic force on the particle if it has 100 excess elementary charges?

$$E = \frac{K_E q}{R^2} = \frac{\text{[illegible]}}{(0.04)^2} = 0.056 \text{ V/m}$$

$$= qE = neE = 100 \times 1.6 \times 10^{-19} \times 0.056 = 9.0 \times 10^{-19} \text{ N}$$

In cgs units,

$$[q = 10^{-14} \times 3 \times 10^9 = 3 \times 10^{-5} \text{ stC}$$

$$\left[E = \frac{\text{[illegible]}}{4^2} = 1.88 \times 10^{-6} \text{ stV/cm}\right]$$

$$[F = 100 \times 4.8 \times 10^{-10} \times 1.88 \times 10^{-6} = 9.0 \times 10^{-14} \text{ dyn}]$$

15.3 ELECTRICAL MOBILITY

When a charged particle is placed in an electric field, it is acted upon by a force F_E (Eq. 15.8). The particle velocity resulting from this force can be determined in a manner similar to that for terminal settling velocity. (See Sections 3.3 and 3.7) For particle motion in the Stokes region, the terminal electrostatic velocity V_{TE} is obtained by equating the electrostatic force to Stokes drag (Eq. 3.18) and solving for velocity:

$$neE = 3\pi\eta V d/C_c \tag{15.14}$$

$$V_{TE} = \frac{neEC_c}{3\pi\eta d} \tag{15.15}$$

Equation 15.15 can be written in terms of the particle mechanical mobility B (Eq. 3.16) as

$$V_{TE} = neEB \tag{15.16}$$

To determine V_{TE} when the particle motion is outside the Stokes region, it is necessary to follow a procedure analogous to that used to calculate V_{TS} for Re > 1. (See Section 3.7.) A value of Re > 1 is more common for electrostatic motion than for settling, because the electrostatic force can be much greater than the force of gravity. Equating Eqs. 15.8 and 3.4, we obtain

$$neE = C_D \frac{\pi}{8} \rho_g d^2 V_{TE}^2 \tag{15.17}$$

and solving for C_D gives

$$C_D = \frac{8neE}{\pi \rho_g d^2 V_{TE}^2} \tag{15.18}$$

Multiplying both sides of Eq. 15.18 by Re^2 gives

$$C_D Re^2 = \frac{8neE\rho_g}{\pi \eta^2} \tag{15.19}$$

$C_D Re^2$ can be calculated without knowing the velocity or Reynolds number at the terminal electrostatic velocity. The terminal electrostatic velocity can then be determined from the value of $C_D Re^2$ by Eq. 3.33 with V_{TS} replaced by V_{TE}, or by the graphical or tabular procedures given in Section 3.7.

The Millikan oil-drop experiment, one of the classical experiments of physics in the early 1900s, used the preceding electrostatic principles to measure the charge of an individual electron. The apparatus used, called a Millikan cell, is shown in Fig. 15.1. A spherical, submicrometer-sized particle (an oil droplet) is introduced between two horizontal parallel plates. The potential difference between the plates can be carefully controlled. The particle is illuminated by a beam of light between the plates and observed by a horizontal microscope positioned perpendicular to the

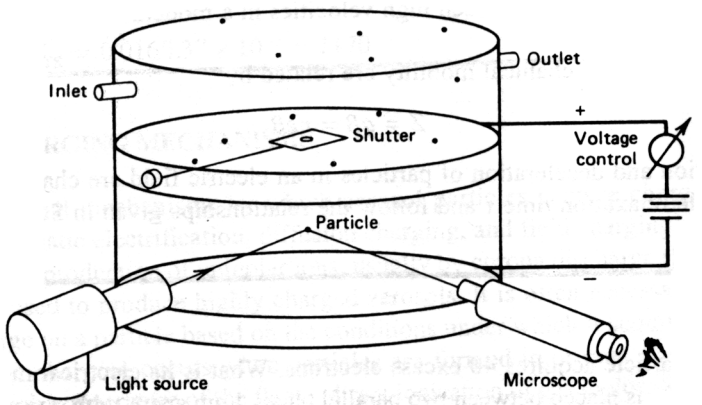

FIGURE 15.1 Apparatus for Millikan oil-drop experiment.

beam . The illuminated particle is seen as a tiny dot of light against a dark background. With no voltage applied to the plates, the diameter of the oil droplet is determined by measuring its settling velocity, as described for the sedimentation cell in Section 3.9. Because of the spray-generation method used, the droplets will ordinarily carry one or more excess electrons. By adjusting the voltage on the upper plate (positive with respect to the lower plate), the upward electrostatic force can be made to balance the force of gravity and the particle held stationary. In this state,

$$neE = \frac{\rho_p \pi d^3 g}{6} \tag{15.20}$$

From thousands of measurements, Millikan found that the value of the charge on a particle was always a whole-number multiple (e, $2e$, $3e$, etc.) of a fundamental unit of charge: the elementary charge, or the charge of an electron, e.

It is convenient to express the ability of a particle to move in an electric field in terms of the particle's *electrical mobility* Z, the velocity of a particle with a charge ne in an electric field of unit strength. Electrical mobility is given by

$$Z = \frac{V_{TE}}{E} = \frac{neC_c}{3\pi\eta d} \quad \text{for Re} < \tag{15.21}$$

$$V_{TE} = ZE \quad \text{for Re} < \tag{15.22}$$

Particle mobility, as given by Eq. 15.21, is based on Stokes drag, and if motion is outside the Stokes region (Re > 1), the true velocity will be greater than that calculated by Eqs. 15.21 and 15.22. Mobility is usually expressed in units of $m^2/V \cdot s$ [$cm^2/stV \cdot s$].

Table 15.2 gives values of mobilities for electrons, ions, and charged aerosol particles with minimum and maximum charge. Ions are charged molecular clusters with an excess or deficiency of one or more electrons, called negative or positive ions, respectively. Air ions are usually singly charged and are formed from air molecules by flames, radiation, or corona discharge. (See Section 15.5.) The ability of highly charged particles to reach high velocities in a moderate electric field is apparent from the table.

Electrical and mechanical mobility are related by

$$Z = qB = neB \tag{15.23}$$

Acceleration and deceleration of particles in an electric field are characterized by the particle relaxation time τ and follow the relationships given in Section 5.2.

EXAMPLE

A 0.6-μm particle acquires 40 excess electrons. What is its electrical mobility? If the particle is placed between two parallel plates 1 cm apart, with one maintained at + 1000 V and the other at –1000 V, what is its terminal electrostatic velocity?

TABLE 15.2 Electrical Mobility of Electrons, Ions, and Aerosol Particles at Standard Conditions

Particle Diameter (μm)	Electrical Mobility ($m^2/V \cdot s$)[a]	
	Singly Charged	Maximum Charge[b]
Electron	6.7×10^{-2}	
Negative air ion	1.6×10^{-4}	
Positive air ion	1.4×10^{-4}	
0.01	2.1×10^{-6}	7.3×10^{-4}
0.1	2.7×10^{-8}	9.3×10^{-4}
1.0	1.1×10^{-9}	$(2.5 \times 10^{-3})^c$
10	9.7×10^{-11}	$(6.7 \times 10^{-3})^c$
100	9.3×10^{-12}	$(1.1 \times 10^{-2})^c$

[a]For mobility in $cm^2/stV \cdot s$, multiply the value shown by 3×10^6.
[b]Based on the ion limit. (See Section 15.6.)
[c]Velocity (m/s) in a unit electric field, but because Re > 1.0, Eq. 15.22 does not hold.

The particle's mechanical mobility can be obtained from Table A11

$$Z = neB = 40 \times 1.6 \times 10^{-19} \times 1.23 \times 10^{10} = 7.9 \times 10^{-8} \text{ m}^2/\text{V} \cdot \text{s}$$

$$[40 \times 4.8 \times 10^{-10} \times 1.23 \times 10^{7} = 0.24 \text{ cm}^2/\text{stV} \cdot \text{s}]$$

$$E = \frac{\Delta W}{} = \frac{+1000 - (-1000)}{0.01} = 200{,}000 \text{ V/m} \quad \left[\frac{2000 \times 0.0033}{1} = 6.6 \text{ stV/cm}\right]$$

$$V_{TE} = ZE = 7.9 \times 10^{-8} \times 200{,}000 = 0.016 \text{ m/s} \quad [0.24 \times 6.6 = 1.6 \text{ cm/s}]$$

Re $66{,}000 \times 0.016 \times 0.6 \times 10^{-6} = 6.3 \times 10^{-4}$ $[6.6 \times 1.6 \times 0.6 \times 10^{-4} = 6.3 \times 10^{-4}]$

Note: $V_{TE}/V_{TS} = 0.016/1.37 \times 10^{-5} = 1170$

15.4 CHARGING MECHANISMS

The principal mechanisms by which aerosol particles acquire charge are flame charging, static electrification, diffusion charging, and field charging. The last two require the production of unipolar ions, usually by corona discharge (Section 15.5), and are used to produce highly charged aerosols. It is often necessary to estimate the charge on a particle based on the conditions under which it acquires the charge.

Flame charging occurs when particles are formed in or pass through a flame. At the high temperature of the flame, direct ionization of gas molecules creates high concentrations of positive and negative ions and thermionic emissions of electrons

or ions from particles. The net charge acquired by the particles depends on the material and is usually symmetric with respect to polarity (equal numbers of positively and negatively charged particles).

Static electrification causes particles to become charged by mechanical action as they are separated from the bulk material or other surfaces. This charging mechanism can produce highly charged particles under the right circumstances, but is not reliable for aerosol charging. It can be extremely important, for example, when dealing with explosive dusts. Particles are usually charged by static electrification during their formation, resuspension, or high-velocity transport. The three primary mechanisms of static electrification that can charge aerosol particles during their generation are electrolytic charging, spray electrification, and contact charging.

Electrolytic charging results when liquids with a high-dielectric constant are separated from solid surfaces. During atomization these liquids strip off charge from the surfaces of the atomizer and produce slightly to moderately charged droplets as the liquids separate from the surfaces. Pure water is a high dielectric liquid that can become charged during atomization. *Spray electrification* results from the disruption of charged liquid surfaces. Due to surface effects, some liquids have a charged surface layer, and when the surface is disrupted during the formation of droplets by atomization or bubbling, charged droplets are produced. *Contact charging*, or triboelectrification, occurs during the separation of dry, nonmetallic particles from solid surfaces. When a particle contacts a surface, charge is transferred between the particle and the surface such that the particle acquires a net positive or negative charge when it separates from the surface. The particle's polarity and the amount of charge on the particle depend on the materials involved and their relative positions in the triboelectric series. Friction increases the amount of charge acquired. Rubbing leather shoes on a woolen rug is a common example of this mechanism. Because it requires dry surfaces, contact charging becomes ineffective at relative humidities greater than about 65%. Most methods of resuspending dry powders involve some friction between the powder and the apparatus and, consequently, produce charged particles.

When an ion collides with a particle, it sticks, and the particle acquires its charge. Particles mixed with unipolar ions (all of the same sign) become charged by random collisions between the ions and the particles. This process is called *diffusion charging* because the collisions result from the Brownian motion of the ions and particles. This mechanism does not require an external electrical field and, to a first approximation, does not depend on the particle material. As the charge accumulates, it produces a field that tends to repel additional ions, reducing the charging rate. The ions, being in equilibrium with the gas molecules, have a Boltzmann distribution of velocities. As the charge on the particle increases, fewer and fewer ions have sufficient velocity to overcome the repulsive force, and the charging rate slowly approaches zero. It never reaches zero, however, because the Boltzmann distribution of velocities has no upper limit.

An approximate expression for the number of charges $n(t)$ acquired by a particle of diameter d_p by diffusion charging during a time t is

$$n(t) = \frac{d_p kT}{2K_E e^2} \ln\left[1 + \frac{\pi K_E d_p \bar{c}_i e^2 N_i t}{2kT}\right] \quad (15.24)$$

where $\bar{c}_i$ is the mean thermal speed of the ions ($\bar{c}_i$ = 240 m/s [2.4 × 10^4 cm/s] at standard conditions) and N_i is the concentration of ions. At standard conditions, for $N_i t > 10^{12}$ s/m^3 [10^6 s/cm^3], Eq. 15.24 is accurate to within a factor of two for particles from 0.07 to 1.5 μm and, for $N_i t > 10^{13}$ s/m^3 [10^7 s/cm^3], to within a factor of two for particles from 0.05 to 40 μm. A more accurate, but less convenient, expression requiring numerical integration is given by Lawless (1996). Even in the presence of an electrostatic field, diffusion charging is the predominant mechanism for charging particles less than 0.2 μm in diameter. A process similar to diffusion charging, but utilizing bipolar ions, is used to discharge highly charged aerosols, see Section 15.7.

Field charging is charging by unipolar ions in the presence of a strong electric field. This mechanism is depicted in Figs. 15.2*a*–15.2*c*, in which the negatively charged plate is at the left and negative ions are present. The rapid motion of ions in an electric field results in frequent collisions between the ions and the particles. When an uncharged spherical particle is placed in a uniform electric field, it distorts the field, as shown in Fig. 15.2*a*. The field lines shown represent the trajectories of ions. The extent of the distortion of the field lines depends on the relative permittivity (dielectric constant) ε of the particle material and the charge on the particle. For an uncharged particle, the greater the value of ε, the greater the number of field lines that converge on the particle.

Ions in this electric field travel along the field lines and collide with the particle where the field lines intersect the particle. All ions on intersecting lines to the left of the particle will collide with the particle and transfer their charge to it. As the particle becomes charged, it will tend to repel the like-charged incoming ions. This situation is shown in Fig. 15.2*b*, in which the particle is partially charged. The presence of the charge on the particle reduces the field strength and the number of field lines converging on the particle from the left and increases these two quantities on the right. Because of these changes, the rate of ions reaching the particle decreases as the particle becomes charged.

Ultimately, the charge builds up to the point where no incoming field lines converge on the particle (Fig. 15.2*c*) and no ions can reach the particle. At this maximum-charge condition, the particle is said to be at *saturation charge*.

When diffusion charging can be neglected, the number of charges, n, acquired by a particle during a time t in an electric field E with an ion number concentration N_i is

$$n(t) = \left(\frac{3\varepsilon}{\varepsilon + 2}\right)\left(\frac{Ed^2}{}\right)\left(\frac{\pi K_E e Z_i N_i t}{}\right) \quad (15.25)$$

where ε is the relative permittivity of the particle and Z_i is the mobility of the ions, approximately 0.00015 m^2/V · s [450 cm^2/stV · s]. In this equation, the first two fac-

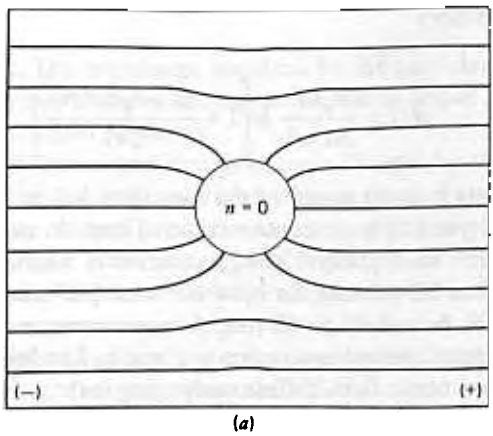

(a)

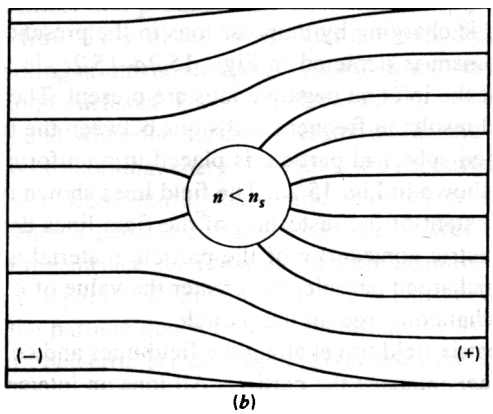

(b)

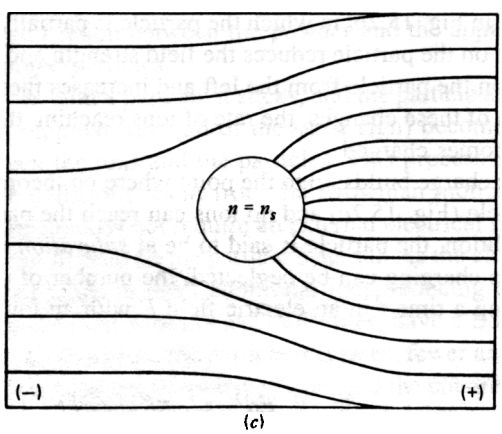

(c)

FIGURE 15.2 Electric field lines for a conducting particle in a uniform field (negative ions and negative plate at left). (*a*) An uncharged particle. (*b*) A partially charged particle. (c) A particle at saturation charge.

tors represent the saturation charge n_s reached after sufficient time at a given charging condition.

$$\left(\frac{3\varepsilon}{\varepsilon+2}\right)\left(\frac{Ed^2}{4K_E e}\right) \tag{15.26}$$

The first factor on the right in Eqs. 15.25 and 15.26 depends only on the material of the particle and ranges from 1.0 for $\varepsilon = 1$ to 3.0 for $\varepsilon = \infty$. The relative permittivity, or dielectric constant ε, reflects the strength of the electrostatic field produced in different materials by a fixed potential relative to that produced in a vacuum under the same conditions. For most materials, $1 < \varepsilon < 10$; ε is 1.0 for a vacuum, 1.00059 for air, 5.1 for DOP, 4.3 for quartz, 80 for pure water, and is infinite for conducting particles. The second factor in Eq. 15.25 indicates that the saturation charge is proportional to the surface area of the particle and to the electrostatic field strength. The final factor is a time-dependent term that reaches a value of 1 when $\pi K_E e Z_i N_i t >> 1.0$. The rate of charging does not depend on the particle size or field strength, but only on the ion concentration. When particles are intentionally charged by field charging, the ion concentration is usually $10^{13}/m^3$ [$10^7/cm^3$] or greater, so charging will be 95% complete in 3 s or less.

The charge that is acquired is proportional to d_p^2 in field charging and to d_p in diffusion charging, so field charging is the dominant mechanism for particles larger than 1.0 μm, and diffusion charging is the dominant mechanism for particles less than 0.1 μm, even in the presence of an electric field. Between these sizes, both mechanisms are operating and the situation is much more complicated. Equations 15.24 and 15.25, while explicit, involve restrictive assumptions and are somewhat oversimplified. More accurate expressions exist, but they are not explicit and usually require computer calculation. Lawless (1996) presents approximations for charging rates that are applicable to diffusion, field, and combined charging. The charging rate obtained must be numerically integrated to get the charge acquired by a particle in a given period. Table 15.3 gives the number of charges acquired in 1 s by particles of various sizes by the diffusion, field, and combined charging mechanisms at an ion concentration of $10^{13}/m^3$ [$10^7/cm^3$]. For the conditions of the table calculations, the field-charging equation, Eq. 15.25, is accurate for particles larger than 5 μm, and Eq. 15.24 is useful from 0.2 to 2 μm. Figure 15.3 shows the number of charges acquired by a particle having $\varepsilon = 5.1$ for various charging conditions.

Figure 15.4 shows particle mobility versus particle size for a typical field-charging condition. Although particle charge decreases with particle size, mechanical mobility increases rapidly with decreasing size; consequently, there is a size for minimum electrical mobility in the submicrometer range. Also, mobility under typical charging conditions is a relatively weak function of particle size in the size range 0.1–1 μm.

EXAMPLE

How many elementary charges are acquired by a 2.0-μm water droplet in 1 s by (a) diffusion charging in an ion concentration of $10^{13}/m^3$ [$10^7/cm^3$] and (b) field

TABLE 15.3 Comparison of Calculation Methods for Charging by Field, Diffusion, and Combined Charging at $N_i t = 10^{13}$ s/m^3 [10^7 s/cm^3]. $\varepsilon = 5.1$.

Particle Diameter (μm)	Number of Elementary Units of Charged Acquired			
	Diffusion Charging		Field Charging E = 500 kV/m [5 kV/cm] Eq. 15.25	Combined Charging E = 500 kV/m [5 kV/cm] Numerical Solution[a]
		Numerical Solution[a]		
0.01	0.10	0.41	0.02	0.42
0.04	0.79	1.6	0.26	1.9
0.1	2.7	4.1	1.6	5.6
0.4	15.7	16.3	25.9	40
1.0	47	41	162	162
4.0	237	163	2580	2680
10	673	407	16,200	16,540
40	3180	1630	259,000	264,000

[a]Lawless (1996)

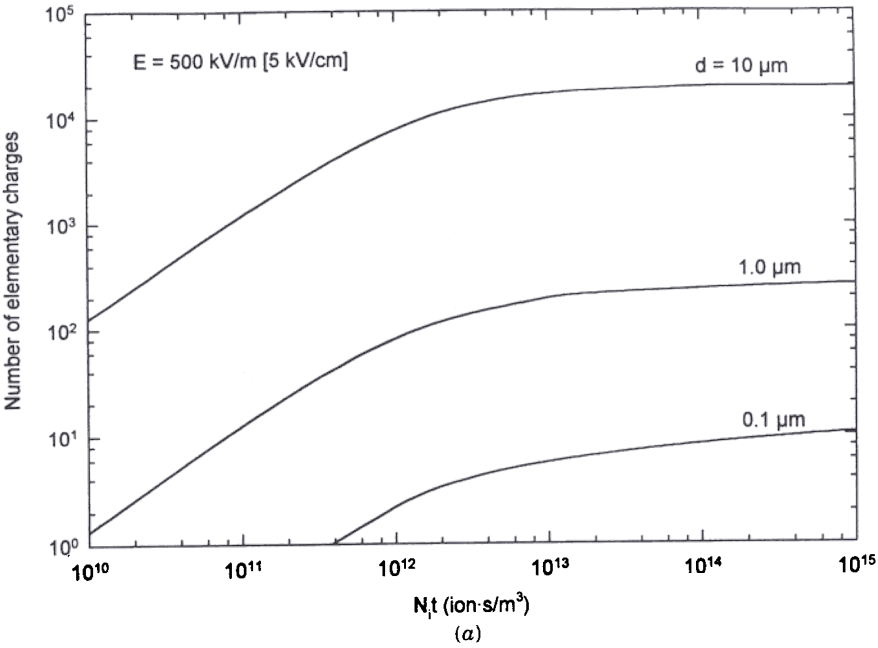

FIGURE 15.3 Field and diffusion charging. (*a*) Number of charges acquired versus $N_i t$ for particle diameters of 0.1, 1, and 10 μm at a field strength of 500 kV/m [5 kV/cm]. (*b*) Number of charges acquired versus particle diameter for field strengths of 0, 100, 1000, and 10,000 V/cm at $N_i t = 10^{13}$ s/m^3 [10^7 s/cm^3]. $\varepsilon = 5.1$.

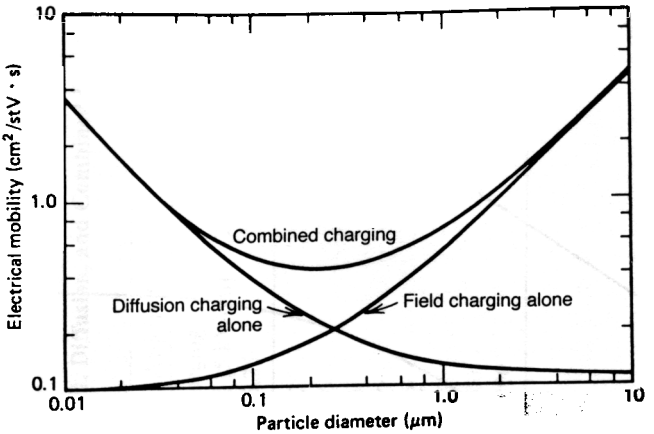

FIGURE 15.4 Electrical mobility versus particle size for diffusion, field, and combined charging at $E = 500$ kV/m [5 kV/cm] and $N_i t = 10^{13}$ s/m^3 [10^7 s/cm^3].

charging in an ion concentration of 10^{13}/m^3 [10^7/cm^3] and an electric field of 600 kV/m [6 kV/cm]?

(a) In SI units,

$$n = \frac{2 \times 10^{-6} \times 1.38 \times 10^{-23} \times 293}{2 \times 9 \times 10^9 \times (1.6 \times 10^{-19})^2} \times \ln\left(1 + \frac{\pi \times 9 \times 10^9 \times 2 \times 10^{-6} \times 240 \times (1.6 \times 10^{-19})^2 \times 10^{13} \times}{2 \times 1.38 \times 10^{-23} \times 293}\right)$$

$$= 17.6 \ln(1 + 430) \quad \mathrm{m \cdot N \cdot m \cdot K^{-1} \cdot K/(N \cdot m^2 \cdot C^{-2} \cdot C^2)} = 106$$

In cgs units,

$$n = \frac{2 \times 10^{-4} \times 1.38 \times 10^{-16} \times 293}{2 \times 1 \times (4.8 \times 10^{-10})^2} \times \ln\left(1 + \frac{\pi \times 1 \times 2 \times 10^{-4} \times 2.4 \times 10^{-4} \times (4.8 \times 10^{-10})^2 \times 10^7 \times}{2 \times 1.38 \times 10^{-16} \times 293}\right)$$

$$= 17.6 \ln(1 + 430) \quad \mathrm{cm \cdot dyn \cdot cm \cdot K^{-1} \cdot K/stC^2} = 106$$

(b) In SI units,

$$\frac{3\varepsilon}{\varepsilon + 2} = \frac{3 \times 80}{80 + 2} = 2.93$$

$$\frac{Ed^2}{4K_E e} = \frac{600{,}000 \times (2 \times 10^{-6})^2}{4 \times 9 \times 10^9 \times 1.6 \times 10^{-19}} = 417 \frac{\text{V} \cdot \text{m}^{-1} \cdot \text{m}^2}{\text{N} \cdot \text{m}^2 \cdot \text{C}^{-2} \cdot \text{C}}$$

$$\pi K_E e Z_i N_i t = \pi \times 9 \times 10^9 \times 1.6 \times 10^{-19} \times 0.00015 \times 10^{13} \times \quad = 6.79 \frac{\text{N} \cdot \text{m}^2 \cdot \text{C} \cdot \text{m}^2 \cdot \text{s}}{\text{C}^2 \cdot \text{V} \cdot \text{s} \cdot \text{m}^3}$$

$$n = 2.93 \times 417 \times \left(\frac{6.79}{6.79 + 1} \right) = 1065$$

In cgs units,

$$\frac{3\varepsilon}{\varepsilon + 2} = \frac{3 \times 80}{80 + 2} = 2.93$$

$$\frac{Ed^2}{4K_E e} = \frac{(6000/300) \times (2 \times 10^{-4})^2}{4 \times 1 \times 4.8 \times 10^{-10}} = 417 \text{ stV} \cdot \text{cm}^{-1} \cdot \text{cm}^2/\text{stC}$$

$$\pi K_E e Z_i N_i t = \pi \times 1 \times 4.8 \times 10^{-10} \times 450 \times 10^7 \times 1 = 6.79 \frac{\text{stC} \cdot \text{cm}^2 \cdot \text{s}}{\text{stV} \cdot \text{s} \cdot \text{cm}^3}$$

$$n = 2.93 \times 417 \times \left(\frac{6.79}{6.79 + 1} \right. = 1065$$

15.5 CORONA DISCHARGE

The field- and diffusion-charging methods described in the previous section require high concentrations of unipolar ions. Because of the mutual repulsion and high mobilities of those ions, their lifetime is brief. Consequently, ions must be continuously produced to use these charging methods. Ions can be created in air by radioactive discharge, ultraviolet radiation, flames, and corona discharge. Only the corona discharge can produce unipolar ions at a high enough concentration to be useful for aerosol charging.

To produce a corona discharge, one must establish a nonuniform electrostatic field, such as that between a needle and a plate or between a concentric wire and a tube, as described in Section 15.2. Air and other gases are normally very good insulators, but in a region of sufficiently high field strength, air undergoes an electrical breakdown and becomes conductive. Depending on the geometry of the field, this breakdown can be an arc or a corona discharge. For a wire-and-tube geometry, the only region with sufficient field strength for breakdown is a thin layer at the surface of the wire. The field strength required for breakdown depends on the wire diameter d_w and is given by the empirical equation (White, 1963),

$$E_b = 3000 + 127 d_w^{-1/2} \text{ kV/m} \quad [30 + 12.7 d_w^{-1/2} \text{ kV/cm}] \qquad (15.27)$$

where d_w is in m [cm]. For a wire diameter of 1 mm, E_b is 7000 kV/m [70 kV/cm]. Figure 15.5 shows the field around a 1-mm wire maintained at 50 kV in a tube with a diameter of 0.2 m [20 cm]. A region 0.8 mm thick around the wire exceeds 7000 kV/m [70 kV/cm] and is the corona discharge region. The low field strength near the tube prevents arcing. This would not be the case for the uniform field between two parallel plates where electrical breakdown would occur in the entire region between the plates and would cause an arc.

In the corona region, electrons are accelerated to a velocity sufficient to knock an electron from an air molecule upon collision and thereby create a positive ion and a free electron. Within the corona region, this process takes place in a self-sustaining avalanche that produces a dense cloud of free electrons and positive ions around the wire called *corona discharge*. The process is initiated by electrons and ions created by natural radiation. If the wire is positive with respect to the tube, the electrons will move rapidly to the wire, and the positive ions will stream away from the wire to the tube in a unipolar "ion wind." If the wire is negative, the positive ions will go to it, and the electrons will be repelled toward the tube. As their velocity slows with the decreasing field strength at greater distances from the wire, the electrons attach to air molecules (if an electronegative gas such as oxygen is present) and form negative ions, which stream across to the tube. In either case, the ions migrate from the wire to the tube in high concentrations of 10^{12}–10^{15}/m^3

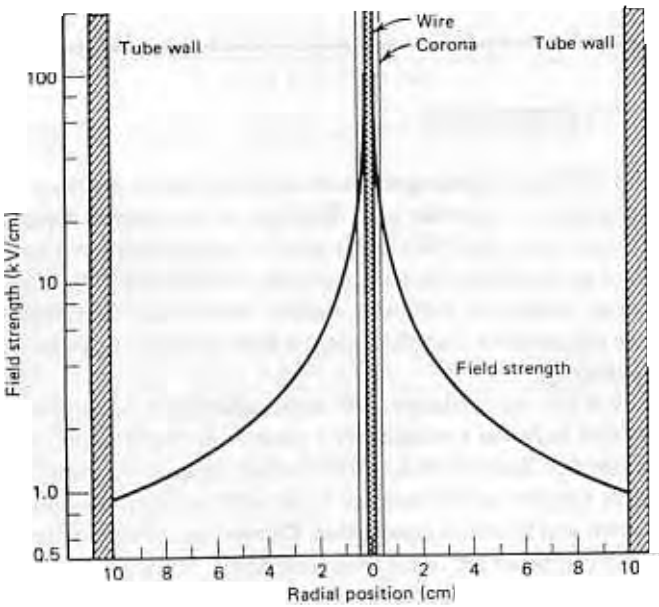

FIGURE 15.5 Field strength in a tube of diameter 0.2 m [20 cm] with a concentric wire 1 mm in diameter at 50 kV. Corona region not to scale.

[10^6–10^9/cm^3] and at high velocities of about 75 m/s [7500 cm/s] for the conditions of Fig. 15.5.

Positive and negative coronas have quite different properties and appearances. With positive corona, the entire region around the wire has a stable, glowing sheath with a characteristic bluish-green color. With negative corona, the corona glow exists in tufts or brushes that appear to be in a dancing motion over the surface of the wire. These tufts may be several millimeters in length. There is sufficient energy in the corona region to produce ozone from oxygen. A negative corona produces about 10 times as much ozone as a positive corona. Indoor and recirculating electrostatic precipitators use positive corona for this reason. Industrial electrostatic precipitators usually use negative corona, because they can be operated at higher voltages and thereby achieve higher efficiencies. Gas temperature, pressure, and composition affect corona generation.

The introduction of aerosol particles into the space between the wire and the tube will result in field charging of the particles to the same polarity as the wire. The field used to create the corona and the ion wind also causes the field charging. If clean air is blown through the tube at high velocity, it will carry the unipolar ions out of the field region, where they may be mixed with aerosol particles for diffusion charging.

15.6 CHARGE LIMITS

There are fundamental limits on the maximum amount of charge that can be acquired by an aerosol particle of a given size. In the presence of strong external electrostatic fields, aerosol particles can exhibit corona discharge. The loss of charge by this mechanism sets an upper limit on the charge for a given particle size that is on the order of the corona onset voltage for a sphere of that size. This type of corona discharge has been observed surrounding raindrops during a thunderstorm and in the laboratory. In the more usual case, where there is no strong external field, a much higher charge can be achieved before the limit of spontaneous charge loss is reached.

For negatively charged solid particles, the maximum charge is reached when the self-generated field at the surface of a particle (see Eq. 15.11) reaches the value required for spontaneous emission of electrons from a surface. When this limit is exceeded, the crowding of electrons on the surface of the particle causes electrons to be ejected from the particle by the force of mutual repulsion. For spherical particles, this limit is

$$n_L = \frac{d_p^2 E_L}{4K_E e} \tag{15.28}$$

where E_L is the surface field strength required for spontaneous emission of electrons, 9.0×10^8 V/m [3×10^4 stV/cm]. This charge limit is proportional to the surface area of the particle, as expected.

A similar limit exists for positively charged particles; the only difference is that a positive ion must be emitted instead of an electron. Howeever, emitting a positive ion is a more difficult process and requires a greater surface field strength. Equation 15.28 can be used with a value of $E_L = 2.1 \times 10^{10}$ V/m [7×10^5 stV/cm] to estimate the limit. Values for the positive and negative limits are shown as a function of particle size in Fig. 15.6.

A different type of limit, called the Rayleigh limit, exists for liquid droplets. When the mutual repulsion of electric charges within a droplet exceeds the confining force of surface tension, the droplet shatters into smaller droplets. The limiting charge is given by

$$n_L = \left(\frac{2\pi\gamma d_p^3}{K_E e^2}\right)^{1/2} \tag{15.29}$$

where γ is the surface tension of the droplet liquid. As shown in Fig. 15.6, the Rayleigh limit is the controlling limit for most water droplets, because it will be reached before the surface emission limits are reached. A moderately charged droplet will become highly charged as it evaporates to a smaller size. Eventually, the droplet will reach the Rayleigh limit and disintegrate. When the droplet disintegrates, the fragments are below the Rayleigh limit because the same amount of charge is now distributed over a larger surface.

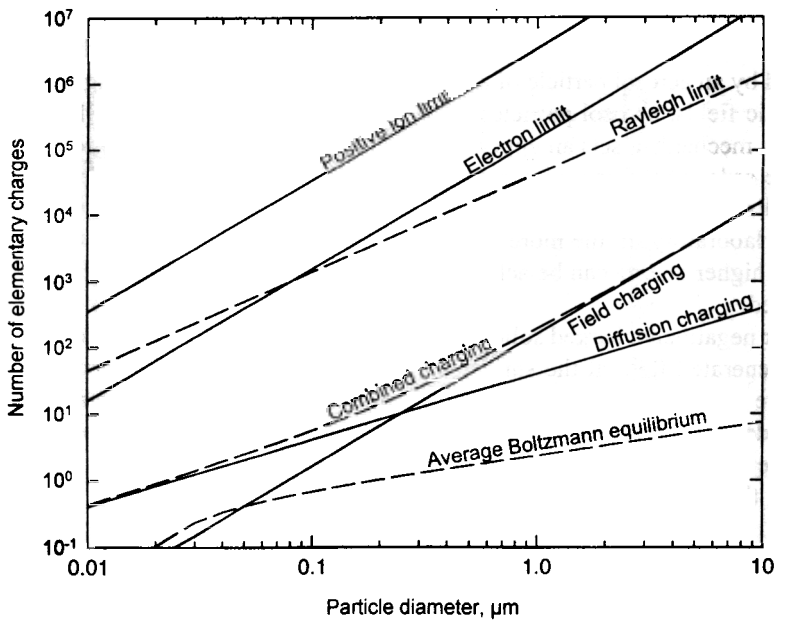

FIGURE 15.6 Particle charge limits. Rayleigh limit for water ($\gamma = 0.073$ N/m [73 dyn/cm]), diffusion charging at $N_i\, t = 10^{13}$ s/m^3 [10^7 s/cm^3] and field charging at $E = 500$ kV/m [5 kV/cm] and $N_i\, t = 10^{13}$ s/m^3 [10^7 s/cm^3]. $\varepsilon = 5.1$.

EXAMPLE

What is the maximum charge for a negatively charged ·μm sphere?

$$n_L = \frac{d_p^2 E_L}{4K_E e} = \frac{(10^{-6})^2 \times 9 \times 10^8}{4 \times 9 \times 10^9 \times 1.6 \times 10^{-19}}$$

$$\left[= \frac{(10^{-4})^2 \times 3 \times 10^4}{4 \times 1 \times 4.8 \times 10^{-10}} \right]$$

15.7 EQUILIBRIUM CHARGE DISTRIBUTION

The minimum charge an aerosol particle can have is zero. This condition is rarely achieved, because of random collisions of aerosol particles with the omnipresent air ions. As explained in Chapter 14, every cubic centimeter of air contains about 10^3 ions with approximately equal numbers of positive and negative ions. Aerosol particles that are initially neutral will acquire charge by collision with ions due to their random thermal motion. Aerosol particles that are initially charged will lose their charge slowly as the charged particles attract oppositely charged ions. These competing processes eventually lead to an equilibrium charge state called the *Boltzmann equilibrium* charge distribution (also called the steady-state, stationary, or bipolar equilibrium charge distribution). The Boltzmann equilibrium charge distribution represents the charge distribution of an aerosol in charge equilibrium with bipolar ions. This minimum amount of charge is very small, with a statistical probability that some particles will have no charge and others will have one or more charges. For equal concentrations of positive and negative ions, a reasonable first approximation for normal air, the fraction of particles f_n of a given size having n positive (or n negative) elementary units of charge is given by

$$f_n = \frac{\exp(K_E n^2 e^2 / d_p kT)}{\sum_{n=-\infty}^{\infty} \exp(K_E n^2 e^2 / d_p kT)} \tag{15.30}$$

For particles larger than 0.5 μm, Eq. 15.30 becomes identical to the equation representing the normal distribution and can be written in an easier-to-use form as

$$f_n = \left(\frac{K_E e^2}{\pi d_p kT} \right)^{1/2} \exp\left(\frac{-K_E n^2 e^2}{d_p kT} \right) \tag{15.31}$$

This equation agrees with Eq. 15.30 to within 7% for particles larger than 0.02 μm and to within 0.04% for particles larger than 0.05 μm. For particles less than about 0.05 μm, both Eq. 15.30 and 15.31 underestimate the fraction of charged particles, and more complicated procedures must be used. [See Hoppel and Frick (1986).]

Table 15.4 gives the percentage of particles of a given size having the indicated charge. The distribution is symmetrical about zero; that is, the fraction of particles with n positive charges equals the fraction with n negative charges. As a practical matter, for particles less than 0.1 μm in diameter, the distribution consists of a fraction that is uncharged and a remaining fraction, which is singly charged with equal fractions charged positively and negatively. The average charge given in the table is the average charge calculated without regard to sign. The average Boltzmann equilibrium charge is compared with other charge conditions in Fig. 15.6. An empirical approximation for the average number of charges $\bar{n}$ is

$$\bar{n} \approx 2.37\sqrt{d_p} \tag{15.32}$$

where d_p is in μm. Equation 15.32 provides satisfactory accuracy (±5%) for particles larger than 0.2 μm.

EXAMPLE

What fraction of 1-μm particles at Boltzmann equilibrium carry +2 charges?

$$\left(\frac{9\times10^{9}\times(1.6\times10^{-19})^{2}}{\pi\times10^{-6}\times1.38\times10^{-23}\times293}\right)^{1/2}\exp\left(\frac{-9\times10^{9}\times2^{2}\times(1.6\times10^{-19})^{2}}{10^{-6}\times1.38\times10^{-23}\times293}\right)=0.107$$

$$\left[\left(\frac{1\times(4.8\times10^{-10})^{2}}{\pi\times10^{-4}\times1.38\times10^{-16}\times293}\right)^{1/2}\exp\left(\frac{-1\times2^{2}\times(4.8\times10^{-10})^{2}}{10^{-4}\times1.38\times10^{-16}\times293}\right)=0.107\right]$$

The rate at which an aerosol reaches the Boltzmann equilibrium charge distribution depends on the concentration of bipolar ions and is given by

$$\frac{n(t)}{n_0} = \exp(-4\pi K_E e Z_i N_i t) \tag{15.33}$$

where $n(t)$ is the number of charges on a particle after it has been exposed to a bipolar ion concentration N_i for a time t if it had n_0 charges at time $t = 0$. The fractional discharge rate does not depend on the particle size or the initial charge. Equation 15.33 is most useful when there is an excess of bipolar ions, so that N_i can be considered constant. The discharge of aerosols to Boltzmann equilibrium depends on the product $N_i t$; that is, the same result is reached for different ion concentrations when the value of $N_i t$ is the same.

Equation 15.33 indicates that rapid discharge of a highly charged aerosol can be achieved by mixing the aerosol with a high concentration of bipolar ions. One method uses an alternating-current corona discharge in a sonic velocity jet of air. The bipolar ions that are produced are swept out of the field region by the sonic

TABLE 15.4 Distribution of Charge on Aerosol Particles at Boltzmann Equilibrium

Particle Diameter (μm)	Average Number of Charges	Percentage of Particles Carrying the Indicated Number of Charges								
		< –3	–3	–2	–1	0	+1	+2	+3	>+3
0.01	0.007				0.3	99.3	0.3			
0.02	0.104				5.2	89.6	5.2			
0.05	0.411			0.6	19.3	60.2	19.3	0.6		
0.1	0.672		0.3	4.4	24.1	42.6	24.1	4.4	0.3	
0.2	1.00	0.3	2.3	9.6	22.6	30.1	22.6	9.6	2.3	0.3
0.5	1.64	4.6	6.8	12.1	17.0	19.0	17.0	12.1	6.8	4.6
1.0	2.34	11.8	8.1	10.7	12.7	13.5	12.7	10.7	8.1	11.8
2.0	3.33	20.1	7.4	8.5	9.3	9.5	9.3	8.5	7.4	20.1
5.0	5.28	29.8	5.4	5.8	6.0	6.0	6.0	5.8	5.4	29.8
10.0	7.47	35.4	4.0	4.2	4.2	4.3	4.2	4.2	4.0	35.4

jet and into a mixing chamber with the charged particles. A more common approach is to use a radioactive source, such as polonium-210 or krypton-85 gas in a thin stainless-steel tube, to ionize the air molecules inside a chamber through which the aerosol to be discharged flows. The volume of the chamber is such that it provides sufficient residence time for the aerosol to be "neutralized," or brought to the Boltzmann equilibrium charge distribution. A value of $N_i t$ of 6×10^{12} ion $\cdot$ s/m^3 [6×10^6 ion $\cdot$ s/cm^3] is required for complete neutralization of highly charged particles. In commercial radioactive aerosol neutralizers, this level of neutralization is achieved in about 2 s. In the atmosphere, where the normal bipolar ion concentration is about 10^9 ions/m^3 [10^3 ions/cm^3], the same effect is achieved in 100 min.

15.8 ELECTROSTATIC PRECIPITATORS

Electrostatic precipitators use electrostatic forces to collect charged particles for aerosol sampling and air cleaning. These forces act only on the particles and can be much greater than the corresponding gravitational or inertial forces. The principles are the same for sampling and air cleaning, but the size scale differs greatly, by a factor of 10^8 in the extreme. The two basic steps are to charge the particles and to subject them to an electric field so that their electrostatic migration velocity causes them to deposit on a collection surface. A third step, that of removing the deposited particles, is necessary for continued operation of air-cleaning precipitators. As a class, these devices are characterized by low pressure drop, high efficiency for small particles, and the ability to handle high dust concentrations.

In an electrostatic precipitator, particles are usually charged by field charging using a corona discharge. Two-stage precipitators have separate sections for charging and precipitation. In a single-stage precipitator the corona wires are in the precipitation section, and the same field that creates the corona also causes the precipitation. Normally, the field and the ion concentration are such that the particles reach their saturation charge in less than a second.

The charged aerosol flows through an electric field oriented perpendicular to the direction of flow and to the collection surface, which is usually the inside of a metal tube or a flat plate. For a laminar-flow precipitator, particle collection is analogous to the gravity-settling chamber described in Section 3.9 and shown in Fig. 3.6. All particles with $V_{TE} > HV_x/L$, where H is the distance from wires to collection plates in a single-stage precipitator and between the plates in a two-stage precipitator, V_x is the flow velocity, and L is the dimension along the flow direction, will be collected with 100% efficiency. For a given charging condition, there is a particle size with minimum mobility (see Fig. 15.4) a laminar-flow precipitator designed to completely capture this size particle will be 100% efficient for all particle sizes.

In air-cleaning electrostatic precipitators, the flow is turbulent and the collection situation is analogous to stirred settling, as described in Section 3.8. Consider the wire-and-tube geometry shown in cross section in Fig. 15.7. In a period dt that is brief compared with that required for turbulent mixing, all particles within a distance $V_{TE}dt$ of the tube wall will be removed. For simplicity, we assume that par-

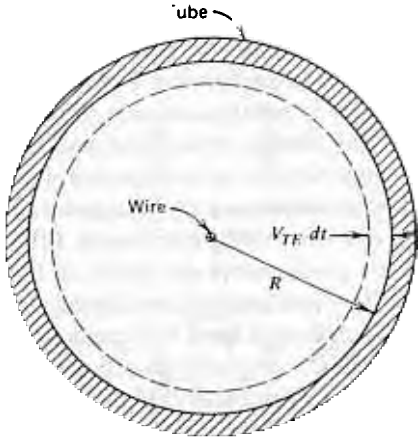

FIGURE 15.7 Cross section of a wire-and-tube electrostatic precipitator.

ticles stick if they touch the wall and are not reentrained. The fraction of particles removed during this period, dN/N, *is* the negative ratio of the area of the annulus, $2\pi R V_{TE} dt$, to the total cross-sectional area of the tube, πR^2, and is given by

$$\frac{dN}{N} = -\frac{2\pi R V_{TE} dt}{\pi R^2} = -\frac{2V_{TE} dt}{R} \tag{15.34}$$

This equation can be integrated to obtain the number concentration after a time

$$\int_{N_0}^{N(t)} \frac{dN}{N} = \int_0^t \frac{-2V_{TE}}{R} dt \tag{15.35}$$

$$\frac{N(t)}{N_0} = \exp\left(\frac{-2V_{TE}t}{R}\right) \tag{15.36}$$

For a tube of length L and a volumetric flow rate Q, the residence time in the tube, $\pi R^2 L/Q$, can be substituted into Eq. 15.36 to get the penetration—the fraction of the inlet concentration that exits the tube:

$$P = \frac{N_{out}}{N_0} = \exp\left(\frac{-2\pi V_{TE} RL}{Q}\right) \tag{15.37}$$

It is customary to express Eq. 15.37 in terms of collection efficiency and the area of the collection surface, $A_c = 2\pi RL$. Doing so gives the Deutsch–Anderson equation,

$$\mathbf{E} = -\exp\left(\frac{-V_{TE} A_c}{Q}\right) \tag{15.38}$$

This is the basic scaling equation for electrostatic precipitators. It assumes that the particles are uniformly distributed across every cross section and become fully charged as soon as they enter the precipitator. It predicts the change in efficiency that will result from changes in precipitator size, flow rate, and V_{TE}. Equations 15.36–15.38 suggest that any change in the precipitator size or flow rate that increases the aerosol residence time in the precipitator will increase its efficiency. Similarly, increasing V_{TE} by increasing the charge on the particles or the field strength will increase the efficiency of the precipitator. Efficiencies for laminar- and turbulent-flow electrostatic precipitators are shown in Fig. 15.8. The 100% efficiency point for laminar-flow precipitators corresponds to the $1 - 1/e$ point for a turbulent-flow precipitator. Although Eq. 15.38 predicts that any efficiency (up to 100%) can be achieved, the efficiency of high-efficiency air-cleaning units is not controlled by that equation, but by secondary effects such as a nonuniform flow distribution, reentrainment, and excess resistivity in the layer of deposited dust.

The point-to-plane type of electrostatic precipitator is used for sampling aerosols for electron microscope studies and for piezoelectric measurement of mass. As shown in Fig. 15.9, the corona and precipitating fields are formed between a corona needle (the point) and a flat collection surface (the plane). Depending on the design, the separation between the point and the plane is from 3 to 40 mm, flow rates are from 0.5 to 5 L/min, and voltages are from 2 to 15 kV. When used for sampling for electron microscopy, the particles are deposited directly onto a carbon-coated electron microscope grid 3 mm in diameter. From simple geometric consideration, this small target results in a low collection efficiency—as low as a few percent. The absolute collection efficiency is not too important, because samples are usually taken to determine the particle size distribution and morphology. More important is the possibility of a particle size bias in the collection efficiency. In the point-to-plane precipitator, charging and precipitation must occur during a fraction of a second, so differences in mobility under these charging conditions can lead to

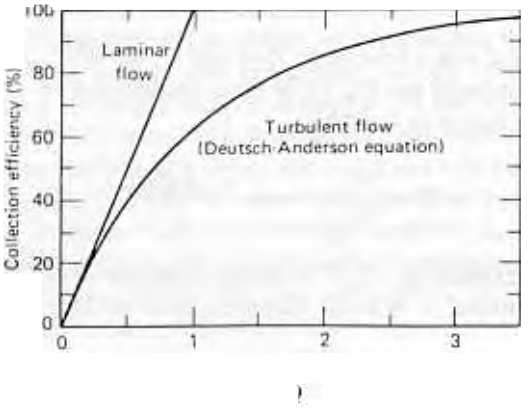

FIGURE 15.8 Efficiency curves for laminar- and turbulent-flow electrostatic precipitators.

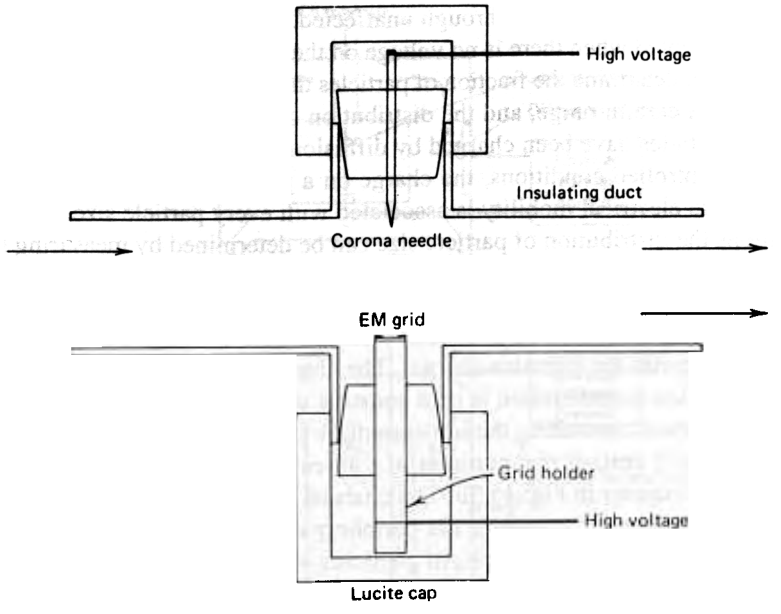

FIGURE 15.9 Cross-sectional diagram of a point-to-plane electrostatic precipitator used to obtain aerosol samples for electron microscopy.

a sampling bias that favors the collection of larger particles (Cheng et al., 1981). The use of a low sampling flow rate and a moderate ion current reduces this bias.

15.9 ELECTRICAL MEASUREMENT OF AEROSOLS

A simple electrical mobility analyzer is shown in Fig. 15.10. Aerosol particles are introduced along the centerline between two oppositely charged parallel plates. Filter samples (or other aerosol measurements) are taken downstream of the device while a specific voltage is maintained on the plates. For a given voltage, all particles with mobility greater than a certain amount will migrate to the plates and be trapped. Those with lower mobility will get through, to be collected on the downstream fil-

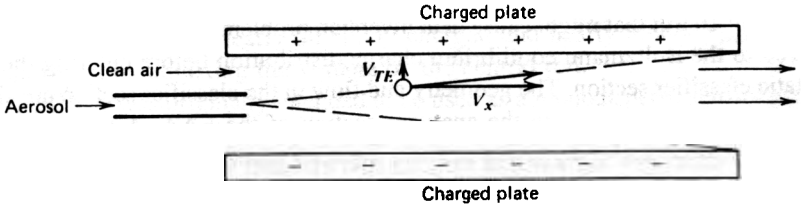

FIGURE 15.10 Diagram of a simple electrical mobility analyzer.

ter. Uncharged particles pass through unaffected. By comparing the mass (or other quantity) sampled when there is no voltage on the plates with that for different voltages, one can determine the fraction of particles that are uncharged, the fraction with mobility in a certain range, and the distribution of electrical mobilities.

If the particles have been charged by diffusion charging under well-defined and carefully controlled conditions, the charge on a particle of a given size is known and a unique electrical mobility is associated with every particle size. Under these conditions the distribution of particle size can be determined by measuring the distribution of electrical mobility. This is the principle of the *electrical aerosol analyzer* (EAA®) manufactured by TSI, Inc., of St. Paul, Minnesota, and shown schematically in Fig. 15.11. Aerosol is drawn into the instrument at 5 L/min and passes through a unipolar-ion diffusion charger. The time in the charger is fixed by the flow rate, and the ion concentration is held constant at $4.6 \times 10^{13}/m^3$ [$4.6 \times 10^7/cm^3$] by a feedback circuit measuring the ion current. A fixed value of $N_i t$ of 10^{13} ion · s/m^3 [10^7 ion · s/cm^3] ensures that particles of a given size receive a predictable number of charges, as shown in Fig. 15.3b. The charged aerosol flows to the mobility analyzer as a thin annular stream at the periphery of a laminar flow of clean air between two concentric cylinders. All particles with mobility less than the cutoff mobility, determined by the voltages on the tubes, pass out of the analyzer section and are collected in a high-efficiency conductive filter.

An electrometer continuously monitors the current produced by the capture of the charged particles in the filter. Since there is a monotonic relationship between mobility and particle size, the difference in current measured at two analyzer voltage settings is related to the number of particles in the size (mobility) range defined by the cutoff sizes of the two voltage settings. The instrument operates with preset voltages to provide the number of particles in each of 10 size ranges from 0.003 to 1.0 μm. In automatic operation, the instrument steps through the 10 size ranges in 2 min. The aerosol must have a stable number concentration and size distribution during this period, and the particles must be solid or nonvolatile liquids. Below 0.02 μm, a substantial, but predictable, fraction of the particles is uncharged. This is compensated for in the calibration of the instrument. The curve of mobility versus size becomes quite flat for particles larger than 0.3 μm (there are only two size ranges greater than this size), and the size resolution deteriorates. The concentration range depends on particle size and goes from 10^7 to $10^{11}/m^3$ [10 to$10^5/cm^3$] for 0.5-μm particles to 2×10^9 to $5 \times 10^{13}/m^3$ [2000 to $5 \times 10^7/cm^3$] for 0.0l-μm particles.

A related instrument is the differential mobility analyzer (DMA®), shown in Figure 15.12. The input aerosol first passes through an impactor to remove particles larger than 10 μm that might cause data inversion problems. The aerosol is then neutralized to the Boltzmann equilibrium charge distribution before entering the electrostatic classifier section. The geometry and flow in the classifier section are similar to the geometry and flow in the analyzer section of the EAA. A laminar flow of clean air is surrounded by a thin annular layer of aerosol as the two fluids travel axially between the central rod and the coaxial tube. The tube is grounded and the voltage on the central rod controlled between 20 and 10,000 V. Near the bottom of the central rod is a gap that allows a small airflow to leave the classifier and exit

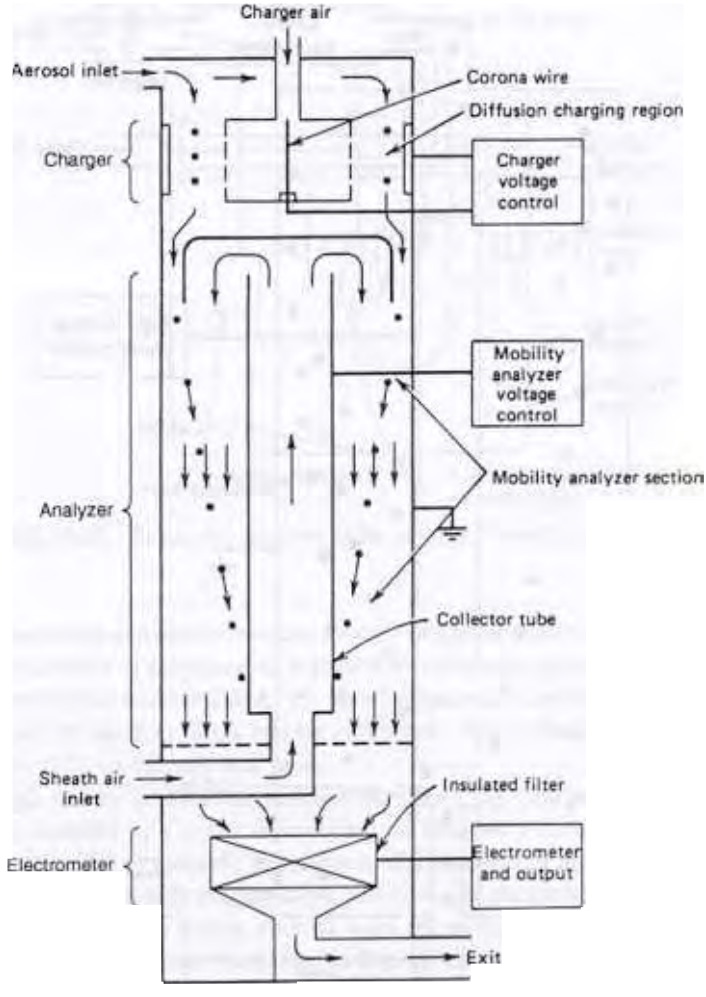

FIGURE 15.11 Schematic diagram of an electrical aerosol analyzer.

through a central tube. Only particles with a narrow range of mobilities can enter the gap. Particles with greater mobility migrate to the central rod before reaching the gap, while those with lower mobility go beyond the gap and are filtered out. The exiting aerosol is nearly all singly charged and nearly monodisperse. Its size is controlled by adjusting the voltage on the central rod.

The DMA was originally intended to be used as a monodisperse aerosol generator to produce submicrometer-sized aerosols for testing and calibration. However, it is used more commonly to measure particle size distribution with high resolution in the submicrometer size range. By monitoring the exit aerosol stream with a CNC (see Section 13.6), the number concentration in a narrow range of mobilities, and thus the particle size, can be determined. The entire submicrometer particle size dis-

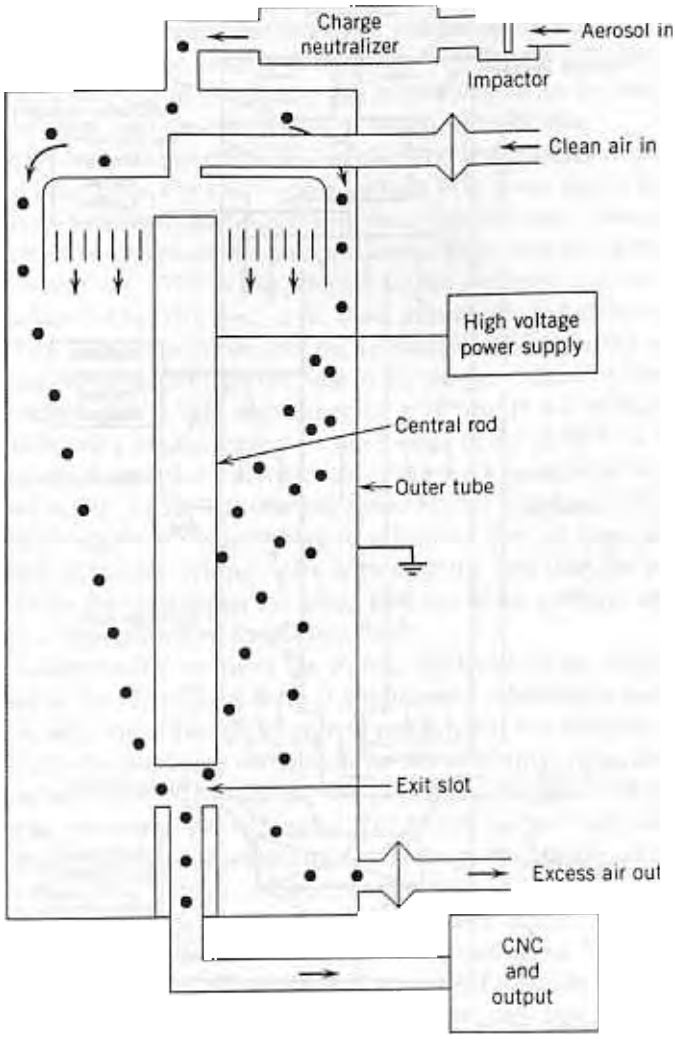

FIGURE 15.12 Schematic diagram of a differential mobility analyzer.

tribution can be obtained by stepping or continuously scanning through the voltage range. The lower size limit and maximum and minimum concentrations that can be measured are determined by the capabilities of the CNC that is used. DMAs can size particles from 0.005 to 1.0 μm at concentrations from 10^6 to $10^{14}/m^3$ [$1–10^8/cm^3$]. One version of this instrument, the TSI, Inc., Model 3934, scans up to 147 size channels under computer control in 1 to 8 minutes.

Two DMAs can be used in series or tandem (TDMA) to study processes that change particle size, such as evaporation, growth by condensation, or chemical reac-

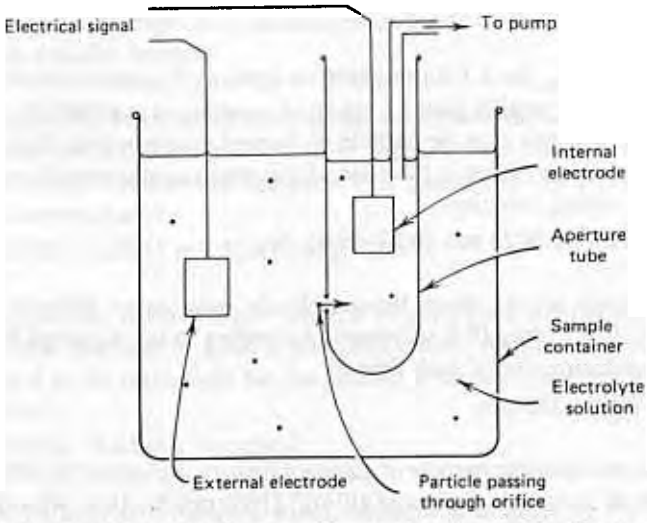

FIGURE 15.13 Schematic diagram of the sensing element of a Coulter counter

tions. A monodisperse submicrometer aerosol of known size is produced by the first DMA. The aerosol is subjected to a growth or shrinkage process, and then its size is measured by the second DMA. By careful operation and data analysis, particle size changes as small as 0.3% can be measured. This method works best for particles in the 0.01-to-0.2-μm size range.

Although not an aerosol-measuring instrument, the Coulter counter, an instrument manufactured by Coulter Electronics, of Hialeah, Florida, uses the electrical resistance principle to measure particle size distributions in liquid suspensions. The instrument is suitable only for insoluble particles, and the particles must be captured directly in a conductive liquid, such as with an impinger, or transferred to such a liquid before measurement. As shown in Fig. 15.13, the liquid flows from one section to the other through a small orifice 10–400 μm in diameter. A current is established through the orifice by platinum electrodes in the liquid on either side of the orifice. Because the particle has an electrical resistance different from that of the liquid, there is a momentary change in the current as the particle passes through the orifice due to the displaced electrolyte. This change, which is directly proportional to the volume of the particle, is sensed electronically and converted to particle size, and these data are accumulated to produce a distribution of particle size weighted by volume. The instrument can be used for particle sizes ranging from 0.3 to 200 μm, but for a given orifice, the range is limited to 2–40% of its diameter. Size calibration is done with polystyrene spheres of known size. (See Section 21.2.) The maximum counting rate is 3000/s. A sample size of about 1 mg is required to determine a size distribution. Wetting agents and ultrasonic energy are used to ensure that all particles are fully dispersed in the liquid.

PROBLEMS

15.1 Determine V_{TE} for a 1.0-μm-diameter sphere of standard density positioned between two parallel plates 1 cm apart maintained at a 9000-V potential difference. Assume that the particle is charged to the average Boltzmann equilibrium charge. What is the ratio of this electrostatic velocity to its gravitational settling velocity?

ANSWER: 0.0023 m/s [0.23 cm/s], 66.

15.2 Raindrops falling from thunderclouds may carry charges as high as 3.3×10^{-11} C/drop [0.1 stC/drop]. According to the Rayleigh limit, what is the minimum size of such drops?

ANSWER: 280 μm.

15.3 A 1.6-μm-diameter particle of standard density is charged by diffusion charging at an ion concentration of $10^{12}/m^3$ [$10^6/cm^3$] for 10 s. What V_{TE} will this charged particle have in an electrostatic field of 300 kV/m [3 kV/cm]?

ANSWER: 0.016 m/s [1.6 cm/s].

15.4 Show that the collision velocity of two equal-sized particles carrying equal and opposite charge is proportional to the inverse of the cube of their diameter, d_p^{-3}. Assume that motion is in the Stokes region. Neglect slip correction.

15.5 An aerosol neutralizer has a volume of 1.7 L and contains a 1.0-mCi Kr-85 source that produces an ion concentration of $3 \times 10^{12}/m^3$ [$3 \times 10^6/cm^3$] inside the cylinder. At a flow rate of 50 L/min, what fraction of the original charge will remain on an aerosol after it has passed through the device?

ANSWER: 6.1×10^{-8}.

15.6 For a uniform electric field of 1200 kV/m [12 kV/cm] and an ion concentration of $10^{14}/m^3$ [$10^8/cm^3$], what is the saturation charge for a 2.0-μm-diameter particle? How long does it take to charge this particle to 95% of its saturation charge? ($\varepsilon = 10$.)

ANSWER: 2080*e*, 0.28 s.

15.7 What is the maximum velocity a 2-μm particle can have in an electrostatic field of 100 kV/m [1 kV/cm]? [*Note*: Motion may be outside the Stokes region.]

ANSWER: 250 m/s [25,000 cm/s].

15.8 What is the average charge on a 0.15-mm-diameter particle in equilibrium with bipolar ions at 293 K [20°C]? Assume that Eq. 15.32 holds.

ANSWER: 1.47×10^{-19} C [4.4×10^{-10} stC]. (*Note*: Equation 15.30 gives an answer that is 7% larger.)

15.9 Show that Rayleigh limit disintegration leads to the formation of charge-stable, smaller droplets.

15.10 Determine the electrostatic velocity and the ratio of this velocity to the settling velocity for a 0.6-μm particle ($\varepsilon = 10$) in a field strength of 1200 kV/m [12 kV/cm]. Assume that the particle is charged to the average Boltzmann equilibrium charge.

ANSWER: 0.0043 m/s [0.43 cm/s], 320.

15.11 Determine the electrostatic migration velocity for a 0.6-μm particle ($\varepsilon = 10$) in a field strength of 1200 kV/m [12kV/cm]. Assume that the particle is charged in the same field for one second at an ion concentration of $10^{14}/m^3$ [$10^8/cm^3$].

ANSWER: 0.44 m/s [44 cm/s].

15.12 What particle size receives equal numbers of charges in 1 s by diffusion charging and by field charging at 2000 kV/m [20 kV/cm]? Assume that each mechanism operates independently and that the ion concentration is $10^{14}/m^3$ [$10^8/cm^3$] for both types of charging. $\varepsilon = 1$. [*Hint*: A trial-and-error spreadsheet approach may be the easiest way to do this problem.]

ANSWER: 0.15 μm.

15.13 What voltage is required to just balance a singly charged (negative) 0.8-μm-diameter particle in a Millikan cell? The plate spacing is 5 mm and particle density is 1000 kg/m^3 [1.0 g/cm^3].

ANSWER: 82 V.

REFERENCES

Cheng, Y-S., Yeh, H-C., and Kanapilly, G. M., "Collection Efficiencies of a Point-to-plane Electrostatic Precipitator," *Am. Ind. Hyg. Assoc. J.*, **42**, 605–610 (1981).

Flagan, R. C., "History of Electrical Aerosol Measurements," *Aerosol Sci. Tech.*, **28**, 301–380 (1998).

Hoppel, W. A., and Frick, G. M., "Ion-Aerosol Attachment Coefficients and the Steady-State Charge Distribution on Aerosols in a Bipolar Environment," *Aerosol Sci. Tech.*, **5**, 1–21 (1986).

Lawless, P. A., "Particle Charging Bounds, Symmetry Relations, and an Analytic Charging Rate Model for the Continuum Regime," *J. Aerosol Sci.*, **27**, 191–215 (1996).

Liu, B. Y. H., and Kapadia, H., "Combined Field and Diffusion Charging of Aerosol Particles in the Continuum Regime," *J. Aerosol Sci.*, **9**, 227–242 (1978).

Liu, B. Y. H., and Pui, D. Y. H., "Electrical Neutralization of Aerosols," *J. Aerosol Sci.*, **5**, 465–472 (1974).

Liu, B. Y. H., Pui, D. Y. H., and Kapadia, H., "Electrical Aerosol Analyzer: History, Principle,

and Data Reduction," in Lundgren, D. A. et al. (Eds.), *Aerosol Measurement*, University Presses of Florida, Gainesville, FL, 1979.

Loeb, L. B., *Static Electrification*, Springer-Verlag, Berlin, 1958.

Smith, W. B., Felix, L. G., Hussey, D. H., Pontius, D. H., and Sparks, L. E., "Experimental Investigations of Fine Particle Charging by Unipolar Ions," *J. Aerosol Sci.*, **9**, 101 (1977).

Whitby, K. T., and Liu, B. Y. H., "The Electrical Behavior of Aerosols," in Davies, C. N. (Ed.), *Aerosol Science*, Academic Press, London, 1966.

White, H. J., *Industrial Electrostatic Precipitation*, Addison-Wesley, Reading, MA, 1963.

Yeh, H.-C., " Electrical Techniques," in Willeke, K., and Baron, P. A. (Eds.), *Aerosol Measurement: Principles, Techniques and Applications*, Van Nostrand Reinhold, New York, 1993.

16 Optical Properties

The optical properties of aerosols are responsible for many spectacular atmospheric effects, such as richly colored sunsets, halos around the sun or moon, and rainbows. They also cause the degradation of visibility associated with atmospheric pollution. The interaction of aerosol particles with light forms the basis for an important class of instruments used for measuring aerosol particle size and concentration. Optical measurement methods have the advantages of being extremely sensitive and nearly instantaneous and of not requiring physical contact with the particles.

The optical phenomena covered in this chapter are all a direct result of the scattering and absorption of light by aerosol particles. Black smoke looks black because the particles absorb visible light. Dense rain clouds, on the other hand, look black even though the droplets have negligible absorption, because the droplet scattering is so complete that light cannot get through the clouds. Fair-weather clouds look white because of the extensive scattering of the incident light from the surface of the cloud. When we see an object, we are seeing primarily the scattered light from that object. The scattered light reaching our eyes contains information about the color, surface texture, and form of the object.

The scattering of light by very small particles—less than 0.05 μm in diameter—is described in relatively simple terms by Rayleigh's theory, the theory of molecular scattering. Scattering by large particles—greater than 100 μm—can be analyzed readily by geometric optics, the tracking of diffracted, reflected, and refracted rays of light through the particle. Between these sizes, an important range of interest for aerosol technology is the Mie scattering region. In this size range, where the particle size and the wavelength of light are the same order of magnitude, the scattering of light by aerosol particles is a complicated phenomenon.

The scientific study of light scattering by aerosols began in the late 1800s with experimental studies by Tyndall and theoretical analysis by Lord Rayleigh. Maxwell's theory of electromagnetic radiation enabled Gustav Mie to develop the general theory of scattering in 1908. Unlike most other areas of aerosol science, the theory of light scattering, although complicated, is exact for spherical, homogeneous particles and thus provides an accurate and reliable tool for measuring properties of aerosols.

The discussion that follows is limited to elastically scattered light—that is, scattered light whose frequency is the same as the frequency of the incident light. Processes such as fluorescence or Raman scattering are not covered here. Nearly all real aerosols are sufficiently dilute that each particle will scatter light independently of its neighbors. Consequently, we follow the microscopic single-particle approach used in the previous chapters.

16.1 DEFINITIONS

Light is defined as visible electromagnetic radiation having a *wavelength* λ between about 0.4 (violet) and 0.7 μm (red) and a *frequency* f between 8×10^{14} and 4×10^{14} Hz. This wavelength band is an extremely narrow portion of the electromagnetic spectrum, which covers a range that is greater than 10^{20}. The center of the visible-light region is green light, with a wavelength of approximately 0.5 μm. Wavelength and frequency are related by

$$c = f\lambda \tag{16.1}$$

where c is the velocity of light in a vacuum, equal to 3.0×10^8 m/s [3.0×10^{10} cm/s].

The ratio of the velocity of light in a vacuum to the velocity of light in a particular material, V_p, is the *index of refraction,* or refractive index, m of that material. For a given wavelength, the index of refraction depends only on the material, but it varies slightly with the wavelength of the light used. For nonabsorbing materials, it is given by

$$m = \frac{}{V_p} \tag{16.2}$$

This is called the *absolute index of refraction* and is always greater than unity.

The index of refraction for absorbing materials—those having appreciable electrical conductivity—is expressed as a complex number

$$m'(1 - ai) = m' - m'ai \tag{16.3}$$

where i is $\sqrt{-1}$, m' is the real refractive index, and a is related to the absorption coefficient of the bulk material A by

$$A = \frac{}{\lambda} \tag{16.4}$$

The imaginary part of the refractive index is zero for nonabsorbing particles. Refractive indices for various materials are given in Table 16.1.

For particles in a two-phase system, a *relative index of refraction* is used. This is defined as the ratio of the velocity of light in the suspending medium, V_m, to the velocity in a particle, V_p:

$$m_r = \frac{V_m}{V_p} = \frac{m_p}{m_m} \tag{16.5}$$

Air has a refractive index that is practically equal to that of a vacuum (see Table 16.1), so that the absolute and relative refractive indices are equal for aerosol particles. For particles suspended in liquids, m_r may be greater or less than unity; m_r is less than unity for gas particles (bubbles) in a liquid.

TABLE 16.1 Index of Refraction of Some Common Materials at $\lambda = 0.589$ μm, the Wavelength of Yellow Sodium Light[a]

Material	Index of Refraction	Material	Index of Refraction
Vacuum	1.0	Quartz (SiO_2)	1.544
Water vapor	1.00025	Polystyrene latex	1.590
Air	1.00028	Diamond	2.417
Water	1.3330	Urban aerosol (avg.)	1.56–0.087*i*
Glycerine	1.4730	Methylene blue	1.55–0.6*i*
Benzene	1.501	Soot	1.96–0.66*i*
Ice (H_2O)	1.305	Carbon[b]	2.0–1.0*i*
Glass	1.52–1.88	Iron	2.80–3.34*i*
Sodium chloride	1.544	Copper	0.47–2.81*i*

[a]Data taken primarily from *Handbook of Chemistry and Physics*, 74th ed., CRC, Boca Raton, FL (1993).
[b]$\lambda = 0.491$ μm.

The *intensity* of electromagnetic radiation arriving at any surface, such as the surface of a detector, is expressed in terms of the radiant power arriving per unit area. When power (energy per unit time) is measured in watts (W), intensity is stated in W/m^2 [W/cm^2]. Intensity of light emitted from a point source is expressed as radiant power emitted into a given solid angle, i.e., watts per steradian (W/sr); for visible light, this intensity can also be expressed in candela (cd), the SI base unit for luminous intensity. The steradian (sr) is the dimensionless solid angle equal to the cone from the center of an imaginary sphere that subtends $1/4\pi$ of the total spherical surface. Thus, there are 4π sr in a sphere. The light scattered from an aerosol particle can be considered as coming from a point source, and its intensity in a given direction may be expressed in any of the units just mentioned.

Although we are concerned primarily with the scattering of visible light, the principles presented here can be applied to electromagnetic radiation of any wavelength. Thus, the scattering of radio waves by artificial satellites, the scattering of microwaves by raindrops, and the scattering of light by aerosol particles are equivalent processes with wavelengths and object sizes that are the same order of magnitude. The scattering in each case is governed by the ratio of the particle size to the wavelength λ of the radiation. This ratio, which is dimensionless, is called the *size parameter* and is given by

$$\alpha = \frac{\pi d}{\lambda} \tag{16.6}$$

The factor π is introduced to simplify certain light-scattering equations and has the effect of making α equal to the ratio of the circumference of the particle to the wavelength. For visible light, the value of α is approximately equal to six times the particle diameter expressed in micrometers.

Light can be considered a stream of photons or a transverse wave. To describe light scattering by aerosol particles, it is convenient to consider light as the elec-

tric wave component of electromagnetic radiation. When the transverse oscillations of the electric vector occur in all directions perpendicular to the direction of propagation, the light is said to be *unpolarized.* Normal light, such as sunlight or incandescent light, is unpolarized. When the electric vector oscillates only in one plane, the light is said to be *polarized* in that plane. Laser light and light that has passed through a polarizing filter are polarized. Any light beam can always be resolved into two perpendicularly polarized components, often called vertical and horizontal polarizations, that may differ in intensity.

16.2 EXTINCTION

Aerosol particles illuminated by a beam of light scatter and absorb some of that light, thereby diminishing the intensity of the beam. This process is called *extinction* and addresses only the attenuation of light along an axis. While all aerosol particles will scatter light, only those made of absorbing material will absorb light. The extinction characteristics of aerosols are important for aerosol measurement and, as will be explained in Section 16.4, for evaluating the effect of aerosols on visibility. We can look directly at the attenuated light of the setting sun because the intensity is reduced by extinction over the long air path. We see a red sun because the extinction is strongest for blue light and weakest for red light.

For a parallel beam of light, such as that shown in Fig. 16.1, the ratio of the light intensity traversing the aerosol, I, to that incident on the aerosol, I_0, is given by Bouguer's law (also known as the Lambert–Beer law),

$$\frac{I}{I_0} = e^{-\sigma_e L} \tag{16.7}$$

where σ_e is the extinction coefficient of the aerosol and L is the path length of the light beam through the aerosol. The extinction coefficient is the fractional loss in

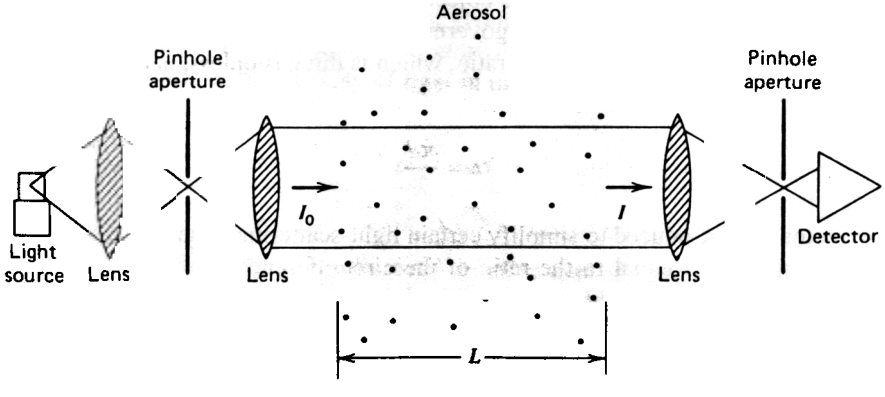

FIGURE 16.1 Schematic diagram of an extinction-measuring apparatus.

intensity per unit path length associated with an elemental thickness dL. The units of σ_e are (length)$^{-1}$, and σ_e and L must be expressed by the same unit of length to make the exponent of Eq. 16.7 dimensionless. The extinction coefficient σ_e is analogous to γ in Eq. 9.11 for penetration through a filter. (Note that Eqs. 16.7 and 9.11 have the same form.)

The aperture and lens arrangement shown in Fig. 16.1 is needed to ensure that the particles are illuminated with a parallel beam of light (i.e., to ensure that all rays are parallel) and that only the attenuated parallel light reaches the detector. Failure to include the lens and aperture at the detector allows forward-scattered light from the particles to reach the detector, in which case Eq. 16.7 does not hold. The extinction produced by a particle is a function of the particle extinction efficiency Q_e.

$$Q_e = \frac{\text{radiant power scattered and absorbed by a particle}}{\text{radiant power geometrically incident on the particle}} \tag{16.8}$$

The geometrically incident power is the amount of energy per second that intercepts the cross-sectional area A_p of the particle. The particle extinction efficiency gives a relative measure of a particle's ability to remove light from a beam compared with simple blocking or interception by the projected area of the particle. The extinction efficiency times the projected area of a particle is the cross-sectional area of light removed from a beam by the particle. A Q_e of 2.0 indicates that a particle removes twice as much light as it would by simple projected-area blocking. Values of Q_e range from 0 to about 5. The particles in a cubic centimeter of a monodisperse aerosol will each remove A_pQ_e watts from a beam of unit intensity. From the definition of the extinction coefficient, a monodisperse aerosol of N particles per unit volume has an extinction coefficient of

$$\sigma_e = NA_pQ_e = \frac{\pi Nd^2Q_e}{4} \tag{16.9}$$

Q_e is defined (Eq. 16.8) in the same way as the combined single-filter efficiency, given in Eq. 9.14. Also, Eqs. 16.7 and 16.9 are analogous to Eq. 9.19 for filters. Both relate macroscopic phenomena—light attenuation and filter penetration—to microscopic-scale particle properties, Q_e and E_Σ, respectively.

The extinction efficiency of a particle is the sum of its scattering efficiency Q_s and its absorption efficiency Q_a,

$$Q_e = Q_s + Q_a \tag{16.10}$$

where Q_s and Q_a are defined by equations equivalent to Eq. 16.8. It follows from Eq. 16.10 that, for monodisperse particles

$$\sigma_e = \sigma_s + \sigma_a \tag{16.11}$$

where σ_s and σ_a are defined by Eq. 16.9 with Q_e replaced by Q_s and Q_a, respectively. For nonabsorbing particles, $Q_e = Q_s$ and $\sigma_e = \sigma_s$. For polydisperse aerosols, Eq. 16.9 holds for each particle size, and the combined effect is given by the sum of the σ_e's for all the particle sizes.

$$\sigma_e = \sum_i \frac{\pi N_i d_i^2 (Q_e)_i}{4} \tag{16.12}$$

where N_i is the number concentration of particles with diameter d_i. For those situations where $(Q_e)_i$ can be treated as a constant ($d > 4$ μm), we can write

$$\sigma_e = \frac{\pi Q_e}{4} \sum N_i d_i^2 = \frac{\pi Q_e}{4} N\overline{d^2} \quad \text{for } d > 4 \text{ μm} \tag{16.13}$$

where N is the total number concentration. For geometrically similar particles, the diameter of average surface area is equal to the diameter of average projected area, and when Q_e is a constant, extinction measurements can be used to determine the surface area concentration (area/m^3 [area/cm^3]) C_s. From Eqs. 16.7 and 16.13,

$$C_s = \frac{-4}{LQ_e} \ln\left(\frac{I}{I_0}\right) \quad \text{for } d > 4 \text{ μm} \tag{16.14}$$

and the diameter of average surface area (the second moment average, see Eq. 4.22) can be obtained as follows if N is known:

$$d_{\bar{s}} = \left(\frac{C_s}{N\pi}\right)^{1/2} \tag{16.15}$$

The use of Eqs. 16.7 and 16.9 for aerosols is straightforward, provided that Q_e is known. There is no single equation that gives Q_e for all particle sizes. Q_e depends on the particle refractive index, shape, and size relative to the wavelength of light. For small particles less than 0.05 μm in diameter, Q_e can be calculated directly from

$$Q_e = \frac{8}{3}\left(\frac{\pi d}{\lambda}\right)^4 \left(\frac{m^2 - 1}{m^2 + 2}\right)^2 \quad \text{for } d < 0.05 \text{ μm} \tag{16.16}$$

In this size range Q_e *is* proportional to d^4 and, consequently, decreases rapidly with decreasing particle size. For gases,

$$\sigma_e = \frac{32\pi^3 (m-1)^2 f}{3\lambda^4 n} \tag{16.17}$$

where m is the bulk refractive index of the gas (see Table 16.1), n is the number concentration of gas molecules, given by $n = pN_A/RT$, and $f = 1.054$ for air at standard conditions (van de Hulst, 1957, 1981).

For large particles ($d > 4$ μm), Q_e approaches, with oscillations, its limiting value of 2.0. For particles between 0.05 and 4 μm, there is no simple equation for Q_e, and its value can be obtained from graphs such as Figs. 16.2 and 16.3 or by computer calculation (see Wilson and Reist, 1994). Nonabsorbing particles have a maximum value of Q_e of about 4 in the size range 0.3–1 μm. Absorbing or irregular particles have only slight maxima and approach their limiting value of $Q_e = 2$ without oscil-

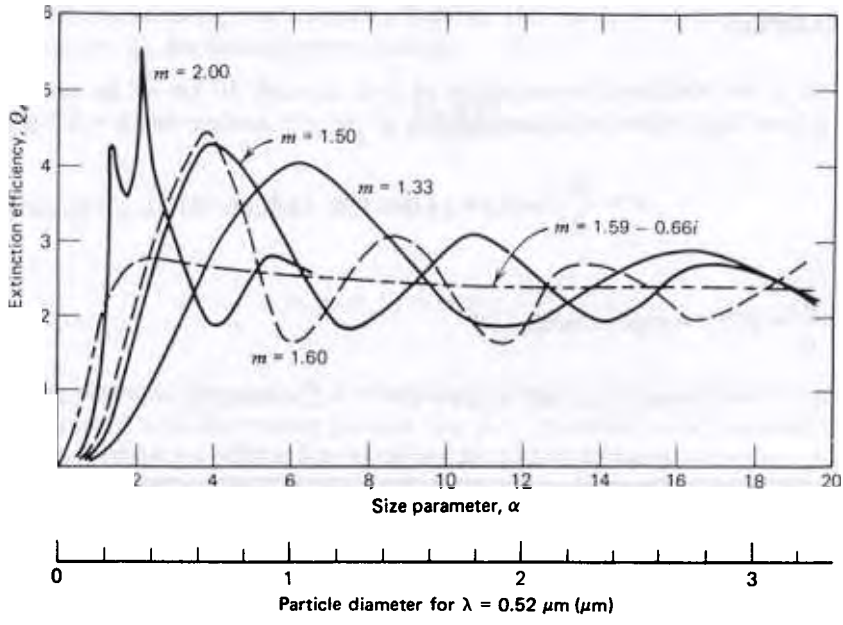

FIGURE 16.2 Extinction efficiency versus particle size for spheres (after Hodkinson, 1966).

lations. The curves for nonabsorbing particles in Fig. 16.2 have been smoothed to remove numerous small bumps and wiggles. These bumps are greatly reduced for absorbing particles. Extinction efficiency decreases rapidly with decreasing α in the region below $\alpha = 2$, as shown in Figs. 16.2 and 16.3.

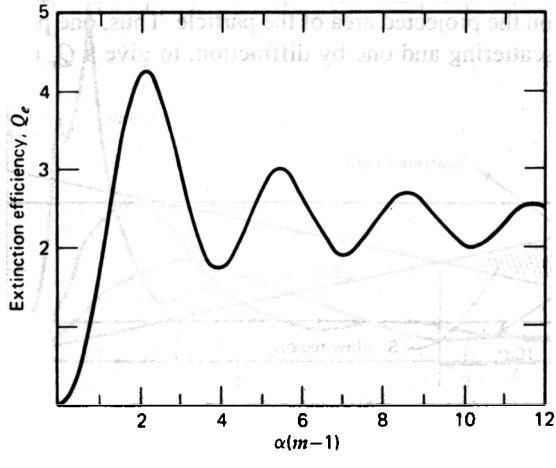

FIGURE 16.3 Extinction efficiency versus $\alpha(m - 1)$ for nonabsorbing spheres with refractive indices between 1.33 and 1.50. Data from Kerker (1969).

EXAMPLE

What is the fractional transmission of light through 10 km of air containing 0.5-μm fog droplets at a concentration of $10^8/m^3$? Assume that $\lambda = 0.5$ μm.

$$\alpha = \frac{\pi 0.5}{0.5} = 3.14 \quad \text{From Fig. 16.2, } Q_e = 2$$

$$\frac{I}{I_0} = e^{-\sigma_e L} = \exp(-\pi N d^2 Q_e L/4)$$

$$= \exp(-\pi \times 10^8 \times (0.5 \times 10^{-6})^2 \times 2 \times 10000/4) = e^{-0.392} = 0.68$$

$$[\exp(-\pi \times 100 \times (0.5 \times 10^{-4})^2 \times 2 \times 10^6/4) = 0.68]$$

The peculiarity of the quantity Q_e converging to a value of 2 for large values of α is called the *extinction paradox* and implies that large particles remove from a light beam an amount of light equal to twice their projected area. The explanation of this paradox is based on the condition that extinction must be observed at a long distance from the particles. As shown in Fig. 16.4, the distance between the object and the detector is such that all the diffracted light is removed from the beam before it reaches the detector. This distance must be large compared to $10d^2/\lambda$, the maximum extent of the shadow. This condition is easily met in the case of aerosol particles, but would require an observation distance greater than 100 km to evaluate the extinction of a coffee cup. Shadows observed in our normal experience seldom meet this criterion. Under proper conditions of observation, it follows from Babinet's principle [see Kerker (1969)] that the amount of light removed by diffraction is equal to that incident on the projected area of the particle. Thus, one projected area of light is removed by scattering and one by diffraction, to give a Q_e of 2.0 when $\alpha > 20$.

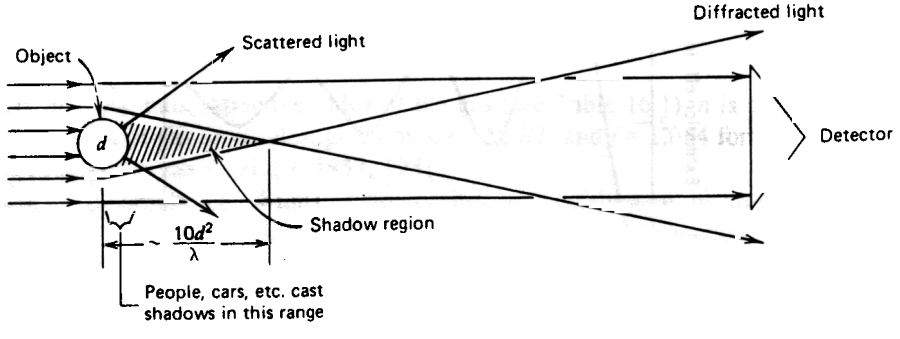

FIGURE 16.4 Diagram of extinction paradox.

It is of interest to express Bouguer's law, Eq. 16.7, in terms of the particle mass concentration C_m for monodisperse aerosols.

$$C_m = \frac{N\rho_p \pi d^3}{6} \tag{16.18}$$

Combining Eq. 16.18 with Eqs. 16.7 and 16.9 gives

$$\frac{I}{} = \exp(-\sigma_e L) = \exp\left(-\frac{3C_m Q_e L}{2\rho_p d}\right. \tag{16.19}$$

For large particles, for which Q_e is a constant, extinction increases (scattering becomes greater) with *decreasing* particle size *for a constant mass concentration.* Figure 16.5 shows the relative scattering per unit mass for three materials as a function of particle size. Because Q_e decreases rapidly ($Q_e \propto d^4$) for small particles, there is a particle size for maximum extinction, as shown in the figure, and a range in which a reduction in size gives an increase in extinction for a given mass concentration. This fact explains why the visual impact of atmospheric aerosols and smokestack plumes is governed by the concentration of particles in the size range from 0.1 to 2 μm and why a reduction in concentration outside this range has little effect on extinction or visibility.

Table 16.2 gives the relative extinction for a given mass of water in the atmosphere in the form of molecules, aerosol particles, or raindrops. For a given mass concentration of water, aerosol particles in the range of 0.1 to 1.0 μm are a million times more effective than vapor molecules and a thousand times more effective than

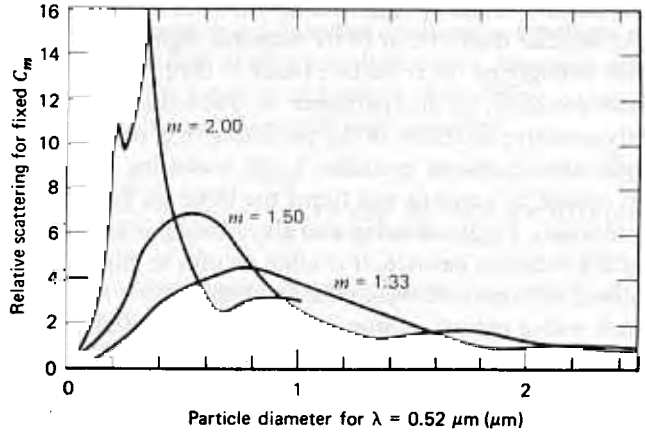

FIGURE 16.5 Relative scattering per unit mass of aerosol versus particle size for light at a wavelength of 0.52 μm.

TABLE 16.2 Extinction and Visual Range in Air Containing 18 g/m³ of Water[a] in Different Forms

Particle Size (μm)	Extinction,[b] $1 - I/I_0$	Visual Range[c] (km)
Vapor	1.8×10^{-7}	220
0.01	3.8×10^{-5}	1.0
0.1	0.29	1.1×10^{-4}
1.0	0.64	3.8×10^{-5}
10	0.052	7.4×10^{-4}
1 mm (rain)	5.3×10^{-4}	0.074

[a]Equivalent to saturation at 293 K [20°C].
[b]L = 1.0 cm and λ = 0.5 μm.
[c]See Section 16.4.

raindrops in attenuating light and creating turbidity in the atmosphere. Thus, even though aerosols are usually present at low concentrations, their visual impact can be great.

The preceding discussion of extinction assumes that single scattering holds. If the aerosol concentration is sufficiently great, the light scattered by each particle will illuminate other particles in a direction that is not parallel to the incident light. This process allows multiple-scattered light, instead of attenuated incident light, to reach the detector, and Eq. 16.7 does not hold. Under favorable conditions, this effect is not significant for I/I_0 greater than 0.1.

16.3 SCATTERING

It is impractical to analyze the refracted and reflected rays of light for particles less than 50 μm, so the interaction of light with a particle in this size range is described in terms of the angular distribution of its scattered light. This angular scattering pattern depends strongly on the refractive index of the particle and the particle diameter, or, more correctly, the size parameter α. The scattered light from a particle is an extremely sensitive indicator of the particle's size, permitting size measurements of single submicrometer particles. Light scattering is responsible for the optical effects caused by aerosols and forms the basis for several types of aerosol measuring instruments. Light scattering also plays an important role in visibility and affects the earth's radiation balance. It is often helpful to think about light scattering as if the illuminated particle were reradiating the light it receives and thus acts as a light source with a unique angular distribution of light intensity.

Standard conventions have been adopted for describing the angular distribution of light scattered by an aerosol particle. As shown in Fig. 16.6, the plane formed by the incident beam and the direction of observation (the scattered beam) is called the *scattering plane.* The *scattering angle* θ is measured in the scattering plane from the direction of the incident beam to the scattered beam. Light that deviates only

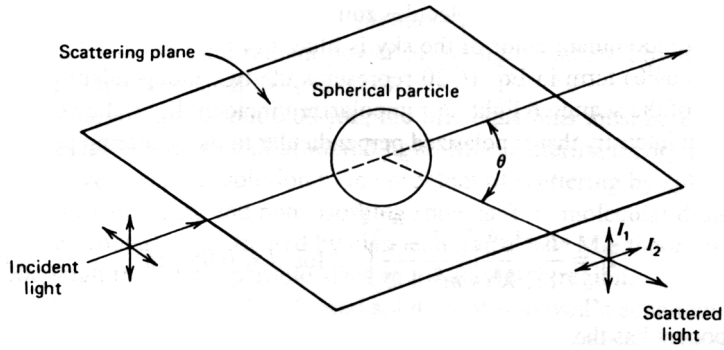

FIGURE 16.6 Diagram showing scattering angle, scattering plane, and the polarized components of scattered light.

slightly from its incident direction has a small scattering angle and is said to be *forward-scattering light.* Light that is reflected or scattered back to the source (i.e., $\theta = 180°$) is called *back-scattered light.* The incident and scattered beams can each be resolved into two independently polarized components, one whose electric vector is perpendicular to the scattering plane (designated by the subscript 1) and one whose electric vector is parallel to the scattering plane (subscript 2).

The general theory of light scattering by aerosols was developed in 1908 by Gustav Mie. The theory gives the intensity of light scattered at any angle θ by a spherical particle with known values of α and m illuminated by light of intensity I_0. The resulting Mie equations are very complicated for particles with sizes greater than the wavelength of light.

When particles are much smaller than the wavelength of light ($d < 0.05$ μm), the much simpler Rayleigh scattering theory can be used. For these particles (and gas molecules), the instantaneous electromagnetic field of the incident light is uniform over the entire particle, creating a dipole that oscillates in synchronization with the incident electromagnetic field. This oscillating dipole reradiates electromagnetic energy in all directions. The intensity and pattern of scattering is known as Rayleigh scattering and, for unpolarized illumination, is given by

$$I(\theta) = \frac{I_0 \pi^4 d^6}{8R^2\lambda^4}\left(\frac{m^2 - 1}{m^2 + 2}\right)^2 (1 + \cos^2\theta) \quad \text{for } d < 0.05\ \mu\text{m} \qquad (16.20)$$

where $I(\theta)$ is the total intensity, at a distance R from the particle, of the light scattered in the direction θ.

Equation 16.20 indicates that the intensity of the scattered light at any angle will be proportional to d^6/λ^4. This is a strong function of diameter and a strong inverse function of wavelength. Rayleigh scattering depends on the particle volume squared and, as a result, is independent of the particle shape. The dependence of scattered light on wavelength (λ^{-4}) accounts for the blue color of the sky: Blue light is scat-

tered (or reradiated) by the air molecules roughly 16 times more strongly than red light, so the predominant color of the sky is blue.

The $(1 + \cos^2\theta)$ term in Eq. 16.20 represents the two independent polarization components of the scattered light. For unpolarized incident light, the component of scattered light intensity that is polarized perpendicular to the scattering plane is given by

$$I_1 = \frac{I_0 \pi^4 d^6}{8R^2\lambda^4}\left(\frac{m^2 - 1}{m^2 + 2}\right)^2 \quad \text{for } d < 0.05\ \mu\text{m} \tag{16.21}$$

This component has the same intensity at all scattering angles. For polarization parallel to the scattering plane,

$$I_2 = \frac{I_0 \pi^4 d^6}{8R^2\lambda^4}\left(\frac{m^2 - 1}{m^2 + 2}\right)^2 \cos^2\theta \quad \text{for } d < 0.05\ \mu\text{m} \tag{16.22}$$

Because of its dependence on $\cos^2\theta$, the I_2 component is equal to I_1 at scattering angles of 0 and 180° and goes to zero at 90°. The angular scattering pattern of both polarizations for Rayleigh scattering is customarily displayed in a polar diagram such as that shown in Fig. 16.7. In such a diagram the scattering angle is shown as the angle between a radial line from the particle and the direction of the incident light. The scattered intensity in that direction is proportional to the length of the line from the particle to the curve. The figure shows that the I_1 component is the same at all angles and the I_2 component is zero at $\theta = 90°$. Thus, light scattered at 90° by gas molecules and small particles will be completely polarized perpendicular to the scattering plane. Similarly, the light scattered from the sky on a clear day will be perpendicularly polarized when it is viewed 90° from the sun, a phenomenon that bees use for navigation. Rayleigh scattering is symmetrical in the forward and backward directions; that is, an equal amount of light is scattered in both directions.

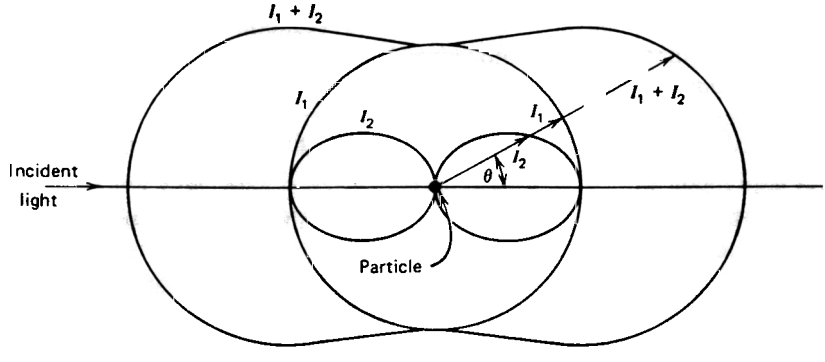

FIGURE 16.7 Polar diagram of Rayleigh scattered light. Scattering plane is parallel to the paper.

When Eq. 16.20 is integrated over the surface of a sphere, the result for nonabsorbing particles is the total radiant power of the light scattered by the particle in all directions, which is equal to $I_0\pi d^2 Q_e/4$.

For particles larger than about 0.05 μm, the Mie equations must be used to determine the angular distribution of scattered light. Mie scattering theory provides a complicated but very general solution to the problem of scattering by spheres. The theory is valid for absorbing and nonabsorbing spheres from molecular dimensions to particles large enough to be treated by classical optics. The Mie theory is identical to the Rayleigh theory for particle sizes in the Rayleigh region.

The Mie solution is the complete formal solution of Maxwell's equations for the combined vector wave equations for the incident wave, the wave inside the particle, and the scattered wave, subject to a set of boundary conditions at the surface of the particle. A derivation of this theory and an explanation of the equations are presented in van de Hulst (1957, 1981) and Kerker (1969).

The Mie solution of Maxwell's electromagnetic equations is a solution to one of the classical problems of physics. Although the solution is exact, its utility was severely limited before the arrival of digital computers, because of the extreme complexity of the computations. With a mechanical calculator, a single solution for one value of m, α, and θ could take from several hours to several months. Efficient computer programs that provide nearly instant solutions to the Mie equations are now available. (See Dave, 1969, and Wilson and Reist, 1994.)

At a distance R in the direction θ from a spherical particle illuminated with unpolarized light of intensity I_0 (W/m^2 [W/cm^2]), the scattered intensity is

$$I(\theta) = \frac{I_0\lambda^2(i_1 + i_2)}{8\pi^2 R^2} \tag{16.23}$$

where i_1 and i_2 are the Mie intensity parameters for scattered light with perpendicular and parallel polarization, respectively. For polarized illumination, the scattered intensity is expressed by

$$\frac{I_0\lambda^2 i_1}{4\pi^2 R^2} \tag{16.24}$$

for perpendicular polarization and by

$$\frac{I_0\lambda^2 i_2}{4\pi^2 R^2} \tag{16.25}$$

for parallel polarization. The Mie intensity parameters i_1 and i_2 are functions of m, α, and θ and are defined by a complicated infinite series involving Legendre polynomials and Bessel functions. Because of the difficulty in calculating the Mie functions it is common to estimate scattered light intensities from values of i_1 and i_2, tabulated as functions of m, α, and θ or to calculate the functions directly using a computer. The use of power series approximations has been reviewed by Kerker (1969). In general, these approximations are restricted to a narrow range of values of α.

EXAMPLE

What is the ratio of backscattered intensity to incident intensity for 0.05-μm particles (m = 1.5) if 10^{12} particles are illuminated and observed at a distance of 0.3 m [30 cm]. Assume that λ = 0.5 μm.

$$\frac{I}{I_0} = 10^{12} \times \left(\frac{\pi^4 \times (0.5 \times 10^{-6})^6}{8 \times 0.3^2 \times (0.5 \times 10^{-6})^4} \right) \left(\frac{1.5^2 - 1}{1.5^2 + 2} \right)^2 (1 + \cos^2(180°)) = 5.9 \times 10^{-6}$$

$$10^{12} \times \left(\frac{\pi^4 \times (0.05 \times 10^{-4})^6}{8 \times 30^2 \times (0.5 \times 10^{-4})^4} \right) \left(\frac{1.5^2 - 1}{1.5^2 + 2} \right)^2 (1 + \cos^2(180°)) = 5.9 \times 10^{-6}$$

Figure 16.8 is a plot of i_1 and i_2 as a function of θ for m = 1.33 and α values of 0.8, 2, and 10. It is apparent that, as the particle size increases, the angular scattering pattern becomes more complicated. The smooth pattern for size parameter, α = 0.8, changes to one that shows large variations in intensity, a factor of 100 or

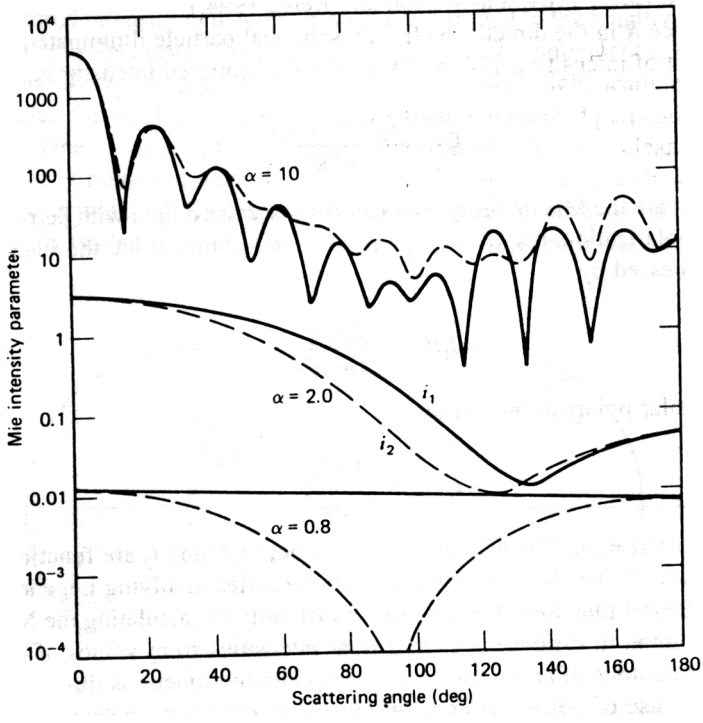

FIGURE 16.8 Mie intensity parameters versus scattering angle for water droplets (m = 1.33) having α = 0.8, 2.0, and 10.0. Solid lines are i_1 and dashed lines are i_2.

more over a few degrees, for an α of 10 or more. As the particles get larger, the scattering in the forward direction becomes much stronger than at other angles. The segment of the curve for $\alpha = 10$ between 0 and about 20° is known as the *forward lobe* and consists primarily of diffracted light. It is absent in Rayleigh scattering. Agglomerated or very irregular particles and absorbing particles tend to smooth out the irregular scattering patterns shown. The irregular scattering patterns shown apply only to single particles or monodisperse aerosols. Most aerosols are polydisperse, and the patterns from many different sizes add together to give much smoother curves.

Figure 16.9 gives the combined Mie intensity parameter for water droplets as a function of the particle size parameter for scattering at $\theta = 30°$ and 90°. These curves

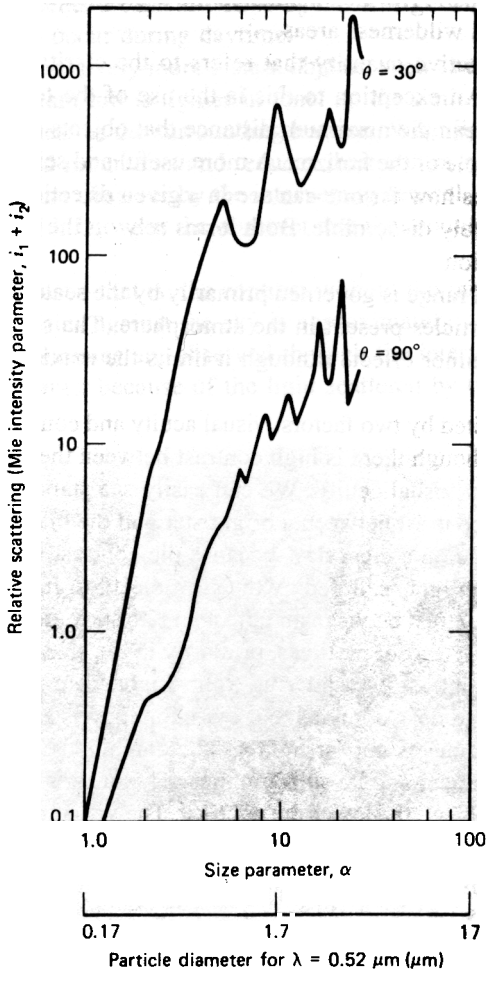

FIGURE 16.9 Relative scattering [Mie intensity parameter $(i_1 + i_2)$] versus size parameter for water droplets ($m = 1.33$) at scattering angles of 30 and 90°.

become smooth and approach a d^6 power curve as the particle size decreases to the Rayleigh region. Curves of scattered intensity versus particle size can be smoothed by accepting scattered light over a range of scattering angles, as is commonly done in light-scattering instruments.

16.4 VISIBILITY

An important application of the theory of light scattering and extinction is the study of visibility in the atmosphere, the most striking feature of particulate pollution. This subject has received considerable attention in the United States since the passage of the Clean Air Act of 1977, which mandated the protection of visibility in American national parks and wilderness areas.

Visibility is a subjective quantity that refers to the clarity with which distant objects can be seen. An exception to this is the use of the term visibility by the aviation industry to mean the maximum distance that objects can be seen throughout at least half the circle of the horizon. A more useful and scientific term is *visual range,* which expresses how far one can see in a given direction, or the distance at which an object is barely discernible. Both terms rely on the psychophysical concept of visual perception.

Atmospheric visual range is governed primarily by the scattering and absorption of light by aerosol particles present in the atmosphere. The scattering by air molecules usually has a minor effect, although it limits the maximum visual range to 100–300 km.

Visual range is limited by two factors: visual acuity and contrast. We cannot read a book at 10 m even though there is high contrast between the letters and the page, because of insufficient visual acuity. We can easily see stars on a clear night because of the extreme contrast between a bright star and the blackness of space. The same stars are invisible on a clear day, because the contrast is reduced to zero by the "air light"—the sunlight scattered by the air molecules. In most situations, it is the lack of apparent contrast between an object and its surroundings that limits how far we can see objects. Aerosol particles, primarily in the size range of 0.1–1.0 μm, reduce the apparent contrast by scattering light. Light from an object is scattered out of the sight path and does not reach our eyes. Sunlight is scattered *into* the sight path and makes dark objects appear lighter. The combined effect is to reduce the contrast between an object and its surroundings. The greater the distance between the observer and the object, the lower the contrast. The visual range is reached when the contrast is reduced to the point where the object is just discernible.

For an isolated object surrounded by a uniform and extensive background, the inherent contrast C_0 is

$$C_0 = \frac{B_0 - B'}{B'} \tag{16.26}$$

where B_0 is the luminance of the object and B' is the luminance of the background. Luminance describes the brightness of a surface and is defined as the luminous intensity per unit solid angle per unit area of surface. The units of luminance are lumens/m^2 · sr, or candelas per square meter (cd/m^2). The sky near the horizon has a luminance of 10^4 cd/m^2 on a clear day and 10^{-4} cd/m^2 on an overcast, moonless night. The luminance of a piece of white paper is 25,000 cd/m^2 in sunlight and 0.03 cd/m^2 in moonlight.

When the luminance of an object and its surrounding background are the same, the contrast is zero, and the object cannot be distinguished from the background. If the object is less luminous than its background, C_0 is negative, reaching a value of -1 for an ideal black object against a white (or lighted) background. When the object is brighter than its background, C_0 can have any positive value. For example, a light at night represents a case in which C_0 has a large value. Contrasts greater than about 10 seldom occur during daytime.

As we look at progressively more distant objects, such as the hills shown in Fig. 16.10, each more distant hill is lighter in tone. At the limit of visibility, the hills have the same brightness as the surrounding horizon. What lightens the appearance of the distant hills and mountains and reduces their contrast relative to the sky is the light scattered to the observer by the intervening aerosol. As the distance is increased, more aerosol is between the observer and the mountains, and they appear lighter.

The inherent contrast—that is, the contrast without the intervening aerosol—of forest-covered mountains against the sky is approximately -1. The apparent contrast C_R when the mountains are observed through the intervening aerosol is less than the inherent contrast because of the light scattered by the aerosol and is defined as

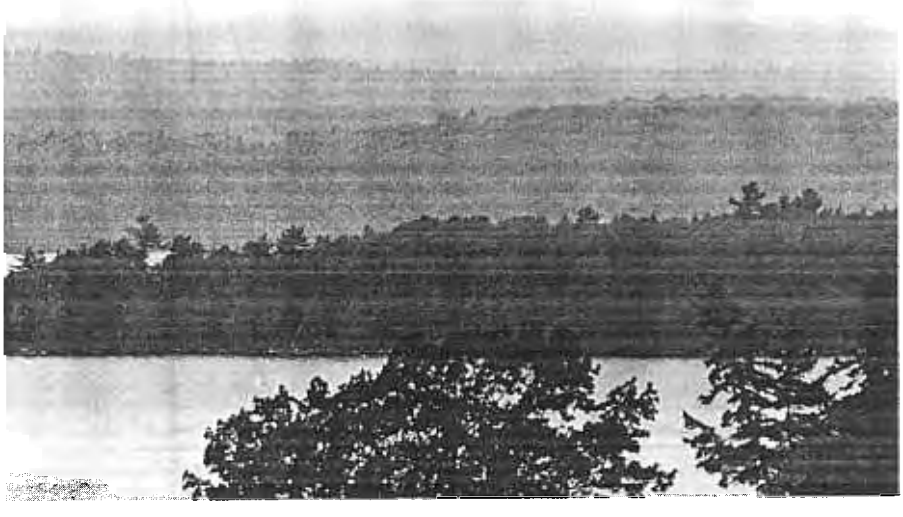

FIGURE 16.10 Photograph showing the increase in the apparent luminance of forest-covered hills with increasing distance. Photograph courtesy of W. L. Hinds.

$$C_R = \frac{B_R - B'_R}{B'_R} \tag{16.27}$$

where B_R and B'_R are the observed luminances of the object and the background, respectively. The apparent contrast is equal to the inherent contrast if there is negligible aerosol (or air) scattering between the observer and the object.

In the common case, shown in Fig. 16.11, of an object viewed against the horizon, the change in luminance, dB, caused by a thin layer dx of a uniform aerosol between the observer and the object is

$$\frac{dB}{dx} = -\sigma_e B + B_a \tag{16.28}$$

where B is the luminance of the object at the thin layer, $\sigma_e B$ is the loss of luminance due to scattering and absorption per unit thickness, and B_a is the luminance of a unit thickness of aerosol due to the skylight scattered to the observer. A similar equation can be written for the horizon sky (the background), but its luminance does not change with position, so dB/dx must equal 0, and

$$B_a = \sigma_e B' = \sigma_e B'_R \tag{16.29}$$

Integrating Eq. 16.28 over the distance L between the object and the observer gives

$$\int_{B_0}^{B_R} \frac{dB}{B_a - \sigma_e B} = \int_0^L dx \tag{16.30}$$

$$B_R = B'_R(1 - e^{-\sigma_e L}) + B_0 e^{-\sigma_e L} \tag{16.31}$$

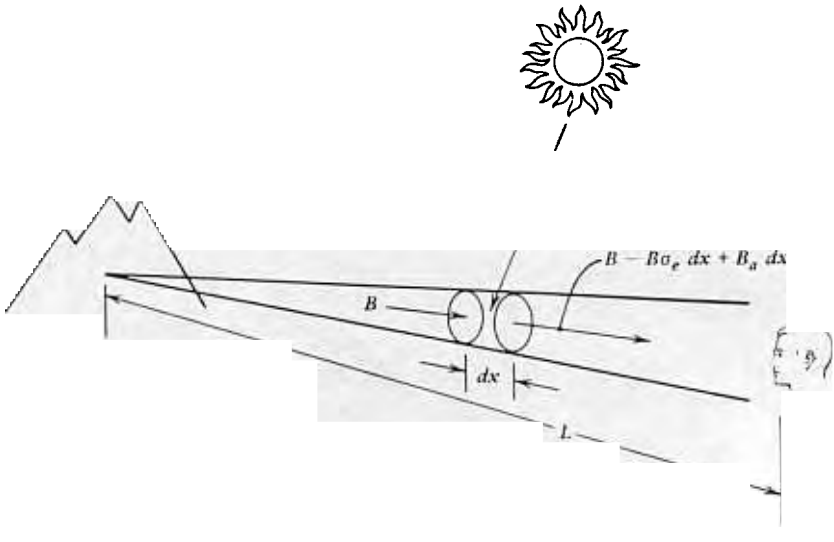

FIGURE 16.11 Diagram for the derivation of Koschmieder's law

where B_a/σ_e has been replaced by B_R' according to Eq. 16.29. Substituting Eqs. 16.29 and 16.31 into 16.27 gives Koschmieder's equation, an expression for the apparent contrast of an object when viewed against the horizon as a function of the distance between the observer and the object:

$$C_R = \left(\frac{B_0 - B_R'}{B_R'}\right) e^{-\sigma_e L} \tag{16.32}$$

$$C_R = C_0 e^{-\sigma_e L} \tag{16.33}$$

A comparison of Eqs. 16.33 and 16.7 reveals that the exponential relationship between contrast and distance is the same as that for extinction. Equation 16.33 holds for horizontal viewing of an object with any value of inherent contrast when the objecct is viewed against the horizon. The extinction coefficient and the illumination of the aerosol must be uniform over the entire viewing distance. If the sight path distance is short or the aerosol sufficiently dilute, $\sigma_e L$ will be approximately zero, and the apparent contrast will equal the inherent contrast, giving nearly perfect viewing. With increasing distance (or increasing σ_e), the apparent contrast gets closer and closer to zero, as shown in Fig. 16.12.

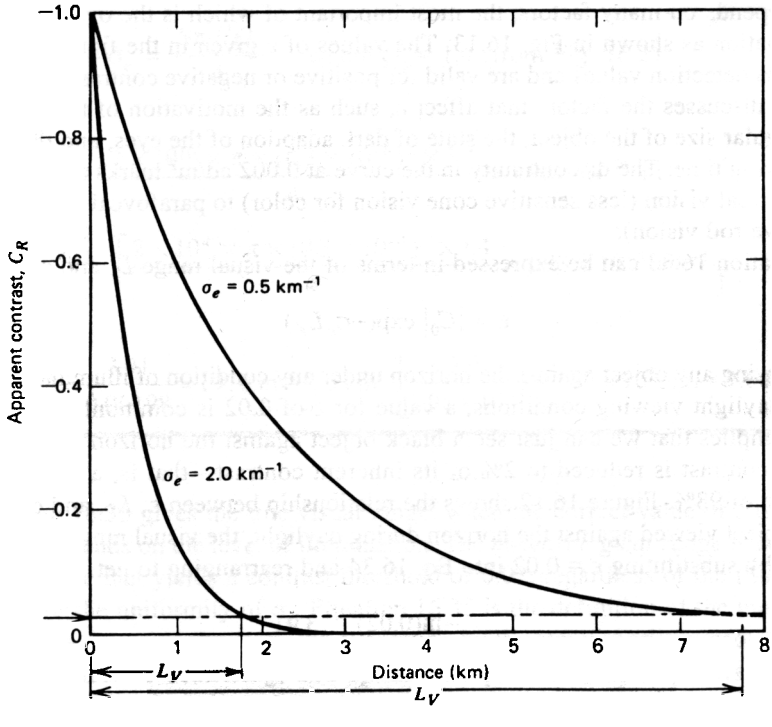

FIGURE 16.12 Apparent contrast versus distance for a dark object against the horizon for two values of extinction coefficient.

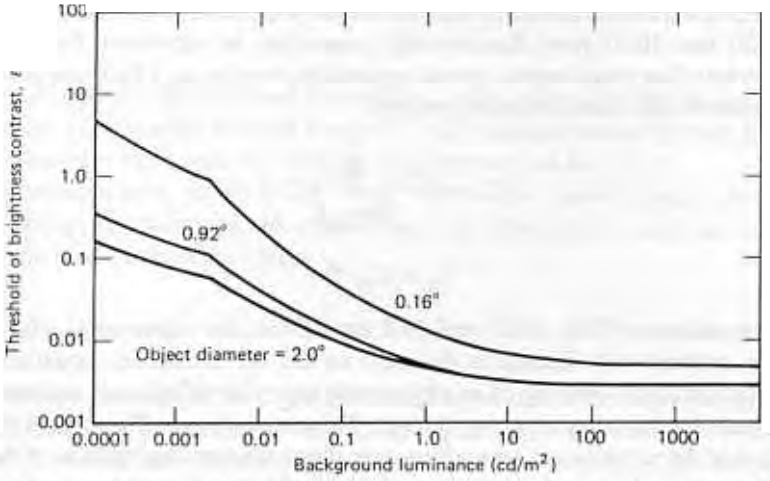

FIGURE 16.13 Threshold of brightness contrast versus background luminance for unlimited viewing time. Parameter is diameter of object, in degrees of arc. Data from Blackwell (1946).

The minimum contrast required to just distinguish an object from its background is called the *threshold of brightness contrast* and is given the symbol ε. The value of ε depends on many factors, the most important of which is the overall level of illumination as shown in Fig. 16.13. The values of ε given in the figure represent the 50% detection values and are valid for positive or negative contrast. Middleton (1952) discusses the factors that affect ε, such as the motivation of the observer, the angular size of the object, the state of dark adaption of the eyes, and the length of viewing time. The discontinuity in the curve at 0.002 cd/m^2 marks the transition from foveal vision (less sensitive cone vision for color) to parafoveal vision (more sensitive rod vision).

Equation 16.33 can be expressed in terms of the visual range L_V and ε as

$$\varepsilon = |C_0| \exp(-\sigma_e L_V \tag{16.34}$$

for viewing any object against the horizon under any condition of illumination. For good daylight viewing conditions, a value for ε of 0.02 is commonly used. This value implies that we can just see a black object against the horizon when its apparent contrast is reduced to 2% of its inherent contrast—that is, a reduction in contrast of 98%. Figure 16.12 shows the relationship between ε, L_V, and σ_e. For a dark object viewed against the horizon during daylight, the visual range can be obtained by substituting ε = 0.02 into Eq. 16.34 and rearranging to get

$$L_v = \frac{-\ln(0.02)}{\sigma_e} = \frac{3.91}{\sigma_e} \tag{16.35}$$

For daylight viewing of a dark object against the horizon, the visual range is a simple inverse function of the atmospheric extinction coefficient. The visual range is given

by Eq. 16.35 in the same units of length in which σ_e is expressed. The equation relates the visual range to σ_e and, consequently, to the aerosol properties of number or mass concentration and particle size by Eq. 16.9, 16.13, or 16.19. When the visual range is greater than 30 km, the effect of scattering by air molecules must be included by summing the extinction coefficients for air (Eq. 16.17) and aerosol.

In 1899, Lord Rayleigh used the preceding visibility principles and Eq. 16.17, a result of the Rayleigh theory, to determine Avogadro's number by visual observation. One clear day, while vacationing in Darjeeling, India, he observed Mount Everest at a distance of about 150 km from the terrace of his hotel. Through simple calculations, he arrived at a value of 3×10^{19} for n (adjusted to sea level), which corresponds to a value of N_a of 6.7×10^{23}. This is remarkably accurate considering the simplicity of the measurement and illustrates the power of light scattering as an atmospheric measuring tool.

EXAMPLE

What is the daylight visual range in polluted air containing 0.3-μm-diameter particles at a concentration of $2 \times 10^{10}/m^3$ [2×10^4 particles/cm^3]? Assume that the particle refractive index is 1.5.

$$\sigma_e = \frac{N\pi d^2 Q_e}{4} \qquad \text{where } Q_e = \ .4 \text{ (from Fig. 16.2)}$$

$$\sigma_e = \frac{2 \times 10^{10} \times \pi \times (0.3 \times 10^{-6})^2 \times 1.4}{4} = 1.98 \times 10^{-3} \text{ m}$$

$$\left[\frac{2 \times 10^4 \times \pi \times (0.3 \times 10^{-4})^2 \times 1.4}{4} = 1.98 \times 10^{-5} \text{ cm} \right]$$

$$L_v = \frac{3.91}{\sigma_e} = \frac{3.91}{0.00198} = 1970 \text{ m} = 2.0 \text{ km} \quad \left[\frac{3.91}{1.98 \times 10^{-5}} = 1.97 \times 10^5 \text{ cm} = 2.0 \text{ km}\right]$$

Equation 16.35 gives the true visual range, when the correct value of ε is 0.02. The latter depends on the level of illumination. The *meteorological range* is defined as the distance that yields a contrast threshold of 0.02, regardless of the illumination level or the uniformity of σ_e. Equation 16.35 is the definition of the meteorological range. In many situations the absorption by the atmospheric aerosol is negligible compared to scattering, and σ_e can be replaced by σ_s (Eq. 16.11). This assumption permits the meteorological range to be estimated by an instrument called an integrating nephelometer (see Section 16.5), which measures σ_s (also called b_{scat})

directly. In polluted urban air, σ_a may be as large as $0.5\sigma_s$, and the total extinction coefficient σ_e must be used.

A review of correlations between the aerosol mass concentration C_m and nephelometer measurements of σ_s by Lodge et al. (1981) found that

$$\frac{C_m}{\sigma_s} = 0.5 \text{ g/m}^2 \tag{16.36}$$

for total mass concentration and

$$\frac{C'_m}{\sigma_s} = 0.3 \text{ g/m}^2 \tag{16.37}$$

for C'_m equal to the mass concentration in the fine-particle mode. The correlation coefficients are 0.6–0.9 for total mass concentration and about 0.9 for the fine-particle mode, suggesting the importance of the latter mode in controlling visibility. At relative humidities greater than 70%, σ_s increases relative to C_m because of droplet formation on hygroscopic particles. Equations 16.36 and 16.37 are averages for many sites, and individual sites may differ significantly. Colored haze, usually brown or yellow, observed in urban areas is caused primarily by wavelength-dependent extinction of aerosols and secondarily by wavelength-dependent extinction of gases such as NO_2.

16.5 OPTICAL MEASUREMENT OF AEROSOLS

Light scattering provides an extremely sensitive tool for the measurement of aerosol concentration and particle size. A single particle as small as 0.1 μm produces a detectable scattered light signal. Light-scattering techniques have the advantage of minimally disturbing the aerosol and providing instantaneous information that is often suitable for continuous monitoring. A disadvantage of light-scattering instruments is that the scattering may be sensitive to small changes in refractive index, scattering angle, particle size, or particle shape, which can lead to confusing or misleading results. These optical measurement methods differ from the microscopy methods described in Chapter 20 in that the particles do not have to be captured and it is not necessary to form an image of them. Kerker (1997) gives a historical overview of light-scattering instruments for aerosol measurement.

A simple laboratory instrument called the *owl,* now primarily of historical interest, can be used to determine rapidly the size of *monodisperse* submicrometer test aerosols (Sinclair, 1950). The aerosol flows through a chamber 70 mm in diameter with a collimated beam of unpolarized, white light passing along a diameter. The aerosol is viewed through a microscope that is free to rotate so that it can view light scattered at any angle from 25 to 155°. The polarization (the ratio of I_2 to I_1) of the light scattered at 90° can be used to determine the diameter of particles between 0.1 and 0.4 μm by comparing the measured values with calculated values. A sec-

ond method relies on the color of the scattered light as a function of angle to determine particle diameters from 0.2 to 1.5 μm. Monodisperse aerosols in this size range produce colored bands in their angular scattering pattern called *higher order Tyndall spectra*, or HOTS. The number or the angular positions of *red* bands can be used to determine the particle size by comparing the observed values with calculated values. The sharpness of the colored bands increases with increasing monodispersity.

Transmissometers, or light-attenuating photometers, are instruments that measure the attenuation (extinction) of light through a path length that may range from a few centimeters to a few kilometers. Stack transmissometers have a focused light source positioned on one side of a stack and directed across the stack to a detector. These instruments measure the extinction by the smoke in the stack when constructed according to Fig. 16.1, but often the detected beam is inadequately collimated, and such instruments detect significant amounts of forward-scattered light. Because of multiple scattering effects at high aerosol concentrations, the transmitted light intensity varies in an unpredictable way with concentration. This unpredictability is not a problem for pure extinction by aerosols. A gravimetric calibration can be used if the particle refractive index and size are constant. To eliminate forward scattering, the size of the pinhole before the detector must have an angular diameter, measured from the center of the preceding lens, of not more than $0.38/\alpha$ radians.

Three types of instruments rely on measurements of light scattered at fixed angles from polydisperse aerosols: photometers, nephelometers, and optical-particle counters. *Photometers* are used to measure relative concentration by measuring the combined light scattered from many particles at once. The aerosol flows continuously through the instrument at several liters per minute. The illumination and collection optics are arranged so that the light scattered at a fixed range of angles reaches the detector. Depending on the design, the instrument may measure the scattered light in the region of 90°, 45°, or less than 30°. Forward-scattering photometers (< 30°) are less sensitive to refractive index than 90° scattering instruments. Photometers are used with monodisperse test aerosols for filter penetration testing. Typical instruments can measure penetrations as low as 0.001%.

In the field of occupational hygiene, portable photometers are used as direct-reading instruments to measure mass concentration. The scattering angles and wavelengths used are selected to reduce the effect of particle size and refractive index on the response of the instrument. Electronic averaging is used to provide a digital readout of mass concentration over the range of 1 $\mu g/m^3$ to 100 mg/m^3. The output of such instruments is sensitive to aerosol material and particle size distribution, and errors in concentration of a factor of two or more are possible with variation in these parameters. Instruments should be calibrated with side-by-side filter samples if they are used for aerosols that differ appreciably from the manufacturer's calibration aerosol. These photometers provide continuous output and are well suited to monitoring concentration changes with time and location, provided that the particle size and chemical composition remain constant. Commercially available photometers and other light-scattering instruments are reviewed by Pui and Swift (1995).

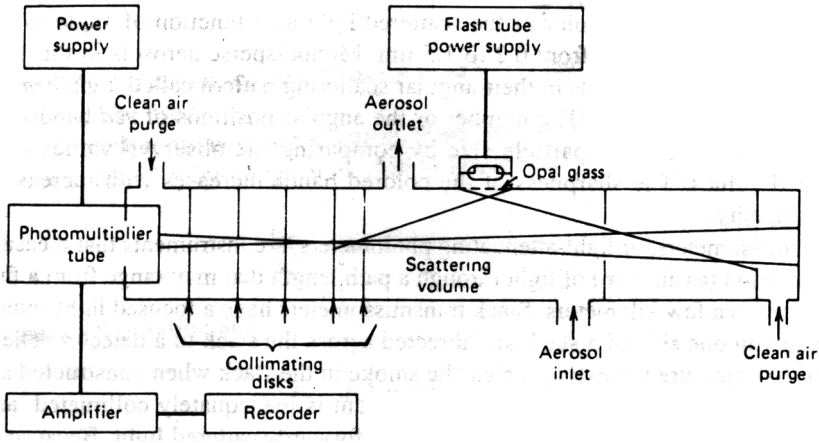

FIGURE 16.14 Diagram of an integrating nephelometer. Reprinted with permission from *J. Air Poll. Control Assoc.*, **17**, 467 (1967).

The *integrating nephelometer* is a photometer designed to measure the light scattered from an aerosol over as wide a range of angles as possible. The instrument shown in Fig. 16.14 measures the scattered light from 8 to 170° and can measure scattering coefficients as small as 10^{-6}/m from a sensitive volume of about 1 L. This instrument provides a measurement of σ_s due to particles and gas molecules. If σ_a is zero, the nephelometer yields a direct measurement of σ_e that provides an instrumental estimate of meteorological range by Eq. 16.35. Integrating nephelometers can be used to estimate mass concentrations with a suitable calibration.

Optical particle counters (*OPC*s), such as that shown in Fig. 16.15, are similar to photometers. However, the aerosol flows through a focused light or laser beam as a thin stream surrounded by sheath air, so that only one particle at a time is illu-

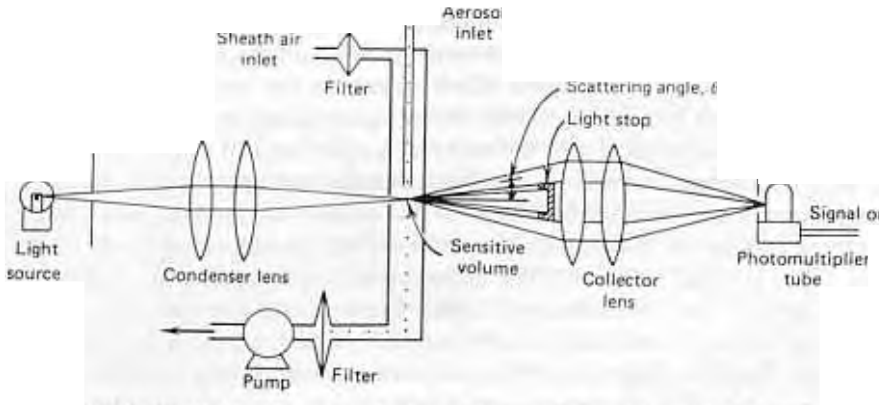

FIGURE 16.15 Diagram of a forward-scattering optical particle counter

TABLE 16.3 Characteristics of Some Optical Particle Counters

Instrument	Particle Size Range (μm)	Number of Channels	Scattering Angle Range (deg)	Sample Flow Rate (cm^3/min)	Maximum Concentration[a] (cm^{-3})
	0.3–>20	16	15–105	28,000	90
	0.1–>0.5	6	15–150	2800	14
	0.19–>5.0	6	15–150	28,000	14
	0.12–>6.0	16	35–120	280	3000
	0.25–>10	6	60–120	28,000	7
	0.065–1.0	32	35–120	2800	8000
	0.09–3	16[f]	35–120	60	7,000
	0.12–7.5	16[f]	35–120	280	3000
	0.2–>5.0	6	60–120	28,000	3.5

[a]Concentration for 10 % coincidence error.
[b]Climet Instruments Co., Redlands, CA.
[c]White light illumination; all others use laser light.
[d]Hiac/Royco, Menlo Park, CA.
[e]Particle Measuring Systems, Inc., Boulder, CO.
[f]Four ranges with 16 channels each.

minated and scatters light to the detector. OPCs have proven to be a valuable tool in aerosol research, air pollution studies, and clean-room monitoring because of their ability to rapidly provide information on aerosol size distributions. Commercial instruments cover the size range 0.05–20 μm, although 0.1–5 μm is most common, and provide measurements of number concentration in 5–16 size channels. As each particle passes through the focused light beam, it scatters a pulse of light to the detector, which is converted to an electrical signal. Electronic pulse height (or area) analysis is used to interpret the pulse and direct a count to the proper size channel, where the total counts in each size range are accumulated. The particle size distribution by count is obtained from the accumulated counts in each size channel. These instruments are based on the assumption that the scattered light intensity is a monotonic function of particle size, but this is not always the case, as is discussed shortly. Also, diluting the aerosol may be necessary so that only one particle passes through the beam at a time.

Characteristics of some commercially available optical particle counters are given in Table 16.3. The choice of scattering angle involves a trade-off of many factors. The forward direction provides stronger signals, but requires special care to reduce background noise, which is least at 90°. Forward scattering is primarily diffracted light, which is less sensitive to the refractive index and to whether the particle is absorbing. Some instruments use bowl-shaped mirrors to collect all the light scattered within a certain range of scattering angles. Instruments that use lasers as their light source have the lowest minimum detectable particle sizes. These instruments have counting efficiencies (ratio of indicated count to true count) of approximately 100% for particles > 0.1 μm. Monodisperse spherical particles of known size and refractive index are used to verify the size calibration of optical particle counters.

As shown in Fig. 16.16, the response of optical particle counters depends on the size and refractive index of the particles. When the refractive index is known, suitable calibration will permit an accurate measurement of the size distribution. For aerosol particles of unknown refractive index, the error in size estimation can be significant. For the response curves shown in Fig. 16.16 this error ranges from –50 to +140%. This large spread limits the usefulness of optical particle counters when a range of refractive indices is present or when the refractive index is not known. For some refractive indices, part of the response curve is not monotonic, usually in the range of 0.5–1.5 μm, and there is more than one size that corresponds to a particular signal strength. For example, a relative signal of 400 for iron in Fig. 16.16 could be due to particles having diameters of either 0.34 or 0.53 μm.

Optical particle counters are restricted by coincidence errors to the measurement of aerosols with relatively low number concentrations, usually less than $10^{10}/m^3$ [$10^4/cm^3$]. Aerosols with higher concentrations must be diluted to this level for unbiased measurement. Coincidence errors arise when two or more particles are in the sensitive volume simultaneously, causing a spurious signal that leads to an underestimation of the particle number concentration and an overestimation of the particle size. The sensitive volume is the region from which signals are generated, defined by the incident and scattered beams and the diameter of the aerosol stream. The ratio of the observed count N_o to the true count N_t is given by

$$\frac{N_o}{N_t} = \exp(-N_t Q\tau) \tag{16.38}$$

where Q is the flow rate through the sensitive volume and τ is the time for a particle to traverse the beam, plus the signal-processing time. Coincidence error can be minimized by reducing the flow rate and the dimensions of the beam; however, small beam dimensions require a small aerosol stream diameter so that nearly all particles will pass through the beam for a high counting efficiency. Some instruments use aerodynamic focusing of the aerosol stream to achieve a stream diameter of less than 0.1 mm. Table 16.3 gives maximum concentrations for a 10% error in count due to coincidence.

Care must be taken in interpreting size distribution data from optical particle counters. The distribution obtained is the size distribution by count or the number distribution, but the number of particles below the lower size limit is unknown and may be large. Plotting the results as counts per micrometer (number divided by channel width) gives an accurate representation of the data. Plotting the fraction per micrometer may be seriously in error if there is uncertainty in the total number of particles.

Another particle-sizing method, called photon correlation spectroscopy (PCS), dynamic light scattering (DLS) or quasi-electric light scattering (QELS), relies on both the light scattering and the Brownian motion of the particles. An ensemble of

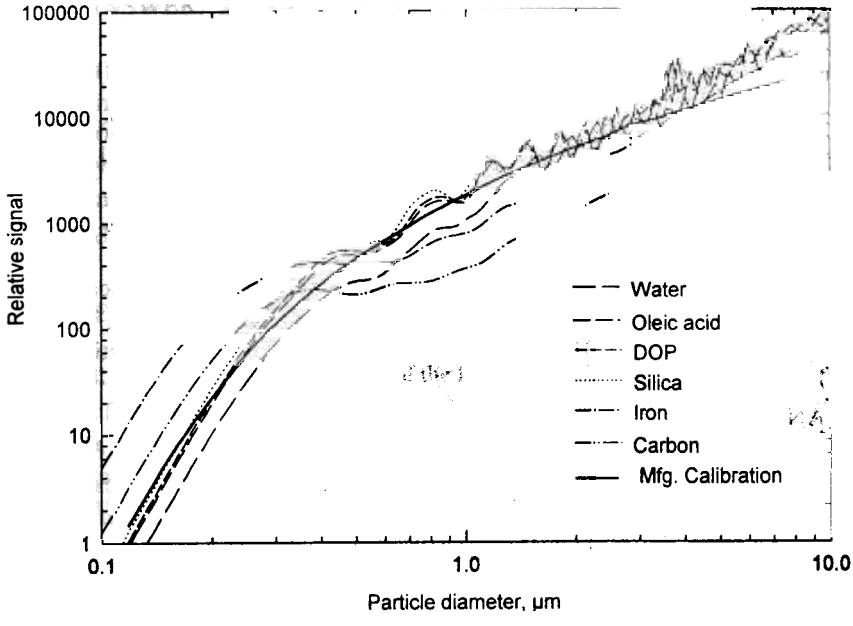

FIGURE 16.16 Calculated response curves for six materials and manufacturer's calibration curve for model LAS-X® (PMS, Inc., Boulder, CO) optical particle counter.

particles is illuminated with a laser beam, and the scattered light is detected at a specific angle. The incident light has a single frequency, but the scattered light has a narrow range of frequencies, due to the Doppler effect and the Brownian motion of the particles. This frequency broadening manifests itself as a low-frequency spectrum in the photomultiplier tube output signal. The signal is analyzed by a spectrum analyzer or a digital autocorrelator (PCS). The width of the spectrum is related to the average diffusion coefficient of the aerosol and thus to the particle size. This method requires a high number concentration, but does not require knowing the particle refractive index. It has been applied to soot formation in flames and to studies of diesel exhaust particles. (See Rader and O'Hern, 1993.)

PROBLEMS

16.1 A tabulation of Mie intensity parameters gives $i_1 = 4.89 \times 10^{-4}$ and $i_2 = 4.43 \times 10^{-8}$ for light scattered at 90° from 0.088-μm polystyrene latex spheres. What error in total scattered intensity at 90° would result if Rayleigh scattering were assumed to hold? $\lambda = 0.55$ μm; $m = 1.59$.

ANSWER: 280%.

16.2 Determine the aerosol number and mass concentration for which the particles and the air in a unit volume of aerosol scatter equal amounts of light. Assume that the particle diameter is 0.5 μm, $m = 1.5$, and $\rho_p = 1000$ kg/m^3 [1.0 g/cm^3].

ANSWER: 2.6×10^7/m^3 [26/cm^3], 1.7 μg/m^3.

16.3 Determine the fractional light transmission through 1 km of air containing 1.0-μm-diameter water droplets at a concentration of 10^8/m^3 [100/cm^3]. Assume that the wavelength of light is 0.52 μm.

ANSWER: 0.73.

16.4 What number concentration of 0.05-μm-diameter particles scatters as much light per cubic centimeter as 1 cm^3 of particle-free air? σ_e for air is 1.5×10^{-5}/m [1.5×10^{-7}/cm]. Assume that $m = 1.5$ for the particles and $\lambda = 0.5$ μm.

ANSWER: 3.4×10^{12}/m^3 [3.4×10^6/cm^3].

16.5 The California ambient air quality standard for visibility requires that the average σ_e be less than 0.23 when the relative humidity is less than 70%. To what visual range does this limit correspond? To what aerosol mass concentration does it correspond? Assume that the particle size is 0.18 μm (SMD for the accumulation mode), the particle refractive index is 1.5, and ρ_p is 1000 kg/m^3 [1.0 g/cm^3].

ANSWER: 17 km [10.6 mi], 110 μg/m^3.

16.6 One sunny day, while measuring the atmospheric aerosol concentration (25 $\mu g/m^3$) on the top of the UCLA Center for Health Sciences building, you notice that you can *just* see Palos Verdes Hill 22 mi away. If you assume that the atmospheric aerosol is monodisperse, what is its particle size? Assume that $Q_e = 1.0$ and $\rho_p = 1000$ kg/m^3 [1.0 g/cm^3] and neglect extinction due to air molecules.

ANSWER: 0.34 μm.

16.7 Repeat problem 16.6, but include the effect of air molecules. Assume that $\lambda = 0.5$ μm.

ANSWER: 0.40 μm.

16.8 You observe the visual range in urban air. If you assume that the range depends solely on the fine-particle mode and that it can be represented by an equivalent nonabsorbing monodisperse aerosol, what is its particle size? Assume that $Q_e = Q_s = 1$ and the particle density is 1500 kg/m^3 [1.5 g/cm^3]. [*Hint*: Use the empirical expression relating visual range to fine-particle mass concentration and Bouguer's law expressed in terms of mass concentration.]

ANSWER: 0.3 μm.

16.9 What is the meteorological range in particle-free air at 20°C at sea level? Assume that $\lambda = 0.5$ μm.

ANSWER: 220 km.

16.10 (a) What is the maximum distance at which one can see a black automobile on a foggy, moonlit night? Assume that the fog consists of 5-μm droplets at 10^{10}/m^3 [10^4/cm^3], that the background luminance is 10^{-3} cd/m^2, and that your eyes are completely dark adapted. (b) Repeat part (a) if the headlights are on and are directed toward you; assume that the inherent contrast is 10^4.

ANSWER: (a) 6.1 m; (b) 30 m.

REFERENCES

Blackwell, H.R., "Contrast Thresholds of the Human Eye," *JOSA*, **36**, 624–643 (1946).

Cadle, R. D., *The Measurement of Airborne Particles,* Wiley, New York, 1975.

Cooke, D. D., and Kerker, M., "Response Calculations for Light Scattering Aerosol Particle Counters," *Appl. Optics,* **14**, 734–739 (1975).

Dave, J. V., "Scattering of Electromagnetic Radiation by a Large, Absorbing Sphere," *IBM J. Res. Develop.,* 302–313 (May 1969).

Dave, J. V., *Subroutines for Computing the Parameters of the Electromagnetic Radiation Scattered by a Sphere*, Rept. No. 320-3237, IBM Scientific Center, Palo Alto, CA, May 1968.

Fenn, R. W., "Optical Properties of Aerosols," in Dennis, R. (Ed.), *Handbook on Aerosols,* USERDA, 1976, TID-26608, Oak Ridge, TN, 1976.

Gebhart, J., "Optical Direct-Reading Techniques: Light Intensity Systems," in Willeke, K., and Baron, P. A. (Eds.), *Aerosol Measurement*, Van Nostrand Reinhold, New York, 1993.

Hodkinson, J. R., "The Optical Measurement of Aerosols," in Davies, C. N. (Ed.), *Aerosol Science,* Academic Press, New York, 1966.

Kerker, M., "Light Scattering Instruments for Aerosol Studies: An Historical Overview," *Aerosol Sci. Tech.*, **27**, 522–540 (1997).

Kerker, M., *The Scattering of Light and Other Electromagnetic Radiation,* Academic Press, New York, 1969.

Lodge, J. P., Waggoner, A. P., Klodt, D. T., and Crain, C. N., "Non-health Effects of Airborne Particulate Matter," *Atm. Env.*, **15**, 431–482 (1981).

Middleton, W. E. K., *Vision through the Atmosphere,* University of Toronto, Toronto, 1952.

Ozkaynak, H., Schatz, A. D., Thurston, G. D., Isaacs, R. G., and Husar, R. B., "Relationships between Aerosol Extinction Coefficients Derived from Airport Visual Range Observations and Alternate Measures of Airborne Particle Mass," *J. Air Pol. Control Assoc.*, **35**, 1176–1185 (1985).

Pui, D. Y. H., and Swift, D. L., "Direct-Reading Instruments for Airborne Particles," in Cohen, B. S., and Hering, S. V. (Eds.), *Air Sampling Instruments*, 8th ed., ACGIH, Cincinnati, 1995.

Rader, D. J., and O'Hern, T.J., "Optical Direct-Reading Techniques: In Situ Sensing," in Willeke, K., and Baron, P. A. (Eds.), *Aerosol Measurement*, Van Nostrand Reinhold, New York, 1993.

Sinclair, D., "Optical Properties of Aerosols," in *Handbook on Aerosols*, USGPO, Washington, DC (1950).

Van de Hulst, H. C., *Light Scattering by Small Particles,* Wiley, New York, 1957; republished by Dover, New York, 1981.

Whitby, K. T., and Willeke, K., "Single Particle Optical Counters: Principles and Field Use," in Lundgren, D. A. et al. (Eds.), *Aerosol Measurement,* University Presses of Florida, Gainesville, FL, 1979.

Wilson, W. E., and Reist, P. C., "A PC-based Mie Scattering Program for Theoretical Investigations of the Optical Properties of Atmospheric Aerosols as a Function of Composition and Relative Humidity," *Atm. Env.*, **28**, 803–809 (1994).

17 Bulk Motion of Aerosols

The analysis of aerosol motion in the preceding chapters has focused exclusively on the motion of individual particles. There are, however, some situations in which individual particle motion is negligible compared with motion on a larger scale. In one such situation, the gas phase of an aerosol has a density that differs from the surrounding gas. For example, the buoyancy of a stack gas plume causes the particles contained in it to rise many meters after leaving the stack. The movement of gases under these circumstances is a subject of fluid mechanics and meteorology and is not covered here. When there is no difference in gas density between an aerosol cloud and its surroundings, there are still situations in which the cloud as an entity can move much faster than the individual particles that make up the cloud. For the purposes of this chapter, an *aerosol cloud* is defined as a region of high aerosol concentration having a definite boundary in a much larger region of clean air. The mechanics of clouds is far more complicated than that of individual particles, and a complete description of the motion of clouds does not exist. In this chapter, we define the order of magnitude of the conditions under which cloud motion can occur.

Since cloud motion depends on the bulk properties of aerosols, we evaluate first the viscosity of an aerosol cloud relative to that of pure air. Consider a monodisperse aerosol of 1-μm spheres of standard density at a mass concentration of 100 g/m^3. This is a very high mass concentration and corresponds to the densest smokes that can be produced. The number concentration of such an aerosol is 2×10^8/cm^3. The average spacing between particles is 17 μm, or 17 times the diameter of the particles, so the aerosol is still mostly air, and the particles are far enough apart to have little effect on each other. The viscosity of such a two-phase system η_c is

$$\eta_c = \eta(1 + 2.5C_v)$$

where C_v is the volume concentration—that is, the volume of particles per unit volume of aerosol. In this example, $C_v = 0.0001$ and the aerosol has a viscosity 0.025% greater than that for pure air, a negligible difference. The density of a cloud exceeds that of particle-free air by an amount equal to the mass concentration of the particles. At a mass concentration of 100 g/m^3, an aerosol has a density 8.3% greater than that of clean air. It is this difference in density that causes bulk motion of aerosols. When such motion is caused by gravity, it is called cloud settling or mass subsidence.

Cloud settling occurs when the aerosol concentration is sufficient to cause the entire cloud to move as an entity at a velocity significantly greater than the indi-

vidual particle settling velocity. This effect can be caused solely by the particles and need not depend on differences in gas density inside and outside the cloud. Why such an effect occurs can be best understood by considering a spherical array of particles—a cloud—with each particle *fixed in space*. Let air be blown at the cloud with a uniform velocity U_0. The air can either pass through the cloud or pass around the cloud, depending on the relative resistance of the two paths. At a low particle concentration, the air will pass through the cloud, and each particle will experience a relative velocity of U_0. The total resistance presented by the particles will be the sum of the drag force on each particle. At a sufficiently high particle concentration, the resistance to airflow through the cloud will be so great that the air will flow around the cloud, that being the path of least resistance. In this case the relative velocity of the particles inside the cloud is zero, and the resistance is caused by the drag force of the air flowing around the spherical cloud. Between these extremes are intermediate conditions under which both mechanisms operate. A completely analogous situation exists for the gravitational settling of a free cloud which may push through the air as a cloud or as individual particles, depending on the aerosol concentration, cloud size, and particle size. These two types of aerosol motion are shown schematically in Fig. 17.1.

Consider a spherical cloud of diameter d_c having N particles per unit volume, each with a diameter d_p and density ρ_p. For the cloud to move as an entity, the gas in which it is suspended and the particles must move together. In a practical sense, the two can be thought of as coupled or completely entrained, since there is negligible relative motion between the gas and the particles within the cloud. In this case, the downward force of gravity on the cloud is equal to the mass of the gas plus the mass of the particles, and the buoyant force is equal to the mass of displaced gas. It is convenient to approach cloud settling in a manner equivalent to particle settling and define a density for the cloud. For a gas density ρ_g and no difference in gas density between the cloud and the surrounding clean air, the *net cloud density* (density minus buoyancy) ρ_c of a spherical cloud is the mass of the cloud minus the mass of the displaced volume of gas, divided by the volume of the cloud, v_c:

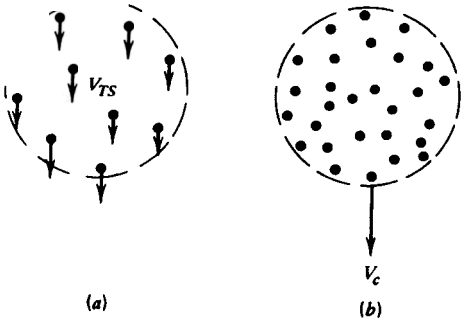

FIGURE 17.1 (a) Individual particle settling. (b) Cloud settling

$$\rho_c = \frac{\rho_g v_c + C_m v_c - \rho_g v_c}{v_c} = C_m \tag{17.2}$$

Thus, the net cloud density is simply the particle mass concentration C_m expressed in appropriate units—kg/m^3 in SI units and g/cm^3 in cgs units. Because clouds are much larger than particles, their Reynolds numbers may be large, and their motion is likely to be outside the Stokes region. The settling velocity V_c of a spherical cloud is obtained by equating the force of gravity to Newton's drag

$$\frac{\rho_c \pi d_c^3 g}{6} = C_D \frac{\pi}{8} \rho_g d_c^2 V_c^2 \tag{17.3}$$

and solving for the cloud settling velocity

$$V_c = \left(\frac{4 \rho_c d_c g}{3 C_D \rho_g} \right)^1 \tag{17.4}$$

Equation 17.4 holds for rigid spheres, but settling clouds develop an internal circulation pattern which reduces the drag force that they experience and increases their settling velocity by a factor of $(6/5)^{0.5}$, or about 10%. For simplicity, this effect has been ignored. Equation 17.4 is equivalent to Eq. 3.29 with ρ_p replaced by ρ_c and d_p by d_c. The procedures for determining the settling velocities of particles at high Reynolds numbers, covered in Section 3.7, can be used to determine the settling velocities of clouds with these substitutions.

EXAMPLE

A spherical cloud of water droplets 5 m in diameter has a mass concentration of g/m^3. What is the terminal settling velocity of the cloud?

$$\rho_c = 0.001 \text{ kg/m}^3 \quad [10^{-6} \text{ g/cm}^3$$

$$C_D \text{ Re} = \frac{4 d_c^3 \rho_c \rho_g g}{3 \eta^2} = \frac{4 \times 5^3 \times 0.001 \times 1.2 \times 9.81}{3 \times (1.81 \times 10^{-5})^2} = 5.99 \times 10^9$$

$$\left[\frac{4 \times 500^3 \times 10^{-6} \times 1.2 \times 10^{-3} \times 981}{3 \times (1.81 \times 10^{-4})^2} = 5.99 \times 10^9 \right]$$

This value is beyond the range of values given in Table 3.4 and is in the region where C_D has a constant value of 0.44. Hence,

$$\left(\frac{5.99 \times 10^9}{0.44}\right)^{1/2} = 1.17 \times 10^5$$

$$V_c = \frac{\text{Re}}{66{,}000 d_c} = \frac{1.17 \times 10^5}{66{,}000 \times 5} = 0.35 \text{ m/s} = \left[\frac{1.17 \times 10^5}{6.6 \times 500} = 35 \text{ cm/s}\right]$$

Thus, this cloud has a settling velocity that is equivalent to the settling velocity of a sphere of standard density 360 μm in diameter.

The settling velocity of an individual particle V_p is given by Eq. 3.21:

$$V_p = \frac{\rho_p d_p^2 g C_c}{18\eta} \tag{17.5}$$

Whether or not cloud settling is significant depends on the quantity G, the ratio of cloud settling velocity (Eq. 17.4) to particle settling velocity (Eq. 17.5). This ratio is

$$G = \frac{V_c}{V_p} = \frac{12\eta}{\rho_p d_p^2 C_c}\left(\frac{3\rho_c d_c}{C_D \rho_g g}\right)^{1/2} \tag{17.6}$$

where C_c is the slip correction factor of the particles. When $G >> 1$, cloud settling is the predominant motion; when $G << 1$, only particle settling occurs; and in between, both mechanisms operate. For simplicity, a value of $G = 1$ will be considered the minimum for cloud settling; it is likely that values of $G >> 1$ are required for prolonged cloud motion, because of the factors, described later in this section, that reduce G with time.

Equation 17.4 holds only for a cloud in the shape of a sphere. Although a cloud may be spherical initially, soon after it begins to move the uneven pressure on its surface will cause it to deform to a nonspherical shape. This deformation will slow the cloud's motion and may cause it to break up into smaller clouds. The size of a settling cloud is gradually reduced with time as its surface is eroded by air currents. Both effects reduce cloud settling velocities. Most cloud aerosols are polydisperse, and the differential settling velocities tend to separate the particles, diluting the cloud and thereby impeding cloud settling. Because of these effects, Eq. 17.4 correctly predicts only the initial motion of a cloud.

The significance of the different variables in Eq. 17.6 is obscured by the drag coefficient C_D, which depends on ρ_c and d_c. For the *special case where cloud motion is in the Stokes region*, $C_D = 24/\text{Re}$, and Eq. 17.6 can be written as

$$G = \frac{\rho_c d_c^2}{\rho_p d_p^2 C_c} = \frac{\pi C_N d_p d_c^2}{6 C_c} \quad \text{for Re}_c < \tag{17.7}$$

where C_c is the slip correction factor of the particles. Equation 17.7 holds only when Re < 1 for the cloud, which usually implies a cloud size smaller than a few centimeters. Cloud settling in the Stokes region is favored by large cloud size, high mass concentration, and small particle size. A mass concentration of only 9.8 mg/m^3 is required for a G value of unity for a cloud 1 cm in diameter with particles 1 μm in diameter.

Table 17.1 gives the minimum mass concentrations required for cloud settling (G = 1). The values were calculated using Eqs. 17.4 and 17.6 and the procedure given in Section 3.7. The table shows the importance of the cloud size and particle size in determining whether cloud settling occurs. It is apparent that most aerosol clouds will, at least initially, have cloud motion, although a value of $G > 100$ is probably required for sustained motion.

Because of the dilution, breakup, and erosion mechanism described earlier, the lifetime of clouds less than a few meters in diameter is brief. Furthermore, a value of G = 1 means only that the cloud settling velocity is equal to the particle settling velocity, a velocity that is very small, particularly for submicrometer-sized particles. Consequently, it is of greater practical significance to identify the concentration required for a cloud to have an appreciable settling velocity, such as 0.01 m/s [1 cm/s], as has been done in Table 17.2. In this case the required mass concentration does not depend on the particle size, although the number concentration does. Note that the mass concentration values are micrograms per cubic meter in Table 17.1 and milligrams per cubic meter in Table 17.2.

When the particle number concentration in a cloud is high, coagulation will rapidly change both the number concentration and the particle size, although the mass concentration will remain constant. As can be seen from Eq. 17.6, an increase in particle size with a constant cloud diameter and mass concentration leads to a rapid decrease in the value of G. Thus, coagulation inhibits cloud settling. In sum, the several effects described here suggest that aerosol clouds often move initially as an entity, but quickly revert to individual particle motion because of the combined effect of erosion, breakup, size distribution, dilution, and coagulation.

Generally, the gas composition and temperature inside a cloud and in the surrounding air will be different. This difference in density is usually much greater than the net cloud density ρ_c, due to the weight of the particles. For example, in natural atmospheric clouds, a temperature difference of 0.2°C produces a buoyant force

TABLE 17.1 Minimum Concentration for Cloud Settling (G = 1) at Standard Conditions

Particle Diameter (μm)	Mass Concentration (μg/m^3)			
	d_c = 0.01 m	d_c = 0.1 m	d_c = 1 m	d_c = 10 m
0.04				
0.1				
0.4				
1.0				

TABLE 17.2 Concentration Required for a Cloud Settling Velocity of 0.01 m/s [1 cm/s] at Standard Conditions

	Mass Concentration (mg/m^3) and [Number concentration (cm^{-3})]			
0.04	4400 [1.3×10^{11}]	100 [3.1×10^{9}]	3.8 [1.1×10^{8}]	0.34 [1.0×10^{7}]
0.	4400 [8.5×10^{9}]	100 [2.0×10^{8}]	3.8 [7.3×10^{6}]	0.34 [6.4×10^{5}]
0.4	4400 [1.3×10^{8}]	100 [3.1×10^{6}]	3.8 [1.1×10^{5}]	0.34 [1.0×10^{4}]
1.0	4400 [8.5×10^{6}]	100 [2.0×10^{5}]	3.8 [7.3×10^{3}]	0.34 [6.4×10^{2}]

equivalent to the force of gravity on a cloud with a particle mass concentration of 1 g/m^3. A similar effect is produced by an absolute humidity difference of 130 Pa [1 mm Hg]. The weight of the particles plays a secondary role in controlling the vertical movement of atmospheric clouds. Some combustion clouds rise initially because of their high gas temperature, and after cooling they settle because of their high CO_2 content. Cloud motion has been observed in experiments with cigarette smoke, an aerosol of high concentration with a gas phase denser than air. (See Martonen, 1992, Chen and Yeh, 1990, and Phalen et al., 1994.)

The special case of an aerosol cloud in the form of a layer overlying clean air can be analyzed in terms of *Rayleigh–Taylor instability*. This phenomenon exists when a denser fluid layer overlays a lighter fluid in a gravitational or other type of force field. Such a configuration can occur naturally in the atmosphere, in dust clouds from volcanos, in the oceans, and in cultures of microorganisms that are denser than water and exhibit negative geotaxis (swim against gravity). Rayleigh–Taylor instability is characterized by an abrupt breakthrough of the heavier layer through the underlying lighter layer. The spacing between the breakthrough points and the rate of fall has been characterized by Plesset and Whipple (1974). Differences in gas density play a major role with this phenomenon, as they do with cloud settling. Small differences in gas density, which have little effect on individual particle settling, can dramatically modify particle motion if they cause Rayleigh–Taylor instability or cloud settling.

All elutriation devices that act as spectrometers have two gas streams: an aerosol stream and a clean carrier gas stream. Consequently, they are susceptible to cloud settling and instability effects. Aerosol centrifuges (see Section 3.9) are particularly susceptible because of the high centrifugal acceleration they exert on the particles and gas streams.

The cloud motion described in this chapter is to be distinguished from the situation in which a cloud entirely fills a container. In this situation, there can be no

cloud settling and only a very slight reduction of particle settling velocity, due to the increase in viscosity of the aerosol at high concentrations and the slight upward velocity of the suspending gas caused by the displaced particle volume. These two effects have only a minor influence (< 0.1%) on the settling velocity of particles in contained aerosols, even extremely dense aerosols.

PROBLEMS

7.1 A cigar smoker blows a smoke ring that falls with a noticeable velocity. If the ring is considered to be a sphere 0.05 m [5 cm] in diameter, what is its cloud settling velocity? Assume that the smoke gas is air at room temperature and the smoke particle concentration is 30 g/m^3. If the smoke particles are 0.4 μm in diameter and of standard density, what is the value of G?

ANSWER: 0.17 m/s [17 cm/s], 25,000.

17.2 Repeat the first part of Problem 17. for a smoke gas-phase density that is 2% greater than that of air.

ANSWER: 0.24 m/s [24 cm/s].

REFERENCES

Chen, B. T. and Yeh, H. C., "Effects of Cloud Behavior on a Cigarette Smoke Aerosol," Lovelace Foundation Report LMF–129, Albuquerque, NM, 1990.

Fuchs, N. A., *The Mechanics of Aerosols*, Pergamon, Oxford, 1964.

Kaiser, G. D., and Griffiths, R. F., "The Accidental Release of Anhydrous Ammonia to the Atmosphere: A Systematic Study of Factors Influencing Cloud Density and Dispersion," *J. Air Poll. Control Assoc.*, **32**, 66–71 (1982).

Martonen, T. B., "Deposition Patterns of Cigarette Smoke in Human Airways," *Am. Ind. Hyg. Assoc. J.*, ***53***, 6–18 (1992).

Maude, A. D., and Whitmore, R. L., "A Generalized Theory of Sedimentation," *Brit. J. Appl. Phys.*, **9**, 477–482 (1958).

Phalen, R. F., Oldham, M. J., Mannix, R. C., and Schum, G. M., "Cigarette Smoke Deposition in the Tracheobronchial Tree: Evidence for Colligative Effect," *Aerosol Sci Tech*, ***20***, 215–226 (1994).

Plesset, M. S., and Whipple, C. G., "Viscous Effects in Rayleigh–Taylor Instability," *Phys. Fluids*, **17**, 1–7 (1974).

Stöber, W., Martonen, T. B., and Osborne, S., Jr., "On the Limitations of Aerodynamical Size Separation of Dense Aerosols with the Spiral Duct Centrifuge," in Shaw, D. T. (Ed.), *Recent Developments in Aerosol Science*, Wiley, New York, 1978.

Wen, C. S., *The Fundamentals of Aerosol Dynamics*, World Scientific, Singapore, 1996.

19 Bioaerosols

Bioaerosols are aerosols of biological origin. They include viruses, living organisms, such as bacteria and fungi; and parts or products of organisms, such as fungal spores, pollen, and allergens from dogs, cats, and insects. Bioaerosols are a special category of aerosols because their biological properties can affect the health of humans, animals, and plants. This aspect demands special analysis, which imposes limitations on collecting and handling samples. This chapter presents a summary of bioaerosol characteristics and sampling.

19.1 CHARACTERISTICS

Bioaerosols are found nearly everywhere, indoors and outdoors, but usually at low concentrations. Only minute amounts of inhaled bioaerosol are needed to cause disease—as little as one bacterium, weighing less than 1 pg. Particle size and the usual range of outdoor concentrations for the most common bioaerosols are shown in Table 19.1. The sources of bioaerosols are plants, animals (including humans), soil, and water. The health effects caused by bioaerosols include (1) infectious disease, (2) sensitization reactions, such as asthma, and (3) reactions to toxins or irritants such as endotoxins (components of the cell walls of certain bacteria) and mycotoxins from fungi. Because of the nature of their growth and aerosolization, bioaerosol particles often occur as agglomerates, as clusters of organisms in droplets, or attached to other airborne debris. Bioaerosols can be subdivided into two main groups: viable and nonviable. Particles of the former group are living organisms that can be identified and quantitated by growing individual organisms with suitable nutrients into visible clusters or colonies. Nonviable bioaerosols, including dead organisms, pollen, animal dander, and insect excreta, require other types of analyses. The most common bioaerosols are bacteria and fungal spores. The concentration of bioaerosols, like that of all aerosols, decays with time due to settling and deposition on surfaces. (See Sections 3.8 and 7.4.) Also, viable bioaerosols show a decline in biological activity with time that depends on the relative humidity, oxygen content, and the concentrations of trace gases in the air. Characteristics of bioaerosols are covered in Burge (1995) and Nevalainen et al. (1993).

Bacteria are single-celled organisms with sizes from 0.3 to 10 μm. They are mostly water with a density that ranges from 1000 to 1500 kg/m^3 [1–1.5 g/cm^3], depending on their degree of hydration. Usually, bacteria are spherical or rod shaped, but they may occur as clusters or chains. More than 1700 species of bacte-

TABLE 19.1 Particle Size and Natural Background Concentration of Bioaerosols[a]

Type of Bioaerosol	Size (μm)	Concentration (number/m^3)
Viruses		
Bacteria		0.5–1000
Fungal Spores		0–10,000
Pollen		0–1000

[a]Data primarily from Jacobson and Morris (1976).

ria have been identified. Those that cause human disease are described as human pathogens. Some examples of infectious diseases known to be caused by aerosolized bacteria are tuberculosis, legionellosis, and anthrax. Opportunistic pathogens are not harmful to healthy people, but can infect those with compromised immune systems. Many environmental bacteria colonize water or soil and are released as aerosols when the water or soil is disturbed. A gram of soil can contain 10^9 bacteria. In indoor environments, bacteria may colonize accumulations of moisture in ventilation systems and become aerosolized by air currents or vibration. Some bacteria release spores called endospores. These are hardy, dormant versions of the bacteria, 0.5 to 3 μm in size, that are easily carried by air currents. Included in this category are actinomycetes associated with hypersensitivity pneumonitis.

Fungi represent a unique group of organisms that are found everywhere in the outdoor environment and in most indoor environments. They may occur as single-celled organisms such as yeast or, more commonly, as microscopic, multicellular branching structures called hyphae. Masses of hyphae are easily visible. Molds and mildew are visible fungal growths on surfaces. Only about 70,000 of the estimated 1.5 million fungi have been identified. The majority of fungi are saprophytes, organisms that get their nutrients from dead organic material and facilitate its decomposition. They are found primarily in soil, in damp locations, and on decaying vegetation. Most fungi disperse by releasing spores into the air. These *fungal spores*, particles of 0.5 to 30 μm in size, are resistant to environmental stresses and adapted to airborne transport. They may be single celled or fragmented hyphae, typically 2–4 μm, or fruiting bodies that form at the end of hyphae. They are aerosolized by air currents or mechanical disturbances. Yeasts, by contrast, do not produce spores, but become airborne by aerosolization of the liquid in which they grow. Inhalation of fungi or spores can cause infectious disease, such as histoplasmosis, or opportunistic infection, such as aspergillosis. Most fungi are associated with allergic diseases (e.g., asthma).

Viruses are intracellular parasites that can reproduce only inside a host cell. They consist of encased RNA or DNA and little else. Although naked viruses range from 0.02 to 0.3 μm, most airborne viruses are found as part of droplet nuclei or attached

to other airborne particles that can have a wide range of sizes. Viruses infect humans, other animals, and plants, although most are specific to one type of host. Infected humans represent the primary reservoir and source for human viruses. Viruses are transmitted by direct contact, through contaminated food or water, or by inhalation of aerosolized viruses. Aeorosolization can occur by coughing, sneezing, or talking. Under favorable conditions, they can survive for weeks on fabric or carpets. Viruses cause infectious diseases such as colds, flu, chicken pox, measles, and hantavirus pulmonary syndrome.

Pollen grains are relatively large, near-spherical particles produced by plants to transmit genetic material to the flowers of other plants of the same species. The grains range in size from 10 to 100 μm, with most between 25 and 50 μm. The average density of pollen grains is 850 kg/m^3 [0.85 g/cm^3]. Anemophilous (wind-pollinated) plants produce abundant bioaerosol pollen; insect-pollinated plants produce sticky pollen that is not readily aerosolized. Pollen has a tough outer coating to protect it from environmental stresses. Wind-borne pollen is produced in the plants' flowers on the end of protruding stalks called anthers. This arrangement facilitates the entrainment of pollen in the wind. The production and release of pollen is seasonal and controlled by wind and weather. Pollen causes allergic diseases of the upper airways, such as hay fever.

Other bioaerosols associated with allergic diseases include aerosolized algae, insect fragments, excreta from dust mites and cockroaches, and saliva and dander from dogs, cats, and birds. Viable aerosols have variable survivability (viability) in air during transport. Some do better at high humidity while others do better at low humidity. Many are affected by temperature and ultraviolet radiation. Oxygen is toxic to some, and trace gases probably affect many others.

All types of bioaerosols are likely to occur in farm and agricultural environments. Bioaerosols in the outdoor, nonfarm environment are dominated by fungal spores with smaller numbers of bacteria and pollen, but concentrations are highly variable and influenced greatly by wind, weather, and local sources. Typical outdoor concentrations of culturable bioaerosols are 100–1000 cfu/m^3 (cfu = colony-forming units; see Section 19.2). In the absence of indoor sources, indoor environments with natural ventilation resemble outdoor environments, but have lower bioaerosol concentrations. In mechanically ventilated office spaces bioaerosol concentrations are low, typically less than 100 cfu/m^3. High concentrations of bioaerosols, 10^4–10^{10} cfu/m^3, can occur in specific work environments, such as farm buildings, food-processing plants, textile plants, and sawmills. Currently, there are no health-based environmental standards for culturable or countable bacteria or fungi or for infectious agents. Nor are there guidelines for acceptable levels of bioaerosols. Information about dose-response relationships for bioaerosols is limited.

19.2 SAMPLING

In sampling for bioaerosols, the objective is to determine the presence or the number concentration of specific species or the total bioaerosol concentration. Sampling

for bioaerosol particles employs many of the methods used for nonbioaerosol particles, but the analytical methods impose certain limitations on the sampling process. There are physical and biological aspects to bioaerosol sampling. The physical aspects are the same for bioaerosols and nonbioaerosols. The biological aspects may require aseptic handling to prevent contamination and special attention to the viability of the organisms during the process of sampling and analysis. Viability, which depends on the organism, the environment, and the sample collection and analysis methods used, introduces significant uncertainty into the quantitation of airborne concentrations of bioaerosols. Estimates of the fraction of viable particles that survive the sampling and analysis process, grow, and are counted range from 0.1 to 0.001 (Macnaughton et al., 1997). Other important factors in bioaerosol sampling are high variability in number concentration, wide particle size range of interest, analytical sensitivity to under- and overloading, and interference by other particles. Comprehensive reviews of bioaerosol sampling methods are given by Nevalainen et al. (1993), Macher (1995), and Willeke and Macher (1998).

There are three stages of bioaerosol sampling. The first concerns the inlet efficiency, which is the same as that for nonbioaerosol particles. This stage is covered in Sections 10.1 and 10.2 on isokinetic and still air sampling. The second stage is the collection or deposition of particles onto glass slides, a semisolid culture medium, or water. This is accomplished by adapting the basic methods used for nonbioaerosols to bioaerosols. The third stage is biological analysis to identify and quantitate the bioaerosol particles present. This stage is unique to bioaerosol sampling. Most bioaerosol analysis involves either microscopic examination or growth in culture medium followed by counting colonies. A discussion of the second stage of bioaerosol sampling follows.

The most common collection methods rely on impaction, the same process as described in Section 5.5 for nonbioaerosols. *Slit impactors* impact particles directly onto a culture medium. For bacteria and fungal spores, the culture medium, called agar, is a semisolid material containing water and nutrients that foster the growth of the viable particles that are collected. For viruses, cell or tissue culture media are used. Typically, the agar fills a 100-mm or 150-mm disposable petri dish, called a culture plate, that is slowly rotated under the slit to provide a history of bioaerosol concentration. Rotating slit impactors have flow rates of 28–50 L/min and cutoff diameters of about 0.5 μm.

Multijet impactors have 100–500 jets impacting directly onto agar culture plates. This action spreads the collected particles to many locations to prevent overloading. Single and multistage impactors are available with cutoff diameters from 0.6 to 8 μm. Shear forces in the high-velocity jet and during impaction may cause loss of viability.

Other types of impactors are used to collect pollen. The pollen grains are impacted directly onto glass slides or adhesive-coated transparent tape for microscopic examination and counting. Culturing is not used for pollen. One type of sampler (the Rotorod® sampler) impacts pollen grains directly onto adhesive-coated polystyrene rods. The rods are transparent for direct microscopic particle counting. The rods are square in cross section, are 60 mm long and 0.5 to 1.6 mm wide, and are

attached to an exposed rotating frame. The cutoff size for collection can be estimated by Eq. 5.23, the definition of the Stokes number, as

$$d_{50} = \left(\frac{18\eta d_r (\mathrm{Stk}_{50})}{\rho_p V_T} \right)^{1/2} \tag{19.1}$$

where d_r is the width of the rod, V_T is the tangential velocity of the rods, Stk_{50} is approximately 0.3. The Stokes number for 85% collection, Stk_{85}, is approximately 1.5.

Impingers (see Section 10.6 and Fig. 10.13) are frequently used to collect bioaerosols in a liquid, such as water, buffered saline solution, or nutrient broth. The two most commonly used impingers are the all-glass impingers, AGI-30 and AGI-4. The numerals refer to the distance in mm from the glass nozzle to the base of the impinger body. Liquid collection prevents desiccation, but the shear forces in the jet and in the turbulent liquid cause loss of viability. The AGI-30 has a cutoff diameter of 0.3 μm; the AGI-4 has a slight lower cutoff, but has a greater loss of viability. Water containing the collected organisms can be applied directly to the culture plates or can be diluted and applied to give the desired surface density of colonies.

The *centrifugal sampler* has a rotating "paddle wheel," open to the environment on one end, with a stationary removable agar-coated plastic strip around the rim of the wheel. Air enters along the axis, and the particles contained in it are driven by centrifugal force onto the collecting strip. Sample flow rates are 40 to 50 L/min.

Membrane filters are also used to collect bioaerosol particles. The collected particles can be examined by an optical microscope (see Section 20.2), or they can be cultured by placing the filter, particle side up, on a culture medium. The filtration process causes significant desiccation of collected microorganisms and loss of viability. This method has been used for bioaerosols in highly contaminated environments.

Bioaerosols can be sampled by allowing them to settle directly onto culture plates, a simple, inexpensive method that allows one to determine the presence of a specific microorganism. The technique, however, is not useful for quantifying airborne concentrations because, after culturing, the size of the initial particle cannot be determined, so V_{TS} and the flux are not known.

Respirable sampling (see Section 11.5) is appropriate for some infectious agents. Inhalable particle sampling (see Section 11.4) is appropriate for all bioaerosol sampling, especially of pollen and other large particles.

An important consideration in bioaerosol sampling is the appropriate surface density for counting organisms or colonies. If the loading is insufficient there will be few counts and high statistical uncertainty. In microscopic counting of organisms, overloading causes overlap with nonbioaerosol particles, making identification difficult. Environmental samples usually have far more nonviable particles than viable particles. In counting colonies, overloading leads to three types of underestimation. First, if two of the same species are sufficiently close to each other, they will be

counted as a single colony. Second, if two different species are sufficiently close, one may inhibit the growth of the other. Finally, due to its chemical nature, a nonbioaerosol particle may inhibit the growth of a nearby viable particle. For a given sampler, the sampling time t to achieve a desired surface density s (colonies or particles per unit area) is given by

$$t = \frac{sA}{\overline{C}_N Q} \tag{19.2}$$

where A is the area onto which particles are deposited, $\overline{C}_N$ is the average number concentration of bioaerosol particles, and Q is the sampler flow rate. For microscopic counting, a surface density of $10^8/m^2$ [10,000/cm^2] gives good results; for counting colonies, a surface density of $10^4/m^2$ [1/cm^2] is desired.

A different approach is taken for multijet impactors. There is a deposition site directly below each jet. After culturing, one cannot tell whether just one or more than one organism has been deposited at a particular site. Regardless of the number of organisms involved, a site with a colony is called a *filled site* or a *positive hole*. Plates are analyzed by counting the number of filled sites. For a given multijet impactor, the more filled sites, the greater the proportion of those filled sites that have multiple organisms. Willeke and Macher (1998) and Macher (1989) give tables with correction factors to estimate the total number of viable organisms collected, based on the number of filled sites. Also given is the statistical uncertainty of these estimates. As shown in Table 19.2, the correction is less than 5% when less than 10% of the sites are filled sites. The correction factor is 2.0 when 80% of the sites are filled sites. For an impactor with N_j jets, the following empirical equation gives

TABLE 19.2 Correction Factors for Multiple Particle Collection in Multijet Impactors[a]

Filled Fraction[b]	Correction Fraction[c]	Filled Fraction	Correction Factor
0.05	1.026	0.55	1.452
0.10	1.054	0.60	1.527
0.15	1.084	0.65	1.615
0.20	1.116	0.70	1.720
0.25	1.151	0.75	1.848
0.30	1.189	0.80	2.012
0.35	1.231	0.85	2.232
0.40	1.277	0.90	2.559
0.45	1.329	0.95	3.154
0.50	1.386	1.00	>5.878

[a]Calculated from Macher (1989).
[b]Fraction of deposition sites with colonies.
[c]Total number of viable particles collected equals the number of filled sites times the correction factor.

the total number of viable organisms collected n_c in terms of the number of filled sites—i.e., those with colonies, n_f,

$$n_c = n_f\left(\frac{1.075}{1.052 - f}\right)^{1.83} \quad \text{for } f < 0.95 \tag{19.3}$$

where, n_f is the number of filled sites with colonies and $f = n_f/N_j$ is the fraction of sites with colonies. Equation 19.3 agrees with tabulated values within 1% for filled fractions less than 0.95.

The only commercially available, direct-reading instrument for bioaerosols is the TSI, Inc. (St. Paul, MN), Model 3312 UV-APS®. This instrument combines time-of-flight measurement of particle size (see Section 5.7) with light-scattering particle detection (see Section 16.5) and single-particle ultraviolet fluorescence measurement. The last of these involves illuminating the particle with an ultraviolet laser beam and measuring the emitted fluorescent intensity at certain wavelengths. This fluorescence is associated with certain molecules produced by living cells. The instrument samples at 1.0 L/min, measures particles from 0.5 to 15 μm, and measures concentrations up to $10^9/m^3$ [$1000/cm^3$].

PROBLEMS

19. An adjustable-speed, rotating slit impactor has a total deposition area of 50 cm^2 for one full rotation. For how long should a sample be taken to get the desired colony surface density if bioaerosol concentration is 1000 cfu/m^3? Assume the sample flow rate is 28 L/min, and that sampling takes place for one full rotation.

ANSWER: 107 s (1.8 min).

19.2 A 400-jet impactor samples a bioaerosol at 28 L/min for 20 minutes. If 344 colonies are counted, what is the average airborne number concentration of viable particles. Assume no loss of viability during sampling.

ANSWER: 1410 cfu/m^3.

REFERENCES

Burge, H. A., Feeley, J. C., Kreiss, K., et al., *Guidelines for the Assessment of Bioaerosols in the Indoor Environment*, ACGIH, Cincinnati, 1989.

Burge, H. A., (Ed), *Bioaerosols*, Lewis, Boca Raton, FL, 1995.

Jacobson, A. R., and Morris, S. C., "The Primary Air Pollutants—Viable Particles, Their Occurrence, Sources, and Effects," in Stern, A. C. (Ed.), *Air Pollution*, 3d ed., Academic Press, New York, 1976.

Macher, J. M., "Positive-Hole Correlation of Multiple-Jet Impactors for Collecting Viable Microorganisms," *Am. Ind. Hyg. Assoc. J.*, **50**, 561–568 (1989).

20 Microscopic Measurement of Particle Size

Microscopic observation of aerosol particles permits direct measurement of particle size. This is in contrast to indirect methods such as sedimentation, impaction, mobility analysis, and light scattering, wherein the particle size is estimated from the measurement of a property related to size. Microscopy also provides the opportunity to observe particle shapes, and it requires only an extremely small amount of sample. Linear measurements made with a microscope can be very accurate and, often serve as a primary measurement for the calibration of other aerosol-sizing methods. However, microscopic methods for determining particle size distributions are, in general, tedious and require consistency, skill, and careful preparation.

20.1 EQUIVALENT SIZES OF IRREGULAR PARTICLES

In measuring particle size with a microscope, it is necessary to assign to each particle a size based on its two-dimensional projected image, or silhouette. For spheres, this is simply the diameter of the circular silhouette observed in the microscope, but for the more common case of irregular particles, we must use equivalent diameters such as those shown in Fig. 20.1. The equivalent diameters shown are based solely on the geometry of the silhouette, in contrast to the equivalent diameters defined in Section 3.5, which are based on the aerodynamic behavior of the particles. The smallest diameter shown is Martin's diameter d_M, the length of the line parallel to a given reference line that divides the projected area (silhouette) of the particle into two equal areas. This diameter is often referred to as a "statistical" diameter, because its value depends on particle orientation, and only its mean value for all particle orientations is unique for a given particle. In practice, orientation averaging is rarely done; instead, in sizing particles, it is more common to measure a single Martin's diameter for each of many particles randomly oriented with respect to a reference line. This procedure has the practical effect of averaging over all orientations. Martin's diameter always passes through the centroid of the particle silhouette, and the average Martin's diameter of a particle represents the mean of all chords through the centroid of the silhouette.

Another "statistical" diameter is Feret's diameter d_F, shown in Fig. 20.1. Feret's diameter is defined as the length of the projection of a particle along a given reference line or the distance between the extreme left and right tangents that are perpendicular to the reference line. It is most convenient to use Feret's diameter when

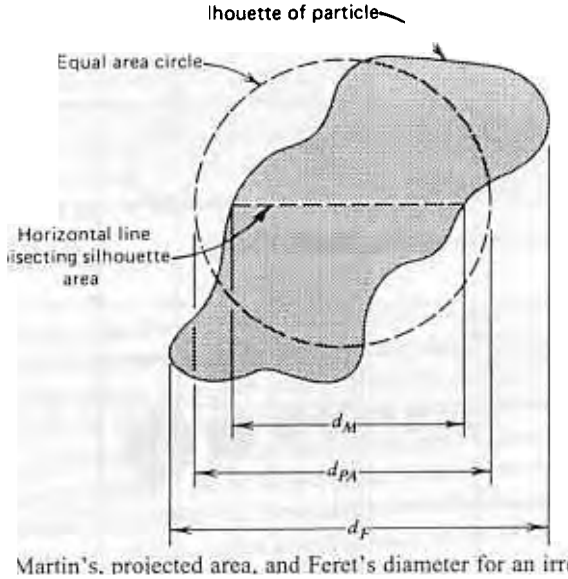

FIGURE 20. Martin's, projected area, and Feret's diameter for an irregular particle

a scale along a given axis is available, such as that in a microscope equipped with a filar micrometer (Section 20.3).

The most commonly used equivalent diameter is the projected area diameter d_{PA}, also shown in Fig. 20.1. The projected area diameter is defined as the diameter of the circle that has the same projected area as the particle silhouette. This diameter has the advantage of providing a unique size for a given silhouette, regardless of its orientation. It is difficult to make an accurate measurement of d_{PA} for a single particle because doing so requires determining the area of an irregular shape. Nevertheless, the projected area diameter is widely used because it can be determined by simple visual comparison between the silhouette area of a particle and standard circles of known area. Such comparisons allow particles to be grouped rapidly into size intervals based on their projected area and the size distribution determined by the methods described in Chapter 4.

In general, $d_M \leq d_{PA} \leq d_F$, with the equality holding only for spheres. For irregular particles of most crushed materials, d_M is only slightly less than d_{PA} (< 10% difference), and they are often assumed to be equal. Feret's diameter is generally about 20% larger than d_{PA} for such materials.

In optical microscopy, the projected area diameter is measured using a set of circles of standard area printed on an eyepiece graticule or reticule. The graticule, a glass disk about 2 cm in diameter with the pattern printed on it, is inserted into the eyepiece of a microscope so that its pattern is superimposed on the magnified image of the particles. A common type is the Porton graticule shown in Fig. 20.2. Each circle on the Porton graticule has twice the area of the next smaller circle; that

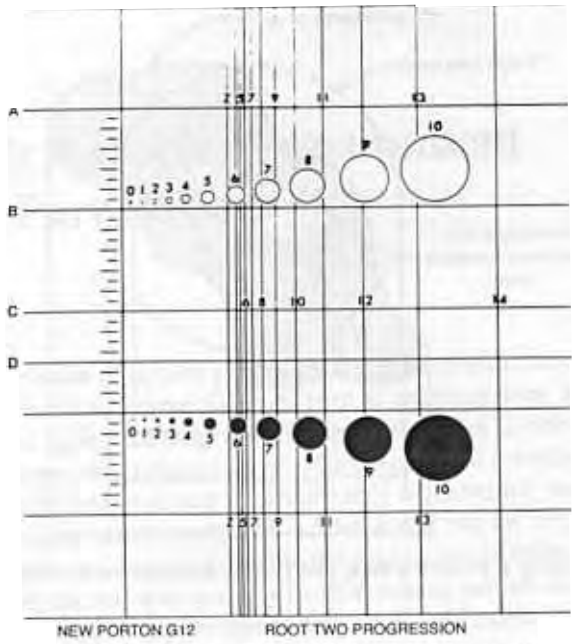

FIGURE 20.2 The Porton eyepiece graticule

is, the circle diameters are in a square-root-of-two geometric progression, and every other diameter differs by a factor of two. The diameter of the nth circle d_n is

$$d_n = d_0(2)^{n/2} \tag{20.1}$$

where d_0 is the base diameter, or the diameter of the zeroth circle. The spacing of the numbered lines from the centerline (labeled Z) follows the same progression as the numbered circles. On the version, shown in the figure, the inside diameter of the open circles follows the same progression. For each microscope, the apparent size of the circles must be calibrated with a stage micrometer, a miniature ruler 1 mm long mounted on a glass slide. As shown in Fig. 20.3, the 1-mm distance is divided into 100 equal segments (numbered by tens), each 10 μm wide. The stage micrometer is placed in the microscope at the location of the sample and is observed with the pattern of the graticule superimposed on it. The vertical distance in Fig. 20.2 between horizontal lines A and F is 200 times the diameter of the zeroth circle. This distance is measured with the stage micrometer, and the sizes of the circles calculated by Eq. 20.1.

EXAMPLE

The apparent distance between lines A and F on a Porton graticule is measured with a stage micrometer in a microscope having a 43× objective and a 10× eyepiece and is found to be 98 μm. The diameter of the zeroth circle is 98/200, or

0.49 μm, and the number-9 circle is $0.49 \times 2^{9/2}$, or 11.1 μm. This result could have been obtained by measuring the number-9 circle directly with the stage micrometer (a less accurate procedure) or by measuring the distance between the center line (Z) and the number-14 line, 63 μm. For the latter measurement, the apparent diameter of the number-9 circle is $63 \times 2^{-5/2}$, or 11.1 μm. The diameters of the other circles can be calculated quickly using the fact that the diameter of every other circle (or line) changes by a factor of two. Thus, circles 7 and 5 are 5.5 and 2.8 μm in diameter, respectively, and circles 8 and 6 are 7.8 and 3.9 μm, respectively.

Sizing is usually done by grouping particles into ranges defined by successive circle sizes and plotting the results on probability graph paper as a cumulative percent for each group versus the upper size limit of that group. The same sizing procedure is applicable to electron microscopy: One uses a photograph of the magnified particles and a transparent overlay of an enlarged Porton graticule to compare the various areas. In practice, particles are grouped into size ranges easily and rapidly because of the factor-of-two difference in area between successive circles. The geometric progression of the circles also provides an even spacing of data points along the size axis of a log-probability graph.

Most aerosol particle size distributions are skewed, so that relatively few large particles are present. To count a meaningful number of large particles involves counting unnecessarily large numbers of small particles. This problem can be

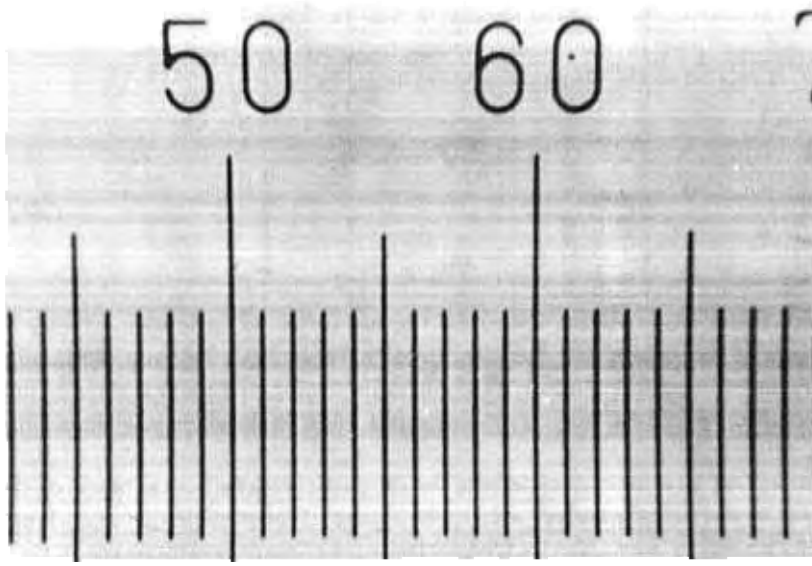

FIGURE 20.3 Portion of a stage micrometer as it appears at 400×. Actual distance between the smallest lines is 10 μm.

avoided by *stratified counting*. As illustrated in Table 20.1, sizing is done by using fields—defined areas such as the box that surrounds the Porton graticule lines or some fraction of it. All particles are sized in the first field. In subsequent fields, only those particles in size ranges having fewer than 10 particles (or another predetermined number) in them are counted. When an adequate number of particles is obtained in each size range of interest, the data are normalized in terms of counts per field, and the normalized results are used to calculate percentages for cumulative or differential distributions. Without stratified counting, the example (Table 20.1) would require sizing about 1250 particles to achieve the same accuracy in the largest size range.

The utility of microscopic size measurements of irregular particles often depends on the ability to convert the measured sizes to other equivalent diameters that describe the behavior rather than the geometry of the particles. The most useful of these diameters is the equivalent volume diameter, which can be combined with the dynamic shape factor (Section 3.5) to describe the aerodynamic properties of a particle. The volume shape factor α_v relates the volume of a particle, v_p, to one of the silhouette diameters described before and is defined, for the projected area diameter, by

$$\alpha_v = \frac{v_p}{d_{PA}^3} \tag{20.2}$$

Similar definitions give α_v in terms of d_F or d_M, but for simplicity, we consider only α_v, defined in terms of d_{PA}. Table 20.2 gives volume shape factors for geometric shapes and mineral dusts. The volume shape factor based on projected area diameter has a maximum value of $\pi/6 = 0.52$, for a sphere. For regular geometric shapes, α_v can be calculated; for irregular shapes, it must be determined experimentally by a combination of two or more measurement methods. The equivalent volume diameter d_e is related to the volume shape factor α_v by

$$v_p = \frac{\pi}{6} d_e^3 = d_{PA}^3 \alpha_v$$

$$d_e = d_{PA}\left(\frac{6\alpha_v}{\pi}\right)^{1/3} \tag{20.3}$$

Except for fibers and platelets, d_e and d_{PA} do not differ by more than a factor of two. Values of the ratio d_a/d_{PA} are also given in Table 20.2. This useful quantity combines the volume shape factor, dynamic shape factor, and particle density into a single factor. Except for very heavy materials, most minerals have values close to unity.

A similar shape factor can be defined for the particle surface area, based on the ratio of the actual particle surface area to the square of the particle diameter. It can be shown by Cauchy's theorem that the surface area of an irregular convex particle is equal to four times its projected area, averaged over all possible particle orienta-

TABLE 20.1 Example of Stratified Counting Procedure

Field Number	Number of Counts in Indicated Size Range						
	>1.4 μm	1.4–2.0 μm	2.0–2.8 μm	2.8–4.0 μm	4.0–5.7 μm	5.7–8.0 μm	Total
					6		250
2					9		12
3							3
4							1
5							3
Total	44	81	75	42	15	12	269
Number per field	44	81	75	42	7.5	2.4	251.9
Percent in size range	17.5	32.1	29.8	16.7	3.0	1.0	100.0
Cumulative percent	17.5	49.6	79.3	96.0	99.0	100.0	

TABLE 20.2 Volume Shape Factor and the Ratio d_a/d_{PA} for Geometric Shapes and Mineral Dusts[a]

Particle	Volume Shape Factor, α_v	d_a/d_{PA}
Geometric shapes		
Sphere	0.52	1.0[b]
Cube	0.38	0.89[b]
Prolate spheroid (axial ratio = 5)	0.33	0.76[b]
Cylinder (axial ratio = 5)	0.30	
Mineral dusts		
Anthracite coal	0.16	0.70
Bituminous coal	0.24	0.88
China clay		0.92
Glass		.08–1.34
Limestone	0.16	
Quartz	0.21	0.97–1.16
Sand	0.26	1.00
Talc	0.16	0.75

[a]Based on projected area diameter determined for particles lying in the most stable position. Data for mineral dusts from Davies (1979) and α_v for geometric shapes from Mercer (1973).
[b]Standard density.

tions. For convex particles having no preferred orientation, the second moment average (rms) of the projected area diameter is equal to the diameter of average surface, $d_{\bar{s}}$.

Liquid aerosol particles are spherical when airborne, but when collected on a glass slide, they spread out to form a lens-shaped (plano-convex) droplet on the surface of the slide. The diameter of the lens is greater than the diameter of the original airborne droplet. The extent of the spreading depends on the properties of the specific liquid and surface involved. Coating a glass slide with an oleophobic surfactant reduces the spreading, as well as the influence of different liquids on spreading. The spreading factor B relates the observed size of a droplet (lens), d_o, on a glass slide to the size of the original airborne droplet, d_p.

$$B = \frac{d_p}{d_o} \tag{20.4}$$

Table 20.3 gives values of B for different liquids and surfaces.

20.2 FRACTAL DIMENSION OF PARTICLES

The shape of an aerosol particles having a complex structure, such as an agglomerated metal fume or soot particle, can be characterized in terms of a fractal dimen-

TABLE 20.3 Spreading Factor for Liquids on Glass Slides[a]

Liquid	Surface Coating[b]	Particle Size Range (μm)	Spreading Factor
DOP[c]	None	2–50	0.30
DOP	L-1429	2–5	0.58
DOP	L-1428	2–50	0.69
DOP	FC-721	10–20	0.74
DOP	L-1083	50–150	0.69
Oleic acid	none	2–50	0.42
Oleic acid	L-1428	2–50	0.70
Oleic acid	FC-721	3–29	0.75
Sulfuric acid	L-1429	0.02–0.07	0.71

[a]Data from Liu, Pui, and Wang (1982); Cheng, Chen, and Yeh (1986); Olan-Figueroa, McFarland, and Ortiz (1982); and John and Wall (1983).
[b]L-1083, L-1428, L-1429, and FC-721 are fluorocarbon oelophobic surfactants manufactured by 3M, Inc., St. Paul, MN.
[c]Di (2-ethylhexyl) phthalate.

sion. Fractals are structures that have geometrically similar shapes at different levels of magnification. This characteristic is called *self-similarity* or *fractal morphology*. The *fractal dimension* relates a property such as the perimeter or surface area of an object to the scale of the measurement.

For example, the length of a coastline can be represented by a continuous series of equal straight-line segments. The size of each segment represents the step size, or "ruler" length, from one contact point to the next. The total length depends on the step size. The smaller the step size, the finer is the detail one can measure and the longer the measured coastline. The relationship between step size and measured length is shown in Figure 20.4 for the coastline of Great Britain. This log–log graph, called a Richardson plot, of the measured coastline length L versus the step size λ approximates a straight line with a negative slope m. The equation for this straight line is

$$L = k\lambda^m = k\lambda^{1-D_f} \tag{20.5}$$

where k is a constant and D_f is the fractal dimension

$$D_f = 1 - m \tag{20.6}$$

In this situation, the fractal dimension, 1.24, is a measure of the complexity of the coastline. Its value lies between 1 and 2. If the coastline were a perfectly smooth straight line, there would be no change in length with the measurement scale, so m would be zero and D_f would be 1.0. As the self-similar complexity of the coastline increases, the fractal dimension increases, approaching its maximum value of 2.0, for this situation. Figure 20.5 shows line segments of increasing complexity and increasing fractal dimension. Since they are all line segments, their topological

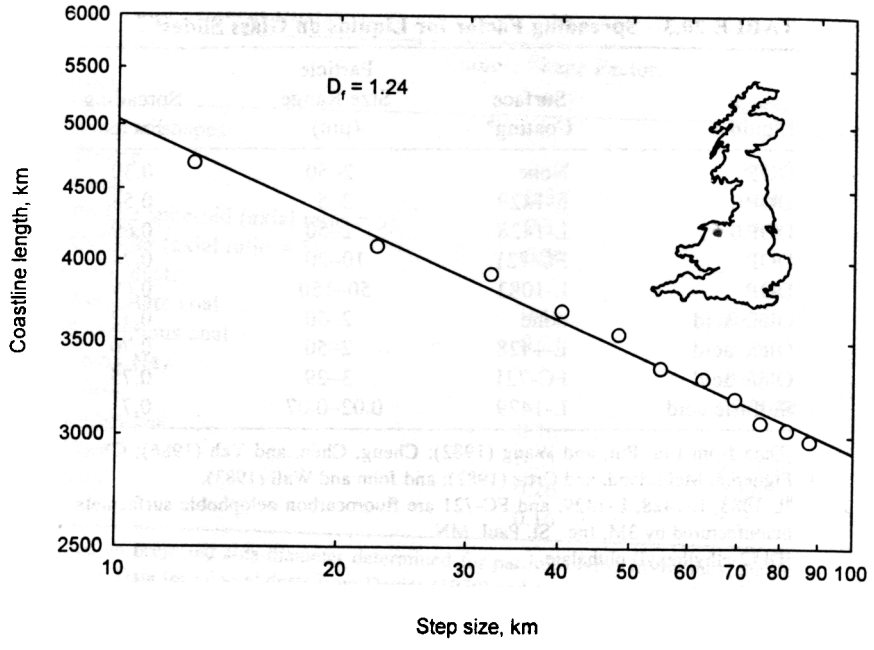

FIGURE 20.4 Measured length of the coastline of Great Britain versus step size (13–88 km). Data from Kaye (1989).

dimension is 1; that is, they would be straight lines if stretched out. The fractal dimension can be thought of as a fractional dimension, in this case intermediate between a straight line with a dimension of 1 and a surface with a dimension of 2.

EXAMPLE

For the data shown in Fig. 20.4, *calculate* the fractal dimension of the coastline of Great Britain and the length of the coastline for a step size of 30 km.

$$m = \frac{\log(y_1/y_2)}{\log(x_1/x_2)} = \frac{\log(5050/2920)}{\log(10/100)} = -0.238$$

$$D_f = 1 - (-0.238) = 1.238$$

$$k = \frac{L}{\lambda^m} = \frac{5050}{10^{-0.238}} = 8740 \text{ km}$$

For $\lambda = 30$ km,

$$L = k\lambda^{1-D_f} = 8740 \times 30^{-0.238} = 3890 \text{ km}$$

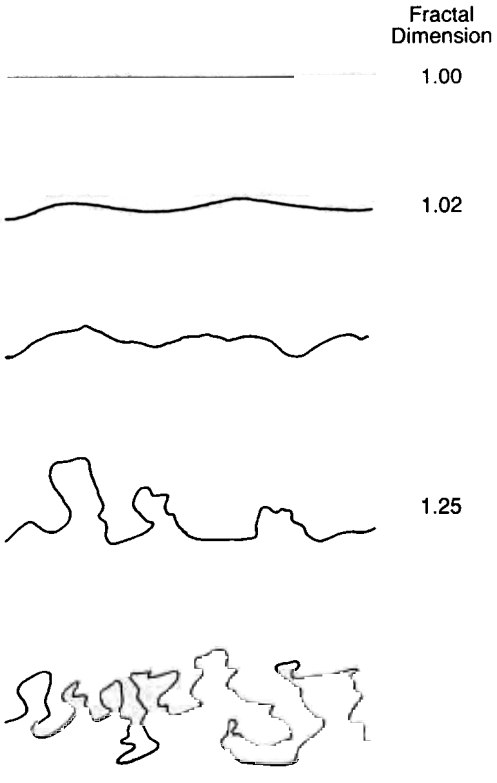

FIGURE 20.5 Line segments having different fractal dimensions. All have topological dimensions of 1.0. After Kaye (1989). Reprinted with permission of Wiley-VCH Verlagsgesellschaft, Weinheim, Germany.

The concept and approach given here for calculating the fractal dimension and the length of the coastline of Great Britain can be applied to the perimeter of any particle. With suitable scaling, the data shown in Fig. 20.4 could apply equally well to an aerosol particle with the same shape. The fractal dimensions would be the same. Graphs such as Fig. 20.4 are usually put in dimensionless (normalized) form by dividing L and λ by the maximum Feret's diameter of the profile of the object, be it Great Britain or an aerosol particle. The appearance of the graph remains the same. Figure 20.6 (Kaye, 1989) shows simulated particle profiles, their fractal dimensions, and normalized graphs of the particle perimeter, P/d_F, versus the normalized step size, λ/d_F.

Fume particles have been measured microscopically and found to have fractal dimensions of 1.3–1.5 (Baron and Willeke, 1993). Soot particles analyzed by Sorenson and Feke (1996) displayed fractal morphology over the range 0.05–400 μm. This range corresponds to agglomerates of 10 to 10^8 primary particles. These same authors found the relationship between the number of primary particles in an

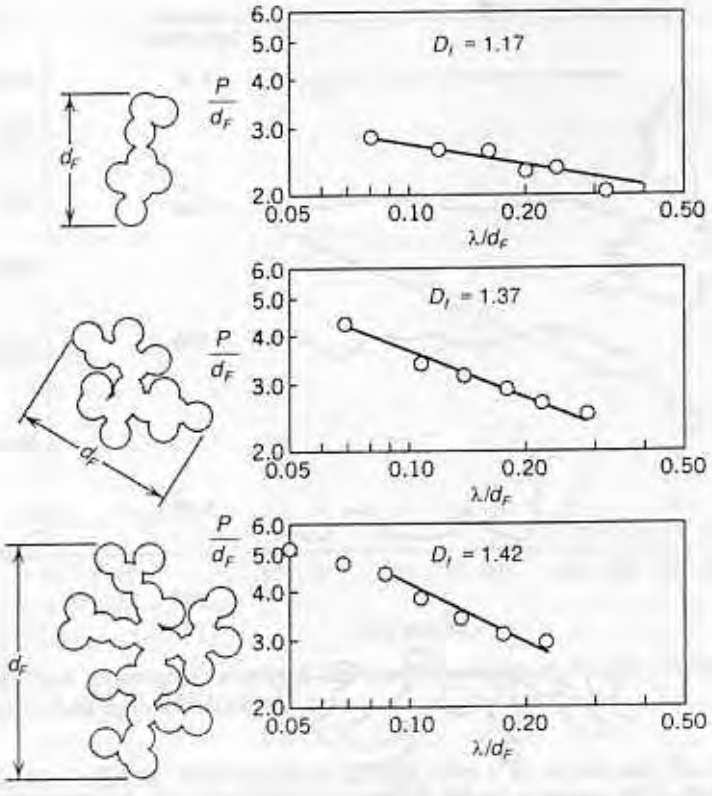

FIGURE 20.6 Profiles of simulated particle agglomerates and their Richardson plots. After Kaye (1989). Reprinted with permission of Wiley-VCH Verlagsgesellschaft, Weinheim, Germany.

agglomerate, N_{pp}, the diameter of the agglomerate, $2R_g$, and the size of the primary particles, d_{pp}, to be

$$N_{pp} = 1.7\left(\frac{2R_g}{d_{pp}}\right)^{1.8} \tag{20.7}$$

where 1.8 is the fractal dimension. R_g is the radius of gyration of the agglomerate, a size measure equal to the rms average distance the particle's mass is from its center of mass. A liquid sphere composed of N_{pp} primary particles of diameter d_{pp} would have a fractal dimension of 3.0 (for $\lambda < 0.5d_p$) and a constant of 3.95 in Eq. 20.7.

Other quantities in the field of aerosol science can also be described as fractals. For example, tracing the path of a particle undergoing Brownian motion by straight-line segments between the positions of the particle at fixed time intervals yields a fractal. As the interval gets shorter, more details are resolved and the path gets

longer, but retains its self-similarity. Other examples of quantities that can be described as fractals are the borders of clouds and smoke plumes, turbulence, and the geometry of the airways of the lungs.

20.3 OPTICAL MICROSCOPY

Because the optical microscope is a common instrument used in many areas of science, only those characteristics of microscopes that are important to particle sizing are covered here. Optical microscopes are most suitable for counting and sizing solid particles having diameters of 0.3–20 μm. While any professional-grade compound microscope can be used to size particles, those with multiple objectives mounted in a nosepiece and a mechanical stage are the most convenient. Figure 20.7 shows the major components of such a microscope. Other desirable features, not shown, are a built-in substage illuminator and binocular eyepieces.

The light path for an optical microscope is shown in Fig. 20.8. Light from an external source, usually a microscope lamp, is reflected up into the condenser by a mirror. The condenser concentrates the light onto the sample from below. The particles to be measured are mounted on a glass slide held in the mechanical stage. A magnified image of the particles is formed by the objective lens positioned just above the slide. The image is located at the eyepiece, which further magnifies it to create a virtual image at a distance comfortable for viewing. In this situation, the

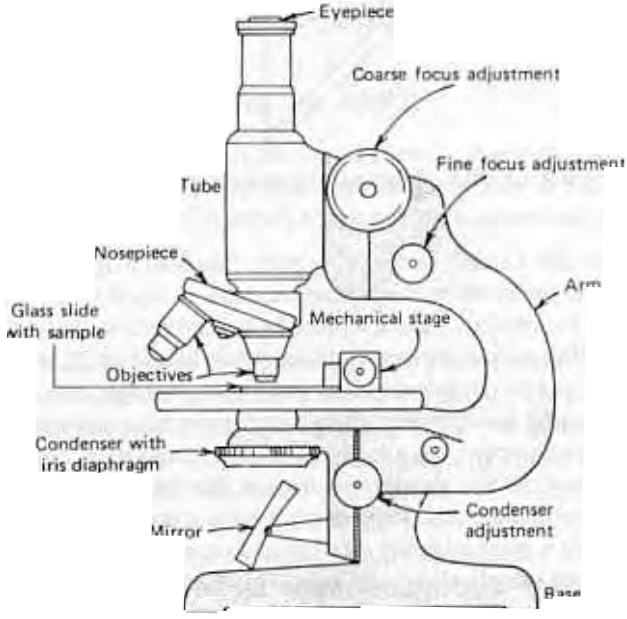

FIGURE 20.7 Diagram of an optical microscope.

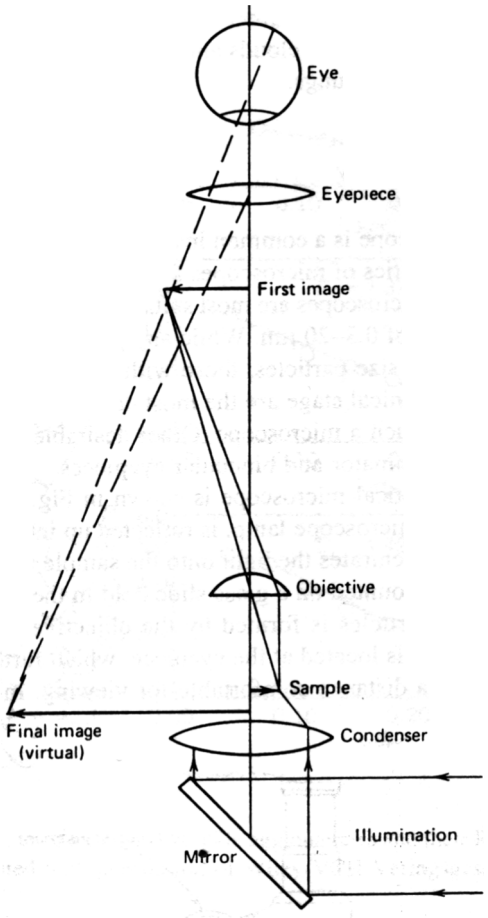

FIGURE 20.8 Light path of an optical microscope.

eyepiece functions like a simple magnifying glass. The total magnification—the ratio of the image size to the particle size—is approximately equal to the product of the magnifications of the objective and eyepiece lenses. Objective lens magnifications range from 10 to 100; eyepiece magnifications range from 5 to 25, with 10, 15, and 20 being the most useful. Eyepieces slide into the microscope tube and are easily interchanged. Focusing is accomplished by moving the tube-and-lens system up or down relative to the sample with a rack-and-pinion mechanism.

At high magnifications it is necessary to use the fine-focusing adjustment, a 500:1 gear system that permits the tube to be positioned to a precision of 1 μm. The mechanical stage holds a glass slide for viewing and provides micrometer adjustment of the position of the sample along two axes. This feature is particularly useful for traversing a nonuniform sample and also enables particle images to be easily positioned for comparison with the standard circles or line spacings of a graticule. The

nosepiece, shown in Fig. 20.7, permits 2–5 objectives to be mounted on the microscope and rotated into place as needed. The objectives are positioned so that, when the microscope is exactly in focus for one objective, the others will also be in focus.

Particles can be captured directly on a glass slide by sedimentation, electrostatic precipitation, or thermal precipitation and viewed directly in a microscope. Powders or bulk dust samples can be spread out on a slide by gentle smearing with a toothpick. The procedure for viewing particles captured on a filter is to cut out a small pie-shaped piece of the filter and place it on a clean glass microscope slide. A drop of immersion oil is allowed to saturate the filter to make it transparent. The filter is covered with a glass coverslip and examined in the microscope. The immersion oil must have the same refractive index as the filter material. The most common type of filter for optical microscope examination of aerosol particles is a cellulose ester membrane of 0.45-μm pore size. These filters have a refractive index of 1.510. Unfortunately, particles having exactly this refractive index are also made transparent and cannot be observed by this method.

Although a total magnification of about 2500× can be obtained with standard objectives and eyepieces, the size of the smallest observable particle is governed not by magnification, but by the limit of resolution, which is controlled by the wavelength of light and the characteristics of the objective lens. The *limit of resolution*, or, more simply, the *resolution*, is the smallest scale of detail that can be observed in the magnified image. Although greater magnification produces a larger image, it does not increase the observable detail beyond the limit of resolution. Resolution is usually defined as the minimum separation distance required for two dots to be observed as two separate dots rather than as one elongated dot. Resolution is characterized by a property of the objective lens called the *numerical aperture*, NA, defined as

$$\text{NA} = m \sin(\theta/2) \tag{20.8}$$

where m is the refractive index of the viewing medium between the objective and the sample and θ is the angular aperture—the angle shown in Fig. 20.9. The limit of resolution, L_R, obtained with an objective having a numerical aperture NA is

$$L_R = \frac{1.22\lambda}{2(\text{NA})} \tag{20.9}$$

where λ is the wavelength of the light used, 0.55 μm for white light.

Characteristics of the three objectives shown in Fig. 20.9 are given in Table 20.4. It is apparent that the maximum value of θ is 180°, so the numerical aperture can exceed unity only when $m > 1$. This is accomplished by filling the space between the objective and the sample with an oil of high refractive index. Such an approach allows numerical apertures as great as 1.4 and yields resolutions of about 0.2 μm for white light. In general, the condenser should be adjusted so that the angle of illumination equals the angular aperture of the objective. For the best resolution, immersion oil should be used to couple the top of the condenser lens to the bottom of the glass slide. A rule of thumb for the selection of eyepieces and objectives is

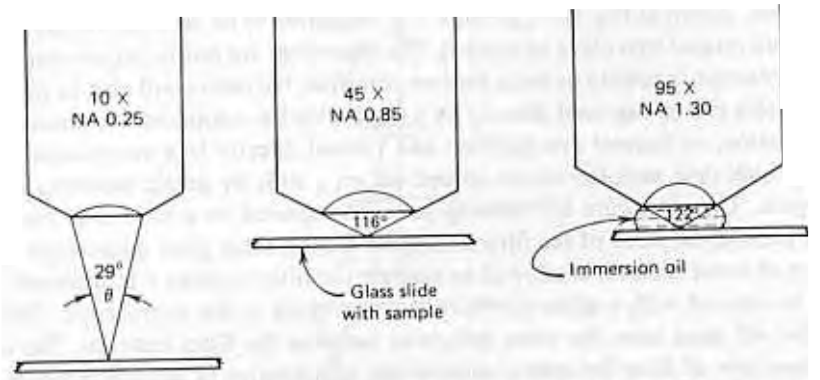

FIGURE 20.9 Comparison of microscope objectives, showing angular aperture

that the maximum useful magnification is equal to 1000 times the numerical aperture of the objective. The depth of field or vertical resolution is the thickness (depth) of the sample region that is simultaneously in focus. This thickness is approximately equal to $L_R/\tan(\theta/2)$. At high magnifications, the small depth of field is a limitation of the optical microscope that makes it difficult to completely observe large particles and to see all particles deposited at different depths in a filter. It is desirable to use a small-pore membrane filter, such as the Millipore HA, for microscopic counting and sizing, because all particles are deposited on or near the surface and can be observed simultaneously.

The filar micrometer and the image-splitting eyepiece are microscope attachments that can be used for particle sizing. Both replace the regular eyepiece. The filar micrometer has a movable crosshair in the field of view that is positioned by a calibrated micrometer screw. Particle size is measured by positioning the crosshair on the left edge of the particle, reading the micrometer setting, moving the crosshair to the right edge of the particle, and reading the setting again. The particle's Feret's diameter is calculated from the difference in the readings. The micrometer is calibrated with a stage micrometer. An image-splitting eyepiece has a prism assembly that creates two images of a particle. When the micrometer screw is in the zero position, both images are superimposed. As the micrometer screw is turned, the images shift, and the micrometer is read when the left edge of one image just touches the right edge of the other. Particle size is calculated from this setting and a calibration obtained with a stage micrometer. Both devices are slower and more tedious, but more accurate, than the circle comparison method. Special types of microscopes used for particle sizing and analysis, such as dark field, phase contrast (used for asbestos counting; see Section 20.5), and polarizing microscopes, are described in Silverman et al. (1971) and Cadle (1975).

20.4 ELECTRON MICROSCOPY

To examine particles smaller than the limit of resolution of optical microscopes, one must use an electron microscope. Of the two common types, scanning electron

TABLE 20.4 Characteristics of Typical Microscope Objectives Used for Particle Sizing

Objective and Nominal Magnification	Focal Length (mm)	Numerical Aperture	θ (deg)	Depth of Field (μm)	Limit of Resolution, λ = 0.55 μm (μm)
10× apochromatic	16	0.25	29	5.19	1.34
45× apochromatic	4	0.85	116	0.25	0.39
95× apochromatic (oil immersion)	1.8	1.30	122	0.14	0.26

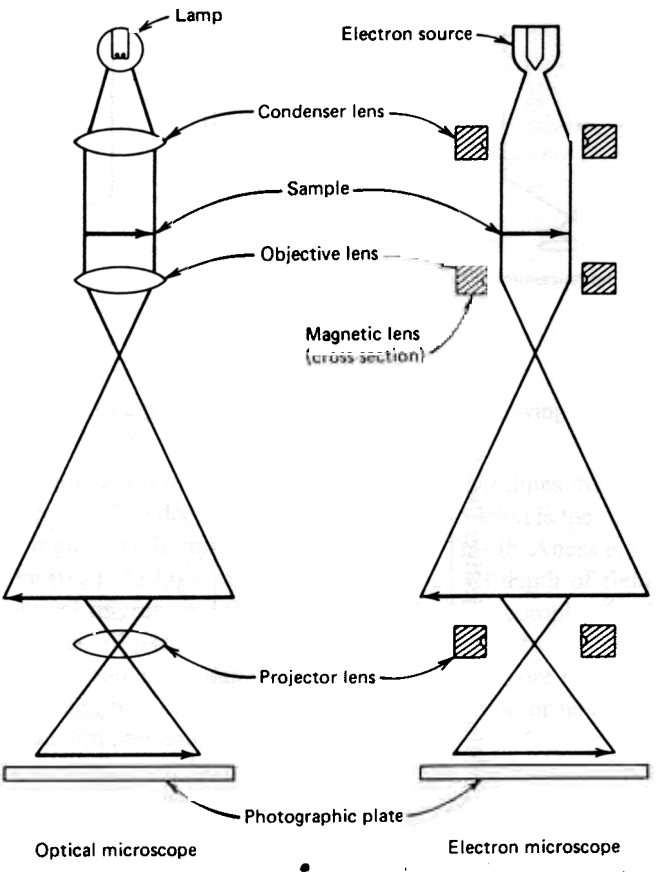

FIGURE 20.10 Comparison of optical and transmission electron microscopes.

microscopes (SEMs) and transmission electron microscopes (TEMs), the latter is most analogous to the light microscope and is covered first. As shown in Fig. 20.10, transmission electron microscopes use electrons in the same way that optical microscopes use light (photons). For purposes of comparison, the optical microscope is shown in the projection mode rather than the direct viewing mode described in Section 20.3. In the TEM, the electrons are generated by thermionic emission from a heated tungsten filament and are focused by magnetic lenses. These serve the same function as optical lenses and are given the same names. Magnetic lenses, however, have the advantage that their focal length can be adjusted by controlling the current through them. The interior of an electron microscope, including the sample area, must be under a high vacuum (less than 0.01 Pa [10^{-7} atm]), to prevent the scattering of the electron beam by air molecules. This is accomplished by a combination of mechanical and oil diffusion vacuum pumps. Particles in the electron beam absorb and scatter electrons to produce a two-dimensional silhouette image similar to

that produced in optical microscopy. The magnified image is viewed by projecting the electron image onto a fluorescent screen or a photographic plate.

The principles of resolution and depth of field discussed in Section 20.3 hold for electron microscopes, but the wavelength of the radiation used in electron microscopes is much less than the wavelength of light. The wavelength of an electron is given by

$$\lambda_e = \frac{0.0012}{\sqrt{V}} \tag{20.10}$$

where λ_e is in μm and the microscope acceleration voltage V is in volts. For a typical acceleration voltage of 70 kV, the wavelength of the electron beam is 4.5×10^{-6} μm, or 100,000 times smaller than the wavelength of light. The resolution, however, is *not* 100,000 times smaller than that of an optical microscope, because of the small value of angular aperture used in electron microscopes to minimize distortion. The limit of resolution for a typical TEM is less than 0.001 μm. The small value of aperture angle used has the advantage of providing a large depth of field, more than 100 times the resolution of the instrument. Table 20.5 compares the magnification, resolution, and depth of field of different types of microscopes.

Transmission electron microscopes permit the smallest aerosol particles to be measured, but these instruments can be used only for solid particles that do not evaporate or degrade under the combined effects of high vacuum and heating by the electron beam. Particles must be deposited on specially prepared 3-mm-diameter grids mounted in a grid holder and inserted into the microscope. The grids are 200 mesh electrodeposited screen with a thin film of carbon or Parlodion (1–4% nitrocellulose in amyl acetate) covering the screen openings. The film is sufficiently thin, compared to the particles, that it causes only slight attenuation of the electron beam. The particles, on the other hand, extensively scatter and absorb the electron beam to form a high-contrast silhouette image. Particles can be deposited directly onto the film surface of a grid by electrostatic precipitation using the miniature type of precipitator described in Section 15.8. In some cases, replication or transfer procedures can be used to deposit particles or their replicas from another surface onto a grid.

Sizing of particles is usually done from photographs made by enlarging a negative exposed to the electron image in the microscope. Special fine-grained, blue-sensitive photographic film is used for this purpose. The sizing procedures are the same as those described in Section 20.1 for optical microscopy, except that a transparent overlay of the Porton graticule or other standard circles is used. The exact magnification of the photographs and the calibration of the overlay are determined by photographing a carbon film replica of a diffraction grating under the same conditions of magnification as that for the particles. The spacing between the grating lines, usually less than 1 μm, is accurately known from independent measurements.

Although the scanning electron microscope (SEM) also uses electron beams, magnetic lenses, and a high vacuum, it operates on a different principle than the TEM does and creates images having a three-dimensional appearance. As shown

TABLE 20.5 Magnification, Resolution, Depth of Field, and Sample Environment for Different Types of Microscopes

Type of Instrument			Ratio of Depth of Field to Resolution	Sample Environment
Eye	1	~200		Air
Magnifying glass	2–10	25–100		Air
Compound optical microscope				
43× objective (dry)	200–850	0.3		Air
Compound optical microscope				
95× objective (oil immersion)	500–1300	0.2	2	Oil
Scanning electron microscope (SEM)	20–100,000	0.01	>1000	Vacuum
Transmission electron microscope (TEM)	1000–1,000,000	<0.001	>100	Vacuum

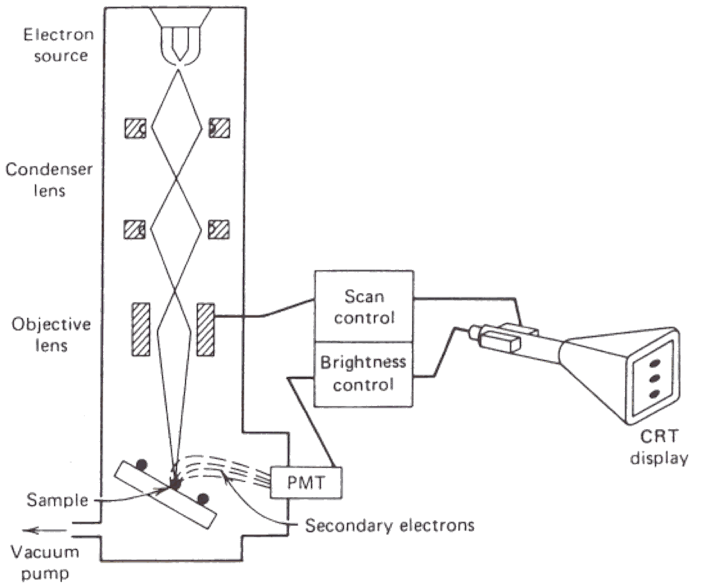

FIGURE 20.11 Schematic diagram of a scanning electron microscope.

in Fig. 20.11, the electron beam is focused to a spot about 0.01 μm in diameter and passed back and forth across the sample in a regular pattern. The electron beam causes secondary electrons to be emitted from the surface of the sample. These low-voltage electrons are attracted to a detector maintained at a positive voltage with respect to the sample. They can follow a curved path to reach the detector (a scintillator plus a photomultiplier tube, or PMT), where they are converted to an electrical signal. The number of secondary electrons emitted and reaching the detector depends on the topography of the surface; high points emit many electrons and valleys emit few. A cathode ray tube (CRT) is scanned in synchronization with the scanning pattern of the electron beam, and the brightness of the picture at any point is made proportional to the number of secondary electrons reaching the detector at that instant. This creates a reconstructed image of the sample surface, with high points appearing bright and valleys appearing dark. By tilting the sample with respect to the electron beam, realistic shadows are produced that give a remarkable three-dimensional effect to the picture. SEM photographs such as those shown in Sections 1.1 and 9.1 are photographed directly from the CRT screen. The sample can be tilted and rotated by external controls while being viewed to reveal all sides of a particle.

The resolution of a typical SEM is about 0.01 μm, not as good as a TEM, but much better than an optical microscope and adequate for most particle studies. Like the TEM, the SEM is limited to solid, nonvolatile particles. Unlike the TEM, the electron beam, in a SEM does not have to penetrate the sample support, so SEM samples are usually mounted on the end of an aluminum cylinder 10–30 mm in

diameter. Precautions must be taken to prevent the buildup of electric charge on the sample surface, which would deflect the electron beam and cause distortion of the image. This is usually done by applying a very thin (< 0.01 μm) coating of gold or carbon to the surface of the particle with a sputter-coating apparatus. Particles can be deposited onto any surface that can be attached to the sample cylinder and made conductive. The smooth surface of a capillary pore membrane filter provides a suitable surface for viewing particles, and particles larger than its pore size can be sampled directly onto the filter surface. Figure 1.4(b) is an example of an SEM sample taken on a capillary pore membrane filter.

Scanning electron microscopes have a depth of field that is more than 300 times greater than that of optical microscopes and a wide range of magnification, 20–100,000×. To measure and evaluate particles, a magnification range of 100–10,000× is most commonly used. The great depth of field and the accurate rendition of surface features make the SEM well suited to particle sizing and morphology studies.

An electron microscope can be used as a microprobe to determine the elemental composition of a particle. The electron beam is focused on a single particle, and the X rays that are emitted are detected by a solid-state X-ray detector. The energy of the X rays is related to the Z number of the elements in the particle and provides an elemental analysis of the particle for $Z > 12$. Microprobe analyses of single particles for elemental or molecular composition are reviewed by Fletcher and Small (1993).

20.5 ASBESTOS COUNTING

The mineral asbestos possesses some unique properties that cause lung injury and necessitate microscopic methods for evaluating its hazard. The characteristic fibrous shape of asbestos particles [see Fig. 1.4(b)] enables them to get past respiratory defense mechanisms and cause asbestosis (scarring of lung tissue), mesothelioma (cancer of the lining of the lung), and lung cancer. Microscopy is used to identify those asbestos fibers whose size and shape enable them to cause these diseases.

Asbestos originates as fiber bundles that break longitudinally into finer and finer fibers during milling. Because of the high strength of the material, fibers of long aspect ratio (length to diameter) are formed. The aerodynamic properties of fibers are such that fibers as long as 50 μm or as big as 3 μm in diameter can reach the alveolar region and are considered respirable. The reason they can do this is that the fibers align themselves with the streamlines and "snake" their way through the narrow airways to the alveolar region. Once lodged in an alveolus, large asbestos fibers cannot be removed by normal clearance mechanisms. They are insoluble in lung fluids, too long to be engulfed by macrophages, and only slightly able to migrate to lymph nodes. It is thought that when macrophages try to engulf long fibers, they leak enzymes that cause fibrosis, the scarring and thickening of alveolar surfaces associated with asbestosis. Asbestos fibers less than about 5 μm in length

are cleared by the normal clearance mechanisms. Each of the asbestos-related diseases is associated with fibers in a specific size range. Fibers 0.15 to 3 μm in diameter and 2–100 μm long are associated with asbestosis, fibers less than 0.1 μm in diameter and 5–100 μm long with mesothelioma, and fibers 0.15–3 μm in diameter and 10 to 100 μm long with lung cancer (Lippmann, 1991). Because the risk of disease depends critically on the shape of the particles, microscopy must be used to evaluate the concentration of those asbestos particles whose size and shape make them hazardous.

The U.S. occupational exposure standard for asbestos is 100,000 fibers/m^3 [0.1 f/cm^3] greater than 5 μm in length and having an aspect ratio greater than 3:1, as determined by the membrane filter method using phase contrast microscopy (PCM). The membrane filter method, or "NIOSH method," is an optical microscope technique used for the quantitative determination of the concentration of asbestos fibers in air. The method consists of collecting breathing zone samples at 0.5–16 L/min on 25-mm membrane filters (mixed cellulose ester membrane filters with a pore size of 0.45–1.2 μm). Open-face filter holders with a 50-mm protective cowl (inlet extension) are used. The sample volume is adjusted to produce a fiber surface density in the optimal range of 100–1300 f/mm^2. A sample volume of 1.0 m^3 [1000 L] is suitable for concentrations of 40,000–500,000 f/m^3 [0.04–0.5 f/cm^3]. The filter is "melted" to a solid, transparent film by hot acetone vapor and is sealed in triacetin. Fibers meeting the size and shape criteria are counted at 400–450× magnification (45× objective, NA = 0.65–0.75, and 10× eyepiece) by phase contrast optical microscopy. (Phase contrast microscopy is used to enhance the contrast of the fibers because the refractive index is near that of the mounting medium.)

Any particle having a length greater than 5 μm and an aspect ratio of 3:1 (length:diameter) or greater is considered a fiber, whether or not it is asbestos. Standard practice in the United States calls for using a Walton–Beckett graticule, shown in Figure 20.12. The Walton–Beckett graticule defines a 100-μm-diameter counting field with standard fiber shapes and sizes around the perimeter for comparison. Fibers meeting the size and shape criteria that are completely within the field are counted as one fiber, while those that are partially within the field are counted as one-half fiber. Sample fibers are also shown in Figure 20.12. Because of the limit of resolution of optical microscopes, this method cannot detect fibers less than 0.25 μm in diameter. Consequently, a significant number of hazardous fibers are too small to be detected by PCM, so the count that is obtained should be considered an index of asbestos concentration, and not the true concentration. Because of the difficulty of sizing particles near the limit of resolution of the microscope, novice counters can underestimate fiber concentrations by a factor of two or more.

More advanced methods of optical and electron microscopy may be used to determine whether a fiber that meets the size and shape requirements is in fact an asbestos fiber. This can be done most definitively by transmission electron microscopy (TEM), which allows observation and measurement of fiber size and shape for even the smallest asbestos fibers. TEM also provides the opportunity for positive identification through elemental analysis by energy-dispersive X-ray analysis

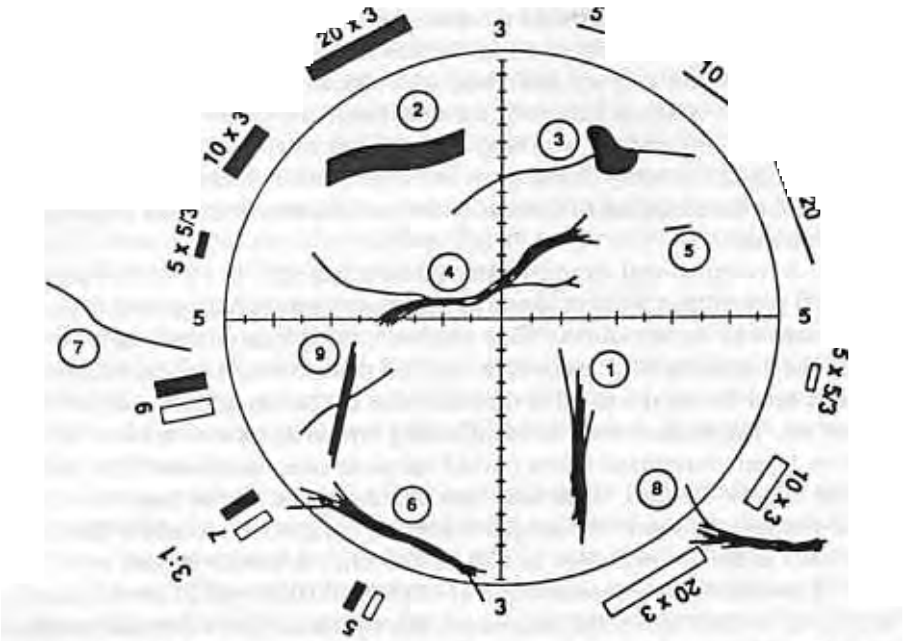

FIGURE 20.12 Walton–Beckett graticule for optical microscope counting of fibers. Particles 1–4 are counted as one fiber, 5–7 are not counted, and 8 and 9 are counted as one-half and two fibers, respectively. From Baron, 1993. Reprinted by permission of John Wiley & Sons, Inc.

(EDXA) and crystal structure by diffraction pattern analysis. TEM samples can be taken on mixed cellulose ester membrane filters, but require special preparation. (See Baron, 1993.)

A portable direct-reading fibrous aerosol monitor, the FAM-1® (MIE, Inc., Bedford, MA), provides rapid measurement of airborne fiber concentrations. Aerosol is sampled at 0.12 m^3/hr [2 L/min] and passes through a 10-mm-diameter sensing tube with laser illumination along its axis. The flow rate through the sensing volume is 10 cm^3/min. The fibers in the aerosol stream line up with an oscillating electric field. The light scattered by fibers pulses at the oscillation frequency while that scattered by compact particles does not. The sharpness of the pulses is related to the fiber length. Fibers meeting the criteria of length and aspect ratio have a characteristic signature that is sensed electronically. Fibers are counted for a preset sampling period and the average number concentration displayed. The correlation between results obtained using the FAM-1 and those obtained using manual counting methods is reasonable.

20.6 AUTOMATIC SIZING METHODS

The visual comparison methods for particle sizing described in Section 20.2 are satisfactory for most particle size analysis, but are slow, tedious, and subject to

operator error or bias. Automated image analysis attempts to overcome these problems by using computer analysis of particle images. First, the image of many particles is scanned, creating a digital image in the form of an array of millions of picture elements (pixels). The image may be from an optical or electron microscope or a photograph. The computer interprets particle size and shape from the arrangement of contiguous dark pixels on a light background or vice versa. The computer can then calculate the projected area diameter, maximum chord, Feret's diameter, Martin's diameter, perimeter, and various shape factors. Mean and standard deviations and moments of these quantities for all particles in the field can be calculated automatically. Measurements can be made on all or selected particles in a field. Image analysis can be combined with elemental analysis in an electron microscope. Here, the microscope is operated under computer control to obtain information about particle size, shape, and elemental composition of many particles automatically. Analysis of hundreds or thousands of particles yields more elaborate information, such as size distributions for selected elemental composition or average concentrations of a specific element versus particle size.

The accuracy, speed, versatility, and ability to make measurements without the possibility of operator bias are the primary virtues of these automatic instruments. They work best with a high-contrast image in which the smallest particles have an image size of several millimeters. When particle images have low contrast with fuzzy, gray edges, the size of the particles measured is controlled by instrument settings that define what gray level constitutes the edge of the particle. In this situation, the entire sizing process, microscopy, photography, and image analysis must be calibrated to yield accurate results that are free from bias. The procedure can be further complicated by overlapping particles and a "noisy" background. Care must be taken that the background texture, such as the holes of a capillary pore membrane (Nuclepore) filter, is not included in the analysis. Such elements are instinctively screened out when we view an image, but the computer does not have our instincts.

PROBLEMS

20.1 Consider an aerosol composed entirely of spherical doublets (particles that consist of two spheres joined at a point). Assume that all spheres are identical with a diameter d. If the particles are viewed perpendicular to the line between their centers:

(a) What is the projected area diameter for these particles?

(b) What is their volume shape factor?

(c) What is the maximum and minimum ratio of Feret's diameter to the projected area diameter?

ANSWER: $1.41d$, 0.37, 1.41, 0.71.

20.2 A straight fiber has an aspect ratio of 5:1. If the fiber is viewed perpendicular to its axis, what is the maximum ratio of Feret's diameter to projected area diameter?

ANSWER: 2.0.

For particles having a square projected cross section, what is the ratio of Feret's diameter (averaged over all orientations) to the projected area diameter?

ANSWER: 1.13.

20.4 A cylindrical fiber has a diameter of 1 μm and a length three times its diameter. What are the projected area diameter and volume shape factor of the fiber when it is viewed perpendicular to its axis?

ANSWER: 2.0 μm, 0.32.

20.5 A particle has a smooth, circular cross section of diameter d_p. The fractal dimension of the particle's perimeter is to be estimated by fitting a four-sided and a six-sided regular inscribed polygon to the circle. Based only on this information, what fractal dimension is estimated for this step size range. [*Hint*: The length b of the side of a regular inscribed polygon with n sides is $b = d_p \times \sin(180/n)$.]

ANSWER: 1.17.

What is the theoretical limit of resolution of a microscope having a 90× objective (angular aperture of 120°) and a 15× eyepiece used with blue light ($\lambda = 0.4$ μm) and with immersion oil having a refractive index of 1.51?

ANSWER: 0.19 μm.

20.7 What is the ratio of the maximum to the minimum size of circle provided by the Porton graticule as shown in Fig. 20.2?

ANSWER: 32.

20.8 Between what two circle numbers on the Porton graticule will the image of a 1-μm particle fall when viewed with a 43× objective and a 15× eyepiece? Circle number 10 has an image diameter of 9.9 mm.

ANSWER: 2 and 3.

REFERENCES

Baron, P. A., "Measurement of Asbestos and Other Fibers," in Willeke, K., and Baron, P. A. (Eds.), *Aerosol Measurement*, Van Nostrand Reinhold, New York, 1993.

Baron, P. A., and Willeke, K., "Aerosol Fundamentals" in Willeke, K., and Baron, P. A. (Eds.), *Aerosol Measurement*, Van Nostrand Reinhold, New York, 1993.

Cadle, R. D., *The Measurement of Airborne Particles*, Wiley, New York, 1975.

Cheng, Y. S., Chen, B. T., and Yeh, H. C., "Size Measurement of Liquid Aerosols," *J. Aerosol Sci.*, **17**, 803–809 (1986).

Davies, C. N., "Particle–Fluid Interaction," *J. Aerosol Sci.*, **10**, 477–513 (1979).

REFERENCES

Fletcher, R. A., and Small, J. A., "Analysis of Individual Collected Particles," in Willeke, K., and Baron, P. A. (Eds.), *Aerosol Measurement*, Van Nostrand Reinhold, New York, 1993.

John, W., and Wall, S. M., "Aerosol Testing Techniques for Size-Selective Samplers," *J. Aerosol Sci.*, **14**, 713–727 (1983).

Kaye, B. H., *A Random Walk through Fractal Dimensions*, Wiley-VCH Verlagsgesellschaft, Weinheim, Germany, 1989.

Lippmann, M., "Industrial and Environmental Hygiene: Professional Growth in a Changing Environment," *Am. Ind. Hyg. Assoc. J.*, **52**, 341–348 (1991).

Liu, B. Y. H., Pui, D. Y. H., and Wang X-Q., "Drop Size Measurement of Liquid Aerosols," *Atm. Environ.*, **16**, 563–567 (1982).

Mandelbrot, B. B., *Fractals, Form, Chance and Dimension*, Freeman, San Francisco, 1977, 1983.

McCrone, W. C., and Delly, J. G., *The Particle Atlas*, 2d ed., Ann Arbor Science, Ann Arbor, MI, 1973.

Mercer, T. T., *Aerosol Technology in Hazard Evaluation*, Academic Press, New York, 1973.

NIOSH, "Asbestos and Other Fibers 7400," in *NIOSH Manual of Analytical Methods*, U.S. Gov. Printing Office, Washington, DC, 1989.

Olan-Figueroa, E., McFarland, A. R., and Ortiz, C. A., "Flattening coefficients for DOP and oleic acid droplets deposited on treated glass slides," *Am. Ind. Hyg. Assoc. J.*, **43**, 395 (1982).

Silverman, L., Billings, C. E., and First, M. W., *Particle Size Analysis in Industrial Hygiene*, Academic Press, New York, 1971.

Sorenson, C. M., and Feke, G. D., "The Morphology of Macroscopic Soot," *Aerosol Sci. Tech*, **25**, 328–337 (1996).

Appendices

Appendix A1. Useful Constants and Conversion Factors

Fundamental units

1 micrometer (μm) = 1 micron (μ) = 10^{-6} m = 10^{-4} cm = 10^{-3} mm = 10^{3} nm = 10^{4} Å = 3.94×10^{-5} in

1 nm = 10^{-3} μm = 10^{-6} mm = 10^{-7} cm = 10^{-9} m

1 m = 39.4 in = 3.28 ft

1 km = 1000 m = 3280 ft = 0.621 mi

1 in. = 0.0254 m = 2.54 cm = 25.4 mm

1 ft = 0.305 m = 30.5 cm = 305 mm

1 newton (N) = 1 kg · m/s^2 = 10^5 dyn = 10^5 g · cm/s^2

1 lb = 0.454 kg = 454 g

K= °C + 273

°F = 1.8(°C) + 32

Volume

1 m^3 = 1000 L = 10^6 cm^3 = 10^9 mm^3 = 35.3 ft^3

1 L = 0.001 m^3 = 1000 cm^3 = 10^6 mm^3 = 0.0353 ft^3 = 61.0 in^3

1 ft^3 = 28,300 cm^3 = 28.3 L = 0.0283 m^3 = 1728 in^3

1 in.^{3} = 16.4 cm^3 = 0.0164 L = 1.64×10^{-5} m^3

Flow rate

1 m^3/s = 2120 ft^3/min = 1000 L/s

1 m^3/h = 16.7 L/min = 35.3 ft^3/h = 0.588 ft^3/min

1 ft^3/min (cfm) = 28.3 L/min (Lpm) = 1.70 m^3/h

1 ft^3/h = 0.47 L/min

Concentration

1 μg/m^3 = 1 ng/L = 1 pg/cm^3

1 mg/m^3 = 1 μg/L = 1 ng/cm^3

1 g/m^3 = 1 mg/L = 1 μg/cm^3

1 mppcf = 35.3 particles/cm^3

Velocity

1 ft/min = 0.305 m/min = 0.508 cm/s

1 ft/s = 0.305 m/s = 30.5 cm/s = 0.68 mph

Velocity of sound in air at 293 K [20°C] = 343 m/s = [34,300 cm/s]

Velocity of light in a vacuum = 3.00×10^8 m/s = [3.00×10^{10} cm/s]

Acceleration

Acceleration of gravity at sea level = 9.81 m/s^2 = [981 cm/s^2]

Pressure

1 atm = 1.01×10^6 dyn/cm^2 = 101 kPa= 14.7 lb/in^2 (psia) = 76 cm Hg
= 760 mm Hg = 1030 cm H_2O = 407 in. H_2O

1 Pa = 1 N/m^2 = 10 dyn/cm^2 = 0.0075 mm Hg = 0.0040 in. H_2O

1 lb/in^2 (psi) = 6.89 kPa = 51.7 mm Hg = 27.7 in. H_2O

1 in. H_2O = 249 Pa = 2490 dyn/cm^2

Vapor pressure of water at 293 K [20°C] = 2.34 kPa = [17.5 mm Hg]

Viscosity

1 Pa · s = 1 N · s/m^2 = 1 kg/m · s = 10 Poise (P) = 10 dyn · s/cm^2 = 10 g/cm · s

Viscosity of air at 293 K [20°C] = 1.81×10^{-5} Pa · s = [1.81×10^{-4} Poise]

Energy

1 J = 1 N · m = 10^7 erg = 0.239 cal = 9.47×10^{-4} Btu

1 cal = 4.19 J = 4.19×10^7 erg = 0.00397 Btu

Ideal Gas Law $Pv = n_mRT$

R = 8.31 J/K · mol (N · m/K · mol) for P in Pa and v in m^3.

R = 82.1 atm · cm^3/K · mol for P in atm and v in cm^3

$R = 8.31 \times 10^7$ dyn · cm/K · mol for P in dyn/cm^2 and v in cm^3

R = 62400 mm Hg · cm^3/K · mol for P in mm Hg and v in cm^3

Volume of 1 mol of ideal gas at 293 K [20°C] = 0.0241 m^3 = 24. L

Avogadro's number = $N_a = 6.02 \times 10^{23}$ molecules/mol

Boltzmann's constant $k = R/N_a = 1.38 \times 10^{-23}$ J/K (N · m/K)
= [1.38×10^{-16} erg/K (dyn · cm/K)]

Dry Air at 293 K [20°C] and 101 kPa (1 atm)

Density = 1.20 kg/m^3 = 1.20 g/L = [1.20×10^{-3} g/cm^3] = 0.074 lb/ft^3

Viscosity = 1.81×10^{-5} Pa · s = [1.81×10^{-4} Poise]

Mean free path = 0.066 μm

Molecular weight = 0.029 kg/mol = [29.0 g/mol]

Specific heat ratio = $\kappa = c_p/c_v = 1.40$
Diffusion coefficient = 2.0×10^{-5} m^2/s = [0.20 cm^2/s]
Composition by volume (dry air)

N_2	78.1%
O_2	20.9%
Ar	0.93%
CO_2	0.031%
Other	0.003%

Water at 293 K [20°C] and 101 kPa (1 atm)
Viscosity = 0.00100 Pa · s [0.0100 dyn · s/cm^2]
Surface tension = 0.0727 N/m = [72.7 dyn/cm]
Saturation vapor pressure = 2.34 kPa = [17.5 mm Hg]

Water vapor at 293 K [20°C] and 101 kPa (1 atm)
Diffusion coefficient = 2.4×10^{-5} m^2/s [0.24 cm^2/s]
Density = 0.75 kg/m^3 = 0.75×10^{-3} g/cm^3

Appendix A2. Some Basic Physical Laws

The inertia of a body is that property of the body which tends to resist change in its state of rest or of motion. Mass is a quantitative measure of inertia.

$$\text{Momentum} = \text{mass} \times \text{velocity} = mV$$

Newton's second law: The rate of change of momentum of a body is proportional to the net force on the body, $\Sigma F = d(mV)/dt$. For a body with constant mass,

$$F = m\left(\frac{dV}{dt}\right) = ma$$

where force is in N (newtons) for m in kg and a in m/s^2, and in dyn for m in g and a in cm/s^2.

Work = force × distance; 1 N · m = 1 J; [1 dyn · cm = 1 erg]
Kinetic energy = $\frac{1}{2}mV^2$; 1 kg · m^2/s^2 = 1 J; [1 g · cm^2/s^2 = 1 erg]
Power = work per unit time; 1 W = 1 J/s = 10^7 erg/s = 0.00134 Hp

$$\text{Centripetal force} = \frac{m(V_T)^2}{R} = mR\omega^2$$

where V_T = tangential velocity, m/s [cm/s]; ω = angular velocity, rad/s; and R = radius of motion.

$V_T = \omega R$

1 radian (rad) = $(\frac{1}{2\pi})$ of a circle = $\frac{360}{2\pi} = 57.3°$

Buoyant force = weight of displaced fluid

Flow in a Duct

Flow rate = velocity × cross-sectional area = $Q = VA$

Residence time = duct volume/flow rate

Properties of a Sphere

Circumference = $2\pi r = \pi d = 3.14d$

Projected area = $\pi r^2 = \frac{\pi d^2}{4} = 0.785d^2$

Surface area = $4\pi r^2 = \pi d^2 = 3.14d^2$

Volume = $\frac{4\pi r^3}{3} = \frac{\pi d^3}{6} = 0.524d^3$

Total solid angle = 4π steradian (sr)

APPENDIX A3. Relative Density of Common Aerosol Materials (Multiply Values by 1000 for Density in kg/m³ and by 1.0 for Density in g/cm³)

Solids			
Aluminum	2.7	Natural fibers	1–1.6
Aluminum oxide	4.0	Paraffin	0.9
Ammonium sulfate	1.8	Plastics	1–1.6
Asbestos	2.0–2.8	Pollens	0.45–1.05
Asbestos, chrysotile	2.4–2.6	Polystyrene	1.05
Carnauba wax	1.0	Polyvinyl toluene	1.03
Coal	1.2–1.8	Portland cement	3.2
Fly ash	0.7–2.6	Quartz	2.6
Fly ash cenospheres	0.7–1.0	Sodium chloride	2.2
Glass, common	2.4–2.8	Sulfur	2.1
Granite	2.6–2.8	Starch	1.5
Ice	0.92	Talc	2.6–2.8
Iron	7.9	Titanium dioxide	4.3
Iron oxide	5.2	Uranine dye	1.53
Limestone	2.7	Wood (dry)	0.4–1.0
Lead	11.3	Zinc	6.9
Marble	2.6–2.8	Zinc oxide	5.6
Methylene blue dye	1.26		
Liquids			
Alcohol	0.79	Mercury	13.6
Dibutyl phthalate	1.045	Oils	0.88–0.94
Dioctyl phthalate [DOP; di-2 (ethylhexyl) phthalate]	0.983	Oleic acid	0.894
		Polyethylene glycol	1.13
Dioctyl sebacate	0.915	Sulfuric acid	1.84
Hydrochloric acid	1.19	Water	1.00

APPENDIX A4. Standard Sieve Sizes

Designation		Nominal	Designation		Nominal
ISO Std.[a] (μm)	Alternate (No.)	Wire Size (μm)	ISO Std.[a] (μm)	Alternate (No.)	Wire Size (μm)
250	60	180	63	230	44
	80	131	53	270	37
150	100	110	45	325	30
125	120	91	38	400	25
106	140	76	32	450	28
90	170	64	25	500	25
75	200	53	20	635	20

APPENDIX A5. Properties of Gases and Vapors at 293 K [20°C] and 101 kPa [1 atm]

Gas or Vapor	Molecular Weight	Relative Density[a]	Viscosity[b]	Diffusion Coefficient[c]
Air (dry)	29.0	1.00	1.81	2.0
Air (saturated)	28.7	0.99	1.79	2.0
CO	28.0	0.967	1.75	
CO_2	44.0	1.52	1.46	1.6
CH_4	16.0	0.554	1.09	
H_2	2.0	0.070	0.88	6.8
H_2O	18.0	0.62	0.96	2.4
N_2	28.0	0.967	1.75	2.0
O_2	32.0	1.10	2.03	2.0

[a]Ratio of density of gas to that of dry air. Multiply by 1.20 to get density in kg/m^3 and by 0.00120 to get density in g/cm^3.
[b]Multiply by 10^{-5} for viscosity in Pa·s and by 10^{-4} for viscosity in P (dyn · s/cm^3).
[c]Diffusion coefficient of gas or vapor in air. Multiply by 10^{-5} for diffusion coefficient in m^2/s and by 0.1 for diffusion coefficient in cm^2/s.

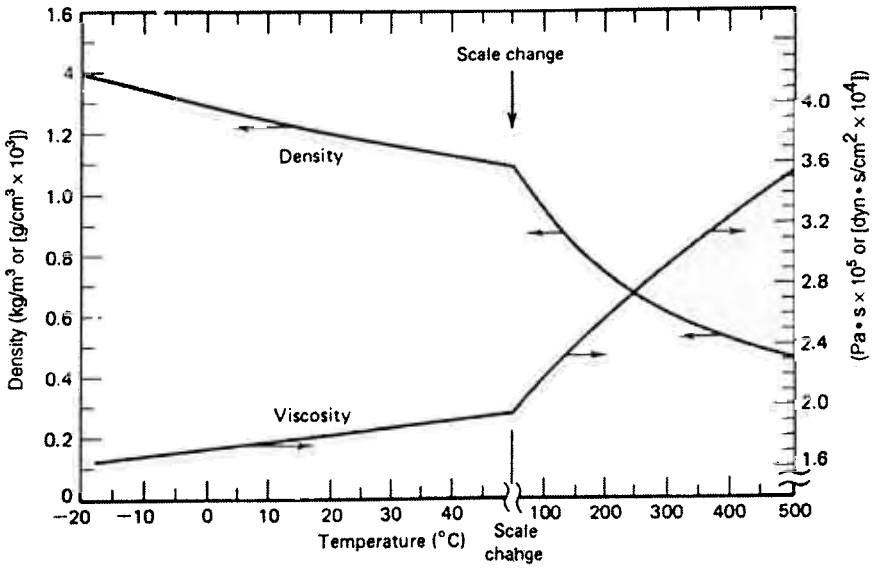

APPENDIX A6. Viscosity and Density of Air versus Temperature

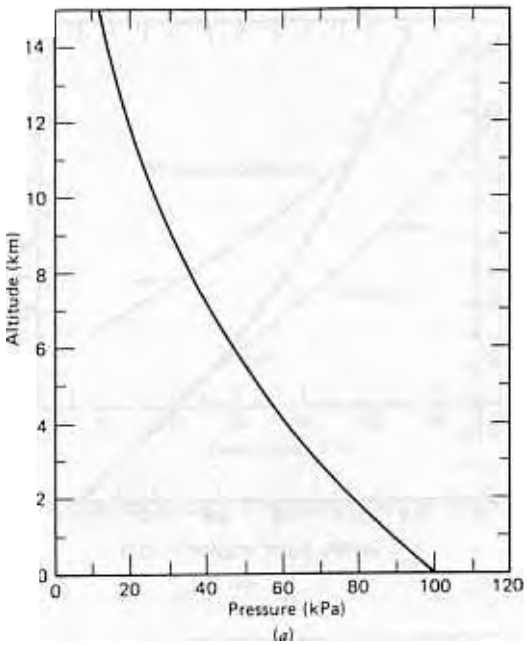

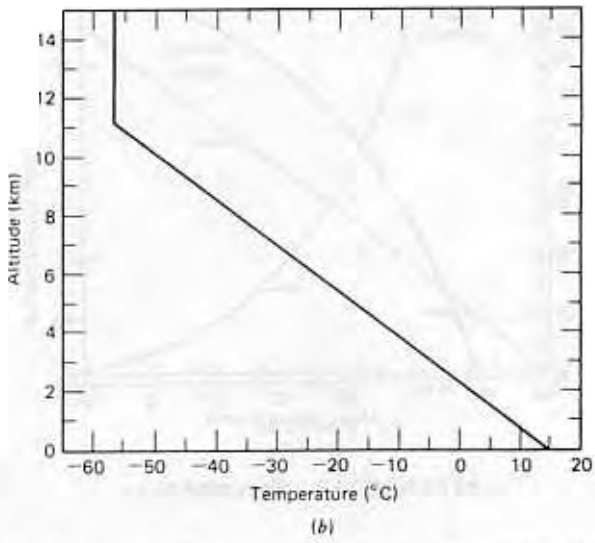

APPENDIX A7. Pressure (a), Temperature (b), Density (c), and Mean Free Path (d) of Air versus Altitude

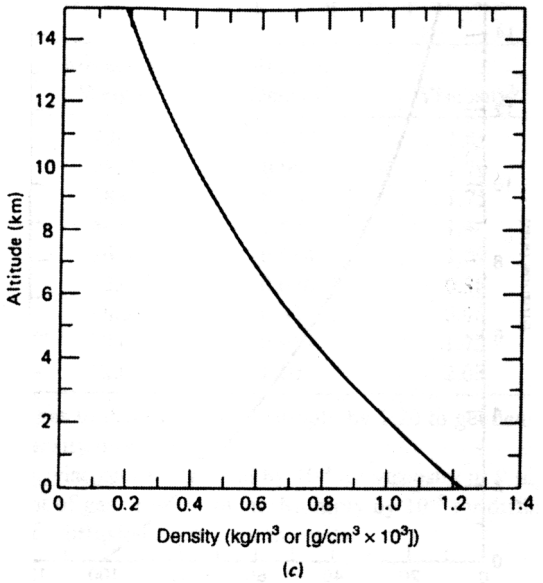

(*c*)

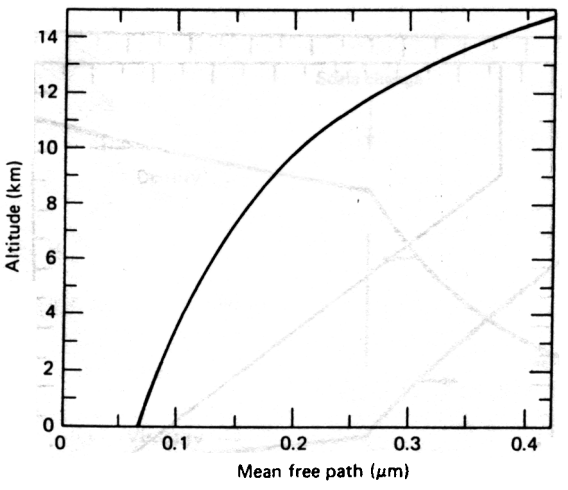

(*d*)

APPENDIX A7. Continued.

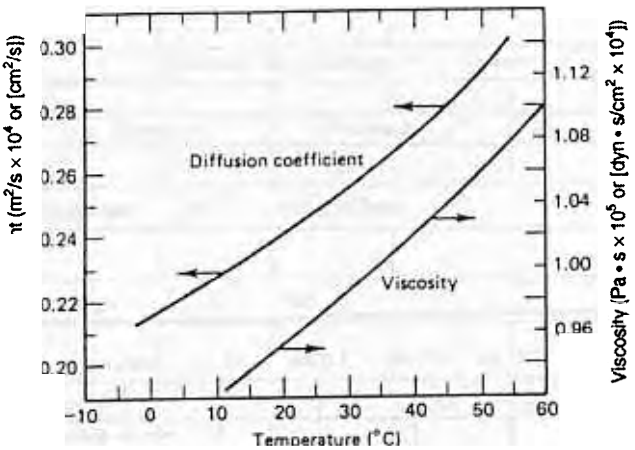

APPENDIX A8. Properties of Water Vapor

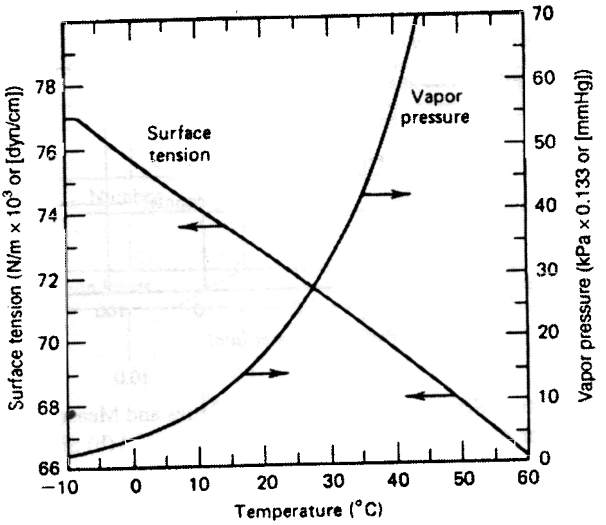

APPENDIX A9. Properties of Water

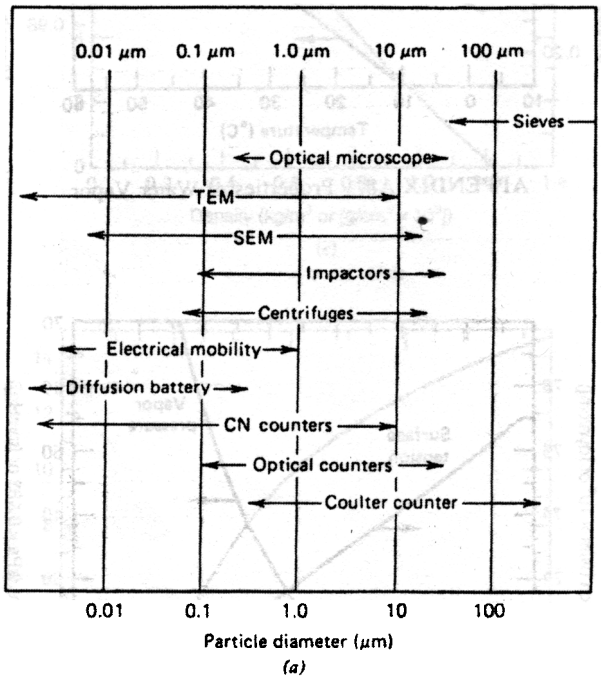

APPENDIX A10. Particle Size Range of Aerosol Properties and Measurement Instruments: (a) Application Range for Aerosol Size Measuring Instruments and (b) Size Range of Aerosol Properties (See Also Fig. 1.6)

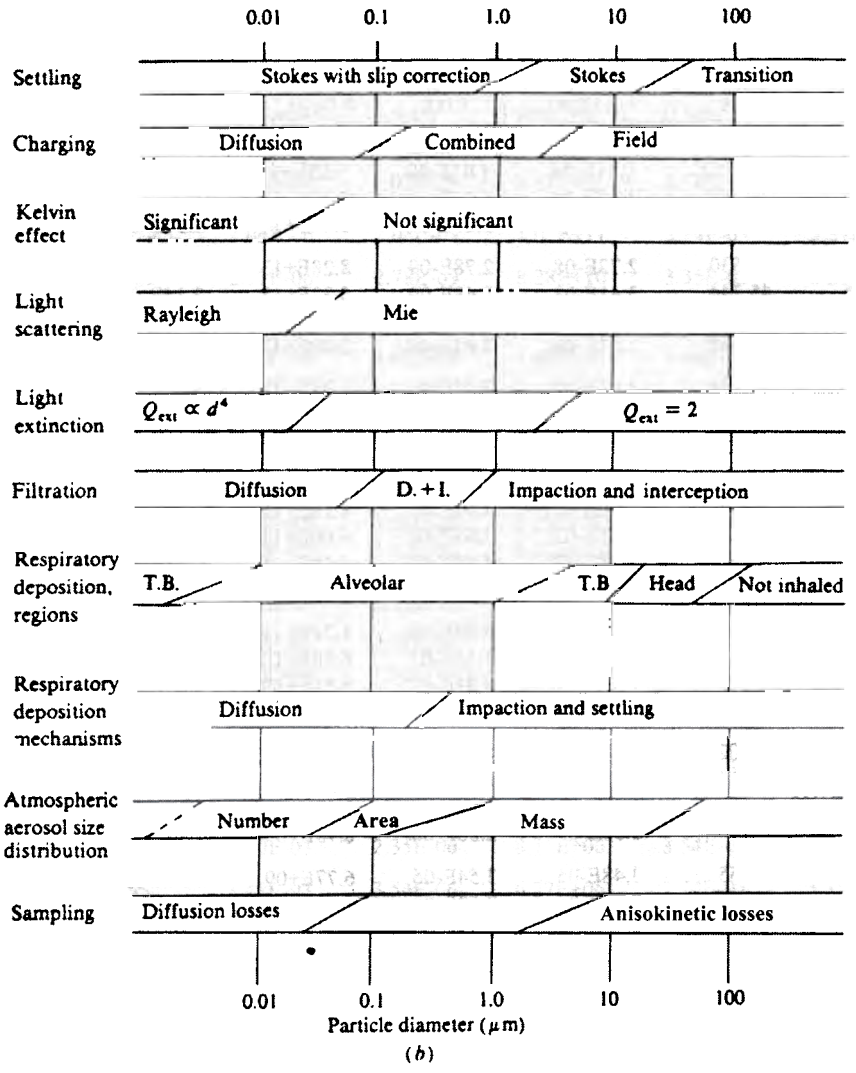

APPENDIX A10. Continued.

APPENDIX A11 (a). Properties of Airborne Particles at Standard Conditions (SI Units)[a]

Particle Diameter d (μm)	Slip Correction Factor C_c	Settling Velocity V_{TS} (m/s)	Relaxation Time τ (s)	Mobility B (m/N · s)	Diffusion Coefficient D (m^2/s)	Coagulation Coefficient K (m^3/s)
0.001	224.332	6.75E-09	6.89E-10	1.32E+15	5.32E-06	3.11E-16
0.0015	149.752	1.01E-08	1.03E-09	5.85E+14	2.37E-06	3.81E-16
0.002	112.463	1.35E-08	1.38E-09	3.30E+14	1.33E-06	4.40E-16
0.003	75.174	2.04E-08	2.08E-09	1.47E+14	5.94E-07	5.39E-16
0.004	56.530	2.72E-08	2.78E-09	8.28E+13	3.35E-07	6.21E-16
0.005	45.344	3.41E-08	3.48E-09	5.32E+13	2.15E-07	6.93E-16
0.006	37.888	4.11E-08	4.19E-09	3.70E+13	1.50E-07	7.56E-16
0.008	28.568	5.51E-08	5.61E-09	2.09E+13	8.46E-08	8.63E-16
0.01	22.976	6.92E-08	7.05E-09	1.35E+13	5.45E-08	9.48E-16
0.015	15.524	1.05E-07	1.07E-08	6.07E+12	2.45E-08	1.09E-15
0.02	11.801	1.42E-07	1.45E-08	3.46E+12	1.40E-08	1.15E-15
0.03	8.083	2.19E-07	2.23E-08	1.58E+12	6.39E-09	1.14E-15
0.04	6.229	3.00E-07	3.06E-08	9.13E+11	3.69E-09	1.07E-15
0.05	5.120	3.85E-07	3.93E-08	6.00E+11	2.43E-09	9.92E-16
0.06	4.384	4.75E-07	4.84E-08	4.28E+11	1.73E-09	9.20E-16
0.08	3.470	6.69E-07	6.82E-08	2.54E+11	1.03E-09	8.03E-16
0.1	2.928	8.82E-07	8.99E-08	1.72E+11	6.94E-10	7.17E-16
0.15	2.220	1.50E-06	1.53E-07	8.68E+10	3.51E-10	5.83E-16
0.2	1.878	2.26E-06	2.31E-07	5.51E+10	2.23E-10	5.09E-16
0.3	1.554	4.21E-06	4.29E-07	3.04E+10	1.23E-10	4.34E-16
0.4	1.402	6.76E-06	6.89E-07	2.06E+10	8.31E-11	3.97E-16
0.5	1.316	9.91E-06	1.01E-06	1.54E+10	6.24E-11	3.76E-16
0.6	1.261	1.37E-05	1.39E-06	1.23E+10	4.98E-11	3.62E-16
0.8	1.194	2.30E-05	2.35E-06	8.75E+09	3.54E-11	3.45E-16
1.0	1.155	3.48E-05	3.54E-06	6.77E+09	2.74E-11	3.35E-16
1.5	1.103	7.47E-05	7.62E-06	4.31E+09	1.74E-11	3.22E-16
2.0	1.077	1.30E-04	1.32E-05	3.16E+09	1.28E-11	3.15E-16
3.0	1.051	2.85E-04	2.90E-05	2.05E+09	8.31E-12	3.09E-16
4.0	1.039	5.00E-04	5.10E-05	1.52E+09	6.15E-12	3.06E-16
5.0	1.031	7.76E-04	7.91E-05	1.21E+09	4.89E-12	3.04E-16
6.0	1.026	1.11E-03	1.13E-04	1.00E+09	4.05E-12	3.03E-16
8.0	1.019	1.96E-03	2.00E-04	7.47E+08	3.02E-12	3.01E-16
10	1.015	3.06E-03	3.12E-04	5.95E+08	2.41E-12	3.00E-16
15	1.010	6.84E-03	6.98E-04	3.95E+08	1.60E-12	2.99E-16
20	1.008	1.21E-02	1.24E-03	2.95E+08	1.19E-12	2.99E-16
30	1.005	2.72E-02	2.78E-03	1.96E+08	7.94E-13	2.98E-16
40	1.004	4.84E-02	4.93E-03	1.47E+08	5.95E-13	2.98E-16
50	1.003	7.55E-02	7.70E-03	1.18E+08	4.76E-13	2.98E-16
60	1.003	1.33E-01	1.11E-02	9.80E+07	3.96E-13	2.98E-16
80	1.002	1.72E-01	1.97E-02	7.34E+07	2.97E-13	2.98E-16
100	1.002	2.49E-01	3.07E-02	5.87E+07	2.37E-13	2.98E-16

[a]Calculated for standard density spheres at 293 K [20°C] and 101 kPa (1 atm).

APPENDIX A11 (b). Properties of Airborne Particles at Standard Conditions (cgs Units)[a]

Particle Diameter d (μm)	Slip Correction Factor C_c	Settling Velocity V_{TS} (cm/s)	Relaxation Time τ (s)	Mobility B (cm/dyn · s)	Diffusion Coefficient D (cm²/s)	Coagulation Coefficient K (cm³/s)
0.001	224.332	6.75E-07	6.89E-10	1.32E+12	5.32E-02	3.11E-10
0.0015	149.752	1.01E-06	1.03E-09	5.85E+11	2.37E-02	3.81E-10
0.002	112.463	1.35E-06	1.38E-09	3.30E+11	1.33E-02	4.40E-10
0.003	75.174	2.04E-06	2.08E-09	1.47E+11	5.94E-03	5.39E-10
0.004	56.530	2.72E-06	2.78E-09	8.28E+10	3.35E-03	6.21E-10
0.005	45.344	3.41E-06	3.48E-09	5.32E+10	2.15E-03	6.93E-10
0.006	37.888	4.11E-06	4.19E-09	3.70E+10	1.50E-03	7.56E-10
0.008	28.568	5.51E-06	5.61E-09	2.09E+10	8.46E-04	8.63E-10
0.01	22.976	6.92E-06	7.05E-09	1.35E+10	5.45E-04	9.48E-10
0.015	15.524	1.05E-05	1.07E-08	6.07E+09	2.45E-04	1.09E-09
0.02	11.801	1.42E-05	1.45E-08	3.46E+09	1.40E-04	1.15E-09
0.03	8.083	2.19E-05	2.23E-08	1.58E+09	6.39E-05	1.14E-09
0.04	6.229	3.00E-05	3.06E-08	9.13E+08	3.69E-05	1.07E-09
0.05	5.120	3.85E-05	3.93E-08	6.00E+08	2.43E-05	9.92E-10
0.06	4.384	4.75E-05	4.84E-08	4.28E+08	1.73E-05	9.20E-10
0.08	3.470	6.69E-05	6.82E-08	2.54E+08	1.03E-05	8.03E-10
0.1	2.928	8.82E-05	8.99E-08	1.72E+08	6.94E-06	7.17E-10
0.15	2.220	1.50E-04	1.53E-07	8.68E+07	3.51E-06	5.83E-10
0.2	1.878	2.26E-04	2.31E-07	5.51E+07	2.23E-06	5.09E-10
0.3	1.554	4.21E-04	4.29E-07	3.04E+07	1.23E-06	4.34E-10
0.4	1.402	6.76E-04	6.89E-07	2.06E+07	8.31E-07	3.97E-10
0.5	1.316	9.91E-04	1.01E-06	1.54E+07	6.24E-07	3.76E-10
0.6	1.261	1.37E-03	1.39E-06	1.23E+07	4.98E-07	3.62E-10
0.8	1.194	2.30E-03	2.35E-06	8.75E+06	3.54E-07	3.45E-10
	1.155	3.48E-03	3.54E-06	6.77E+06	2.74E-07	3.35E-10
5	1.103	7.47E-03	7.62E-06	4.31E+06	1.74E-07	3.22E-10
	1.077	1.30E-02	1.32E-05	3.16E+06	1.28E-07	3.15E-10
	1.051	2.85E-02	2.90E-05	2.05E+06	8.31E-08	3.09E-10
4	1.039	5.00E-02	5.10E-05	1.52E+06	6.15E-08	3.06E-10
5	1.031	7.76E-02	7.91E-05	1.21E+06	4.89E-08	3.04E-10
6	1.026	1.11E-01	1.13E-04	1.00E+06	4.05E-08	3.03E-10
8	1.019	1.96E-01	2.00E-04	7.47E+05	3.02E-08	3.01E-10
10	1.015	3.06E-01	3.12E-04	5.95E+05	2.41E-08	3.00E-10
15	1.010	6.84E-01	6.98E-04	3.95E+05	1.60E-08	2.99E-10
20	1.008	1.21E+00	1.24E-03	2.95E+05	1.19E-08	2.99E-10
30	1.005	2.72E+00	2.78E-03	1.96E+05	7.94E-09	2.98E-10
40	1.004	4.84E+00	4.93E-03	1.47E+05	5.95E-09	2.98E-10
50	1.003	7.55E+00	7.70E-03	1.18E+05	4.76E-09	2.98E-10
60	1.003	1.33E+01	1.11E-02	9.80E+04	3.96E-09	2.98E-10
80	1.002	1.72E+01	1.97E-02	7.34E+04	2.97E-09	2.98E-10
100	1.002	2.49E+01	3.07E-02	5.87E+04	2.37E-09	2.98E-10

[a]Calculated for standard density spheres at 293 K [20°C] and 101 kPa [1 atm].

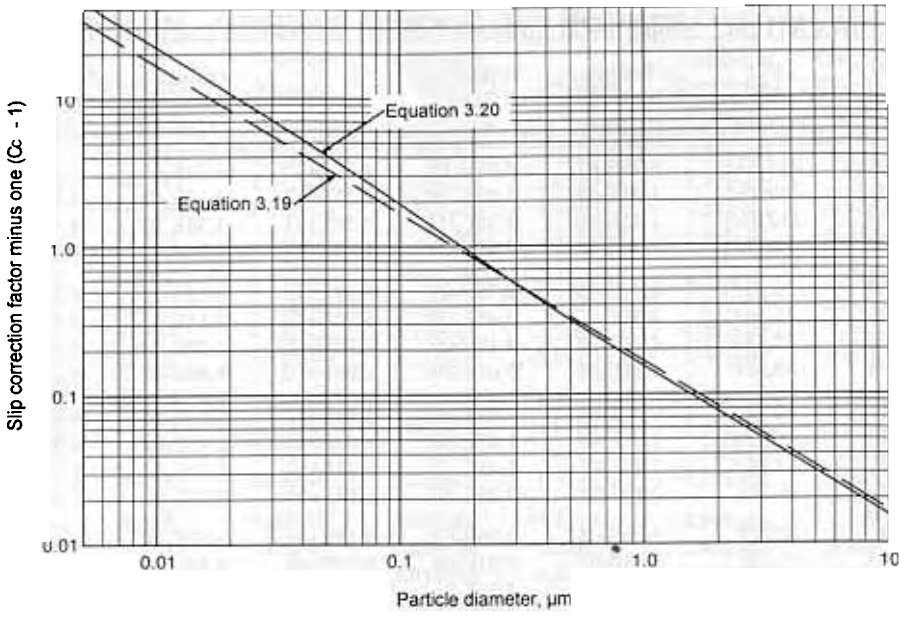

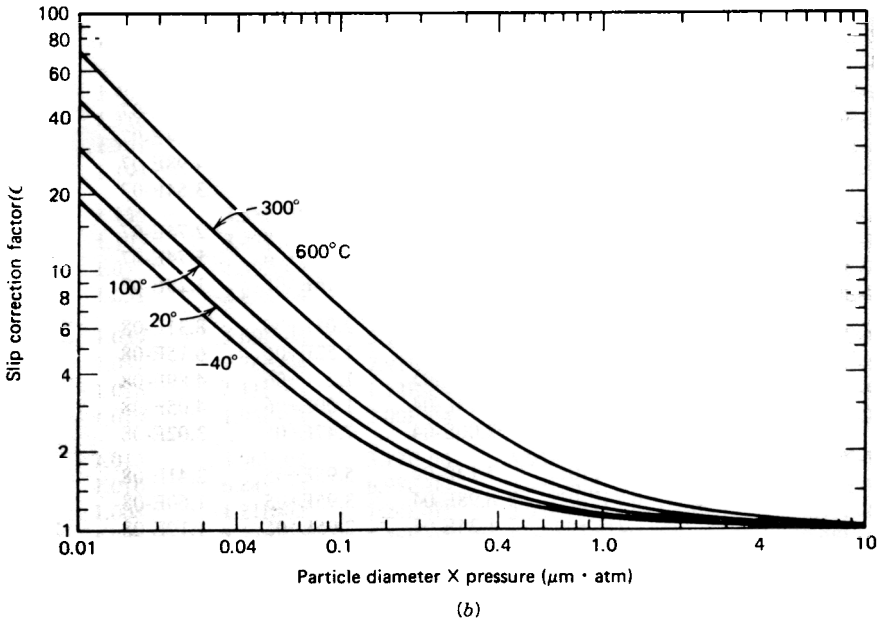

(b)

APPENDIX A12. Slip Correction Factor for Standard and Nonstandard Conditions: (a) Slip Correction Factor Minus One versus Particle Diameter at Standard Conditions; (b) Slip Correction Factor versus Particle Diameter Times Pressure for Temperatures from 233 to 893 K [–40 to 600°C][a]

[a]Calculated by Eqs. 2.25, and 3.20.

APPENDIX A13. Properties of Selected Low-Vapor-Pressure Liqui

Liquid	Molecular Weight	Relative Density[a]	Viscosity at 293 K [20°C] (Pa · s)	Surface Tension (N/m × 10^5) or [dyn/cm]	Boiling Temperature (°C)	Vapor Pressure[b] at 293 K [20°C] Pa [mmHg]	Refractive Index
	278				340	0.012 [9×10^{-5}]	
DOP (DEHP)[d]	391	0.984	0.082	31	350	3.5×10^{-6} [2.6×10^{-8}]	1.484
DOS (DEHS)[e]	426	0.9?5	0.027	32	248		1.448
PAO[f](3004)		0.819	0.027	29	401	—	1.456
Glycerol	92	1.26	1.4	63	290 (decomposition)	0.027 [2×10^{-4}]	1.475
Mineral oil[g]		0.86–0.88	(0.6)		95% >360		1.48
Oleic acid	283	0.894			360 (decomposition)	0.012 [9×10^{-5}]	1.458
PEG[h]	380–420	1.13	0.11	45	range		465
Silicone oil[i]		0.97–1.	0.1–1	3–21			

—Indicates data not available.

[a]Density relative to water. Multiply by 1000 for density in kg/m^3 or by 1.0 for density in g/cm^3.

[b]Extrapolated to 293 K [20°C] from published data.

[c]Di-butyl phthalate.

[d]Di (2-ethylhexyl) phthalate.

[e]Di (2-ethylhexyl) sebacate.

[f]Poly alpha olefin, Emery 3004.

[g]White mineral petroleum oil, USP.

[h]Polyethylene glycol, PEG 400, Union Carbide.

[i]Range for DC 200, 550, and 710 cS. Dow Corning.

APPENDIX A14. Reference Values for Atmospheric Properties at Sea Level and 293.15 K [20°C][a]

Property		Value, (SI Units)	Value, (cgs Units)
Absolute Temperature[b]	T	293.15 K	293.15 K [20°C]
Acceleration of Gravity[c]	g	9.8066 m/s^2	980.66 cm/s^2
Atmospheric Pressure[c, d]	p	1.0132×10^5 Pa	1.0132×10^6 dyn/cm^2
Avogadro Constant[c]	N_a	6.0222×10^{23} /mol	6.0222×10^{23} /mol
Boltzmann Constant[c]	k	1.3806×10^{-23} J/K	1.3806×10^{-16} dyn·cm/K
Density[e]	ρ_g	1.2041 kg/m^3	1.2041×10^{-3} g/cm^3
Diffusion Coefficient[f]	D	1.99×10^{-5} m^2/s	0.199 cm^2/s
Mean Free Path[g]	λ	0.066 μm	0.066 μm
Molar Volume[e]	v_m	0.024053 m^3/mol	24.053 L/mol
Molecular Concentration[e]	n	2.5036×10^{25} m^{-3}	2.5036×10^{19} cm^{-3}
Molecular Weight[c]	M	0.028964 kg/mol	28.964 g/mol
Molecular Collision Diameter[h]	d_m	3.7×10^{-10} m	3.7×10^{-8} cm
Molecular Velocity (mean)[e]	$\bar{c}$	462.90 m/s	46290 cm/s
Ratio of Specific Heats (c_p/c_v)[i]	κ	1.400	1.400
Speed of Sound[e]	V_s	343.23 m/s	34323 cm/s
Universal Gas Constant[c]	R	8.3143 J/mol·K	8.3143×10^7 dyn·cm/K·mol
Viscosity, Dynamic[j]	η	1.8134×10^{-5} Pa·s	1.8134×10^{-4} Poise

[a]Values rounded off to five significant figures where available.
[b]Value given is the standard temperature used in this book. It differs from the adopted sea level temperature of 288.15 K [15°C] used in USSA (1976).
[c]USSA (1976) value.
[d]Also 760 mm Hg exactly, USSA (1976).
[e]USSA (1976) value adjusted to the standard temperature of 293.15 [20°C].
[f]Bolz and Tuve (1973) value.
[g]Calculated by Eq. 2.25 using the adopted value of 0.37 nm for the molecular collision diameter. (Note, this value of λ differs slightly from the USSA (1976) value corrected to 293.15 [20°C] because of a different adopted value (0.365 nm) for molecular collision diameter.)
[h]Adopted value. This value differs slightly from the adopted value used in USSA (1976) of 0.365 nm. (Note, this affects the mean free path as calculated by Eq. 2.25.)
[i]USSA (1976) adopted value.
[j]USSA (1976) value adjusted to the standard temperature of 293.15 [20°C] by the Southerland equation (see the example problem in Section 2.4).

References

USSA, *U.S. Standard Atmosphere, 1976*, National Oceanic and Atmospheric Administration (NOAA), National Aeronautics and Space Administration (NASA), and United States Air Force (USAF), Washington, DC, 1976.

Bolz, R. E. and Tuve, G. L., *CRC Handbook of Tables for Applied Engineering Sciences*, 2d ed., CRC Press, Boca Raton, FL, 1973.

APPENDIX A15. Greek Symbols Used in This Book

A α	Alpha	Θ θ	Theta	Σ σ	Sigma
B β	Beta	K κ	Kappa	T τ	Tau
Γ γ	Gamma	Λ λ	Lambda	Φ ϕ	Phi
Δ δ ∂	Delta	M μ	Mu	X χ	Chi
E ϵ ε	Epsilon	Π π	Pi	Ω ω	Omega
H η	Eta	P ρ	Rho		

SI Prefixes

	Prefix				Symbol
10^{9}	giga	G	10^{-3}	milli	m
10^{6}	mega	M	10^{-6}	micro	μ
10^{3}	kilo	k	10^{-9}	nano	n
10^{-2}	centi	c	10^{-12}	pico	p